Matter-wave Optics of Dark-state Polaritons: Applications to Interferometry and Quantum Information

Dissertation

Frank E. Zimmer

Vom Fachbereich Physik der Technischen Universität
Kaiserslautern zur Verleihung des akademischen Grades
„Doktor der Naturwissenschaften" genehmigte Dissertation

Betreuer: Prof. Dr. Michael Fleischhauer
Zweitgutachter: Prof. James R. Anglin, Ph. D.

Datum der wissenschaftlichen Aussprache: 28.07.2006

D 386

Contents

Kurzfassung

Die vorliegende Arbeit ,,*Materwave Optics with Dark-state Polaritons: Applications to Interferometry and Quantum Information*" befaßt sich im Weiteren mit dem Thema Dunkelzustände und im Speziellen mit den im Zusammenhang mit der Speicherung von Photonenwellenpaketen in optisch dichten Medien eingeführten Dunkelzustandspolaritonen. Diese lassen sich als Superposition von Licht- und Materiewellen auffassen. Im Rahmen der Arbeit werden die besonderen optischen und materiewellenoptischen Eigenschaften dieser Anregungen untersucht. Zum einen wird ein neues Verfahren vorgestellt, das zur räumlichen Erhöhung der Anregungsdichte benutzt werden kann, zum anderen werden die Eigenschaften zur Konstruktion eines neuen Sagnac-Interferometers verwendet. Die Arbeit gliedert sich in vier Teile:

In einem Einführungskapitel werden die zum Verständnis der Arbeit notwendigen Begriffe, wie elektromagnetisch induzierte Transparenz (EIT), Dunkelzustandspolaritonen und Sagnac-Effekt erläutert. Außerdem werden zum späteren Vergleich die *state-of-the-art* Quantenlimites für Laser- und Materiewellen-Gyroskope angegeben.

Das zweite Kapitel der Arbeit betrachtet das von A. André und M. D. Lukin entwickelte Verfahren zur Erzeugung stationärer optischer Wellenpakete in speziell präparieren EIT-Medien. Es wird, unter Betrachtung eines selbstkonsistenten Gleichungssystems für ein schwaches Probefeld, und durch Einführung angepaßter Normalmoden gezeigt, dass die Absorption einer der Moden zum Phänomen des *pulse-machtings* und damit zu einem diffusiven Verhalten der anderen Normalmode führt. Alle bis zu diesem Punkt durchgeführten Untersuchungen basieren auf einer homogenen und symmetrischen Konfiguration der Präparationslaser. Wird diese Symmetrie aufgeben, so erkennt man, dass der diffusiven Verbreiterung der nichtabsorbierten Normalmoden eine Driftbewegung superponiert ist. Durch die Wahl einer speziellen Präparationslaserkonfiguration kann die Driftbewegung so modifiziert werden, dass sie zu einer effektiven Kraft führt, welche die diffusive Verbreiterung kompensiert. Insbesondere kann die effektive Kraft so stark werden, dass die Feldverteilung dieser Normalmode komprimiert wird. Der hier beschriebene Prozess kann mittels einer Fokker-Planck Gleichung vom Ornstein-Uhlenbeck-Typ beschrieben werden, deren Lösung einer Lösung des gedämpften harmonischen Oszillator sehr ähnlich ist. Es zeigt sich, dass das Komprimieren der Feldverteilung zu einer Anregung höherer Moden der allgemeinen Ornstein-Uhlenbeck Lösung führt, welche wesentlich schneller zerfallen als der Grundzustand. Im letzten Abschnitt dieses Kapitels wird dieser Anregungsprozess näher untersucht und es werden Bedingungen angegeben, die zu einer Verringerung bzw. Vermeidung der Anregung höherer Moden führen. Alle in diesem Kapitel gemachten Aussagen werden durch numerische Simulationen ergänzt.

Im dritten Kapitel werden die materiewellenoptischen Eigenschaften der Dunkelzustandspolaritonen untersucht. Diese werden dazu benutzt, um ein neuartiges Licht-Materiewellen Hybrid Sagnac Interferometer zu konstruieren. Zunächst werden der prinzipielle Aufbau und die Funktionsweise eines solchen Interferometers skizziert. Anschließend wird die Dynamik der Materie-Licht-Wechselwirkung in einem rotierenden Bezugssystem erläutert und die relevanten Bewegungsgleichungen werden abgeleitet. Diese bilden die Grundlage für die darauffolgende Untersuchungen der Dunkelzustandspolari-

tonendynamik ohne und unter Einfluß von externen Fallenpotentialen für den Materiewellenanteil. Wir zeigen, dass eine Sensitivitätserhöhung des Hybrid-Gyroskopes gegenüber eines gewöhnlichen, passiven Laser-Gyroskopes selber Fläche zu erwarten ist, wenn anfänglich das beteiligte gasförmige Medium sich in einem suprafluiden Quantenzustand in einer Ringfalle befindet. Außerdem wird aufgezeigt, dass ein simultaner Impuls- und Kohärenztransfer für die Arbeit des Interferometers notwendig ist. Im letzten Teil des Kapitels wird die zu erwartende Sensititivät des neuen Gyroskopes am Schrotrauschlimit durch Betrachtung der Einteilchen-Dichtematrixgleichungen ermittelt. Insbesondere wird der Einfluß der Teilchenbewegung bei diesen Berechnungen mit berücksichtigt. Dazu werden die Maxwell-Bloch-Gleichungen störungstheoretisch in der gesuchten Rotationsrate behandelt und die Suszeptibilität des betrachteten 3-Niveau-Systems in beliebiger Ordnung des Probefeldes bestimmt. Schließlich wird die so gefundene Sensitivität des Hybrid-Gyroskopes mit *state-of-the-art* Laser- und Materiewellen Sagnac Interferometern verglichen.

Das letzte Kapitel der Arbeit ist durch ein gemeinsames theoretisches und experimentelles Projekt im Rahmen eines Praktikums in der AG Bergmann enstanden. Das Praktikum wurde durch das Graduiertenkolleg 792: „Ultrakurzzeitphysik und nichtlineare Optik" initiiert. Dieser Abschnitt behandelt nicht mehr direkt die oben diskutierten Dunkelzustandspolaritonen sondern greift den allgemeineren Begriff des Dunkelzustands auf. Durch experimentelle Arbeiten konnten erstmals die von E. Arimonodo et al. vorhergesagten geschwindigkeitsselektiven transienten Dunkelzustände nachgewiesen werden. Das Kapitel führt zunächst in den Begriff des geschwindigkeitsselektiven Dunkelzustands am Beispiel einer Λ-Kopplung ein. Die Systemdynamik für diesen Fall wird in der speziellen Basis aus Hell- und Dunkelzuständen näher erläutert und führt schließlich zur Einführung des transienten Dunkelzustandes. Danach werden die zur theoretischen Beschreibung notwendigen Gleichungen abgeleitet, da diese im darauffolgenden Abschnitt zur numerischen Simulation des Systems benötigt werden. Diese Simulationen basieren auf der Lösung der verallgemeinerten Bloch-Gleichungen, welche die Schwerpunktsbewegung der Atome ebenfalls berücksichtigen. Unter Zuhilfenahme dieser und Untersuchungen mittels eines resolventheoretischen Ansatzes werden Bedingungen zur Beobachtbarkeit der transienten Dunkelzustände angegeben. Schließlich werden die experimentellen Voraussetzungen und die Messmethode vorgestellt und die experimentellen mit den theoretischen Resultaten verglichen.

Abstract

The present work "Materwave Optics with Dark-state Polaritons: Applications to Interferometry and Quantum Information" deals in a broad sense with the subject of dark-states and in particular with the so-called dark-state polaritons introduced by M. Fleischhauer and M. D. Lukin to discribe the coherent and reversible storage of photonic wavepackets in optical dense media. The dark-state polaritons can be regarded as combined excitation of electromagnetic fields and spin/matter-waves. Within the framework of this thesis the special optical properties of the combined excitation are studied. On one hand a new procedure to spatially manipulate and to increase the excitation density of stored photons is described and on the other hand the properties are used to construct a new type of Sagnac Hybrid interferometer. The thesis is devided into four parts.

In the introduction all notions necessary to understand the work are described, e. g. : electromagnetically induced transparency (EIT), dark-state polaritons and the Sagnac effect. Moreover, for later comparison the standard quantum limits for state-of-the-art laser and matterwave gyroscopes are provided.

The second chapter considers the method developed by A. André and M. D. Lukin to create stationary light pulses in specially dressed EIT-media. In a first step a self-consistent set of field equations is derived and simplified by introducing a new set of normal modes. The absorption of one of the normal modes leads to the phenomenon of *pulse-matching* for the other mode and thereby to a diffusive spreading of its field envelope. This is further studied by considering the equations of motion for the first two momenta of the non-absorbed normal mode. All these considerations are based on a homogeneous and symmetrical field setup of the EIT preparation laser. If this restriction is dismissed one finds that a drift motion is superimposed to the diffusive spreading. By choosing a special laser configuration the drift motion can be tailored such that an effective force is created that counteracts the spreading. Moreover, the force can not only be strong enough to compensate the diffusive spreading but also to exceed this dynamics and hence to compress the field envelope of the excitation. The compression can be discribed using a Fokker-Planck equation of the Ornstein-Uhlenbeck type. The general solution of this equation is quite similar to the solution of the damped harmonic oscillator. The investigations show that the compression leads to an excitation of higher-order modes of the general Ornstein-Uhlenbeck solution which decay very fast. In the last section of the chapter this exciation will be discussed in more detail and conditions will be given how the excitation of higher-order modes can be avoided or even suppressed. All results given in the chapter are supported by numerical simulatons.

In the third chapter the matterwave optical properties of the dark-state polaritons will be studied. They will be used to construct a light-matterwave hybrid Sagnac interferometer. First the principle setup of such an interferometer will be sketched and the relevant equations of motion of light-matter interaction in a rotating frame will be derived. These form the basis of the following considerations of the dark-state polariton dynamics with and without the influence of external trapping potentials on the matterwave part of the polariton. It will be shown that a sensitivity enhancement compared to a passive laser gyroscope can be anticipated if the gaseous medium is initially in a

superfluid quantum state in a ring-trap configuration. To achieve this enhancement a simultaneous coherence and momentum transfer is furthermore necessary. In the last part of the chapter the quantum sensitivity limit of the hybrid interferometer is derived using the one-particle density matrix equations incorporating the motion of the particles. To this end the Maxwell-Bloch equations are considered perturbatively in the rotation rate of the noninertial frame of reference and the susceptibility of the considered 3-level Λ-type system is derived in arbitrary order of the probe-field. This is done to determine the optimum operation point. With its help the anticipated quantum sensitivity of the light-matterwave hybrid Sagnac interferometer is calculated at the shot-noise limit and the results are compared to state-of-the-art laser and matterwave Sagnac interferometers.

The last chapter of the thesis originates from a joint theoretical and experimental project within the Graduiertenkolleg 792: "Ultrakurzzeitphysik und nichtlineare Optik". It is based on a laboratory in the AG Bergmann. This chapter does no longer consider the dark-state polaritons of the last two chapters but deals with the more general concept of dark states and in particular with the transient velocity selective dark states as introduced by E. Arimondo et al. In the experiment we could for the first time measure these states. The chapter starts with an introduction into the concept of velocity selective dark states as they occur in a Λ-configuration. Then the system dynamics will be described in a special basis set namley the dark- and bright-states of the present system. This leads us to the introduction of the transient velocity selective dark-states as they occur in an particular extension of the Λ-system. For later use in the simulations the relevant equations of motion are derived in detail. The simulations are based on the solution of the generalized optical Bloch equations which also incooperate the center-of-mass motion of the atoms. With the help of these simulations and a resolvent ansatz conditions for the parameters to meausre those states are presented. Finally the experimental setup and procedure are explained and the theoretical and experimental results are compared.

Outline

The subject of this thesis are matterwave properties of dark-state polaritons (DSP) introduced by M. Fleischhauer and M. D. Lukin [1] to solve the light-storage problem in media showing electromagnetically induced transparency (EIT) [2]. These dark-state polaritons are combined excitations of electromagnetic fields and atomic Raman transitions [3]. The main theme of this thesis is: can we use the special superposition nature of the DSP for applications that outperform conventional or matterwave optics. This rather general problem is discussed for two different, more specific subjects. The first is: "Can we use the special properties of the DSPs to construct an efficient quantum logic gate?" and the second: "Is it possible to make use of the matterwave component of the DSP in interferometry (especially when constructing a DSP-gyroscope)?". Since the whole thesis can be divided according to these two questions we motivate both parts separately.

Quantum information technologies requires methods to coherently store, transfer and manipulate quantum states. The dark-state polariton approach has made considerable progress in terms of the first two requirements. Ensembles of atoms with long-lived atomic states provide reliable storage units for quantum information. The transfer is mediated by photons which are quite robust and are an efficient realization of *flying* qubits. However, the development of high fidelity quantum logic gates operating on single quantum excitations is a still unsolved problem. To date a number of proposals based on the DSP approach have been considered, for example: scattering of DSP in optical lattices [4], dipole-dipole interaction of slow-light pulses via Rydberg states [5] and entanglement of photons via N-shaped atomic configurations schemes [6]. All these approaches suffer, however, from several drawbacks.

The first one is the limited interaction time. For example in head-on type collisions between two polaritons the interaction time stays constant irrespectively of the group velocity v_{gr} of the polaritons. Thus in order to achieve a long interaction time copropagating pulses were considered [6]. However, this configuration leads to nonhomogeneous interaction and spectral broadening of the wave packets. Hence, the latter ansatz has limited suitability for quantum information processing as well.

A second drawback becomes apparent if we want to reach the required nonlinear interaction to entangle two DSPs, moving with a small group velocity $v_{\mathrm{gr}} \ll c$, via the nonlinear part of the susceptibility. In this case we run into trouble since the number of photons in the DSP-pulse decreases by the factor v_{gr}/c when it enters the medium. Hence, the usable interaction energy decreases by the same factor. For small group velocities the major part of excitation is transfered to the matterwave part of the polariton which is

5

not available for nonlinear interaction via the susceptibility. In this case one might argue that an extension of the interaction time would help, however, a longer interaction time is accompanied by decoherence which has to be avoided.

The reduced photonic part of slow moving polaritons might be compensated by the resonant enhancement of the nonlinear susceptibility in EIT media [7, 8]. As found by S. Harris [9] nonlinear optical processes become efficient already at energy densities of one photon per atomic cross section [10]. This requires however tight spatial confinement of the photonic excitation in addition to the long interaction time.

To fulfill the requirements of long interaction time and tight spatial confinement we consider not the standard slow-light scheme but an extension introduced by A. André and M. D. Lukin [11, 12]. This scheme allows for the creation of long-lived stationary photonic excitations in the medium. All main ingredients for the construction of a quantum logic gate are provided by the stationary light scheme except that the excitation density on the single excitation level is not high enough. A coherent and quantum state preserving spatial compression of the excitation is required to profit from the resonant enhanced nonlinear susceptibility. That this can be achieved will be shown in chapter 2.

Let us turn now to the second question, i. e. whether it is possible to make use of the matterwave part of the DSP in interferometry. Recently U. Leonhardt and P. Piwnicki [13] pointed out that one might anticipate a sensitivity enhancement c/v_gr of a gyroscope using slow-light in an EIT-medium as compared to a standard optical Sagnac gyroscope. This suggestion lead to an intense research since at the same time L. V. Hau and coworkers [14] showed that it is possible to reach incredible low group velocities on the order of meters per second in EIT-media. There exists a large interest for high sensitivity gyroscopes as they are used in many commercial applications such as orientation sensors for airplanes. They are also interesting from a pure scientific point of view since they can help to decide between different gravitation theories.

In this thesis we discuss a slow-light gyroscope that makes use of the possible free motion of the atoms in a gaseous medium [15]. We show that a sensitivity enhancement is only achievable if the momentum transfer from the light to the matterwave part of the dark-state polariton is taken into account. This statement is controversially discussed in the community [16].

The thesis is structured as follows: The first chapter gives an introduction in the concepts used. The standard Hamiltonian of quantum optics in the length-gauge is derived with special emphasis on a separation of relative and center-of-mass coordinates since we are also interested in the quantum mechanical treatment of the center-of-mass variable. In a second step we explain electromagnetically induced transparency which is a phenomenon at the heart of the dark-state polariton concept. Furthermore, we introduce slow-light and explain its limitations with respect to light-storage. We can cope with its limitations by using explicitly time-dependent electromagnetically induced transparency. This finally leads us to the dark-state polariton mechanism which allows for a state and shape preserving storage and release of light pulses. At the end of the Introduction chapter we give a brief review of the Sagnac effect and stated the quantum limits of gyroscopes based on the corresponding effect.

Chapter 2 is devoted to the detailed analysis of the stationary light scheme and the

coherent manipulation of stationary light. We first derive a self-consistent set of field equations which describe the dynamics of electromagnetic fields in an EIT-media dressed in a special way. The introduction of new set of variables, i. e. normal modes, leads to a clearer representation of the ongoing dynamics. Absorption of one of the normal modes, which is equivalent to the phenomenon of pulse matching, leads to a diffusive behavior of the other mode. This dynamics is discussed in more detail. Finally by choosing an appropriate dressing of the EIT-medium the stationary field can spatially be compressed. All the analytical calculation are supported by numerical simulations.

The 3rd chapter is devoted to the detailed analysis of the proposed polariton based Sagnac interferometer. In a first step we derive the relevant equations of motion in the rotating frame. The conceptual basics of the gyroscopes are introduced afterwards. We show that an enhancement of the interferometers sensitivity is only possible if the atoms – matter part of the polariton – are initially prepared in a superfluid quantum state in a ring-trap type configuration. Finally we derive the minimum detectable rotation rate at the optimal operation point of the gyroscope by calculating the signal-to-noise ratio.

The last chapter originates form a joint experimental and theoretical project in the ,,Graduiertenkolleg 792: Ultrakurzzeitphysik und nichtlineare Optik". Together with Dr. F. Vewinger I was able to measure for the first time the transient dark state in the velocity selective coherent population trapping (VSCPT) scheme. The corresponding chapter gives first an introduction into the concepts of VSCPT. In a second step we review the theoretical concepts used later on for our numerical simulations. At the end of the chapter the experimental and numerical results are compared.

Chapter 1

Introduction

1.1 Hamiltonian of quantum optics

In this thesis we consider the interaction of radiation with matter, either in the form of optically dense ensembles of Λ-like 3-level atoms or of a beam of two level atoms. We therefore introduce the concept of the interaction of quantized electromagnetic fields with non-stationary atoms. We do this to establish the notation used later on and to give a brief conceptual overview. To this end we introduce first the minimal coupling Hamiltonian (see [17, 18] and references therein). To simplify the discussion we assume a very simple atom model which is however sufficient for this thesis. Since we will treat the center-of-mass motion of atoms quantum mechanically in chapter 3 and 4, we will show how the initial minimal coupling Hamiltonian transforms to center-of-mass coordinates. For convenience and later use we will derive the length or $\hat{\mathbf{E}} \cdot \hat{\mathbf{r}}$-gauge form of the corresponding Hamiltonian using the Power-Zienau-transformation. Last but not least, a brief derivation of the Hamiltonian for stationary Λ-like 3-level atoms will be given. The interaction of such atoms with electromagnetic fields is the major topic of this thesis.

1.1.1 Interaction of neutral atoms with electromagnetic fields

Transformation to center-of-mass coordinates

We will restrict ourselves within this thesis to the class of atoms with a single valence electron, e. g. alkali atoms, since most relevant experiments in this field are conducted on their basis [14, 19, 20]. Alkali-metal atoms can be treated fairly well in the one-electron approximation with a heavy nuclei and an outer, much lighter valence electron. The electric charge of the core is in general screened by the inner electrons and the core therefore possesses the screened charge q. Let e be the electric charge of the electron with mass m_e and position $\hat{\mathbf{r}}_\mathrm{e}$. The mass and position of the core shall be denoted by m_c and $\hat{\mathbf{r}}_\mathrm{c}$ respectively.

In non-relativistic quantum theory the standard Hamiltonian that describes the inter-

action between quantized electromagnetic fields and atoms is given by

$$H = H_{\mathrm{a}} + H_{\mathrm{aa}} + H_{\mathrm{f}}. \tag{1.1}$$

Here H_{a} is the minimal coupling Hamiltonian that is responsible for the light-matter-interaction, H_{aa} is the part that stands for the atom-atom interaction and the last term is the Hamiltonian of the free electromagnetic field. We will neglect the atom-atom interaction due to collisions in this thesis. This is valid as long as the considered atomic ensemble, which we assume to be gaseous, is sufficiently dilute. Collisions will be taken into account only indirectly by including, if necessary, dephasing or decay rates into the equations of motion for the atomic variables.

The minimal coupling Hamiltonian distinguishes itself from others by the invariance of its corresponding Schrödinger equation under local gauge phase transformations [21, 22]. For the electron-core system it is given by

$$H_{\mathrm{a}} = \frac{(\hat{\mathbf{p}}_{\mathrm{c}} - q\hat{\mathbf{A}}(\hat{\mathbf{r}}_{\mathrm{c}}))^2}{2\,m_{\mathrm{c}}} + \frac{(\hat{\mathbf{p}}_{\mathrm{e}} - e\hat{\mathbf{A}}(\hat{\mathbf{r}}_{\mathrm{e}}))^2}{2\,m_{\mathrm{e}}} + V_{\mathrm{ec}}\left(\hat{\mathbf{r}}_{\mathrm{e}}, \hat{\mathbf{r}}_{\mathrm{c}}\right), \tag{1.2}$$

where V_{ec} denotes the effective (screened) Coulomb potential between the outer valence electron and the core. $\hat{\mathbf{p}}_{\mathrm{e}}$ and $\hat{\mathbf{p}}_{\mathrm{c}}$ are the canonical momenta corresponding to the electron and core position coordinates. In eq. (1.2) $\hat{\mathbf{A}}$ denotes the vector potential. The fundamental dynamical variables for the motion of electron and core obey the following commutation relations

$$[\hat{r}_{\alpha,\mathrm{i}}, \hat{r}_{\beta,\mathrm{j}}] = [\hat{p}_{\alpha,\mathrm{i}}, \hat{p}_{\beta,\mathrm{j}}] = 0, \tag{1.3}$$

$$[\hat{r}_{\alpha,\mathrm{i}}, \hat{p}_{\beta,\mathrm{j}}] = \mathrm{i}\,\hbar\,\delta_{\alpha,\beta}\,\delta_{\mathrm{i,j}} \ \ \text{with} \ \ i,\,j = x, y, z \ \ \text{and} \ \ \alpha, \beta = e, c. \tag{1.4}$$

The free electromagnetic field is described in the Coulomb-gauge, i. e. $\nabla \cdot \hat{\mathbf{A}} = 0$, and in second quantization by the following Hamiltonian

$$H_{\mathrm{f}} = \frac{\epsilon_0}{2} \int \mathrm{d}^3 r' \left\{ \left[\frac{\hat{\mathbf{\Pi}}_{\perp}(\mathbf{r}')}{\epsilon_0}\right]^2 + c^2 \left[\nabla' \times \hat{\mathbf{A}}_{\perp}(\hat{\mathbf{r}}')\right]^2 \right\}, \tag{1.5}$$

with c being the speed of light in vacuum and ϵ_0 the dielectric constant. The subscript $\perp$ denotes transversal vectors fields[1]. In the Coulomb-gauge the dynamical variables of the system are $\hat{\mathbf{A}}_{\perp}$ and $\hat{\mathbf{\Pi}}_{\perp} = -\hat{\mathbf{D}}_{\perp} = \epsilon_0 \partial_t \hat{\mathbf{A}}_{\perp}$. One determines the electric and magnetic fields from these by $\hat{\mathbf{E}}_{\perp} = -\partial_t \hat{\mathbf{A}}_{\perp}$ and $\hat{\mathbf{B}}_{\perp} = \nabla \times \hat{\mathbf{A}}_{\perp}$. The representation of the field operators in terms of creation ($\hat{a}_{\mathbf{k}\boldsymbol{\epsilon}}$) and annihilation ($\hat{a}^\dagger_{\mathbf{k}\boldsymbol{\epsilon}}$) operators of the field modes $\{\mathbf{k}, \boldsymbol{\epsilon}\}$ are given in the Schrödinger picture by

$$\hat{\mathbf{A}}_{\perp}(\mathbf{r}) = \hat{\mathbf{A}}_{\perp}^{(+)}(\mathbf{r}) + \hat{\mathbf{A}}_{\perp}^{(-)}(\mathbf{r}) = \sum_{\mathbf{k}\boldsymbol{\epsilon}} \mathcal{A}_{\omega_{\mathrm{k}}} \left[\hat{a}_{\mathbf{k}\boldsymbol{\epsilon}}\boldsymbol{\epsilon} e^{\mathrm{i}\mathbf{k}\cdot\mathbf{r}} + \hat{a}^\dagger_{\mathbf{k}\boldsymbol{\epsilon}}\boldsymbol{\epsilon} e^{-\mathrm{i}\mathbf{k}\cdot\mathbf{r}}\right], \tag{1.6}$$

$$\hat{\mathbf{E}}_{\perp}(\mathbf{r}) = \hat{\mathbf{E}}_{\perp}^{(+)}(\mathbf{r}) + \hat{\mathbf{E}}_{\perp}^{(-)}(\mathbf{r}) = \sum_{\mathbf{k}\boldsymbol{\epsilon}} \mathrm{i}\,\mathcal{E}_{\omega_{\mathrm{k}}} \left[\hat{a}_{\mathbf{k}\boldsymbol{\epsilon}}\boldsymbol{\epsilon} e^{\mathrm{i}\mathbf{k}\cdot\mathbf{r}} - \hat{a}^\dagger_{\mathbf{k}\boldsymbol{\epsilon}}\boldsymbol{\epsilon} e^{-\mathrm{i}\mathbf{k}\cdot\mathbf{r}}\right], \tag{1.7}$$

$$\hat{\mathbf{B}}_{\perp}(\mathbf{r}) = \hat{\mathbf{B}}_{\perp}^{(+)}(\mathbf{r}) + \hat{\mathbf{B}}_{\perp}^{(-)}(\mathbf{r}) = \sum_{\mathbf{k}\boldsymbol{\epsilon}} \mathrm{i}\,\mathcal{B}_{\omega_{\mathrm{k}}} \left[\hat{a}_{\mathbf{k}\boldsymbol{\epsilon}}(\boldsymbol{\kappa} \times \boldsymbol{\epsilon}) e^{\mathrm{i}\mathbf{k}\cdot\mathbf{r}} - \hat{a}^\dagger_{\mathbf{k}\boldsymbol{\epsilon}}(\boldsymbol{\kappa} \times \boldsymbol{\epsilon}) e^{-\mathrm{i}\mathbf{k}\cdot\mathbf{r}}\right], \tag{1.8}$$

---

[1]The vector field $\mathbf{F}(\mathbf{r})$ is a transversal field if $\nabla \cdot \mathbf{F}(\mathbf{r}) = 0$.

where $\mathcal{E}_{\omega_{\mathbf{k}}} = \sqrt{\hbar\omega_k/2\epsilon_0 V}$ is the electric field per photon in the quantization volume V and we have $\mathcal{A}_{\omega_{\mathbf{k}}} = \mathcal{E}_{\omega_{\mathbf{k}}}/\omega_k$ and $\mathcal{B}_{\omega_{\mathbf{k}}} = \mathcal{E}_{\omega_{\mathbf{k}}}/c$. In eq. (1.6) $\hat{\mathbf{A}}_{\perp}^{(+)}$ corresponds to the positive and $\hat{\mathbf{A}}_{\perp}^{(-)}$ to the negative frequency part of the transverse vector potential. The notation also hold for the electric and magnetic fields. For the polarization unit vector of the electric field and the vector potential we have used the symbol $\boldsymbol{\epsilon}$ and $\boldsymbol{\kappa} = \mathbf{k}/|\mathbf{k}|$ denotes the normalized wave vector. In the following we will for notational simplicity omit the subscript $\perp$. The equal time commutation relation for the vector components of the field operators

$$\left[\hat{A}_i(\mathbf{r},t), \hat{A}_j(\mathbf{r}',t)\right] = \left[\hat{\Pi}_i(\mathbf{r},t), \hat{\Pi}_j(\mathbf{r}',t)\right] = 0, \tag{1.9}$$

$$\left[\hat{A}_i(\mathbf{r},t), \hat{\Pi}_j(\mathbf{r}',t)\right] = \mathrm{i}\hbar\delta_{ij}^{\perp}(\mathbf{r}-\mathbf{r}') \quad \text{with} \quad i,j \in \{1,2,3\}, \tag{1.10}$$

can either be deduced from the commutator relation $[\hat{a}_{\mathbf{k}\boldsymbol{\epsilon}}, \hat{a}_{\mathbf{k}'\boldsymbol{\epsilon}'}^{\dagger}] = \delta_{\boldsymbol{\epsilon}\boldsymbol{\epsilon}'}\delta_{\mathbf{k}\mathbf{k}'}$ of the creation and annihilation operators or have to be postulated in the course of a canonical quantization. $\delta_{i,j}^{\perp}(\mathbf{R}-\mathbf{r}')$ in eq. (1.10) denotes the transversal delta function [17].

In a first step we rewrite eq. (1.2) using the center-of-mass variables defined by

$$\hat{\mathbf{R}} = \frac{m_{\mathrm{c}}\hat{\mathbf{r}}_{\mathrm{c}} + m_{\mathrm{e}}\hat{\mathbf{r}}_{\mathrm{e}}}{m}, \tag{1.11}$$

$$\hat{\mathbf{P}} = m\,\dot{\hat{\mathbf{R}}} = m_{\mathrm{c}}\dot{\hat{\mathbf{r}}}_{\mathrm{c}} + m_{\mathrm{e}}\dot{\hat{\mathbf{r}}}_{\mathrm{e}} = \hat{\mathbf{p}}_{\mathrm{c}} + \hat{\mathbf{p}}_{\mathrm{e}}, \tag{1.12}$$

where $m = m_{\mathrm{c}} + m_{\mathrm{e}}$ is the total mass of the atom and $\hat{\mathbf{R}}$ and $\hat{\mathbf{P}}$ is the center-of-mass coordinate and the corresponding conjugate momentum. In addition one defines the relative coordinate and momentum respectively,

$$\hat{\mathbf{r}} = \hat{\mathbf{r}}_{\mathrm{c}} - \hat{\mathbf{r}}_{\mathrm{e}}, \tag{1.13}$$

$$\frac{\hat{\mathbf{p}}}{\mu} = \frac{\mathrm{d}\hat{\mathbf{r}}}{\mathrm{d}t} = \frac{\hat{\mathbf{p}}_{\mathrm{c}}}{m_{\mathrm{c}}} - \frac{\hat{\mathbf{p}}_{\mathrm{e}}}{m_{\mathrm{e}}}, \tag{1.14}$$

using the reduced mass $\mu = m_{\mathrm{c}}\,m_{\mathrm{e}}/m$. With these definitions the commutator relations eq. (1.3, 1.4) transform to

$$[\hat{r}_{\mathrm{i}}, \hat{r}_{\mathrm{j}}] = [\hat{p}_{\mathrm{i}}, \hat{p}_{\mathrm{j}}] = \left[\hat{r}_{\mathrm{i}}, \hat{R}_{\mathrm{j}}\right] = \left[\hat{r}_{\mathrm{i}}, \hat{P}_{\mathrm{j}}\right] = \left[\hat{R}_{\mathrm{i}}, \hat{p}_{\mathrm{j}}\right] = \left[\hat{R}_{\mathrm{i}}, \hat{R}_{\mathrm{j}}\right] = 0, \quad \text{and} \tag{1.15}$$

$$[\hat{r}_{\mathrm{i}}, \hat{p}_{\mathrm{j}}] = \left[\hat{R}_{\mathrm{i}}, \hat{P}_{\mathrm{j}}\right] = \mathrm{i}\,\hbar\,\delta_{\mathrm{i},\mathrm{j}} \quad \text{with} \quad i,j \in \{1,2,3\} \tag{1.16}$$

Substituting the inverse transformations of eqs. (1.11-1.14), i. e.

$$\hat{\mathbf{r}}_{\mathrm{e}} = \hat{\mathbf{R}} - \frac{m_{\mathrm{c}}}{m}\,\hat{\mathbf{r}}, \tag{1.17}$$

$$\hat{\mathbf{r}}_{\mathrm{c}} = \hat{\mathbf{R}} + \frac{m_{\mathrm{e}}}{m}\,\hat{\mathbf{r}}, \tag{1.18}$$

and

$$\hat{\mathbf{p}}_{\mathrm{e}} = \frac{m_{\mathrm{e}}}{m}\,\hat{\mathbf{P}} - \hat{\mathbf{p}}, \tag{1.19}$$

$$\hat{\mathbf{p}}_{\mathrm{c}} = \frac{m_{\mathrm{c}}}{m}\,\hat{\mathbf{P}} + \hat{\mathbf{p}}, \tag{1.20}$$

into the minimal coupling Hamiltonian, eq. (1.2), one arrives, after applying the dipole

approximation with respect to the exchange of transverse photons and using the commutativity of $\hat{\mathbf{P}}$ and $\hat{\mathbf{p}}$ with $\hat{\mathbf{A}}$ in the Coulomb gauge, at

$$H_{\mathrm{a}} = \frac{\hat{\mathbf{P}}^2}{2m} + \frac{\hat{\mathbf{p}}^2}{2\mu} - \frac{q+e}{m}\hat{\mathbf{A}}(\hat{\mathbf{R}}) \cdot \hat{\mathbf{P}} + \left(\frac{q}{m_{\mathrm{e}}} - \frac{e}{m_{\mathrm{e}}}\right)\hat{\mathbf{A}}(\hat{\mathbf{R}}) \cdot \hat{\mathbf{p}}$$
$$+ \frac{1}{2}\left(\frac{q^2}{m_{\mathrm{c}}} + \frac{e^2}{m_{\mathrm{e}}}\right)\hat{\mathbf{A}}(\hat{\mathbf{R}})^2 + V_{\mathrm{ec}}(\hat{\mathbf{R}}, \hat{\mathbf{r}}). \tag{1.21}$$

The dipole or long-wavelength approximation, used in the derivation of eq. (1.21), is applicable as long as the vector potential does not change significantly over the size of the atom, i. e. if $a_0 \ll \lambda$, where a_0 is the *radius* of the corresponding atom and λ the wavelength of the transversal photon.

In this thesis we will only deal with electrically neutral atoms, hence the total charge $q + e$ is zero and the third term in eq. (1.21) vanishes. Eq. (1.21) together with the additional term of the free electromagnetic field Hamiltonian and the atom–atom interaction contribution represent the full Hamiltonian of quantum optics for neutral atoms in center-of-mass and relative variables. Using again the fact that we restrict ourselves to neutral atoms we can simplify eq. (1.21) applying $q = -e$ (neutral atom) and

$$\frac{q^2}{m_{\mathrm{c}}} + \frac{e^2}{m_{\mathrm{e}}} = \frac{q^2}{\mu}, \tag{1.22}$$

$$\frac{e}{m_{\mathrm{e}}} - \frac{q}{m_{\mathrm{c}}} = -\frac{q}{\mu}. \tag{1.23}$$

With the help of these relations we rewrite eq. (1.21) and find

$$H_{\mathrm{a}} = \frac{\hat{\mathbf{P}}^2}{2m} + \frac{1}{2\mu}\left[\mathbf{p} - q\,\hat{\mathbf{A}}(\hat{\mathbf{R}})\right]^2 + V_{\mathrm{ec}}(\hat{\mathbf{R}}, \hat{\mathbf{r}}). \tag{1.24}$$

Transformation to the length- or $\mathbf{E} \cdot \mathbf{r}$-gauge

We note that not the vector potential but the electric field is the gauge invariant observable. Hence, it is desirable to express the above Hamiltonian in terms of the latter. To go from the Coulomb- to the length-gauge of the Hamiltonian (1.24) we apply the unitary transformation [17]

$$U = \exp\left[-\frac{\mathrm{i}}{\hbar}q\,\hat{\mathbf{r}} \cdot \hat{\mathbf{A}}(\hat{\mathbf{R}})\right]. \tag{1.25}$$

This transformation is called Power-Zienau transformation [23]. Applying U to the dynamical variables of the system leads to the following substitution rules:

$$\hat{\mathbf{p}} \rightarrow \hat{\mathbf{p}} + q\hat{\mathbf{A}}(\hat{\mathbf{R}}) \tag{1.26}$$

$$\hat{\mathbf{E}} \rightarrow \hat{\mathbf{E}} + \hat{\mathbf{P}}/\epsilon_0. \tag{1.27}$$

The rest of the variables remain invariant. Eq. (1.24) reads in the new gauge

$$H_{a'} = H_{a'}^{(cen)} + H_{a'}^{(rel)} = \frac{\hat{\mathbf{P}}^2}{2m} + \frac{\mathbf{p}^2}{2\mu} + V_{ec}(\hat{\mathbf{R}}, \hat{\mathbf{r}}), \tag{1.28}$$

where the prime denotes that this is a Hamiltonian with respect to the length gauge. The distinction between relative and center-of-mass motion is given by the superscripts (cen) and (rel). The transformation of the free electromagnetic field Hamiltonian is not as straight forward. To this end we need to apply the following transformation rule [24]

$$e^{-\alpha A} B e^{\alpha A} = B - \alpha\left[A, B\right] + \frac{\alpha^2}{2}\left[A, [A, B]\right] - \dots \tag{1.29}$$

and the commutator relations eq. (1.9) and (1.10). This leads to

$$H_{f'} = \frac{\epsilon_0}{2}\int \mathrm{d}^3 r' \left\{ \left[\frac{\hat{\mathbf{\Pi}}(\mathbf{r'})}{\epsilon_0}\right]^2 + c^2\left[\nabla' \times \hat{\mathbf{A}}(\mathbf{r'})\right]^2 \right\} + q\mathbf{r} \cdot \frac{\hat{\mathbf{\Pi}}(\mathbf{R})}{\epsilon_0} \tag{1.30}$$

$$+ \frac{\epsilon_0}{2}\int \mathrm{d}^3 r' \sum_{i,j}\left(\frac{qr_j}{\epsilon_0}\right)^2 \delta_{i,j}^{\perp}(\mathbf{R} - \mathbf{r'})$$

The first term is again the free electromagnetic field Hamiltonian, the second one is the interaction Hamiltonian in dipole approximation and length-gauge. The last term is the dipolar self energy that would lead to an infinite contribution and needs to be renormalized. We will neglect it in the forthcoming because the renormalization leads to constant energy shift which we assume to be absorbed into $H_{a'}^{(rel)}$ [25, 26].

Hamiltonian for a Λ-like 3-level atom

Starting from the general results given in the last section we now want to derive a Hamiltonian for a simplified atom model with three relevant states in a Λ-type configuration as shown in fig. 1.1. In a first step we assume that we can in principle find the spectral decomposition of the Hamiltonian describing the relative motion of core and electron. This means we can write

$$H_{a'}^{(rel)} = \sum_{\nu} E_{\nu}|\nu\rangle\langle\nu|, \tag{1.31}$$

where the ν is an abbreviation for all relevant quantum numbers which are necessary to specify the atomic states. Using eq. (1.25) and therefore eq. (1.30) we have restricted our considerations to electric dipole transitions. This is sufficient for most of the applications in quantum optics because it is the dominant type of transition occuring in nature. For higher order multipole contributions see [17, 18]. The dipole interaction term in eq. (1.30) may be identified with the polarization of the medium. The idea of polarization considers a charge distribution, here the electron of the atom, with respect to a reference distribution,
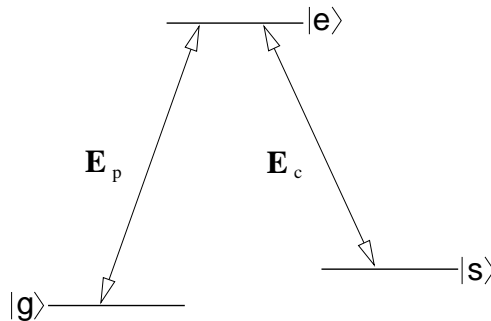
Figure 1.1: A Λ-type 3-level atomic system with the (meta)-stable levels $|g\rangle$ and $|s\rangle$ as well as the excited unstable state $|e\rangle$. The two fields leading to dipole allowed transition are called probe $\mathbf{E}_p$ and control-field $\mathbf{E}_c$. Shown here is a resonant configuration between electromagnetic fields and Bohr frequencies.

the core. In this thesis the main focus is on atomic ensembles. In the case of an ensemble of N-atoms the polarization of the medium is

$$\hat{\boldsymbol{P}}(\mathbf{r}) = \sum_{j=1}^{N} \hat{\mathbf{d}}_j \, \delta(\mathbf{r} - \mathbf{R}_j) = \sum_{j=1}^{N} \sum_{\mu_j, \nu_j} \left(\mathbf{d}_{\mu_j \nu_j} \hat{\sigma}_{\mu_j, \nu_j} + \text{h.a.} \right) \delta(\mathbf{r} - \mathbf{R}_j), \qquad (1.32)$$

where $\mathbf{d}_{\mu_j \nu_j} = \langle \mu | \mathbf{d}_j | \nu \rangle = e \langle \mu | \mathbf{r}_j | \nu \rangle$ is the dipole moment of the j-th atom mediating the transition $|\mu\rangle \leftrightarrow |\nu\rangle$ and $\hat{\sigma}_{\mu_j, \nu_j} = |\mu_j\rangle \langle \nu_j|$ are the corresponding single atom spin-flip operators. The atom is assumed to be localized at $\mathbf{R}_j$. The expression after the second equal sign corresponds to a representation of the polarization operator in the basis of eigenstates of the Hamiltonian eq. (1.31). As can be seen from parity considerations only two dipole allowed transition can exist in a Λ-like 3-level atom as shown in fig. 1.1. The polarization of the system is, in the interaction picture with respect to the 3-level Hamiltonian of eq. (1.31) and after a rotating wave approximation, given by

$$\hat{\boldsymbol{P}}_\Lambda(\mathbf{r}) = \sum_{j=1}^{N} \left(\mathbf{d}_{eg} \hat{\sigma}_{eg} e^{\mathrm{i}\omega_{eg} t} + \mathbf{d}_{es} \hat{\sigma}_{es} e^{\mathrm{i}\omega_{es} t} + \text{h.a.} \right) \delta(\mathbf{r} - \mathbf{R}_j). \qquad (1.33)$$

The Bohr frequencies used in eq. (1.33) are defined by $\omega_{\mu\nu} = \omega_\mu - \omega_\nu$, where $\omega_\mu = E_\mu/\hbar$. We assume that the dipoles are randomly distributed over the interaction region according to the probability density

$$p(\mathbf{R}_1, \ldots, \mathbf{R}_N) = p(\mathbf{R}_1) \cdot \cdots \cdot p(\mathbf{R}_N), \quad \text{with} \quad \int \mathrm{d}^{3N} R \, p(\mathbf{R}_1, \ldots, \mathbf{R}_N) = 1. \quad (1.34)$$

By writing eq. (1.34) we assumed that the probability $p(\mathbf{R}_j)$ to find a dipole at $\mathbf{R}_j$ is independent of the probability $p(\mathbf{R}_i)$ to find an other dipole at $\mathbf{R}_i$ (with $i \neq j$). This assumption is valid as long as the interaction between the dipoles is negligible and the densityare of the sample is small enough such that local-field corrections are unimportant.

The averaged polarization of a medium consisting of Λ-like 3-level atoms is then given by

$$
\begin{aligned}
\mathbf{P}_\Lambda(\mathbf{r}) &= \int \mathrm{d}^3 R_1 \ldots \int \mathrm{d}^3 R_N \, p(\mathbf{R}_1, \ldots, \mathbf{R}_N) \, \hat{\boldsymbol{P}}_\Lambda(\mathbf{r}) \\
&= p(\mathbf{r}) N \left(\mathbf{d}_{eg} \hat{\sigma}_{eg} e^{\mathrm{i}\omega_{eg}t} + \mathbf{d}_{es} \hat{\sigma}_{es} e^{\mathrm{i}\omega_{es}t} + \mathrm{h.a.} \right).
\end{aligned}
\tag{1.35}
$$

We now assume that $p(\mathbf{r})$ is a uniform distribution. Thus the probability density to find a dipole at $\mathbf{r}$ is $1/V$. Using eq. (1.35) and eq. (1.30) we can easily determine the Hamiltonian for the interaction of Λ-like 3-level atoms with two electromagnetic fields. In the interaction picture and after a rotating wave approximation we have

$$
\begin{aligned}
H_{int} &= \int \mathrm{d}^3 r \, \hat{\mathbf{P}}_\Lambda(\mathbf{r}) \cdot \frac{\hat{\mathbf{\Pi}}(\mathbf{r})}{\epsilon_0} = -\int \mathrm{d}^3 r \, \hat{\mathbf{P}}_\Lambda(\mathbf{r}) \cdot \frac{\hat{\mathbf{D}}(\mathbf{r})}{\epsilon_0} \\
&= -\frac{N}{V} \int \mathrm{d}^3 r \left[\wp \, \hat{\sigma}_{eg} \hat{\mathsf{E}}_p^{(+)}(\mathbf{r}) e^{-\mathrm{i}(\omega - \omega_{eg})t} + \wp' \, \hat{\sigma}_{es} \hat{\mathsf{E}}_c^{(+)}(\mathbf{r}) e^{-\mathrm{i}(\omega_c - \omega_{es})t} + \mathrm{h.a.} \right],
\end{aligned}
\tag{1.36}
$$

where $\wp = \mathbf{d}_{eg} \cdot \boldsymbol{\epsilon}_p$ and $\wp' = \mathbf{d}_{es} \cdot \boldsymbol{\epsilon}_c$. Here $\boldsymbol{\epsilon}_p$ and $\boldsymbol{\epsilon}_c$ are the unit vectors for the polarization of the probe and control field respectively. The (near) resonant optical transitions $|g\rangle \leftrightarrow |e\rangle$ and $|s\rangle \leftrightarrow |e\rangle$ are mediated by the probe and control field with main carrier frequencies ω and ω_c respectively. The quantities $\hat{\mathsf{E}}_p^{(+)}$ and $\hat{\mathsf{E}}_c^{(+)}$ denote the envelope functions of the positive frequency parts of the corresponding fields. We will only consider strong classical control-fields within the framework of this thesis, i. e. $\hat{\mathbf{E}}_c \to \langle \hat{\mathbf{E}}_c \rangle$, and therefore introduce for notational simplicity the Rabi frequency of the control-field via $\Omega_c = \wp' \langle \hat{\mathsf{E}}_c^{(+)} \rangle / \hbar$.

Equations of motion for electromagnetic fields

Before we discuss the special features of the interaction of electromagnetic fields with Λ-type atoms of fig. 1.1, we will briefly summarize the equations of motion for electromagnetic fields in media with polarization $\hat{\mathbf{P}}$. By determining the Heisenberg equations for the dynamical field variables $\{\hat{\mathbf{A}}, \hat{\mathbf{\Pi}}\}$ we find

$$
\partial_t \hat{\mathbf{\Pi}}(\mathbf{r}, t) = -\frac{1}{\mu_0} \nabla \times (\nabla \times \hat{\mathbf{A}}(\mathbf{r}, t)),
\tag{1.37}
$$

$$
\partial_t \hat{\mathbf{A}}(\mathbf{r}, t) = \frac{1}{\epsilon_0} \hat{\mathbf{\Pi}}(\mathbf{r}, t) + \frac{1}{\epsilon_0} \hat{\mathbf{P}}(\mathbf{r}, t),
\tag{1.38}
$$

where μ_0 denotes the free space permeability. From these equations we can derive the two coupled Maxwell equations (without current density because we disregard free charges). To this end we use $\hat{\mathbf{B}}(\mathbf{r}, t) = \nabla \times \hat{\mathbf{A}}(\mathbf{r}, t)$ and the relation between the conjugate momentum and the displacement operator in a dielectric medium consisting of neutral atoms given by [18]

$$
\hat{\mathbf{\Pi}}(\mathbf{r}, t) = -\hat{\mathbf{D}}(\mathbf{r}, t) = -\left[\epsilon_0 \hat{\mathbf{E}}(\mathbf{r}, t) + \hat{\mathbf{P}}(\mathbf{r}, t) \right].
\tag{1.39}
$$

The two coupled Maxwell equations then read

$$\partial_t \hat{\mathbf{E}}(\mathbf{r}, t) = c^2 \, \nabla \times \hat{\mathbf{B}}(\mathbf{r}, t) - \frac{1}{\epsilon_0} \partial_t \hat{\mathbf{P}}_\perp(\mathbf{r}, t) \Leftrightarrow \partial_t \hat{\mathbf{D}}(\mathbf{r}, t) = \frac{1}{\mu_0} \nabla \times \hat{\mathbf{B}}(\mathbf{r}, t), \tag{1.40}$$

$$\partial_t \hat{\mathbf{B}}(\mathbf{r}, t) = -\nabla \times \hat{\mathbf{E}}_\perp(\mathbf{r}, t). \tag{1.41}$$

From this set of equations we obtain the wave-equation in dielectric media

$$\left[\partial_t^2 - c^2 \Delta \right] \hat{\mathbf{E}}(\mathbf{r}, t) = -\frac{1}{\epsilon_0} \partial_t^2 \hat{\mathbf{P}}_\perp(\mathbf{r}, t). \tag{1.42}$$

In chapter 2 we will need a decomposition of the electromagnetic field in forward $(+)$ and backward propagating $(-)$ components. To this end we make the following ansatz for the positive frequency part of the electric field $\hat{\mathbf{E}}^{(+)}$ and the polarization $\hat{\mathbf{P}}^{(+)}$ or that of an arbitrary vector field $\hat{\mathbf{F}}^{(+)}$

$$\hat{\mathbf{F}}^{(+)} = \hat{\mathbf{F}}_+^{(+)} + \hat{\mathbf{F}}_-^{(+)} \tag{1.43}$$

with $\hat{\mathbf{F}}_\pm^{(+)}(\mathbf{r}, t) = \hat{\mathbf{F}}_\pm(\mathbf{r}, t) \exp\left[-\mathrm{i}(\omega t \mp kz)\right]$. Using this ansatz we finally find the paraxial wave equation

$$\left[\partial_t \pm c\partial_z + \frac{c}{2\mathrm{i}k} \Delta_\perp \right] \hat{\mathbf{E}}_\pm(\mathbf{r}, t) = -\frac{\omega}{2\mathrm{i}\epsilon_0} \hat{\mathbf{P}}_\pm(\mathbf{r}, t). \tag{1.44}$$

To derive eq. (1.44) we have applied the slowly-varying envelope approximation (SVEA) [21], i. e. we have assumed that the characteristic length scale L on which the field envelope $\hat{\mathbf{F}}$ changes is much larger than the optical wavelength $\lambda = 2\pi/k$. Analog arguments were applied to the time domain.

1.2 Electromagnetically induced transparency (EIT) and slow-light

The concepts of electromagnetically induced transparency and slow-light can most easily be understood in terms of of dark-state polaritons which we are using throughout this thesis. Hence it is worth studying them briefly.

Using Electromagnetically Induced Transparency (EIT) a medium that is otherwise optically thick, i. e. opaque, for a probe-field is rendered transparent by the appropriate application of an additional control-field. It is based on the coherent preparation [27] of 3-level type atoms as shown for example in fig. 1.2. It was first experimentally been observed by Boller et al. [28] in Strontium. For the atoms to show EIT it is not necessary to be in a Λ-like configuration, we will restrict, however, ourselves to this configuration.

The coherent preparation not only leads to the modification of the absorptive properties but also to very useful changes of the dispersive properties. The modified properties of EIT-media can be used to generate pulses with a very small group velocity [29, 14], to effectively control nonlinearities [30, 7] and for high precision magnetometry [31].
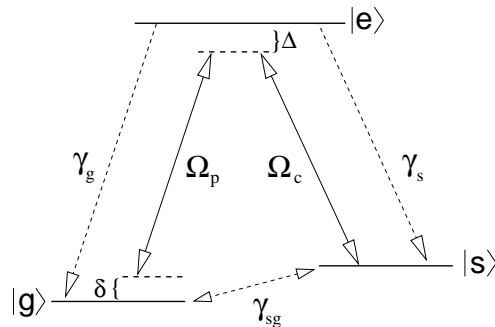
Figure 1.2: Λ-type 3-level atomic system with the (meta)-stable levels $|g\rangle$ and $|s\rangle$ as well as the excited state $|e\rangle$. The control-field is denoted by Ω_c and the signal field by $\Omega_p = \wp\langle\hat{\mathsf{E}}_p\rangle/\hbar$. Δ and δ are one- and two-photon detuning respectively (see main text). γ_g and γ_s are the population decay rates of the excited state into the two lower levels and γ_{gs} denotes the decay rate of the Raman coherence.

In general the interaction of light with atoms depends on the frequency of the incident light field [21, 17]. If the frequency of the light field equals the Bohr frequency of a particular transition, a resonance condition occurs and is accompanied by a dispersive/dissipative back-action of the medium on the radiation field. In the linear response limit, which we are generally interested in, the back-action is described by the linear polarization of the medium

$$\mathsf{P}(z,\omega) = \epsilon_0\left[\epsilon_r(\omega) - 1\right]\mathsf{E}(z,\omega) = \epsilon_0\left[\chi'(\omega) + i\chi''(\omega)\right]\mathsf{E}(z,\omega). \tag{1.45}$$

Here ϵ_r is the relative electric permittivity and χ' and χ'' are the real and imaginary part of the complex susceptibility χ. The later determines the corresponding back-action [32]. In general we can safely ignore the magnetic properties of the atomic system. In most cases the magnetic reponse is many orders of magnitude smaller than the electric one. Hence, we set the magnetic permeability equal to unity. The next section will discuss EIT by the examination of an idealized, homogeneously broadend 3-level Λ-system in detail.

1.2.1   The model system of EIT

Various ways exist to describe the phenomenon of EIT. In this section we analyze the linear susceptibility derived from a density matrix ansatz based on the work of Imamoğlu and Harris [33]. To do so we examine a system consisting of Λ-type 3-level atoms as indicated in fig. 1.2. For simplicity we assume that the only relevant mode in the electric field expansion of eq. (1.7) is given by the resonance frequency ω, hence we can define a common coupling constant

$$g = \frac{\wp}{\hbar}\sqrt{\frac{\hbar\omega}{2\epsilon_0 V}}. \tag{1.46}$$

With the help of this the interaction Hamiltonian eq. (1.36) is given, in a frame co-rotating with the optical frequencies by

$$H_{\text{int}} = -\frac{N}{V} \int \mathrm{d}^3 r \hbar \left\{ \Delta \, \hat{\sigma}_{ss} + (\delta + \Delta) \, \hat{\sigma}_{gg} + \left[\Omega_c(\mathbf{r}, \mathbf{t}) \, \hat{\sigma}_{es} + g \hat{\mathcal{E}}_p(\mathbf{r}, t) \, \hat{\sigma}_{eg} + \text{h.a.} \right] \right\}.$$
(1.47)

In the above Hamiltonian we have used a calligraphic symbol for the electric field operator. We changed the notation since the corresponding electric field is now a dimensionless variable. The transformation to this new, scaled variables is straight forward. Finally $\Delta = \omega_{es} - \omega_c$ as well as $\delta = \omega_{sg} - (\omega - \omega_c)$ respresent the one-photon detuning of the control-field as well as the two-photon detuning of probe- and control-field from the Raman transition $|g\rangle \leftrightarrow |s\rangle$.

Under the assumption that the thermal occupancy of the relevant radiation field modes is completely negligible, which is justified for optical frequencies [17], one finds the following equations of motion for the off-diagonal spin operators $\hat{\sigma}_{ge}$ and $\hat{\sigma}_{gs}$

$$\dot{\hat{\sigma}}_{ge} = -\left(\gamma_{ge} + i\left(\delta + \Delta\right)\right) \hat{\sigma}_{ge} - i\,g\hat{\mathcal{E}}_p(\mathbf{r}, t)(\hat{\sigma}_{ee} - \hat{\sigma}_{gg}) + i\,\Omega_c(\mathbf{r}, t)\hat{\sigma}_{gs} + \hat{F}_{ge},$$
(1.48)

$$\dot{\hat{\sigma}}_{gs} = -\left(\gamma_{gs} + i\,\delta\right) \hat{\sigma}_{gs} - i\,g\hat{\mathcal{E}}_p(\mathbf{r}, t)\hat{\sigma}_{es} + i\,\Omega_c^*(\mathbf{r}, t)\hat{\sigma}_{ge} + \hat{F}_{gs}.$$
(1.49)

These can be derived from the Hamiltonian (1.47) by calculating the Heisenberg-Langevin equations. The $\hat{F}_{\mu\nu}$ are the Langevin noise forces corresponding to the decay rates $\gamma_{\mu\nu}$ [34].

The transverse decay rate $\gamma_{ge} = (\gamma_g + \gamma_s)/2 + \gamma_{\text{phase}}$ is determined by the radiative decay rates γ_g and γ_s on the transition $|e\rangle \to |g\rangle$ respectively $|e\rangle \to |s\rangle$ and a dephasing term primarily due to collisions [35]. Since the transition $|g\rangle \leftrightarrow |s\rangle$ is not dipole allowed the major contribution here is given by non-radiative dephasing mechanisms, like collisions or fluctuations of external fields.

By treating the ratio of the collective Rabi frequency $g\langle\hat{\mathcal{E}}\rangle$ of the probe field over the Rabi frequency of the control field Ω_c as a perturbation parameter we find, assuming that initially all population is in state $|g\rangle$, i. e. $\hat{\sigma}_{gg}^{(0)} = 1$, in first order

$$\dot{\hat{\sigma}}_{ge}^{(1)} = -\left(\gamma_{ge} + i\left(\delta + \Delta\right)\right) \hat{\sigma}_{ge}^{(1)} + i\,g\hat{\mathcal{E}}_p(\mathbf{r}, t) + i\,\Omega_c(\mathbf{r}, t)\hat{\sigma}_{gs}^{(1)},$$
(1.50)

$$\dot{\hat{\sigma}}_{gs}^{(1)} = -\left(\gamma_{gs} + i\,\delta\right) \hat{\sigma}_{gs}^{(1)} + i\,\Omega_c^*(\mathbf{r}, t)\hat{\sigma}_{ge}^{(1)}.$$
(1.51)

Within the present approach we keep all orders of the strong field Ω_c, which coherently couples the states $|e\rangle$ and $|s\rangle$, but treat the probe-field only in first order of the above perturbation expansion. This is sufficient to derive the linear susceptibility [35]. If we additionally assume that the polarization of the ensemble of atoms is given by the average polarization of each atom times the number of atoms N devided by the quantization/interaction volume, i. e. $\hat{\mathcal{P}}^{(+)} = \wp N \hat{\sigma}_{ge}/V$, then the susceptibility reads [36]

$$\chi = i\,\frac{2\,N\,g^2}{\omega} \left[\frac{\gamma_{gs} + i\,\delta}{(\gamma_{ge} + i\,(\delta + \Delta))(\gamma_{gs} + i\,\delta) + |\Omega_c|^2} \right].$$
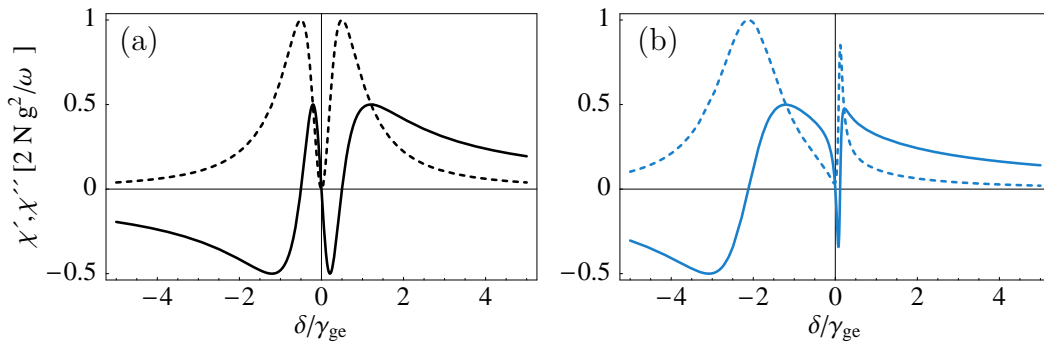(1.52)

Figure 1.3: Real (solid line) and imaginary (dashed line) parts of the linear susceptibility (in units of $\frac{2Ng^2}{\omega}$) as a function of the normalized detuning δ/γ_{ge} width $\Omega_c = 0.5\gamma_{ge}$ and (a) $\gamma_{gs} = 0$ and $\Delta = 0$ as well as (b) $\gamma_{gs} = 10^{-2}\gamma_{ge}$ and $\Delta = 2\gamma_{ge}$.

To obtain eq. (1.52) we have solved the eqs. (1.50-1.51) in steady state, i. e. we set all time derivatives to zero. This assumes that the evolution of the atomic system is much faster than the temporal change of the radiation field. Using the above equation one easily finds the real (χ') and imaginary part (χ'') of the complex susceptibility $\chi = \chi' + i\chi''$

$$\chi'(\delta, \Delta) = \frac{2Ng^2}{\omega} \frac{\gamma_{gs}((\Delta+\delta)\gamma_{gs} + \delta\gamma_{ge}) - \delta(\gamma_{ge}\gamma_{gs} - \delta(\Delta+\delta) + |\Omega_c|^2)}{(\gamma_{ge}\gamma_{gs} - \delta(\Delta+\delta) + |\Omega_c|^2)^2 + ((\Delta+\delta)\gamma_{gs} + \delta\gamma_{ge})^2}, \quad (1.53)$$

$$\chi''(\delta, \Delta) = \frac{2Ng^2}{\omega} \frac{\gamma_{ge}(\gamma_{gs}^2 + \delta^2) + \gamma_{gs}|\Omega_c|^2}{(\gamma_{ge}\gamma_{gs} - \delta(\Delta+\delta) + |\Omega_c|^2)^2 + ((\Delta+\delta)\gamma_{gs} + \delta\gamma_{ge})^2}. \quad (1.54)$$

The linear susceptibility, as shown in fig. 1.3, displays a number of the prominent features of EIT. First of all one immediately recognizes that at two-photon resonance, $\delta = 0$, both real and imaginary part of the susceptibility vanish in the limit of vanishing decay rate of the Raman coherence $\gamma_{gs} = 0$. This is called the ideal limit since it is not realized in nature.

However, even in the case $\gamma_{gs} \neq 0$, one obtains, for $\sqrt{\gamma_{gs}\gamma_{ge}} \ll |\Omega_c| \ll \gamma_{ge}$, a very sharp dip in the imaginary part of the susceptibility which corresponds to a dip in the absorption spectrum. Its width $\Delta\omega_{tr}$ is proportional to the intensity of the applied control-laser field, $\Delta\omega_{tr} \sim |\Omega_c|^2/\gamma_{ge}$ [37]. This sharp dip-like feature calls for a quantum interference explanation rather than simple line splitting argumentation as is for example the case for Autler-Townes splitting [2, 38]. The transparency obtained at two-photon resonance is independent from the one-photon detuning of the control-field as we can see from fig. 1.3 (b). With increasing one-photon detuning, the absorption spectrum slowly turns into that of a two-level system with an additional narrow Raman peak close to two-photon resonance. The *effective two-level system* can be identified in fig. 1.3 (b) by its broad Lorentzian lineshape in the imaginary part of the susceptibility and steep slope of the real part. The spectrum of the real and imaginary part of the susceptibility are very asymmetric in this case.

In general, due to external disturbances like atomic collisions, the Raman decay rate
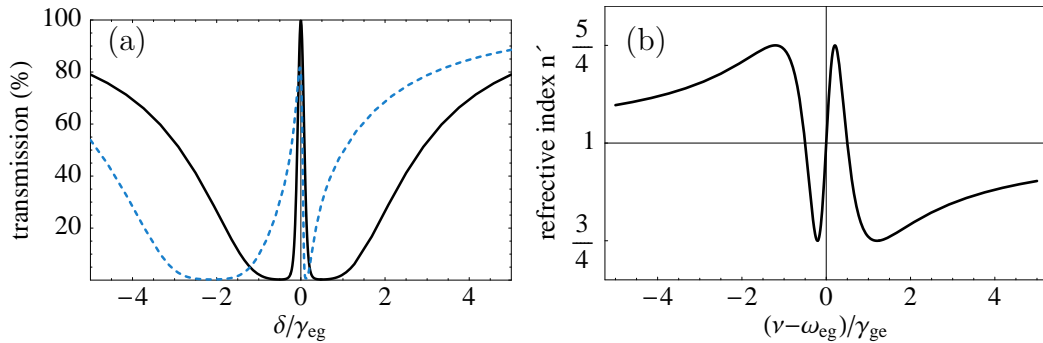
Figure 1.4: (a) Transmission spectra for an optical depth of the medium of $OD = L/L_{\rm abs} = 6$ and for the two cases of figure 1.3 (solid line case (a) and dashed line case (b)). (b) Refractive index as a function of the probe-field frequency for the parameters of fig. 1.3 (a) (here $\omega_{eg} = 0$ without loss of generality is assumed).

does not vanish. However, even in this case most of the important properties of EIT remain observable as long as the Rabi frequency of the coupling field satisfies [27]

$$|\Omega_c|^2 \gg \gamma_{ge}\gamma_{gs}. \tag{1.55}$$

Due to the resonance in the absorption spectrum the medium becomes transparent as we can see by inspecting the properties of the intensity transmission coefficient T of the probe-field. This coefficient is defined by $T(L,\delta) = I(L,\delta)/I_0$, where I_0 is the initial intensity of the probe-beam before entering the cell containing the atomic ensemble and $I(L,\delta)$ is the intensity after passing through the cell of length L. Using the time-independent shortend wave equation for the probe-field, i. e. $\partial_z \hat{\mathcal{E}}_p = ik\chi\hat{\mathcal{E}}_p$ and applying the definition of the absorption length $L_{\rm abs} = c\gamma_{ge}/g^2N$ in absence of EIT, we find

$$T(\delta) = \exp\left\{-\chi''(\delta)kL\right\} = \exp\left\{-\tilde{\chi}''(\delta)\frac{L}{L_{\rm abs}}\right\}. \tag{1.56}$$

After the second equal sign of eq. (1.56) we have introduced the normalized susceptibility $\tilde{\chi}$. It is defined by $\tilde{\chi} = \gamma_{ge}\omega(g^2N)^{-1}\chi$. We use this definition because it most easily allows to see that the exponent of eq. (1.56) is completely defined by the decay rates and detunings as well the ratio $L/L_{\rm abs}$. The latter is called optical depth. For the optically dense media under consideration it is (much) bigger than unity [39, 36]. Eq. (1.56) was used to create fig. 1.4 (a).

So let us discuss now fig. 1.4. In the case of non vanishing relaxation of the Raman coherence the real part χ' of the complex susceptibility is still equal to zero but the imaginary part χ'' in eq. (1.54) is proportional to γ_{gs} at two-photon resonance. Hence complete transparency, $T = 1$, is only obtained in the ideal case of a vanishing relaxation rate of the corresponding coherence. In this case quantum interference completely suppresses absorption at Raman resonance [40]. For a small detuning δ the interference is no longer perfect and the medium becomes absorbing. Thus, following the earlier argumentation

about the sharpness of the absorption resonance, the transparency peak that appears in the transmission spectrum is typically very narrow (see figure 1.4 (a)). The interference turns more robust and the spectral width $\Delta\omega_{tr}$ of the transparency window increases even more the larger the Rabi frequency of the coupling field turns, i. e. the better condition (1.55) is fullfilled. This property allows to increase the tolerance of EIT to two-photon frequency mismatch. We note that the asymmetry of the susceptibility in fig. 1.3 (b) also appears in the transmission spectrum.

Finally, we want to consider the dispersive properties of the dressed medium in order to determine the group and phase velocity of the probe-field. To this end we calculate the real part of the index of refraction using its definition $n = n' + i\,n''$ and its relation to the permittivity [41, 42]

$$n^2 = \epsilon_r(z,\omega)\mu_r(z,\omega) \simeq \epsilon_r(z,\omega). \tag{1.57}$$

We find the following set of equations

$$\chi' = (n')^2 - (n'')^2 - 1, \tag{1.58}$$
$$\chi'' = 2n'n'', \tag{1.59}$$

that can be solved to give [21]

$$n' = \left\{ \frac{[(1+\chi')^2 + \chi''^2]^{1/2} + (1+\chi')}{2} \right\}^{1/2}, \tag{1.60}$$

$$n'' = \left\{ \frac{[(1+\chi')^2 + \chi''^2]^{1/2} - (1+\chi')}{2} \right\}^{1/2} \mathrm{sgn}(\chi''). \tag{1.61}$$

In the ideal case of vanishing Raman dephasing the probe-field experiences at two-photon resonance no absorption and a vanishing real susceptibility. Therefore the refractive index n', shown in fig. 1.4 (b), is equal to unity. This implies that the phase velocity of the probe-field in the medium is equal to that in vacuum. On the other hand, due to absorptive interference and the symmetry of the states, the refractive index n' has a large normal dispersion, i. e. $\omega\,\mathrm{d}n/\mathrm{d}\omega \gg 1$, in the vicinity of the two-photon resonance. This leads via

$$v_{gr} = \frac{c}{n + \omega\frac{\mathrm{d}n}{\mathrm{d}\omega}} \tag{1.62}$$

to a very small group velocity v_{gr}. In addition there is no group velocity dispersion, i. e. $\mathrm{d}^2n/\mathrm{d}\omega^2 = 0$, which is essential for the formstable propagation of pulses in the medium. A non-vanishing group velocity dispersion would lead to pulse distortion [29]. From the statements of this section we see that EIT-media are suitable for the distortion-free slow-down of electromagnetic fields. This is one essential component necessary for the construction of a quantum memory.

1.2.2 Slow-light and its limitations

In this section we will show that even though the large frequency dispersion of EIT-media $|\omega \, dn/d\omega| \gg 1$, can be used to slow down a field pulse to incredibly low group velocities, of the order of $10 - 10^2$ m/s [43, 44, 14, 45, 46], this is not enough to construct an efficient quantum memory [3]. To store photons or to manipulate them coherently would require a non destructive storage and retrieval of the quantum state of a photon. In order to show this deficiency we consider the propagation dynamics of a weak probe field in an atomic ensemble of Λ-like atoms in more detail.

Weak probe-field limit and the adiabatic approximation

To discuss later on the limitations of slow-light we derive first the equation of motion for a weak probe field in an EIT-medium. Furthermore we assume that the characteristic time T in which the probe field respectively the control field changes is much longer than the decay time of the optical coherence γ_{ge}^{-1}, i. e. we have $T\gamma_{ge} \gg 1$. To derive the equation of motion of the probe field we solve the equations (1.50) and (1.51) for the optical and spin coherence respectively

$$\hat{\sigma}_{gs}^{(1)} = -\frac{g}{\Omega_c}\hat{\mathcal{E}}_p - \frac{\mathrm{i}}{\Omega_c}\left[\left(\frac{\partial}{\partial t} + \gamma_{ge}\right)\hat{\sigma}_{ge}^{(1)} - \frac{\mathrm{i}}{\Omega_c}\hat{F}_{ge}\right], \tag{1.63}$$

$$\hat{\sigma}_{ge}^{(1)} = -\frac{\mathrm{i}}{\Omega_c^*}\left(\frac{\partial}{\partial t} + \gamma_{gs}\right)\hat{\sigma}_{gs}^{(1)} + \frac{\mathrm{i}}{\Omega_c^*}\hat{F}_{gs}. \tag{1.64}$$

Substituting eq. (1.64) in eq. (1.63) and using furthermore that the interaction of a probe-field pulse can be described using the shortened wave equation (1.44) with the polarization of the medium given by $\hat{\mathcal{P}} = g \, N \, \hat{\sigma}_{ge}^{(1)}$, we find the following set of equations

$$\left(\frac{\partial}{\partial t} + c\frac{\partial}{\partial z}\right)\hat{\mathcal{E}}_p(z,t) = \frac{gN}{\Omega^*}\left(\frac{\partial}{\partial t} + \gamma_{gs}^{(1)}\right)\hat{\sigma}_{gs}(z,t) - \frac{gN}{\Omega_c^*}\hat{F}_{gs}, \tag{1.65}$$

$$\hat{\sigma}_{gs}^{(1)}(z,t) = -\frac{g}{\Omega_c(z,t)}\hat{\mathcal{E}}_p(z,t) - \frac{\mathrm{i}}{\Omega_c(z,t)}\left[\left(\frac{\partial}{\partial t} + \gamma_{ge}\right)\left\{-\frac{\mathrm{i}}{\Omega_c^*(z,t)}\left(\frac{\partial}{\partial t} + \gamma_{gs}\right)\hat{\sigma}_{gs}^{(1)}\right\}\right.$$
$$\left. + \left(\frac{\partial}{\partial t} + \gamma_{ge}\right)\left(\frac{\mathrm{i}}{\Omega_c^*(z,t)}\hat{F}_{gs}(t)\right) - \frac{\mathrm{i}}{\Omega_c(z,t)}\hat{F}_{ge}(t)\right]. \tag{1.66}$$

This set can be simplified considerably if we work in the adiabatic limit [47, 8, 9, 6]. By introducing a normalized time τ via $\tau = t/T$, where T is the characteristic time scale on which the probe- as well the control-field changes we can expand the right hand side of eq. (1.66) in powers of $1/T$. This yields

$$\hat{\sigma}_{gs}^{(1)} = -\frac{g}{\Omega_c}\hat{\mathcal{E}}_p - \frac{\mathrm{i}}{\Omega_c}\left[\left(\frac{1}{T}\frac{\partial}{\partial \tau} + \gamma_{ge}\right)\left\{-\frac{\mathrm{i}}{\Omega_c^*}\left(\frac{1}{T}\frac{\partial}{\partial \tau} + \gamma_{gs}\right)\hat{\sigma}_{gs}^{(1)}\right\}\right.$$
$$\left. + \left(\frac{1}{T}\frac{\partial}{\partial \tau} + \gamma_{ge}\right)\left(\frac{\mathrm{i}}{\Omega_c^*}\frac{1}{\sqrt{T}}\hat{F}_{gs}\right) - \frac{\mathrm{i}}{\Omega_c}\frac{1}{\sqrt{T}}\hat{F}_{ge}\right], \tag{1.67}$$

where we have used that $\langle \hat{F}_{\mu\nu}(t)\hat{F}_{\alpha\beta}(t')\rangle \propto \delta(\tau - \tau')/|T|$ holds in the Markov-limit. In the lowest non-vanishing order of the perturbation expansion with respect to the small parameter $1/T$, we obtain from eq. (1.67)

$$\hat{\sigma}_{gs}(z,t) = -\frac{g}{\Omega_c(z,t)}\hat{\mathcal{E}}_p(z,t). \tag{1.68}$$

To derive eq. (1.68) we have once more applied the EIT-condition (1.55). Substituting eq. (1.68) into the field equation (1.65) yields the propagation equation of the quantized probe-field

$$\left(\frac{\partial}{\partial t} + c\frac{\partial}{\partial z}\right)\hat{\mathcal{E}}_p(z,t) = -\frac{g^2 N}{\Omega_c^*(z,t)}\left(\frac{\partial}{\partial t} + \gamma_{gs}\right)\frac{\hat{\mathcal{E}}_p(z,t)}{\Omega_c(z,t)} + \hat{F}_{\mathcal{E}}. \tag{1.69}$$

The term proportional to γ_{gs} describes absorption of the probe field due to decay of the ground state coherence. If we restrict ourselves to a timescale much shorter than γ_{gs}^{-1}, which we will do in the forthcoming, this term can be neglected. The operator $\hat{F}_{\mathcal{E}}$ is an abbreviation for the Langevin force term corresponding to the decay of the probe field operator. Its explicit representation is not of interest here. The shortened wave equation (left hand side) together with the time derivate of the right hand side lead to slow-light and light storage as we will show in the next sections.

Slow-light and its limits

The adiabatic approximation of the last section assumes that the dynamics in terms of frequencies takes place within the narrow transparency window as shown in fig. 1.4 (a). If the pulse is too short, or its spectrum too broad relative to the transparency width, absorption and higher-order dispersion can not be neglected. To be more precise we discuss once more the intensity transmission function of the medium. By assuming a spatially homogeneous control-field, one finds that close to two-photon resonance, the transmission function is given by

$$T(\delta,z) = \exp\left\{-k\,L\,\text{Im}[\chi(\delta)]\right\} \approx \exp\left\{-\delta^2/\Delta\omega_{\text{tr}}^2\right\}, \tag{1.70}$$

where we have assumed that the probe-pulse traversed a medium of length L. The transparency width

$$\Delta\omega_{\text{tr}} = \left[\frac{c}{\gamma_{ge}L}\frac{|\Omega_c|^2}{n_{gr}}\right]^{1/2} = \frac{1}{\sqrt{OD}}\frac{|\Omega_c|^2}{\gamma_{ge}} \tag{1.71}$$

decreases with increasing group index which is given by [3]

$$n_{\text{gr}} = \frac{g^2 N}{|\Omega_c|^2} \tag{1.72}$$

and which is related to the group velocity of the probe field pulse by

$$v_{\text{gr}} = \frac{c}{1 + n_{\text{gr}}}. \tag{1.73}$$

The optical depth (opacity) of the medium is denoted by $OD = L/L_{\text{abs}}$, where $L_{\text{abs}} = c\gamma_{ge}/g^2 N$ is the absorption length in absence of EIT. One notices from eq. (1.71) that a reduction of the group velocity of the probe pulse leads to a decreasing transparency width. We express the transparency width in terms of the probe-pulse delay time $\tau_d = (1/v_{\text{gr}} - 1/c)L = n_{gr}L/c$ to find a more intuitive expression [29, 48, 49]. The equation

$$\Delta\omega_{\text{tr}} = \sqrt{OD}\,\frac{1}{\tau_d}. \tag{1.74}$$

states that an increasing delay time τ_d implies a narrowing of the transparency window. A narrow transparency window requires on the other hand long probe pulses. When the group velocity is too small or in orther words the pulse delay time too long, the transparency window becomes smaller than the spectral width of the pulse. In this case is the adiabatic condition violated, and the medium absorbs the pulse. However, this line of argumentation holds only if the spectral width of the pulse stays constant while propagating through the medium. This is the case if we consider a time independent control-field. Unlike this does the time-dependent control-field case, discussed in section 1.3.3, allow a simultaneous narrowing of the spectral pulse and the transmission transparency window width.

To show that the spectral pulse width stays constant while the pulse is propagating through the medium let us consider the propagation equation (1.69). For $\Omega(z,t) = \Omega(z)$ one easily shows that the equation implies

$$\left[\frac{\partial}{\partial t} + v_{\text{gr}}(z)\frac{\partial}{\partial z}\right]\hat{\mathcal{E}}_p(z,t) = 0, \tag{1.75}$$

where the space dependence of the group velocity origins from the corresponding space dependence of the control-field. By introducing new coordinates according to

$$\tau = t - \int_0^z \mathrm{d}z'\frac{1}{v_{\text{gr}}(z')}, \tag{1.76}$$

$$\xi = z, \tag{1.77}$$

we can further simplify the propagation equation (1.75) and find

$$\frac{\partial}{\partial\xi}\hat{\mathcal{E}}_p(\xi,\tau) = 0. \tag{1.78}$$

The solution of the present Cauchy problem is

$$\hat{\mathcal{E}}_p(z,t) = \hat{\mathcal{E}}_p\left(0, t - \int_0^z \mathrm{d}z'\frac{1}{v_{\text{gr}}(z')}\right). \tag{1.79}$$

Eq. (1.79) describes a pulse propagating with a spatially varying group velocity v_{gr} and an invariant temporal shape. Here $\hat{\mathcal{E}}_p(0,t')$ denotes the field entering the interaction region

at $z = 0$. According to eq. (1.75) the slow down of the quantized probe-field in the adiabatic limit is a lossless and linear process and hence all properties of the quantum pulse are conserved. As explained in [21] the power-spectrum is given in terms of a two-time correlation function of the corresponding radiation field. Under stationary conditions the correlation function $\langle \hat{\mathcal{E}}_p^\dagger(t) \hat{\mathcal{E}}_p(t') \rangle$ only depends on the time difference $\tau = t' - t$. Using the solution (1.79) we see that the corresponding spectrum of the pulse is constant

$$S(z, \omega) = \int\limits_{-\infty}^{\infty} \mathrm{d}\tau \langle \hat{\mathcal{E}}_p^\dagger(t) \hat{\mathcal{E}}_p(t - \tau) \rangle e^{-\mathrm{i}\omega\tau} = S(0, \omega). \tag{1.80}$$

In particular the spectral width of the probe pulse

$$\Delta\omega_p(z) = \Delta\omega_p(0) \tag{1.81}$$

remains unchanged. Hence, in the case the probe field pulse is slowed down by a spatially decreasing control field the spectral width of the pulse stays constant. However, the reduction of the control field intensity also leads to a reduction of the transparency width of the EIT-window as stated before. Sooner or later this leads to absorption of the field pulse which makes slow-light as introduced here not usable for light-storage.

1.3 Storage of light in an optically dense medium

In section 1.2.2 we have already mentioned the existence of a remedy to cure the problems of slow-light with respect to light storage. In the same section we argued that for EIT to be effective in eliminating dissipation, the spectrum of the light pulse should lie within the transparency window during the whole storage procedure. The essential limitation of EIT as a storage mechanism in a *quantum light memory* is the inverse proportionality between the spectral transmission width and the pulse delay time, eq. (1.74). Thus even if the initial width of the pulse spectrum is smaller than the transmission width, the group velocity reduction sooner or later leads to the absorption of the probe-pulse.

This problem can be cured using techniques similar to those used in *stimulated Raman adiabatic passage (STIRAP)* [50]. To this end we assume that the control-field now only depends on time and ignore its space-dependence. To include the latter does not change the principle results but would make the presentation more involved. To solve the propagation and later on the storage problem for a quantized probe-field we follow M. Fleischhauer and M. D. Lukin [1, 3] and introduce a new set of variables. We will see, that they can be identified with a new type of quasi-particles the so called *bright-* and *dark-state polaritons*. Using the corresponding ansatz we will show that if the initial spectral width of the probe pulse was smaller than the spectral width of the transmission window it will be during the whole slow-down and storage process. This makes the present approach suitable for the coherent storage of light.

1.3.1   Definition of dark- and bright-state polaritons

To simplify the forthcoming considerations we assume a spatially homogeneous and real control-field $\Omega = \Omega(t) = \Omega(t)^*$. The equations of motion (1.65, 1.66) for the physically relevant variables $\hat{\mathcal{E}}_p$ and $\hat{\sigma}_{gs}$ can be simplified by applying a unitary transformation

$$\begin{bmatrix} \hat{\Psi}(z,t) \\ \hat{\Phi}(z,t) \end{bmatrix} = \begin{bmatrix} \cos\theta(t) & -\sin\theta(t) \\ \sin\theta(t) & \cos\theta(t) \end{bmatrix} \begin{bmatrix} \hat{\mathcal{E}}_p(z,t) \\ \sqrt{N}\hat{\sigma}_{gs}(z,t) \end{bmatrix}, \tag{1.82}$$

which defines a new pair of quantum fields. The mixing angle $\theta(t)$ used in eq. (1.82) is defined via the group index, i. e.

$$\tan^2\theta(t) = \frac{g^2 N}{\Omega_c^2(t)} = n_{gr}. \tag{1.83}$$

For reasons which will become apparent later on we will call $\hat{\Psi}$ dark-state and $\hat{\Phi}$ bright-state polariton. We transform the equations of motion for the electric field and the collective atomic spin variable using the inverse transformation of eq. (1.82) into field equations for the new variables. After some algebra we finds

$$\left[\frac{\partial}{\partial t} + c\cos^2\theta(t)\frac{\partial}{\partial z} \right] \hat{\Psi}(z,t) = -\frac{\partial\theta}{\partial t}\hat{\Phi}(z,t) - \sin\theta\cos\theta c\frac{\partial\theta}{\partial z}\hat{\Phi}(z,t) \tag{1.84}$$

$$\hat{\Phi}(z,t) = \frac{\sin\theta}{g^2 N}\left(\frac{\partial}{\partial t} + \gamma_{ge} \right)\left(\tan\theta\frac{\partial}{\partial t} \right)\left(\sin\theta\hat{\Psi} - \cos\theta\hat{\Phi} \right) + i\frac{\sin\theta}{g\sqrt{N}}\hat{F}_{ge}, \tag{1.85}$$

For the derivation of the above equations one has to keep in mind that the mixing angle θ is now a function of time.

1.3.2   Dynamics in the adiabatic limit

Introducing the adiabaticity parameter $\epsilon = (g\sqrt{N}T)^{-1}$ with T being the same characteristic time as of section 1.2.2, one expands the equations of motion (1.84) and (1.85) in powers of ϵ. In lowest order, i. e. in the adiabatic limit one finds

$$\hat{\Phi}(z,t) \approx 0, \tag{1.86}$$

and

$$\left[\frac{\partial}{\partial t} + c\cos^2\theta(t)\frac{\partial}{\partial z} \right] \hat{\Psi}(z,t) = 0. \tag{1.87}$$

Using (1.86) we find furthermore in this limit

$$\hat{\mathcal{E}}_p(z,t) = \cos\theta(t)\hat{\Psi}(z,t), \tag{1.88}$$

$$\sqrt{N}\hat{\sigma}_{gs}(z,t) = -\sin\theta(t)\hat{\Psi}(z,t). \tag{1.89}$$

Eq. (1.87) describes a shape and quantum-state preserving propagation with an instantaneous group velocity given by $v_{gr}(t) = c \cos^2 \theta(t)$. Applying the coordinate transformation

$$\xi = z - \int_0^t v_{gr}(\tau) \mathrm{d}\tau, \tag{1.90}$$

$$\tau = t, \tag{1.91}$$

we find in analogy to section 1.2.2 a simple equation which can be integrated to solve the initial value problem

$$\hat{\Psi}(z,t) = \hat{\Psi}\left(z - \int_0^t v_{gr}(\tau)\mathrm{d}\tau, 0\right). \tag{1.92}$$

Eq. (1.92) describes an amplitude and shape-preserving propagation of the dark-state polariton which can be modified by changing the intensity of the control field in time. We will use this results now to show that the polariton approach is suitable to achieve a distortion-free storage of a light pulse in an optically dense EIT-medium. Before we discuss this in more detail, we note that during the process of adiabatic slowing, the spatial profile and, in particular, the length of the wavepacket (Δl) remains unaffected, as long as the group velocity is only a function of time. In other words,

$$\Delta l = \Delta l_0. \tag{1.93}$$

By inspecting equation (1.88) we see, that at the same time the amplitude of the field gets reduced. In addition its temporal profile gets stretched due to the reduction of the probe-pulse group velocity. The opposite happens when the group velocity is increased. From eqs. (1.88, 1.92) one finds

$$\hat{\mathcal{E}}_p(z,t) = \frac{\cos\theta(t)}{\cos\theta(0)}\hat{\mathcal{E}}_p\left(z - \int_0^t v_{gr}(\tau)\mathrm{d}\tau, 0\right). \tag{1.94}$$

Determing with this the power-spectrum of the probe-field, we see that it now changes during the propagation process and especially during the slow-down of the dark-state polariton. Assuming that $\cos\theta$ changes only slow compared to the field amplitudes one finds

$$S(z,\omega) = \frac{\cos^2\theta(t)}{\cos^2\theta(0)} S\left(0, \frac{\omega}{\cos^2\theta(t)}\right). \tag{1.95}$$

In particular, the spectral width narrows (broadens) according to

$$\Delta\omega_p(t) \approx \Delta\omega_p(0)\frac{\cos^2\theta(t)}{\cos^2\theta(0)}. \tag{1.96}$$
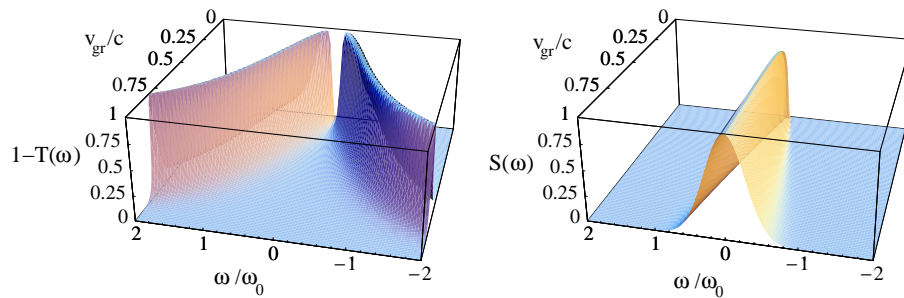
Figure 1.5: Simultaneous narrowing of the transparency window (left) and probe-pulse spectrum (right) in the case of a time-dependent variation of the group velocity v_{gr}.

From eq. (1.71) we see that by reducing the group velocity the transparency window decrease as well

$$\Delta\omega_{\mathrm{tr}}(t) = \frac{\cot^2\theta(t)}{\cot^2\theta(0)}\Delta\omega_{\mathrm{tr}}(0). \tag{1.97}$$

Thus the ratio of the pulse and transparency width remains finite,

$$\frac{\Delta\omega_p(t)}{\Delta\omega_{\mathrm{tr}}(t)} = \frac{\sin^2\theta(t)}{\sin^2\theta(0)}\frac{\Delta\omega_p(0)}{\Delta\omega_{\mathrm{tr}}(0)}. \tag{1.98}$$

In the practically relevant regime $\sin^2\theta(t)/\sin^2\theta(0)$ is always close to unity since one has to start with an already slowed probe-field pulse, i. e. $v_{\mathrm{gr}} \ll c$ and $\sin\theta \approx 1$. Thus absorption can be prevented in the dynamical light-trapping method as long as the input pulse spectrum lies within the transparency window,

$$\Delta\omega_p(0) \ll \Delta\omega_{\mathrm{tr}}(0). \tag{1.99}$$

The simultaneous reduction of the transparency window and the probe-pulse bandwidth is illustrated in fig. 1.5.

In conclusion the simultaneous reduction of the width of the EIT transparency window and the bandwidth of the probe-puls makes the present method applicable for the coherent storage of a light pulses. Since the derived theory is valid also in the quantum regime, i. e. eq. (1.87) is a linear operator equation, is it possible to store even single-photon states in an ensemble of Λ-like 3-level atoms. In the next section we will discuss the storage procedure in more detail. The state of a stored photonic excitation in an atomic ensemble is the starting point of the considerations presented in chapter 2.

1.3.3 Coherent and adiabatic storage of photonic wave-packets

We start to describe the storage procedure based on the dark-state polaritons of the last section in the Schrödinger picture, i. e. by considering the dark states of the present system and show how they are connected to the former. Historically one understands

under dark states superpostions of atomic states which are decoupled from the light-matter interaction, i. e. they are eigenstates of the interaction Hamiltonian with vanishing dipole moment. In this section we will see that they will turn out to be the actual storage units of the considered quantum memory. In the case of a quantized probe field not only one such state exists but a whole family of states into which the atoms are driven [3, 1, 51, 52]. One of the these dark states is given by

$$|D_n^k\rangle = \sum_{m=0}^{n} \binom{n}{m}^{1/2} (-\sin\theta(t))^m (\cos\theta(t))^{n-m} |(n-m)^{(k)}\rangle |s_k^{(m)}\rangle, \qquad (1.100)$$

where $|n^{(k)}\rangle$ denotes the quantum field state with n photons in mode k and $|s_k^{(m)}\rangle$ is a Dicke-like atomic state of the atomic ensemble containing m atoms in the Raman (spin)-single atom state $|s\rangle$ [53, 35, 54]. These states are defined by

$$|s^{(0)}\rangle = |g_1, g_2, \ldots, g_N\rangle, \qquad (1.101)$$

$$|s_k^{(1)}\rangle = \frac{1}{\sqrt{N}} \sum_{j=1}^{N} |g_1, \ldots, s_j, \ldots, g_N\rangle \, f_k(\mathbf{r}_j), \qquad (1.102)$$

$$|s_k^{(2)}\rangle = \frac{1}{\sqrt{2N(N-1)}} \sum_{i \neq j=1}^{N} |g_1, \ldots, s_i, \ldots, s_j, \ldots, g_N\rangle \, f_k(\mathbf{r}_i) \, f_k(\mathbf{r}_j), \qquad (1.103)$$

$$\vdots$$

where the $f_k(\mathbf{r})$ are modefunctions for the k-th mode. The mode functions of the radiation field form a orthonormal system, i. e.

$$\sum_j f_k(\mathbf{r}_j) \, f_{k'}(\mathbf{r}_j) = \delta_{kk'}. \qquad (1.104)$$

To find a connection between this state description and the last section we consider a plane-wave decomposition of dark- and bright-state polaritons, i. e.

$$\hat{\Psi}(z,t) = \sum_k \hat{\Psi}_k(t) \, e^{\mathrm{i}kz}, \qquad (1.105)$$

$$\hat{\Phi}(z,t) = \sum_k \hat{\Phi}_k(t) \, e^{\mathrm{i}kz}. \qquad (1.106)$$

Their equal time commutation relations read

$$\left[\hat{\Psi}_k, \hat{\Psi}_{k'}^\dagger \right] = \delta_{k,k'} \left[\cos^2\theta + \sin^2\theta \frac{1}{N} \sum_{j=1}^{N} (\hat{\sigma}_{gg}^j - \hat{\sigma}_{ss}^j) \right], \qquad (1.107)$$

$$\left[\hat{\Phi}_k, \hat{\Phi}_{k'}^\dagger \right] = \delta_{k,k'} \left[\sin^2\theta + \cos^2\theta \frac{1}{N} \sum_{j=1}^{N} (\hat{\sigma}_{gg}^j - \hat{\sigma}_{ss}^j) \right], \qquad (1.108)$$

$$\left[\hat{\Psi}_k, \hat{\Phi}_{k'}^\dagger \right] = \delta_{k,k'} \sin\theta \cos\theta \left[1 - \frac{1}{N} \sum_{j=1}^{N} (\hat{\sigma}_{gg}^j - \hat{\sigma}_{ss}^j) \right]. \qquad (1.109)$$

In the weak probe-field limit, i. e. if the number density of the photons in the initial probe-field pulse is much smaller than the number density of atoms in the ensemble, they reduce to those of bosonic *quasi-particles*, i. e.

$$\left[\hat{\Psi}_k, \hat{\Psi}_{k'}^{\dagger}\right] = \left[\hat{\Phi}_k, \hat{\Phi}_{k'}^{\dagger}\right] \approx \delta_{k,k'} \text{ and } \left[\hat{\Psi}_k, \hat{\Phi}_{k'}^{\dagger}\right] \approx 0. \tag{1.110}$$

We have assumed again that all atoms have initially been prepared in state $|g\rangle$. In this limit $\hat{\sigma}_{gg}^j \approx 1$ and $\hat{\sigma}_{ss}^j \approx 0$ is justified. Hence, we can associate bosonic quasi-particles (polaritons) with these operators. Furthermore, one can verify that all the number states created by $\hat{\Psi}_k^{\dagger}$ are the dark-states mentioned above

$$|D_n^k\rangle = \frac{1}{\sqrt{n!}} \left(\hat{\Psi}_k^{\dagger}\right)^n |0\rangle |s^{(0)}\rangle, \tag{1.111}$$

where $|0\rangle$ denotes the field vacuum and $n \ll N$. This is the reason these quasi-particles are called dark-state polaritons. Similarly one finds that the elementary excitations created by $\hat{\Phi}_k$ correspond to the bright-states of the 3-level system.

For simplicity we consider in the forthcoming only a single-photon wavepacket in the description of the storage procedure. The initial state of the probe-field is assumed to be $|1\rangle = \sum_k \xi_k |1_k\rangle$ with $|1_k\rangle = a_k^{\dagger}|0\rangle$, where the Fourier amplitudes ξ_k are normalized according to $\sum_k |\xi_k|^2 = 1$. Since the initial state of the ensemble is $|s^{(0)}\rangle$, the initial state of the compound system of radiation field and atomic ensemble equals, for $\theta = 0$, to the dark-state $|D_1\rangle = \sum_k \xi_k |D_1^k\rangle$. The limit $\theta = 0$, i. e. $\Omega^2 \gg g^2 N$, corresponds to the case of electromagnetically induced transparency. The dark-state polariton has in this limit only photonic character, i. e. it is given by $\hat{\Psi} \approx \hat{\mathcal{E}}_p$ and according to eq. (1.87) it propagates with the speed of light in vacuum.

By adiabatically, continuously decreasing the control-field Rabi frequency to zero we can change the character of the polariton from completely photonic into spin-like, $\hat{\Psi} = -\sqrt{N}\hat{\sigma}_{gs}$. Thereby we reduce the velocity of the excitation to zero and transfer it to an immobile Raman-coherence $\hat{\sigma}_{gs}$. The reduction of the control-field Rabi frequency corresponds to a change of the mixing angle from $\theta = 0$ to $\theta = \pi/2$ and rotates the dark-state from

$$|D_1(\theta = 0)\rangle = |1\rangle \otimes |s^{(0)}\rangle \rightarrow |D_1(\theta = \pi/2)\rangle = -|0\rangle \otimes |s^{(1)}\rangle, \tag{1.112}$$

i. e. the initial photon is mapped, using this adiabatic rotation, onto the collective spin state $|s^{(1)}\rangle$. Here we have defined in accordance with the single-photon definition $|0\rangle = \Pi_k |0_k\rangle$ and in addition we have introduced the multimode single-spin excitation by $|s^{(1)}\rangle = \sum_k \xi_k |s_k^{(1)}\rangle$. Due to the linearity of eq. (1.87) the quantum state as well as the shape of the dark-state polariton remains unchanged during the slow down and storage procedure. Adiabatically increasing the control-field Rabi-frequency, i. e. to a value much bigger than the collective Rabi-Frequency of the probe-field, $\Omega^2 \gg g^2 N$, allows us to reaccelerate the polariton and to transfer the quantum state stored in the collective spin state $|s^{(1)}\rangle$ back into its initial form of a single-photon wave packet.

The propagation of a dark-state polariton is plotted in fig. 1.7. The figure shows
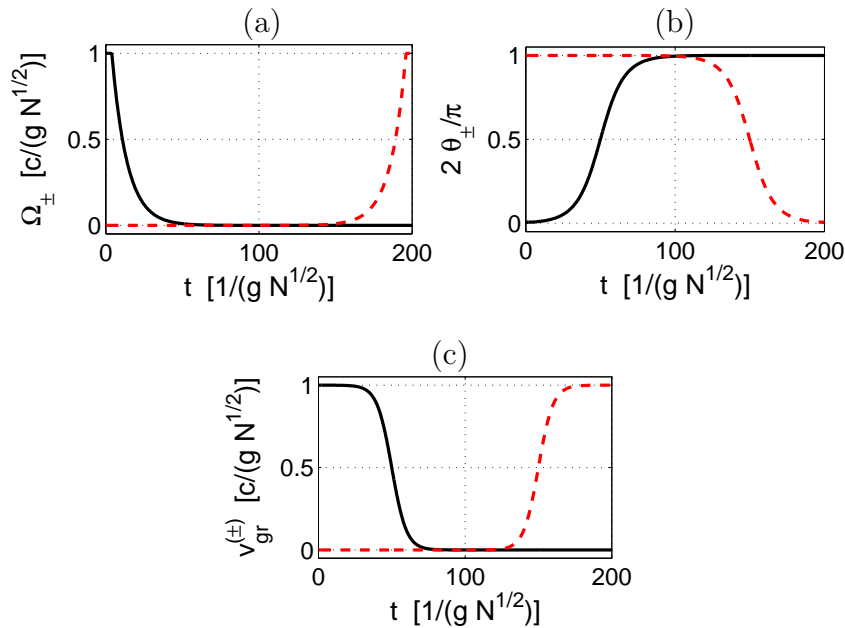
Figure 1.6: The group velocity is controlled externally via $\Omega_\pm$ according to $v_{\text{gr}}^{(+)} = c * 0.5 * (1 - \tanh(0.1 * (t - 50)))$ for the forward $(+)$ and according to $v_{\text{gr}}^{(-)} = c * 0.5 * (1 + \tanh(0.1 * (t - 150)))$ for the backward direction $(-)$. In (a) the solid (black) line corresponds to the forward control-field and the dashed (red) line to the backward one. (b) and (c) show respectively the corresponding mixing angles $\theta_\pm$ and group velocities $v_{\text{gr}}^{(\pm)}$.

storage of a forward (positive z-direction) propargating probe-field and its later read out into the backward direction [55]. The adiabatic rotation of the mixing angle using the time-dependent control-field is shown in figure 1.6. The essential point of the described technique is not the storage of the energy or of the momentum carried by the photon but the storage of its quantum state. Most part of the energy of the probe-field photon is carried away by the control-field in the stimulated Raman scattering process. Only in the case of energetically non-degenerated lower-levels does the medium absorb some energy. However, we disregard in this section the influence of such processes. An extension of the theory with respect to recoil transfer will be given in chapter 3. There the recoil transfer will become a major ingredient of the proposal.

1.4   The Sagnac effect

As we have noted in the Outline, the second major topic of this thesis is connected to the Sagnac effect. The third chapter shows that dark-state polaritons can be used to increase the sensitivity of a Sagnac interferometer. As a preparation we will now give a brief explanation of the Sagnac effect and derive the anticipated sensitivity limits for light and matterwave Sagnac gyroscopes.

The Sagnac-effect is the rotation induced phase difference of two counter-propagating
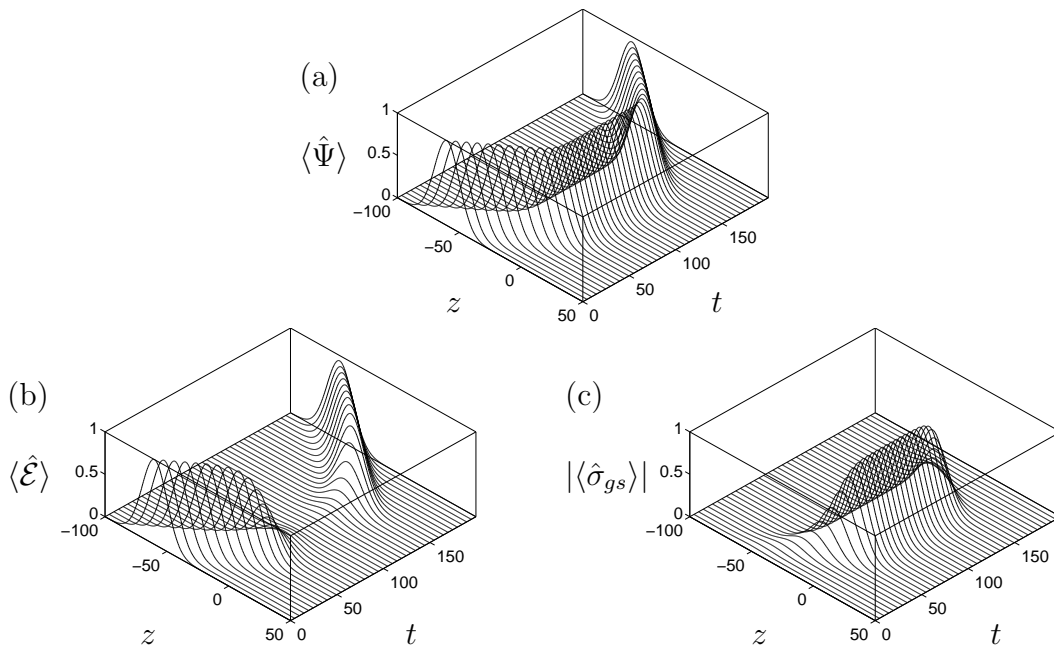
Figure 1.7: The plot shows the storage of a forward propagating light pulse and subsequent read-out into the backward direction. Propagation of a dark-state polariton with Gaussian envelope $10^{-4}/(\sqrt{2\pi}\sigma)\exp\left(-1/2*(z-z_0)^2/\sigma^2\right)$, where $\sigma = 10$ and $z_0 = -60c/(g\sqrt{N})$. In (a) the coherent amplitude of the dark-state polariton $\langle\hat{\Psi}\rangle$ is shown. The electric field amplitude $\langle\hat{\mathcal{E}}_p\rangle$ as well as the Raman coherence component $|\langle\hat{\sigma}_{gs}\rangle|$ are given in (b) and (c) respectively. The time t is given in units of $g\sqrt{N}$ and the position z in units of $c/g\sqrt{N}$. $\langle\hat{\Psi}\rangle$, $\langle\hat{\mathcal{E}}_p\rangle$ and $|\langle\hat{\sigma}_{gs}\rangle|$ are normalized with respect to their maximal value within the integration interval. Since the atoms do not move the spin coherence is stationary in space.

coherent waves in a rotating Mach-Zehnder interferometer. With the help of this effect it is possible to determine the state of rotation of the local frame of reference by means of an intrinsic measurement. Intrinsic means in this case that a reference to other frames, as for example by optical means, is not allowed.

The Sagnac-effect was first measured by the German student F. Harres in 1911 in his doctor thesis [56]. He unfortunately misinterpreted his excellent experimental results. However, independently from Harres similar experiments were carried out by G. Sagnac in 1913. In contrast to Harres, Sagnacs intention was to find the rotationally induced shift of interference fringes. He already noted in his first publication that the phase shift is proportional to the rotation rate $\boldsymbol{\Omega}$ of the interferometer according to [57]

$$\Delta\phi_{\text{Sagnac}} = \frac{\mathbf{A}\cdot\boldsymbol{\Omega}}{\lambda v}, \tag{1.113}$$
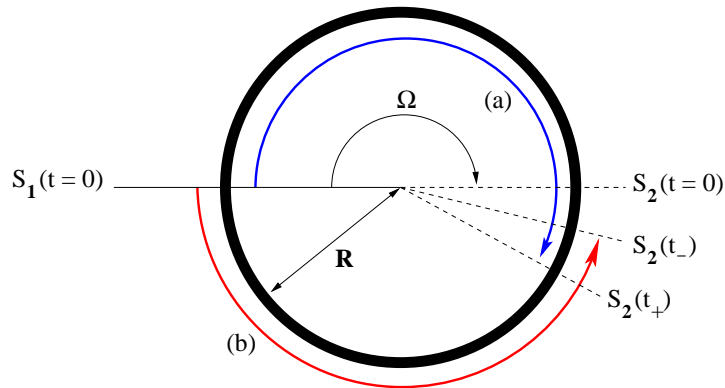
Figure 1.8: A simplified Sagnac configuration consisting of a ring-interferometer with two beam splitters which either couple the waves into the interferometer (S_1) or which are used to couple the radiation and leads it to the detector unit (S_2). The beam co-propagating with the interferometer needs longer (t_+) to arrive at the second beam splitter S_2 as the counter-propagating beam (t_-). Hence, there is a difference in arrival times $\Delta t = t_+ - t_-$ between co- and counter-propagating beam. This corresponds to the Sagnac phase shift.

where $\mathbf{A}$ is the enclosed area in the Mach-Zehnder type interferometer, λ the wavelength and v phase velocity of the used wave phenomenon. Sagnac and Harres used light for their measurements, however, as we will see later, the restriction to electromagnetic waves is not necessary.

1.4.1   A brief explanation

In this section we want to give a classical, kinematical derivation of the Sagnac phase shift eq. (1.113). To this end we consider the situation shown in fig. 1.8. The propagation of coherent waves is assumed to be constrained to follow a circular path of radius R. We calculate the time difference between clockwise (a) and counter-clockwise (b) circulation. Let us consider now the situation from an inertial frame of reference. If the interferometer is not rotating with respect to this frame, the time needed to traverse the semi circle is $t = \pi R/v$, irrespectively whether the wave propagates clockwise or counter clockwise. Hence, the arrival time difference between waves traveling from beam splitter S_1 to S_2 for the two directions is zero. This leads to a vanishing phase difference.

This is however different, when we consider a rotating interferometer. Let us assume that the beams leave the first beam splitter S_1 at $t = 0$. The counter clockwise beam, traveling in the opposite direction as the direction of rotation, meets the second beam splitter S_2 at t_-, whereas the clockwise beam traveling in the same direction arrives at S_2 at t_+. In the case the whole interferometer rotates with an angular velocity Ω the time for the counter-clockwise beam to go to S_2 is given by

$$t_- = \frac{\pi R - \Omega R t_-}{v} = \frac{\pi R}{v}\left(1 + \frac{R\Omega}{v}\right)^{-1}, \tag{1.114}$$

since S_2 moves in the semi-circle transit-time towards the first beam splitter S_1. A similar result holds for the clockwise beam

$$t_+ = \frac{\pi R}{v} \left(1 - \frac{R\Omega}{v}\right)^{-1}, \tag{1.115}$$

however, it takes longer for the wave to catch-up with the beam splitter which moves away from the approaching wave. The time difference between clockwise and counter-clockwise beams is then given by

$$\Delta t = t_+ - t_- = \frac{2\Omega\pi R^2}{v^2} \left(1 - \left(\frac{\Omega R}{v}\right)^2\right)^{-1} \approx \frac{2\Omega\pi R^2}{v^2}, \tag{1.116}$$

where the last approximate holds if $\Omega R \ll v$, i. e. if we consider reasonable small radii. This corresponds to a difference in (optical) path length of $\Delta L = v\Delta t$ and hence to phase shift of

$$\Delta\phi = \Delta L k = \frac{4\pi^2 R^2 \Omega}{\lambda v}, \tag{1.117}$$

with respect to a considered wave with wavelength $\lambda = 2\pi/k$. In this derivation we considered a ring configuration which can, however, be generalized to arbitrary interferometer shapes [58]. From the considerations above we see that the Sagnac effect is based on the rotationally induced difference in the (optical) path length. Furthermore, we see that the derivation of the Sagnac formula does in principle not depend on the nature of the wave phenomenon, i. e. whether one uses light or matterwaves. As we will see in the next section this is different when we determine the sensitivity of Sagnac effect based gyroscopes. Finally, we note that measuring a phase difference allows us, according to eq. (1.113), not only to state that the local frame is rotating but also to determine the rate of rotation. To this determination we will turn now.

1.4.2   Quantum limit of laser and matter-wave gyroscopes

In this section we derive the quantum limit of the minimal detectable rotation rate of light and matterwave gyroscopes. In chapter 3 we will compare the results given here with the result derived for the dark-state polariton based gyroscope. For the derivation of the quantum limit we assume that the minimum detectable phase shift is given by the shot noise limit [21]

$$\Delta\phi_{min} = \frac{1}{\sqrt{n}}, \tag{1.118}$$

where n is number of particles, either photons or atoms depending on the nature of the considered interferometer. The number of quanta is given by the flux j of quanta hitting the detector by jt_m, where t_m is the measurement time. In case of a laser gyroscope

the flux is given by the power P divided by the photon energy $\hbar\omega$. Hence, by equating eq. (1.117) and (1.118) we find the minimum detectable rotation rate to be

$$\Omega_{\min}^{\text{light}} = \frac{\hbar}{Am_\gamma}\sqrt{\frac{\hbar\omega}{Pt_m}}, \qquad (1.119)$$

where $m_\gamma = \hbar\omega/c^2$ is the effective photon mass. If we, instead of a laser gyroscope, consider a matterwave interferometer, we will have to substitute the wavelength in eq. (1.117) by the de-Broglie wavelength $\lambda_{\text{dB}} = \hbar/mv$ of the atom. In this case the minimum detectable rotation rate is given by

$$\Omega_{\min}^{\text{light}} = \frac{\hbar}{2\pi A\,m}\frac{1}{\sqrt{jt_m}}. \qquad (1.120)$$

We note here that if the enclosed are A and the flux would be the same for laser and matterwave gyroscope the matterwave gyroscopes would be more sensitive by a factor $m/m_\gamma = mc^2/\hbar\omega \approx 10^{10}$ for typical laser wavelengths. However, these conditions can not be fulfilled with state-of-the-art technologies. As we will show in chapter 3, it is to some extend possible to use the superposition nature of the dark-state polaritons, i. e. that they are a superposition of light and matterwaves, to have a sensitivity enhancement of a dark-state polariton gyroscope as compared to conventional light and matterwave gyroscopes.

1.4.3   Overview: state-of-the-art gyroscopes

For later comparison we finally state briefly the current sensitivity limits of Sagnac gyroscopes. But first we note that not all gyroscopes are based on the Sagnac effect. Other physical principles can be used for rotation sensing, as are e. g. the Josephson effect in superfluid ^{3}He and ^{4}He [59] or nuclear spin precession [60, 61]. Even mechanical gyroscopes which work quite well in low gravity environments are under discussion [62].

Gyroscopes based on the Sagnac effect have so far achieved a sensitivity of 2×10^{-10} rad s^{-1} Hz$^{-1/2}$ using a ring laser with an enclosed area of 1 m^2 [63] and 6×10^{-10} rad s^{-1} Hz$^{-1/2}$ using an atomic interferometer with a path length of 2 m [64] (a value for the area was not given). Compact fiber-optic gyroscopes have a reported sensitivity of 2×10^{-8} rad s^{-1} Hz$^{-1/2}$ [61]. Even though the later are less sensitive they are very robust and are used in commercial airplanes [65].

Chapter 2

Coherent spatial control of stationary light

2.1 Motivation

The success of quantum-information (QI) processing will strongly depend on the ability to construct a scalable quantum network, i. e. a set-up capable of storing, transferring and handling the units of quantum information (qubits). The various physical requirements for such a network have been summarized by DiVincenzo [66].
A number of systems are at present under investigation to achieve this goal, some of these are for example: ion traps [67], nuclear magnetic resonance schemes (NMR) [68, 69, 70], high-Q optical cavities [71, 72, 73] and superconducting quantum interference devices (SQUIDs) [74]. To date none of these approaches fullfills all the requirements posed for the construction of a complete and scalable quantum network. Among the various considered attempts we here consider one based upon photons as *flying* qubits, i. e. information carriers, and atomic ensembles as storage and processing units. As stated in the introduction, a number of techniques for a reliable transfer of quantum information between light and atomic ensembles have been proposed [1, 3, 75] and, in part, experimentally realized over the last couple of years [19, 20, 76]. The first experimental demonstrations were based upon classical fields. Only recently it was possible to demonstrate these storage techniques on the single photon level [77, 78, 79].
Despite the progress in storage and transfer of single photons the implementation of an information processing unit, i. e. a set of a high-fidelity, scalable quantum logic gates with photonic qubits, is still challenging. At present two major directions are actively explored. The first one is a *probabilistic* approach based on linear optical elements and photodectors [80, 81, 82]. The non-linear dynamics necessary for quantum information processing is here a part of the detection process. We are here however interested into the second approach that aims at *deterministic* entanglement between pairs of single photons. Due to the almost negligible interaction energy per photon, this turns out to be a very difficult task since entanglement between photons requires a sufficiently strong non-linear interaction between these [9, 10, 5]. We can only meet this requirement if we spatially

confine the (photonic) excitation very tightly and use a sufficiently long interaction time. This would, due to the locality of most interactions, lead to high enough interaction energy. Even for long-range interactions, as e. g. for the dipole-blockade scheme discussed in [83], tight spatial confinement would be desirable [84, 85].

In the present chapter we will discuss a method to coherently and spatially manipulate the shape of collective excitations of stationary pulses of light in atomic ensembles. This method will allow us to increase the excitation density. The scheme to create stationary pulses of light has been introduced by A. André and M. D. Lukin [11, 86] and has in addition been experimentally verified shortly afterwards by the same group [12]. It is a combination of the earlier mentioned light-storage and retrieval technique [1, 27] with techniques of Bragg reflection on absorptive periodic structures.

The procedure is to first store a light pulse by adiabatically rotating the corresponding dark-state polariton, from a freely propagating electromagnetic field pulse, see fig. 2.2 (a), into a stationary Raman coherence[1]. Stored in this coherence, the excitation is well protected from environmental influences for a rather long time. This is an essential feature of a quantum memory. However, it makes the excitation also immobile and limits the possibilities of spatial manipulation to the atomic degrees of freedom. Unless one actively changes the spatial distribution of the atoms the only way to manipulate the spatial shape of stored excitation is to partially convert it back to light but to keep it trapped in a special kind of artificial high Q-cavity such that it does not leave the medium. To this end Lukin et al. [12] used a weak retrieval field, created by *two counter-propagating control lasers* forming a *standing wave pattern*, and created a quasi stationary pulse of light as shown in fig. 2.1. The illumination by the two counter-propagating fields has several interesting consequences: first of all, everywhere except for the nodes of the control-fields the spin coherence is partially converted back into the probe-field. This leads to a periodic structure of the probe-field amplitude imprinted by the control-field. Second, the control-field dresses the medium in such a way that the absorption of the probe-field is suppressed again everywhere except at the nodes of the control-field. This results in a sharply peaked, periodic modulation of the atomic absorption for the probe-field (see fig. 2.1). Even if the retrieved photonic component is at all times very small, the process renders the excitation sufficiently mobile to follow the profile of the retrieval lasers. It provides a potential mechanism to manipulate and coherently control the spatial shape of the excitation, using the external control-fields, while keeping most of its probability amplitude in the well-protected collective spin coherence.

The chapter is organized as follows. First we state the fundamental equations of motion for this system. In particular we give the relevant equations in secular approximation and in the weak probe field limit. Then we briefly introduce a new stationary light scheme which circumvents the need of a secular approximation and adds some new freedom to the system. Using the fundamental equations we derive a self-consistent set of equations of motion for the forward and backward propagating probe fields in the adiabatic limit. These are simplified by introducing a new set of normal modes. In the new representation

---

[1]The storage phase mentioned is in principle not necessary; adiabatically turning on the second control-field while the probe-pulse is propagating through the EIT-medium is sufficient [87]. See also section 2.3
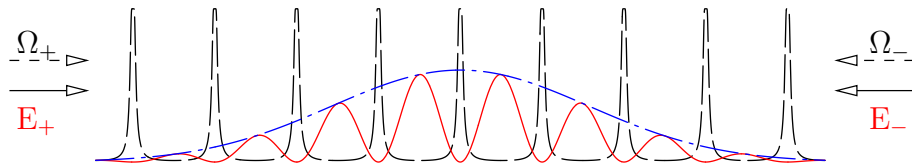
Figure 2.1: The dashed dotted (blue) line is the envelope of the spin coherence in which the information of the initial probe pulse is stored. The dashed line (black) corresponds to the absorption profile for the probe-field due to the dressing of the medium by the control-field standing wave. The solid line (red) represents the partially retrieved probe-field.

we see that one of the normal modes is absorbed leading to pulse matching phenomenon which we discuss in more detail. Subsequently we consider the configuration of spatially homogeneous control fields. This topic can furthermore be divided into the two cases of equal and unequal field intensities of the forward and backward propagating control fields. The first case leads to the discussion of diffusion in the stationary light scheme and the second to the introduction of a drift motion. Both phenomena turn out to be important for the last part of the chapter the discussion of spatially nonhomogeneous control fields. A special configuration of nonhomogeneous control fields can lead to effective forces which counteract the diffusive spreading and can be used to compress the spatial probe field distribution. At the end of the chapter we discuss the effectivity of this process.

2.2   The stationary light system

2.2.1   The absorptive stationary light scheme

Linear response of the dressed EIT-medium

Stationary light is created in a Λ-type 3-level medium with strong, counter-propagating control-fields on the $|e\rangle-|s\rangle$-transition, having the same one-photon detuning $\Delta = \omega_{es}-\omega_c$. This configuration is shown in fig. 2.2 (b). The control-field dresses the medium in such a way that the weak probe-field experiences EIT and travels with a reduced group veloctiy through the medium. Furthermore we allow for a detuning $\delta = \omega_{sg} - (\omega - \omega_c)$ from the two-photon Raman transition $|g\rangle - |s\rangle$. In the interaction picture and in a slowly varying time frame as well as using the undepleted control-field approximation [88] the Hamiltonian of the system is given by

$$\hat{H}(t) = -\frac{N}{V} \int d^3\mathbf{r}\, \hbar \left\{ \Delta\, \hat{\sigma}_{ss}(\mathbf{r},t) + (\delta + \Delta)\, \hat{\sigma}_{gg}(\mathbf{r},t) + \left[\Omega(\mathbf{r},\mathbf{t})\, \hat{\sigma}_{es}(\mathbf{r},t) + \text{h.a.} \right] \right.$$
$$\left. + g\left[\hat{E}^{(+)}(\mathbf{r},t)\, \hat{\sigma}_{eg}(\mathbf{r},t) + \text{h.a.} \right] \right\} \tag{2.1}$$

where $g = \frac{\wp}{\hbar}\sqrt{\frac{\hbar\omega_{eg}}{2\epsilon_0 V}}$ is the atom-field coupling constant of the probe-field with the dipole moment $\wp$ and the quantization volume V. N is the number of atoms in this volume.
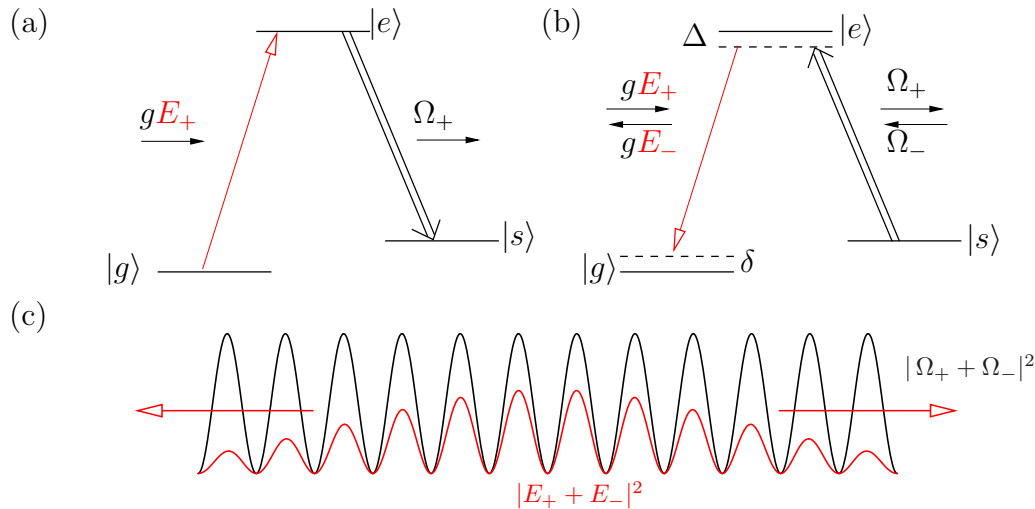
Figure 2.2: (a) Storage of light scheme for a probe pulse E_+, where the storage process is mediated by adiabatically reducing the control-field Ω_+ to zero. (b) Subsequent partial regeneration of stationary probe light with counter-propagating components $E_\pm$ by applying two control-fields $\Omega_\pm$ which form a standing wave. (c) The total field distribution of the retrieved probe-field approaches due to a pulse matching phenomenon diffusively (indicated by the red arrow) the control-field envelope.

For simplicity, and without loss of generality, we consider g to be real. To describe the quantum properties of the medium we use collective atomic operators

$$\hat{\sigma}_{\mu\nu}(\mathbf{r}, t) = \frac{1}{N_{\mathbf{r}}} \sum_{j}^{N_{\mathbf{r}}} \hat{\sigma}_{\mu\nu}^{j}(t), \tag{2.2}$$

where the sum is taken over all atoms within a small but macroscopic volume containing $N_{\mathbf{r}} \gg 1$ atoms around the position $\mathbf{r}$ [89]. The $\hat{\sigma}_{\mu\nu}^{j}$ are the single-atom spin-flip operators at position $\mathbf{r}_j$. In the continuum limit, the collective operators obey the commutator relation

$$[\hat{\sigma}_{\alpha\beta}(\mathbf{r}, t), \hat{\sigma}_{\mu\nu}(\mathbf{r}', t)] = \frac{V}{N} \delta(\mathbf{r} - \mathbf{r}') \left(\delta_{\beta,\mu} \hat{\sigma}_{\alpha\nu}(\mathbf{r}, t) - \delta_{\nu,\alpha} \hat{\sigma}_{\mu\beta}(\mathbf{r}, t) \right). \tag{2.3}$$

The equations of motion for these collective atomic operators are given by the Heisenberg-Langevin equations [21]

$$\frac{\partial \hat{\sigma}_{\mu\nu}(\mathbf{r}, t)}{\partial t} = -\gamma_{\mu\nu} \hat{\sigma}_{\mu\nu}(\mathbf{r}, t) - \frac{\mathrm{i}}{\hbar} \left[\hat{\sigma}_{\mu\nu}(\mathbf{r}, t), \hat{H}(t) \right] + \hat{F}_{\mu\nu}(\mathbf{r}, t). \tag{2.4}$$

According to the dissipation-fluctuation theorem [21], that states that dissipation is always accompanied by fluctuation and visa versa, we had to add rapidly and randomly fluctuating noise forces when including the transverse decay rates $\gamma_{\mu\nu}$ into equation

(2.4). Due to these forces the commutation relations for the collective atomic operators will stay preserved at all times [34]. In the Markovian limit, the first order correlation function of the Langevin noise force $\hat{F}_{\mu\nu}$-operators are δ-correlated, i. e. we have $\langle \hat{F}_{\mu\nu}(t)\hat{F}_{\alpha\beta}(t')\rangle = D_{\mu\nu\alpha\beta}\delta(t-t')$. Using the Einstein relations, which hold in the Markovian limit, the diffusion coefficients $D_{\mu\nu\alpha\beta}$ may be calculated from the drift constants of the problem. The determination of the latter is possible at least perturbatively. Finally the noise forces have to have a vanishing expectation value $\langle \hat{F}_{\mu\nu}(t)\rangle = 0$. They do not change the dynamics for the expectation values of the collective atomic operators [35].

Finally, we summarize the Heisenberg-Langevin equations for the Hamiltonian (2.1). The corresponding equations for the diagonal elements of the spin operators are

$$\dot{\hat{\sigma}}_{gg} = \gamma_{gg}\hat{\sigma}_{ee} - ig\left[\hat{E}^{(+)}(\mathbf{r},t)\hat{\sigma}_{eg} - \hat{E}^{(-)}(\mathbf{r},t)\hat{\sigma}_{ge}\right] + \hat{F}_{gg}(\mathbf{r},t), \tag{2.5}$$

$$\dot{\hat{\sigma}}_{ss} = \gamma_{ss}\hat{\sigma}_{ee} + i\left[\Omega^*(\mathbf{r},t)\hat{\sigma}_{se} - \Omega(\mathbf{r},t)\hat{\sigma}_{es}\right] + \hat{F}_{ss}(\mathbf{r},t), \tag{2.6}$$

$$\dot{\hat{\sigma}}_{ee} = -\left[\gamma_{gg} + \gamma_{ss}\right]\hat{\sigma}_{ee} + i\left[\Omega(\mathbf{r},t)\hat{\sigma}_{es} - \Omega^*(\mathbf{r},t)\hat{\sigma}_{se}\right]$$
$$+ ig\left[\hat{E}^{(+)}(\mathbf{r},t)\hat{\sigma}_{eg} - \hat{E}^{(-)}(\mathbf{r},t)\hat{\sigma}_{ge}\right] + \hat{F}_{ee}(\mathbf{r},t), \tag{2.7}$$

and the ones for the collective coherence operators are

$$\dot{\hat{\sigma}}_{ge} = -\left[i(\delta + \Delta) + \gamma_{ge}\right]\hat{\sigma}_{ge} - ig\hat{E}^{(+)}(\mathbf{r},t)\left[\hat{\sigma}_{ee} - \hat{\sigma}_{gg}\right] + i\Omega(\mathbf{r},t)\hat{\sigma}_{gs} + \hat{F}_{ge}(\mathbf{r},t), \tag{2.8}$$

$$\dot{\hat{\sigma}}_{gs} = -\left[i\,\delta + \gamma_{gs}\right]\hat{\sigma}_{gs} - ig\hat{E}^{(+)}(\mathbf{r},t)\hat{\sigma}_{es} + i\Omega^*(\mathbf{r},t)\hat{\sigma}_{ge} + \hat{F}_{gs}(\mathbf{r},t), \tag{2.9}$$

$$\dot{\hat{\sigma}}_{se} = -\left[i\,\Delta + \gamma_{se}\right]\hat{\sigma}_{se} + ig\hat{E}^{(+)}(\mathbf{r},t)\hat{\sigma}_{sg} - i\Omega(\mathbf{r},t)\left[\hat{\sigma}_{ee} - \hat{\sigma}_{ss}\right] + \hat{F}_{se}(\mathbf{r},t). \tag{2.10}$$

In our approach we assume that the transverse decay rates are given by $\gamma_{ge} = (\gamma_{gg} + \gamma_{ss})/2 = \gamma_{se}$, where the $\gamma_{\mu\mu}$, with $\mu \in \{g,s\}$, are the population decay rates of the $|e\rangle \rightarrow |\mu\rangle$-transitions.

Since we are interested only in the linear response we treat eqs. (2.5-2.10) perturbatively in the probe-field. By assuming that the collective Rabi frequency of the probe-field is much smaller than the control-field Rabi frequency, and the number of photons in the probe-field is much smaller than the number of atoms N in the quantization volume [48], such a perturbation is justified, and we find in first order

$$\partial_t\hat{\sigma}_{ge} = -(\gamma_{ge} + i(\Delta + \delta))\hat{\sigma}_{ge} + ig\hat{E}^{(+)}(\mathbf{r},t) + i\Omega\hat{\sigma}_{gs} + \hat{F}_{ge}, \tag{2.11}$$

$$\partial_t\hat{\sigma}_{gs} = -(\gamma_{gs} + i\delta)\hat{\sigma}_{gs} + i\Omega^*\hat{\sigma}_{ge} + \hat{F}_{ge}. \tag{2.12}$$

To derive (2.11) and (2.12) we have assumed that the medium was initially prepared in the ground state $|g\rangle$, i. e. $\sigma_{gg} \simeq 1 \gg \sigma_{ee}, \sigma_{ss}$. In order to describe a standing control field wave we make the following ansatz

$$\Omega(\mathbf{r},\mathbf{t}) = \Omega_+e^{ik_cz} + \Omega_-e^{-ik_cz}. \tag{2.13}$$

We also decompose the signal field into forward $(+)$ and backward $(-)$ propagating spatially slowly varying variables

$$\hat{E}^{(+)}(\mathbf{r},t) = \hat{E}_+(\mathbf{r},t)\,e^{ikz} + \hat{E}_-(\mathbf{r},t)\,e^{-ikz}. \tag{2.14}$$

Furthermore, we assume that the polarization $P = N \wp \hat{\sigma}_{ge}$ of the $|g\rangle \leftrightarrow |e\rangle$-transition, and hence the collective operator $\hat{\sigma}_{ge}$, follows the behavior of the probe-field and can be decomposed in the same way. After introducing all these decompositions into the equations of motion of the collective atomic operators we can perform a secular approximation, i. e. we neglect fast oscillating terms of the form $\exp(\pm i 2 k_c z)$ or $\exp(-i(k + k_c)z)$. By introducing the following transformations

$$\hat{E}_\pm(\mathbf{r}, t) = \hat{\mathcal{E}}_\pm(\mathbf{r}, t) e^{\pm i \Delta k z}, \tag{2.15}$$

$$\hat{\sigma}_{ge}(\mathbf{r}, t) = \hat{\sigma}_{ge}^{(+)}(\mathbf{r}, t) e^{i \Delta k z} + \hat{\sigma}_{ge}^{(-)}(\mathbf{r}, t) e^{-i \Delta k z}, \tag{2.16}$$

with $\Delta k = k_c - k = \Delta \omega / c$, we finally find

$$\partial_t \hat{\sigma}_{\text{ge}}^{(\pm)} = - \left[i(\delta + \Delta) + \gamma_{\text{ge}} \right] \hat{\sigma}_{\text{ge}}^{(\pm)} + i g \hat{\mathcal{E}}_\pm + i \Omega_\pm \hat{\sigma}_{\text{gs}}, \tag{2.17}$$

$$\partial_t \hat{\sigma}_{\text{gs}} = - \left[i \, \delta + \gamma_{\text{gs}} \right] \hat{\sigma}_{\text{gs}} + i \left(\Omega_+^* \hat{\sigma}_{\text{ge}}^{(+)} + \Omega_-^* \hat{\sigma}_{\text{ge}}^{(-)} \right). \tag{2.18}$$

In addition we note that the propagation equations for the probe modes of the plus $(+)$ and minus $(-)$ direction are given in this case, in paraxial approximation, by

$$\left(\partial_t \pm c \partial_z + \frac{c}{2 i k} \Delta_\perp \right) \hat{\mathcal{E}}_\pm = -i \Delta \omega \, \hat{\mathcal{E}}_\pm + i g N \hat{\sigma}_{ge}^{(\pm)}. \tag{2.19}$$

Eqs. (2.17-2.19) are the starting point for the derivation of a self-consistent set of equations for the two probe-field modes in the linear response regime of our *model* medium of Λ-type 3-level atoms. Before we go on to discuss the probe field dynamics in such a stationary light configuration we first introduce a new stationary light scheme which does not require a secular approximation and provides some additional degrees of freedom which may be useful in practical applications.

2.2.2 The 2V-scheme for stationary light

In this section we introduce a new scheme that also shows the phenomenon of stationary light. Let us consider to counter-propagating control-fields in a $\sigma^+ - \sigma^-$-configuration as shown in fig. 2.3. Furthermore, we assume that also the probe-fields are in a corresponding configuration. In contrast to the scheme by A. André and M. D. Lukin [11, 12] the considered configuration is not based on the Bragg scattering from the spatially periodic absorption maxima. In the present case the interaction Hamiltonian in a frame co-rotating with the optical frequencies is given by

$$H_{\text{int}} = -\frac{N}{V} \int \mathrm{d}\mathbf{r} \, \hbar \Big\{ (\Delta_+ + \Delta_+^{(c)}) \hat{\sigma}_{e_+ e_+} + (\Delta_- + \Delta_-^{(c)}) \hat{\sigma}_{e_- e_-} + $$
$$+ \left[\Omega_+ \hat{\sigma}_{e_+ s} + \Omega_- \hat{\sigma}_{e_- s} + \text{h.a.} \right] + \left[\hat{E}_+^{(+)} \hat{\sigma}_{e_+ s} + \hat{E}_-^{(+)} \hat{\sigma}_{e_- s} + \text{h.a} \right] \Big\}. \tag{2.20}$$

Using eq. (2.4) we can again determine the Heisenberg-Langevin equations for the collective spin operator. These are very similar to the earlier equations, however, they
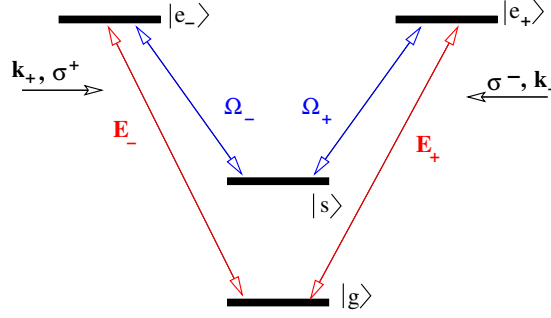
Figure 2.3: Sketch of the 2V-coupling scheme exhibiting stationary light. The figure displays the one- and two-photons resonance.

incooperate a few more terms. Therefore, we give them here explicitly. The equations for the diagonal terms read

$$\dot{\hat{\sigma}}_{\text{gg}} = \gamma_{\text{g}+}\hat{\sigma}_{\text{e}_+\text{e}_+} + \gamma_{\text{g}-}\hat{\sigma}_{\text{e}_-\text{e}_-} - ig\left[\hat{E}_+^{(+)}(\mathbf{r},t)\hat{\sigma}_{\text{e}_+\text{g}} + \hat{E}_-^{(+)}(\mathbf{r},t)\hat{\sigma}_{\text{e}_-\text{g}} - \text{h.a}\right] + \hat{F}_{gg}(\mathbf{r},t),$$
(2.21)

$$\dot{\hat{\sigma}}_{\text{ss}} = \gamma_{\text{s}+}\hat{\sigma}_{\text{e}_+\text{e}_+} + \gamma_{\text{s}-}\hat{\sigma}_{\text{e}_-\text{e}_-} + i\left[\Omega_+^*(\mathbf{r},t)\hat{\sigma}_{\text{se}_+} + \Omega_-^*(\mathbf{r},t)\hat{\sigma}_{\text{se}_-} - \text{h.a}\right] + \hat{F}_{ss}(\mathbf{r},t),$$
(2.22)

$$\dot{\hat{\sigma}}_{\text{e}_\pm\text{e}_\pm} = -\left[\gamma_{\text{g}\pm} + \gamma_{\text{s}\pm}\right]\hat{\sigma}_{\text{e}_\pm\text{e}_\pm} + i\left[\Omega_\pm(\mathbf{r},t)\hat{\sigma}_{\text{e}_\pm\text{s}} - \Omega_\pm^*(\mathbf{r},t)\hat{\sigma}_{\text{se}_\pm}\right]$$
$$+ ig\left[\hat{E}_\pm^{(+)}(\mathbf{r},t)\hat{\sigma}_{\text{e}_\pm\text{g}} - \hat{E}_\pm^{(-)}(\mathbf{r},t)\hat{\sigma}_{\text{ge}_\pm}\right] + \hat{F}_{e_\pm e_\pm}(\mathbf{r},t),$$
(2.23)

and the ones for the coherence operators are

$$\dot{\hat{\sigma}}_{\text{ge}_\pm} = -\left[i(\Delta_\pm + \Delta^{(c)})_\pm + \gamma_{\text{ge}_\pm}\right]\hat{\sigma}_{\text{ge}_\pm} - ig\hat{E}_\pm^{(+)}(\mathbf{r},t)\left[\hat{\sigma}_{\text{e}_\pm\text{e}_\pm} - \hat{\sigma}_{\text{gg}}\right]$$
$$+ i\Omega_\pm(\mathbf{r},t)\hat{\sigma}_{\text{gs}} - ig\hat{E}_\mp^{(+)}(\mathbf{r},t)\hat{\sigma}_{\text{e}_\mp\text{e}_\pm}\hat{F}_{ge}(\mathbf{r},t),$$
(2.24)

$$\dot{\hat{\sigma}}_{\text{gs}} = -\gamma_{\text{gs}}\hat{\sigma}_{\text{gs}} - ig\hat{E}_+^{(+)}(\mathbf{r},t)\hat{\sigma}_{\text{e}_+\text{s}} - ig\hat{E}_-^{(+)}(\mathbf{r},t)\hat{\sigma}_{\text{e}_-\text{s}}$$
$$+ i\Omega_+^*(\mathbf{r},t)\hat{\sigma}_{\text{ge}_+} + i\Omega_-^*(\mathbf{r},t)\hat{\sigma}_{\text{ge}_-} + \hat{F}_{gs}(\mathbf{r},t),$$
(2.25)

$$\dot{\hat{\sigma}}_{\text{se}_\pm} = -\left[i\left(\Delta_\pm + \Delta_\pm^{(c)} + \gamma_{\text{se}}\right]\hat{\sigma}_{\text{se}_\pm} + ig\hat{E}_\pm^{(+)}(\mathbf{r},t)\hat{\sigma}_{\text{sg}} - i\Omega_\pm(\mathbf{r},t)\left[\hat{\sigma}_{\text{e}_\pm\text{e}_\pm} - \hat{\sigma}_{\text{ss}}\right]$$
$$- i\Omega_\mp\hat{\sigma}_{\text{e}_\mp\text{e}_\pm} + \hat{F}_{se_\pm}(\mathbf{r},t),$$
(2.26)

$$\hat{\sigma}_{e_+e_-} = -\left[i((\Delta_+ - \Delta_-) + (\Delta_+^{(c)} - \Delta_-^{(c)})) + \gamma_{e_+e_-}\right]\hat{\sigma}_{e_+e_-}$$
$$+ i\Omega_-\hat{\sigma}_{e_+s} - i\Omega_+^*\hat{\sigma}_{se_-} + ig\hat{E}_-^{(+)}\hat{\sigma}_{e_+g} - ig\hat{E}_+^{(-)}\hat{\sigma}_{se_-}.$$
(2.27)

In the weak-probe field limit we can treat these equations perturbatively. By assuming that initially all population is in the ground state, i. e. $\hat{\sigma}_{gg} = 1$ and $\hat{\sigma}_{\mu\nu} \approx 0$ for the rest, we find in first order a set of six equations. However, we immediately see that these separate

into two sets of three equations respectively. We only note here the ones relevant for us

$$\dot{\hat{\sigma}}_{\text{ge}_\pm} = -\left[\text{i}(\Delta_\pm + \Delta_\pm^{(c)}) + \gamma_{\text{ge}_\pm}\right]\hat{\sigma}_{\text{ge}_\pm} + \text{i}g\hat{E}_\pm^{(+)}(\mathbf{r}, t)N + \text{i}\Omega_\pm(\mathbf{r}, t)\hat{\sigma}_{\text{gs}} + \hat{F}_{ge}(\mathbf{r}, t),$$
(2.28)

$$\dot{\hat{\sigma}}_{\text{gs}} = -\gamma_{\text{gs}}\hat{\sigma}_{\text{gs}} + \text{i}\Omega_+^*(\mathbf{r}, t)\hat{\sigma}_{\text{ge}_+} + \text{i}\Omega_-^*(\mathbf{r}, t)\hat{\sigma}_{\text{ge}_-} + \hat{F}_{gs}(\mathbf{r}, t).$$
(2.29)

For simplicity we have omitted the superscripts denoting the perturbation order. We note that these equations are formally identical to eq. (2.17) and (2.18) for the Λ-scheme. The difference here is that no secular approximation was necessary and that the single-photon detunings $\Delta_\pm$ can now be different for the forward and backward direction.

2.2.3 Self-consistent probe-field equations

Effective field equations in the adiabatic limit

In this section we use the Heisenberg-Langevin equations and the shortened wave equation as found in section 2.2.1 to derive a self-consistent set for the weak forward and backward propagating probe fields. Using this we will discuss the probe field dynamics for a few control-field configurations. To this end, we note that the decay rate γ_{ge} of the optical transition $|g\rangle - |e\rangle$ is in general much larger than the decay rate of the Raman coherence, therefore we may adiabatically eliminate the first [21]. In an intuitive picture this means that the temporal evolution of the optical coherence happens on a much shorter time scale than that of the Raman coherence. Furthermore we assume that this also holds for the characteristic time of the dynamics of the probe and control-field. Hence, we can set the time derivative of $\hat{\sigma}_{ge}^{(\pm)}$ in eq. 2.17 equal to zero and obtain

$$\hat{\sigma}_{ge}^{(\pm)} = \frac{\text{i}g\hat{\mathcal{E}}_\pm + \text{i}\Omega_\pm\hat{\sigma}_{gs}}{\text{i}(\delta + \Delta) + \gamma_{\text{ge}}}.$$
(2.30)

Using this result as well as the definition of the total control-field Rabi frequency

$$|\Omega|^2 = |\Omega_+|^2 + |\Omega_-|^2,$$
(2.31)

we can eliminate the polarization of probe-field from the atomic dynamics. To do this we substitute eq. (2.30) into eq. (2.18). Solving the resulting equation for the spin coherence we find

$$\hat{\sigma}_{gs} = -\frac{g(\hat{\mathcal{E}}_+\Omega_+^* + \hat{\mathcal{E}}_-\Omega_-^*) + (\text{i}(\delta + \Delta) + \gamma_{\text{ge}})\partial_t\hat{\sigma}_{gs}}{(\text{i}\,\delta + \gamma_{\text{gs}})(\text{i}(\delta + \Delta) + \gamma_{\text{ge}}) + |\Omega|^2}.$$
(2.32)

Equations (2.30) and (2.32) describe the dynamics of the spin coherence adiabatically followed by the optical coherence. In order to find a self-consistent set of equations for the probe-field amplitudes alone, we perform a perturbation expansion based on the temporal change of the spin coherence. To this end, we introduce a normalized time $\tilde{t} = t/T$, where T is the characteristic time for the changes of the Raman coherence $\hat{\sigma}_{gs}$. By expanding

the right-hand side of eq. (2.32) in terms of $1/T$ we can ignore in zeroth order the time derivative of the coherence. If we would expand the above equation only up to this order we would, however, neglect all interesting effects we want to study. The approximation would mean that the characteristic probe pulse time and hence the characteristic time of change of the Raman coherence is much larger than the time the probe pulse needs to transverse the medium. Hence, it would not allow for a finite group velocity of the considered probe pulse. To include the group velocity, we will have to expand the series up to first order. Using the abbreviations

$$\Gamma_{\text{ge}} \equiv \text{i}(\delta + \Delta) + \gamma_{\text{ge}}, \tag{2.33}$$

$$\Gamma_{\text{gs}} \equiv \text{i}\,\delta + \gamma_{\text{gs}}, \tag{2.34}$$

and $\Gamma^2 = \Gamma_{\text{ge}}\Gamma_{\text{gs}}$ we find up to first order

$$
\begin{aligned}
\hat{\sigma}_{gs} = {} & g\hat{\mathcal{E}}_+ \left[\frac{\Gamma_{\text{ge}}}{(\Gamma^2 + |\Omega|^2)^2} \left(\partial_t \Omega_+^* - \frac{\Omega_+^*}{\Gamma^2 + |\Omega|^2} \partial_t |\Omega|^2 \right) - \frac{\Omega_+^*}{\Gamma^2 + |\Omega|^2} \right] \\
& + g\hat{\mathcal{E}}_- \left[\frac{\Gamma_{\text{ge}}}{(\Gamma^2 + |\Omega|^2)^2} \left(\partial_t \Omega_-^* - \frac{\Omega_-^*}{\Gamma^2 + |\Omega|^2} \partial_t |\Omega|^2 \right) - \frac{\Omega_-^*}{\Gamma^2 + |\Omega|^2} \right] \\
& + g \frac{\Gamma_{\text{ge}}}{(\Gamma^2 + |\Omega|^2)^2} \left(\Omega_+^* \partial_t \hat{\mathcal{E}}_+ + \Omega_-^* \partial_t \hat{\mathcal{E}}_- \right).
\end{aligned} \tag{2.35}
$$

Here we have allowed for a possible explicit time-dependence of the control-fields. Finally we substitute this expression into the optical coherence (2.30) and subsequently into the paraxial wave equation for the $(+)$- and $(-)$-modes of the probe-field. After some algebra we find

$$
\begin{aligned}
& \left(\partial_t \pm c\partial_z + \frac{c}{2\text{i}k}\Delta_\perp \right) \hat{\mathcal{E}}_\pm = -\text{i}\Delta\omega\,\hat{\mathcal{E}}_\pm \\
& - \frac{g^2 N}{\Gamma_{\text{ge}}} \left(\frac{|\Omega_\mp|^2 \hat{\mathcal{E}}_\pm - \Omega_\pm \Omega_\mp^* \hat{\mathcal{E}}_\mp}{\Gamma^2 + |\Omega|^2} \right) - \frac{g^2 N}{\Gamma_{\text{ge}}} \left(\frac{\Gamma^2}{\Gamma^2 + |\Omega|^2} \right) \hat{\mathcal{E}}_\pm \\
& - \frac{g^2 N}{(\Gamma^2 + |\Omega|^2)^2} \left(\hat{\mathcal{E}}_+ \left[\Omega_\pm \partial_t \Omega_+^* - \frac{\Omega_\pm \Omega_+^*}{\Gamma^2 + |\Omega|^2} \partial_t |\Omega|^2 \right] + \hat{\mathcal{E}}_- \left[\Omega_\pm \partial_t \Omega_-^* - \frac{\Omega_\pm \Omega_-^*}{\Gamma^2 + |\Omega|^2} \partial_t |\Omega|^2 \right] \right) \\
& - \frac{g^2 N}{(\Gamma^2 + |\Omega|^2)^2} \Omega_\pm \left(\Omega_+^* \partial_t \hat{\mathcal{E}}_+ + \Omega_-^* \partial_t \hat{\mathcal{E}}_- \right).
\end{aligned} \tag{2.36}
$$

In the following we will summarize conditions, which are well justified for EIT-systems, that we are going to use to simplify the system of equations (2.36) for the forward and backward propagating modes $\hat{\mathcal{E}}_\pm$.

Simplifying conditions

To further simplify the above expressions, the following assumptions are made:

$$\gamma_{gs}\gamma_{ge} \ll |\Omega|^2, \tag{2.37}$$

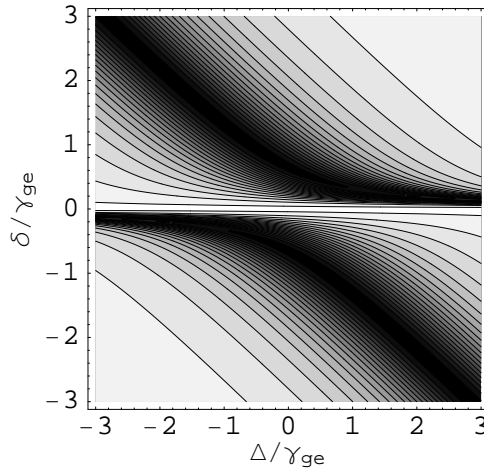$$\delta(\delta + \Delta) \ll |\Omega|^2. \tag{2.38}$$

Figure 2.4: Contour plot of the imaginary part of the susceptibility χ' as a function of the one-photon detuning of the control-field from the excited state and of the two-photon detuning of the probe and control-fields from the Raman transition. Dark area corresponds to high absorption and white area to low absorption. The transparency window at two-photon resonance, $\delta = 0$, is clearly visible. Parameters for the plot: $\Omega = 0.65\gamma_{ge}$ and $\gamma_{gs} = 10^{-2}\Omega$.

Both conditions are necessary to achieve EIT [27]. The first one states that the time to establish EIT, i. e. $\gamma_{ge}/|\Omega|^2$, should be much shorter than the decoherence time γ_{gs}^{-1} of the Raman coherence. The interpretation of the second relation is also straight forward; it says, that the dynamical Stark shift $|\Omega|^2/(\delta+\Delta)$ of the excited state should be much larger than a possible two-photon detuning δ [27]. The second condition can also be understood in the dark- and bright-state basis. The coupling of the dark-state to the bright-state of the 3-level Λ-system under consideration, is either proportional to non-adiabatic processes or to a finite two-photon detuning δ. The latter is negligible as long as $|\delta| \ll |\Omega|^2/|\Delta|$ [90]. If the two-photon detuning is to large, i. e. larger than the narrow EIT-transparency window, the probe-field is being absorbed as shown in fig. 2.4. In addition we want to make the following approximation

$$\frac{1}{(\Gamma^2 + |\Omega|^2)^2} \approx \frac{1}{|\Omega|^4}, \tag{2.39}$$

which holds if

$$\delta\gamma_{ge} \ll |\Omega|^2, \qquad \text{and} \qquad \Delta\gamma_{gs} \ll |\Omega|^2, \tag{2.40}$$

where we have used that in general $\gamma_{gs} \ll \gamma_{ge}$ [39]. These conditions can be understood in a similar fashion as the conditions above. They lead to a restriction of the possible operation time. The most serious condition is eq. (2.37) since the others can by fulfilled by choosing one- and two-photon resonance. As we will see later, we will have to slightly violate the exact two-photon resonance condition because of a phase matching which

has to be fulfilled. This does, however, not lead to a violation of the above conditions. To summarize this section: the entire dynamics has to take place, as in the standard slow-light and light storage experiments, within the EIT-window shown in fig. 2.4.

Introduction of mixing angles

Based on this approximations we can simplify (2.36) and obtain

$$
\begin{aligned}
\left(\partial_t \pm c\partial_z + \frac{c}{2ik}\Delta_\perp\right)\hat{\mathcal{E}}_\pm &= -i\Delta\omega\,\hat{\mathcal{E}}_\pm \\
&- \frac{g^2 N}{|\Omega|^2}\left(\frac{|\Omega_\mp|^2\hat{\mathcal{E}}_\pm - \Omega_\pm\Omega_\mp^*\hat{\mathcal{E}}_\mp}{\Gamma_{\text{ge}}}\right) - \frac{g^2 N}{|\Omega|^2}\Gamma_{\text{gs}}\hat{\mathcal{E}}_\pm \\
&- \frac{g^2 N}{|\Omega|^4}\left(\hat{\mathcal{E}}_+\left[\Omega_\pm\partial_t\Omega_+^* - \frac{\Omega_\pm\Omega_+^*}{|\Omega|^2}\partial_t|\Omega|^2\right] + \hat{\mathcal{E}}_-\left[\Omega_\pm\partial_t\Omega_-^* - \frac{\Omega_\pm\Omega_-^*}{|\Omega|^2}\partial_t|\Omega|^2\right]\right) \\
&- \frac{g^2 N}{|\Omega|^4}\Omega_\pm\left(\Omega_+^*\partial_t\hat{\mathcal{E}}_+ + \Omega_-^*\partial_t\hat{\mathcal{E}}_-\right).
\end{aligned}
\tag{2.41}
$$

This result suggest the introduction of the following mixing angles

$$
\sin^2\theta = \frac{g^2 N}{g^2 N + |\Omega|^2} \qquad \text{and} \qquad \cos^2\theta = \frac{|\Omega|^2}{g^2 N + |\Omega|^2},
\tag{2.42}
$$

as well as

$$
\sin^2\varphi = \frac{|\Omega_-|^2}{|\Omega|^2} \qquad \text{and} \qquad \cos^2\varphi = \frac{|\Omega_+|^2}{|\Omega|^2}.
\tag{2.43}
$$

For simplicity we choose the Rabi frequencies of the control-fields to be real, i. e. $\Omega_\pm = \Omega_\pm^*$. Using furthermore the expression $v_{\text{gr}} = c\cos^2\theta$ as an abbreviation, we find

$$
\begin{aligned}
\left(\partial_t + v_{\text{gr}}\partial_z + \frac{v_{\text{gr}}}{2ik}\Delta_\perp\right)\hat{\mathcal{E}}_+ &= -\left(i\Delta\omega\,\cos^2\theta + \Gamma_{\text{gs}}\sin^2\theta\right)\hat{\mathcal{E}}_+ \\
&- \sin^2\theta\frac{\Omega^2}{\Gamma_{\text{ge}}}\sin\varphi\left(\sin\varphi\,\hat{\mathcal{E}}_+ - \cos\varphi\,\hat{\mathcal{E}}_-\right) \\
&- \sin^2\theta\sin\varphi\left(\cos\varphi\,\partial_t\hat{\mathcal{E}}_- - \sin\varphi\,\hat{\mathcal{E}}_+\right) \\
&- \sin^2\theta\cos\varphi\,\Omega^2\left[\hat{\mathcal{E}}_+\partial_t\left(\frac{\cos\varphi}{\Omega}\right) + \hat{\mathcal{E}}_-\partial_t\left(\frac{\sin\varphi}{\Omega}\right)\right]
\end{aligned}
\tag{2.44}
$$

and

$$
\begin{aligned}
\left(\partial_t - v_{\text{gr}}\partial_z + \frac{v_{\text{gr}}}{2ik}\Delta_\perp\right)\hat{\mathcal{E}}_- &= -\left(i\Delta\omega\,\cos^2\theta + \Gamma_{\text{gs}}\sin^2\theta\right)\hat{\mathcal{E}}_+ \\
&+ \sin^2\theta\frac{\Omega^2}{\Gamma_{\text{ge}}}\cos\varphi\left(\sin\varphi\,\hat{\mathcal{E}}_+ - \cos\varphi\,\hat{\mathcal{E}}_-\right) \\
&+ \sin^2\theta\cos\varphi\left(\cos\varphi\,\partial_t\hat{\mathcal{E}}_- - \sin\varphi\,\hat{\mathcal{E}}_+\right) \\
&- \sin^2\theta\sin\varphi\,\Omega^2\left[\hat{\mathcal{E}}_+\partial_t\left(\frac{\cos\varphi}{\Omega}\right) + \hat{\mathcal{E}}_-\partial_t\left(\frac{\sin\varphi}{\Omega}\right)\right].
\end{aligned}
\tag{2.45}
$$

As we will see later on is v_{gr} not the true group velocity of the field modes. However, for convenience we will stick to this definition since it is the definition for the group velocity in the case of standard slow-light [1, 3, 27]. The structure of the above equations suggests the introducution of a new set of *normal* modes. We will see in the next section that this will turn them into a more transparent form.

2.2.4 Normal modes

In order to approximately decouple the field equations we introduce the following normal modes

$$
\begin{bmatrix} \hat{\mathcal{E}}_S \\ \hat{\mathcal{E}}_D \end{bmatrix} = \begin{bmatrix} \cos\varphi & \sin\varphi \\ -\sin\varphi & \cos\varphi \end{bmatrix} \begin{bmatrix} \hat{\mathcal{E}}_+ \\ \hat{\mathcal{E}}_- \end{bmatrix}. \tag{2.46}
$$

Using the unitary transformation (2.46) we define a new pair of normal modes which we will term sum- ($\hat{\mathcal{E}}_S$) and difference-mode ($\hat{\mathcal{E}}_D$). In the new representation we find the following set of differential equations

$$
\left(\partial_t + v_{\mathrm{gr}} \cos 2\varphi \, \partial_z + \frac{v_{\mathrm{gr}}}{2\mathrm{i}k} \Delta_\perp \right) \hat{\mathcal{E}}_S = - \left(\dot{\theta} \tan\theta + \mathrm{i}\Delta\omega \, \cos^2\theta + \Gamma_{\mathrm{gs}} \sin^2\theta \right) \hat{\mathcal{E}}_S
$$
$$
+ \left(\dot{\varphi} \cos^2\theta + v_{\mathrm{gr}} \sin 2\varphi \, \partial_z \right) \hat{\mathcal{E}}_D
$$
$$
+ v_{\mathrm{gr}} \varphi' \left(\sin 2\varphi \, \hat{\mathcal{E}}_S + \cos 2\varphi \, \hat{\mathcal{E}}_D \right), \tag{2.47}
$$

and

$$
\left(\partial_t - c \cos 2\varphi \, \partial_z + \frac{c}{2\mathrm{i}k} \Delta_\perp \right) \hat{\mathcal{E}}_D = - \left[\mathrm{i}\Delta\omega + \left(\Gamma_{\mathrm{gs}} + \frac{\Omega^2}{\Gamma_{\mathrm{ge}}} \right) \tan^2\theta \right] \hat{\mathcal{E}}_D
$$
$$
- \left(\dot{\varphi} - c \sin 2\varphi \, \partial_z \right) \hat{\mathcal{E}}_S
$$
$$
+ c \, \varphi' \left(\cos 2\varphi \, \hat{\mathcal{E}}_S - \sin 2\varphi \, \hat{\mathcal{E}}_D \right). \tag{2.48}
$$

We have taken into account here that the mixing angles θ and φ can depened on both space and time. For simplicity we have neglected the transversal dependence of the mixing angles. The dot denotes, as usual, the derivative with respect to time and the prime denotes the derivative with respect to the z-coordinate. In eq. (2.47) we have used $\sin^2\theta \, \partial_t \ln\Omega = -\tan\theta \partial_t\theta$ which we find by differentiation of $\tan\theta(z,t) = g\sqrt{N}/\Omega(z,t)$.

Equations (2.47) and (2.48) are the first major result of this chapter. We will give now a brief discussions of the occuring terms. The above equations are a set of coupled first order (in z and t), linear differential equations. The second term of each left-hand side is the group velocity of the corresponding normal mode. It is remarkable that both group velocities can be altered using the external control-fields via the factor

$$
\cos 2\varphi(z,t) = \frac{\Omega_+^2(z,t) - \Omega_-^2(z,t)}{\Omega_+^2(z,t) + \Omega_-^2(z,t)}. \tag{2.49}
$$

This additional factor in the group velocity of the sum- and difference-mode is a signature of the phenomenon of stationary light [12, 11]. The first line on the right hand side of each equation describes a phase shift of the fields due to a wavevector mismatch and due to detuning or correspondingly the fields' absorption. By appropriately choosing one- and two-photon detuning we can avoid this phase shift. As long as the decay rate of the Raman coherence is not negligible, absorption always occurs.

A non-vanishing time derivative of the mixing angle φ describes non-adiabatic coupling between the normal modes. In a first approach we will neglect this coupling. The second expressions in the same brackets will turn out to be the most important ones for the forthcoming sections and include a number of phenomena such as diffusion and spatial compression of the fields. The last line of each equation shows that cross-coupling between the normal modes occurs as long as the spatial change of the control-fields is not negligible. We see that the set of equations decouples if, and only if, the external control-fields do not change in space and time and one of the two control-fields is zero, i. e. $\sin 2\varphi = 0$. This is the earlier studied case of slow light which we will not consider here [1]. Before we proceed we apply to the above set of equations the *phase matching* condition

$$\delta = -\Delta\omega \cot^2\theta = -\Delta k\, c\, \Omega^2/(g^2 N) \tag{2.50}$$

and neglect for simplicity the transversal derivatives , which simplifies the equations to

$$\begin{aligned}
\left(\partial_t + v_{\mathrm{gr}}\cos 2\varphi\, \partial_z\right)\hat{\mathcal{E}}_S = &-\left(\dot\theta\tan\theta + \gamma_{\mathrm{gs}}\sin^2\theta\right)\hat{\mathcal{E}}_S \\
&+ \left(\dot\varphi\cos^2\theta + v_{\mathrm{gr}}\sin 2\varphi\, \partial_z\right)\hat{\mathcal{E}}_D \\
&+ v_{\mathrm{gr}}\varphi'\left(\sin 2\varphi\,\hat{\mathcal{E}}_S + \cos 2\varphi\,\hat{\mathcal{E}}_D\right),
\end{aligned} \tag{2.51}$$

and

$$\begin{aligned}
\left(\partial_t - c\cos 2\varphi\, \partial_z\right)\hat{\mathcal{E}}_D = &-\left[\left(\gamma_{\mathrm{gs}} + \frac{\Omega^2}{\Gamma_{\mathrm{ge}}}\right)\tan^2\theta\right]\hat{\mathcal{E}}_D \\
&- \left(\dot\varphi - c\sin 2\varphi\, \partial_z\right)\hat{\mathcal{E}}_S \\
&+ c\,\varphi'\left(\cos 2\varphi\,\hat{\mathcal{E}}_S - \sin 2\varphi\,\hat{\mathcal{E}}_D\right).
\end{aligned} \tag{2.52}$$

In the case of a small group-velocity, i. e. if $v_{\mathrm{gr}} \ll c$, the *phase matching* condition (2.50) does not lead to a violation of the EIT condition eq. (2.38) and hence the probe-field will not be absorbed. This is since

$$\delta = -\Delta\omega \cot^2\theta = -\Delta\omega \frac{v_{\mathrm{gr}}}{c - v_{\mathrm{gr}}} \approx -\Delta\omega \frac{v_{\mathrm{gr}}}{c}, \tag{2.53}$$

i. e. the two-photon detuning can be chosen arbitrarily small in the small group veloctiy regime. The condition can easily be accomplished experimentally [88] and leads in addition to a transversal guiding of the probe-fields as explained in [86]. Since we do not take transversal effects into account, we will here not discuss this issue any further. For simplicity we will drop the terms proportional to $\partial_t\varphi$ and $\partial_t\theta$. We will cosider them in section 2.5.2 where we take nonadiabatic corrections into account. To make the discussion in the next sections more transparent we will also set the Raman coherence decay rate $\gamma_{gs} = 0$.

2.2.5 Pulse matching and adiabatic elimination

Pulse matching

When considering the set of equations (2.51) and (2.52) one makes the following observations: In the case of a non-vanishing Raman decay rate γ_{gs} both normal modes are absorbed. Even in the non-realistic limiting case of $\gamma_{gs} = 0$, one recognizes from eq. (2.52) that the difference mode is strongly absorbed with a rate

$$\frac{\Omega^2}{\Gamma_{ge}} \tan^2 \theta = \frac{g^2 N}{\Gamma_{ge}}. \tag{2.54}$$

As a consequence the amplitudes of the retrieved fields approach a configuration where the difference mode vanishes, i. e. $\hat{\mathcal{E}}_D \to 0$, which means that the probe-field amplitudes match those of the control-fields

$$\frac{\mathcal{E}_+}{\mathcal{E}_-} \to \cot \varphi = \frac{\Omega_+}{\Omega_-}. \tag{2.55}$$

The phenomenon of *shape matching of pulses* is well known for EIT systems and was observed first by Harris [91]. One may understand eq. (2.55) by considering the semi-classical version, i. e. classical field and quantized atom, of the model considered here. In this case the dark-state is given by

$$|DS\rangle = \frac{\Omega_c |g\rangle - \Omega_p |s\rangle}{\sqrt{\Omega_p^2 + \Omega_c^2}}, \tag{2.56}$$

where Ω_c and Ω_p are the Rabi frequencies of the control and probe-fields respectively. In our four-wave mixing scheme the dark-state (2.56) is either established by $\Omega_{p,+}$ and $\Omega_{c,+}$ or by its backward propagating counterpart. One immediately verifies that these two dark-states $|DS_+\rangle$ and $|DS_-\rangle$ coincide if the fields fulfill eq. (2.55), i. e. $\Omega_{p,+}/\Omega_{p,-} = \Omega_{c,+}/\Omega_{c,-}$ [92]. Hence, coupling of the forward and backward propagating modes via the common dark-state leads to pulse matching of the participating fields. In our case due to phase-matching and due to the Doppler-freeness this pair is given either by Ω_p^+ and Ω_c^+ or by the backward propagating couple. It should be noted that even if the ratio of the control-field envelopes is spatially constant but not equal to unity the difference mode will be generated out of the sum mode until the latter is constant in space. This is the coupling mentioned above, which will give rise to a slow spatio-temporal evolution.

Adiabatic elimination of the difference mode

Before discussing several control-field configurations we will adiabatically eliminate the difference mode in the set of eqs. (2.51) and (2.52). To this end we introduce the characteristic time T_D of changes and length L_D of changes inside the medium for the difference mode. In the limit of $|\Gamma_{ge}|/g^2 N T_D \ll 1$ and $|\Gamma_{ge}|c/g^2 N L_D \ll 1$ we can negelect the left hand side of eq. (2.52). If we furthermore assume that the control-field changes sufficiently

slow in space such that $c|\varphi'||\Gamma_{ge}|/g^2 N \ll 1$, we can also drop the term proportional to the difference mode in the last bracket on the right hand side of eq. (2.52). Using this we find

$$\hat{\mathcal{E}}_D(z,t) = \frac{\Gamma_{ge}c}{g^2 N}\Big[\varphi'\cos(2\varphi) + \sin(2\varphi)\partial_z\Big]\hat{\mathcal{E}}_S(z,t). \tag{2.57}$$

To gain a simple physical understanding of these assumptions we consider the case of one- and two-photon resonance, i. e. $\Delta = \delta = 0$. In this case the first of the above conditions simplifies to $L_{\text{abs}} \ll cT$ and the second one to $L_{\text{abs}}/L \ll 1$, where $L_{\text{abs}} = c\gamma_{ge}/g^2 N$ is the absorption length of the probe-field in absence of EIT. Hence, the first condition states that the absorption length should be much less the typical vacuum-pulse length and the second one that the optical density of the medium $OD = L/L_{\text{abs}}$ should be much larger than unity. Since we consider optically thick media, the second condition is fulfilled by definition. To give some judgement about the first condition we consider the light storage experiments. In this case the typical length of the light pulse is on the order of some kilometer due to the requirement, that the pulse spectrum has to fit initially into the EIT-window. The absorption length on the other hand is on the order of some millimeter for optically thick media. Thus the first condition is also satisfied. In the case of one- and two-photon resonance eq. (2.57) reads

$$\hat{\mathcal{E}}_D(z,t) = L_{\text{abs}}\Big[\varphi'\cos(2\varphi) + \sin(2\varphi)\partial_z\Big]\hat{\mathcal{E}}_S(z,t). \tag{2.58}$$

2.3 Spatially *homogeneous* retrieval beams

Within this subsection we will restrict ourselves to the discussion of spatially homogeneous and time independent retrieval beams, which means that $\dot{\varphi} = 0$ and $\varphi' = 0$. Furthermore we set the Raman coherence decay rate to zero, which means that all the process happen on a time scale which is much shorter than γ_{gs}^{-1}. The field configuration to realize the spatial homogeneous case is given by paraxial laser beams with a negligible curvature of the phase fronts, i. e. we work in the plain wave regime. In this case the propagation equations for the sum and difference mode simplify to

$$(\partial_t + v_{\text{gr}}\cos 2\varphi\,\partial_z)\,\hat{\mathcal{E}}_S = v_{\text{gr}}\sin 2\varphi\,\partial_z\hat{\mathcal{E}}_D, \tag{2.59}$$

and

$$(\partial_t - c\cos 2\varphi\,\partial_z)\,\hat{\mathcal{E}}_D = -\frac{g^2 N}{\Gamma_{\text{ge}}}\hat{\mathcal{E}}_D + c\sin 2\varphi\,\partial_z\,\hat{\mathcal{E}}_S. \tag{2.60}$$

2.3.1 Equal control-field amplitudes

Within this section we want to study the case of equal control-field intensities. This amounts to

$$\cos 2\varphi = 0, \tag{2.61}$$
$$\sin 2\varphi = 1, \tag{2.62}$$

and hence the set of equations for the sum and difference mode simplify to

$$\partial_t \hat{\mathcal{E}}_S = v_{\text{gr}} \, \partial_z \hat{\mathcal{E}}_D, \tag{2.63}$$

$$\partial_t \hat{\mathcal{E}}_D = -\frac{g^2 N}{\Gamma_{\text{ge}}} \hat{\mathcal{E}}_D + c \, \partial_z \, \hat{\mathcal{E}}_S. \tag{2.64}$$

One immediately realizes that this choice of control-fields leads to a vanishing of the group velocity terms in the propagation equations. The dressing of the medium changes the propagation properties in a very drastic way, as we will see now.

Telegraph equation in a dielectric medium

In order to find a deeper understanding of the field dynamics we rewrite in a first step the above set of field equations (2.63) and (2.64) into a second order partial differential equation. One can easily verify that the equation holds for both the sum and the difference mode. The calculation results in

$$\partial_z^2 \hat{\mathcal{E}}(z,t) = \left[\frac{1}{c v_{\text{gr}}} \partial_t^2 + \frac{1}{v_{\text{gr}} L_{\text{abs}}} \partial_t \right] \hat{\mathcal{E}}(z,t). \tag{2.65}$$

Eq. (2.65) is a representation of the telegraph equation which is usually used to describe the propagation of electromagnetic waves along transmission lines.

If the absorption length of the medium in absence of EIT L_{abs} tends to infinity the equation reduces to the free space wave equation. This is because in this limit the group velocity v_{gr} tends to the vacuum speed of light. By applying a spatial and temporal Fourier transformation to eq. (2.65) we find that the dispersion relation of the dressed medium is given by

$$k^2 = \left(\frac{\omega}{c} \right)^2 \frac{c}{v_{\text{gr}}} \left[1 + \mathrm{i} \frac{c}{\omega L_{\text{abs}}} \right]. \tag{2.66}$$

Solving equation (2.66) for the angular frequency we find

$$\omega(k) = -\frac{\mathrm{i}c}{2 L_{\text{abs}}} \pm c \sqrt{\frac{v_{\text{gr}}}{c} k^2 - \frac{1}{4 L_{\text{abs}}^2}}, \tag{2.67}$$

which is depicted in fig. 2.5. We note that the considered dispersion relation is given with respect to the slowly varying sum or difference mode, i. e. not to freely propagating modes and hence the interpretation is not as straight forward. The figure shows that in the low-Fourier-frequency or the long-wavelength limit the free propagation of the sum and difference mode are forbidden. Furthermore, we see that if the free propagation of the modes is allowed it is accompanied by absorption.

If the Fourier wavenumber k is much smaller than the critical wavenumber

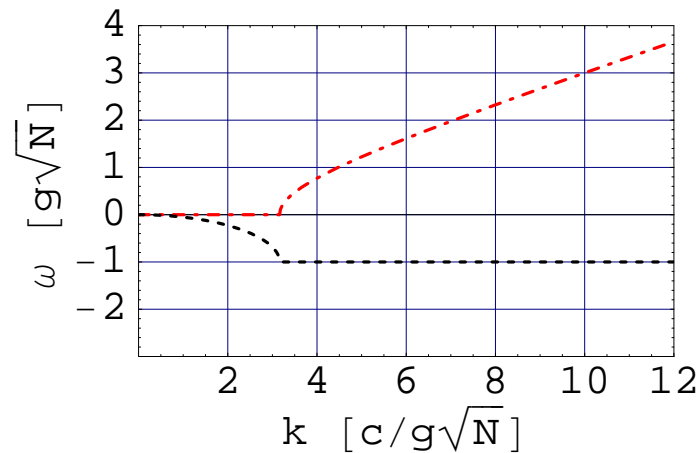$$k_c = \sqrt{\frac{c}{v_{\text{gr}}} \frac{1}{2 L_{\text{abs}}}}, \tag{2.68}$$

Figure 2.5: Dispersion relation for stationary light. The dash-dotted (red) line is the real part of the complex angular frequency eq. (2.67), the dashed (black) line represents the imaginary part. The parameters for this plot are $L_{\mathrm{abs}} = 1\,c/g\sqrt{N}$ and $v_{\mathrm{gr}} = 0.1\,c$.

which we determine by setting the radicand equal to zero in eq. (2.67), the k^2-term in eq. (2.67) and hence the term proportional to the second order time derivative in eq. (2.65) are negligible. In this case the considered wave equation reduces to a diffusion equation which we will discuss in more detail in the next section. For a Fourier transform limited pulse this means that its spatial variance should not be smaller than the critical wavelength $\lambda_c = 2\pi/k_c$. In the small group velocity regime this characteristic length

$$\lambda_c = 4\pi\sqrt{\frac{v_{\mathrm{gr}}}{c}}\,L_{\mathrm{abs}}, \tag{2.69}$$

is much smaller than the absorption length in absence of EIT. As we will show later on our considerations are restricted to wave packets with a width $\sigma \geq L_{\mathrm{abs}}$, hence this term is negligible. Even though the description using the telegraph equation is generally valid, we simplify the considerations by making use of the property that the examined medium is optically thick. As noted in section 2.2.5 the optical thickness of the medium allows us to adiabatically eliminate the difference mode, i. e. we assume that its dynamics takes place on a time scale which is much larger than L_{abs}/c.

Adiabatic elimination - the diffusion equation

Following the argumentation presented in section 2.2.5 we adiabaticly eliminate the difference mode in eq. (2.64) and find a diffusion equation for the sum mode

$$\partial_t\,\hat{\mathcal{E}}_S = v_{\mathrm{gr}}\,L_{\mathrm{abs}}\,\partial_z^2\,\hat{\mathcal{E}}_S. \tag{2.70}$$

The dynamics of the sum-mode resembles that of a Brownian particle in an emulsion. The dynamics of the fields in this specifically dressed dielectric vapor is characterized by a
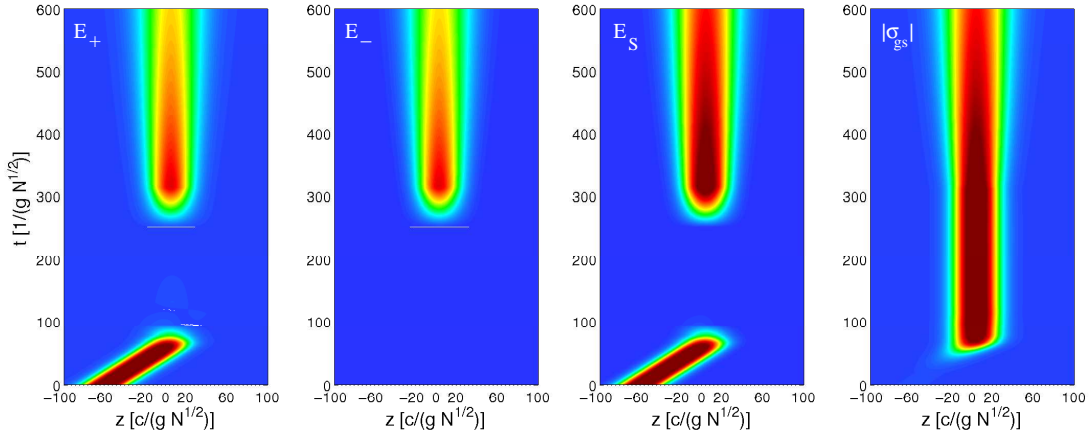
Figure 2.6: Numerical simulation of the storage and partial retrieval of a light pulse. The color code represents the amplitude of the probe-field components. A forward propagating field ($\mathcal{E}_+$) is stored. Subsequently the spin coherence (σ_{gs}) is read out by two counter-propagating control-fields. In the retrieval process also a backward ($\mathcal{E}_-$) propagating component is excited as well as the sum mode ($\mathcal{E}_S$). The diffusively spreading dynamics of the fields is accompanied by an adiabatically following spin coherence. The parameters used for the simulations are: $\delta = \Delta = \Delta\omega = 0$, $\gamma_{ge} = 1\, g\sqrt{N}$, $\gamma_{gs} = 0$, $\Omega_\pm(0) = 100\, g\sqrt{N}$ and the initial width of the Gaussian wave-packet was $\Delta z_0 = \sqrt{2} * 10\, c/(g\sqrt{N})$.

diffusion constant $D = v_{gr}L_{\mathrm{abs}}$. Here $v_{\mathrm{gr}} = c\cos^2\theta$ is the earlier introduced group velocity and L_{abs} is the absorption length of the probe-field in absence of EIT. The constant combines two important physical quantities. These are: (a) the mean velocity v_{gr} of a photon wave-packet traveling through a medium of randomly distributed scatterers and (b) the mean free path L_{abs} of the photons in the medium. The *Brownian motion* is shown in one dimension in fig. 2.6 as a false color image. Due to the positivity of the diffusion constant D the dynamics of the system leads to a spreading of the wave-packet. In fig. 2.6 we see that the initial field distribution, which starts to propagate into the positive z-direction at $z(t=0) = -60\, c/g\sqrt{N}$, is being stored into the collective spin coherence $\hat{\sigma}_{gs}$ at $t \approx 100\,(g\sqrt{N})^{-1}$. Later at $t \approx 200\,(g\sqrt{N})^{-1}$, the coherence is read out again using two counter-propagating control-fields. The control-field behavior as well as the corresponding group velocities for the forward and backward direction are shown in fig. 2.7. The data for the false color images fig. 2.6 are obtained by a numerical integration of the full set of atomic density matrix equations (2.5-2.10) plus the reduced wave equation (2.19). These equations are implemented into the programs after the secular approximation, mentioned in section 2.2.1. The diffusive spreading occurs also in the spin coherence $\hat{\sigma}_{gs}$. This happens since the spin coherence follows according to

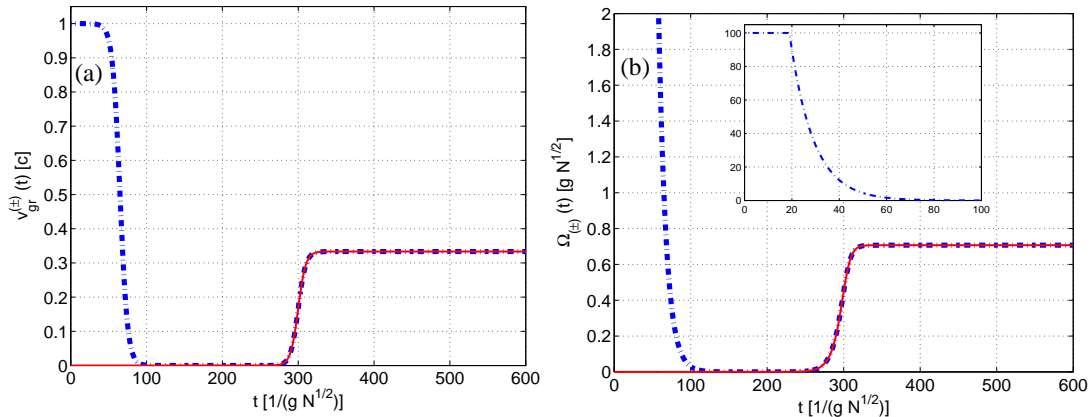$$\hat{\sigma}_{gs} = -\frac{1}{\sqrt{N}}\tan\theta\,\hat{\mathcal{E}}_S \tag{2.71}$$

Figure 2.7: The figures show (a) the group velocities $v_{gr}^{\pm} = c \cos^2 \theta_{\pm}$ and (b) the control-field amplitudes $\Omega_{\pm}$ as function of time. Both subplots show the storage and retrieval phase. The forward control-field Ω_{+} is used for both the storage and retrieval procedure and represented by a dash-dotted (blue) line. The corresponding group velocity has the same color code. To achieve stationary light both the forward and backward propagating control fields have to be simultaneously switched on. This is done at $t \approx 290(g\sqrt{N})^{-1}$. The backward direction is represented by the solid red lines.

adiabatically the dynamics of the sum normal mode. The expression can be derived from eq. (2.32) in lowest order of the adiabatic approximation, i. e. by neglecting the time derivative of the spin coherence and applying the conditions derived in section 2.2.3. Fig. 2.8 shows cuts through the field distribution of the forward propagating mode as well as the spin coherence for fixed times. After a short, initial time period the control-fields nolonger change in time (see fig. 2.7), i. e. at this point in time the simulation enters the diffusion phase. In this phase the field maxima decrease, as shown in fig. 2.8, whereas the width of the field distributions increase. This is a clear indication of a diffusive type of process. A more quantitative tests of the properties of a diffusion process will be given in the forthcoming section, especially in section 2.3.2.

Properties of the quasi-stationary field in the diffusion limit

It is well known that for quantities following a diffusion equation such as the sum field $\mathcal{E}_S$ the zeroth moment

$$\langle \mathcal{F} \rangle_0(t) = \int\limits_{-\infty}^{\infty} \mathcal{F}(z,t) \, \mathrm{d}z \tag{2.72}$$

is a constant of motion. Because of eq. (2.57) and (2.71) the difference mode and the spin coherence adiabatically follow the diffusive behavior of the sum mode. Hence, also these field variables obey a diffusion equation. This property can also be found numerically as is shown in fig. 2.9, where after an initial period of varying control fields, the system reaches
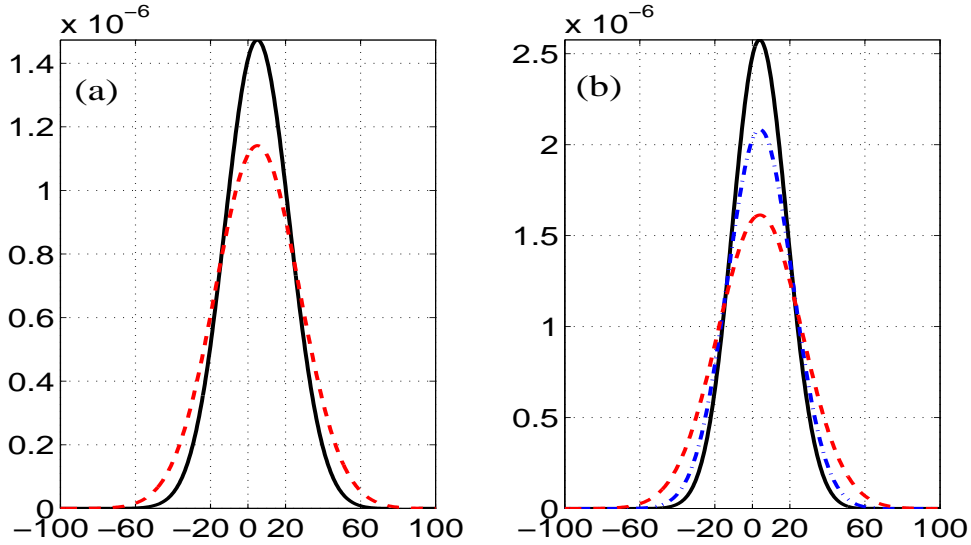
Figure 2.8: The figures show (a) cuts through the field distribution of the forward propagating mode ($\mathcal{E}_+$) at time $t = 400(g\sqrt{N})^{-1}$ (solid black line) and at $t = 600(g\sqrt{N})^{-1}$ (dashed red line). The cuts in (b) at $t = 200(g\sqrt{N})^{-1}$ (solid black line), $t = 400(g\sqrt{N})^{-1}$ (dashed-dotted blue line) and at $t = 600(g\sqrt{N})^{-1}$ (dashed red line) are cuts through the spin coherence (σ_{gs}) presented in fig. 2.6. The picture clearly shows that the fields spread in the course of time.

the diffusion regime. The numerical data for these plots are taken from a simulation without any previous storage period, i. e. the control-fields are adjusted such that the pulse is immediately transfered into a stationary light pulse. This is the standard approach in experiments [87].

Furthermore, we can see by comparing fig. (2.9) (a) & (b) with (c) that the definition of the sum mode can be applied to find the height of the zeroth moment of the sum mode for large times, i. e. we have $2\langle\mathcal{E}_\pm\rangle_0/\sqrt{2} = \langle\mathcal{E}_S\rangle_0$. The zeroth order moment of the difference mode only gets excited in this example due to non-adiabatic processes. This excitation vanishes very fast and the difference mode turns out to be a purely odd function with vanishing zeroth moment (integral).

Finally we can see that almost the whole probe pulse is stored in the spin coherence, fig. 2.9 (c), since the pulse area of the spin coherence is only slightly smaller than the initial probe pulse area given by 10^{-4} (see fig. 2.9 (a) for $t = 0$). This reflects the fact that we work in the small group velocity regime.

We continue by considering the temporal evolution of the total number of quanta in the diffusion limit of stationary light. This is of particular interest since for quantum information applications there should be a minimum loss of total excitations. Two major loss channels exist within the system of which one is the decay of ground state coherence and the other one spontaneous emission from the excited level. The origin of the first channel are either collisions between the relevant atoms or fluctuations of external fields. These processes lead to decoherence or dephasing of the Raman coherence. In the second
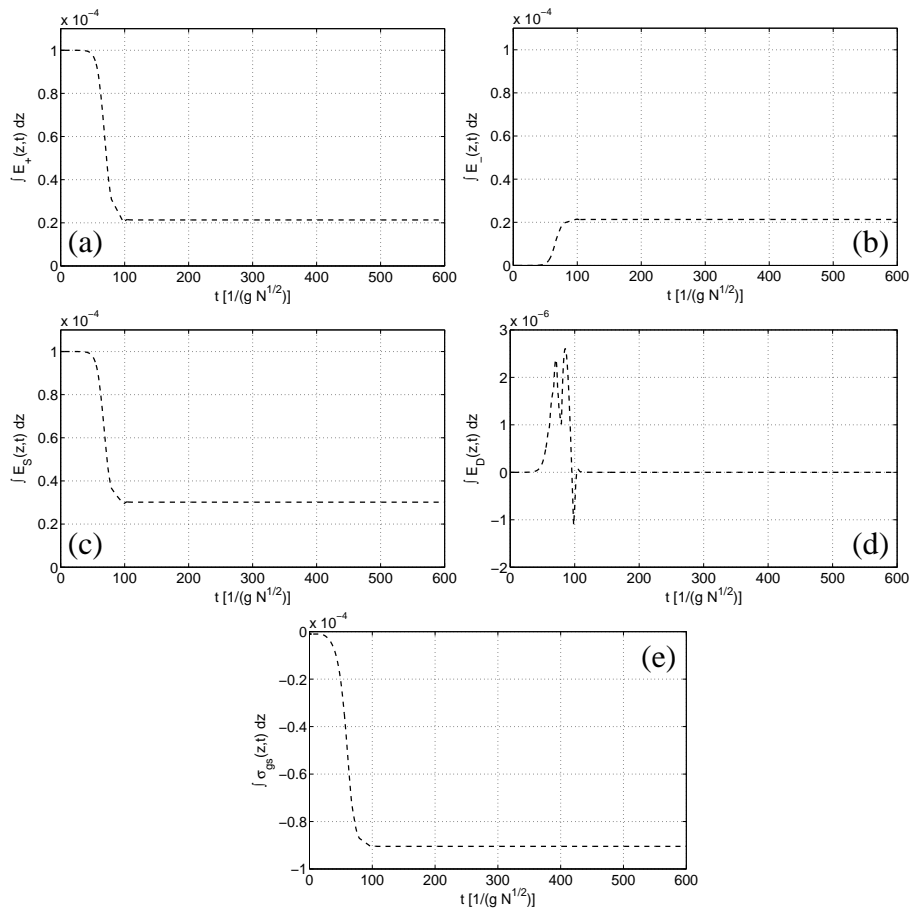
Figure 2.9: Temporal evolution of the zero moment of the (a) forward, (b) backward, (c) sum and (d) difference mode as well as of (c) the Raman spin coherence.

case loss of the excitation occurs due to spontaneous emission. To study the phenomenon of excitation loss, we consider the equation of motion for the number of photons in the stationary light field.

$$
n = n_+ + n_- = \int\limits_{-\infty}^{\infty} \left[|\mathcal{E}_+|^2 + |\mathcal{E}_-|^2 \right] \, \mathrm{d}z,
\tag{2.73}
$$

is the number of photons in the forward (n_+)/backward (n_-) probe-mode. Since the transformation between the forward and backward modes and the sum and difference modes is unitary, we have

$$
n = \int\limits_{-\infty}^{\infty} \left[|\mathcal{E}_D|^2 + |\mathcal{E}_S|^2 \right] \, \mathrm{d}z.
\tag{2.74}
$$

In the adiabatic limit under consideration the equations of motion for the sum and difference mode are given by

$$\partial_t \mathcal{E}_S = D\partial_z^2 \mathcal{E}_S, \tag{2.75}$$

$$\partial_t \mathcal{E}_D = 0, \tag{2.76}$$

which leads to following equation

$$\partial_t n = -2\,D \int (\partial_z \mathcal{E}_S(z,t))(\partial_z \mathcal{E}_S^*(z,t))\,\mathrm{d}z. \tag{2.77}$$

To derive eq. (2.77) we have used $\partial_t |\mathcal{E}_D|^2 = 0$, which is true because of eq. (2.76). The numerical simulation in fig. 2.10 (b) shows that this is strictly speaking not correct. Since $\int |\mathcal{E}_D(z,t)|^2 \mathrm{d}z$ yields however only a negligible contribution to n this is of no consequence here. Eq. (2.77) shows that the total number of excitations in the quasi-stationary light field decays in time. In the following we want to determine the relevant decay time. To this end we assume, that the field is regenerated in form of a Gaussian distribution from the spin coherence, i. e.

$$\mathcal{E}(z,t) = \frac{\mathcal{E}_0}{2\sqrt{2\pi}\sigma(t)}\,\exp\left(-\frac{1}{2}\left(\frac{z}{\sigma(t)}\right)^2\right), \tag{2.78}$$

with $\sigma(t) = \sqrt{\sigma(0) + 2\,D\,t}$. Making use of this ansatz equation (2.77) reads

$$\partial_t\,n = -\frac{D}{2\sqrt{\pi}\sigma(t)^3}|\mathcal{E}_0|^2. \tag{2.79}$$

and can easily be solved. The solution is

$$n(t) = n(t_0)\left\{1 + \left[\frac{\sigma(t_0)}{\sqrt{\sigma(t_0)^2 + 2\,D\,t}} - \frac{\sigma(t_0)}{\sqrt{\sigma(t_0)^2 + 2\,D\,t_0}}\right]\right\}. \tag{2.80}$$

or setting $t_0 = 0$:

$$n(t) = n(0)\frac{\sigma(0)}{\sqrt{\sigma(0)^2 + 2\,D\,t}}. \tag{2.81}$$

One recognizes that the number of photons decreases non-exponentially, proportional to one over the sum-field width. The latter depends on the group velocity as well as the absorption length. The non-exponential decay can qualitatively be seen in fig. 2.10. It compares very well with the numerical simulation. In order to have negligible losses, the time over which a stationary pulse can be maintained is limited by

$$t \ll \frac{\sigma^2(0)}{D} = \frac{\sigma^2(0)}{v_{\mathrm{gr}}L_{\mathrm{abs}}}, \tag{2.82}$$

which is exactly the characteristic time for the spread of the initial wave-packet.
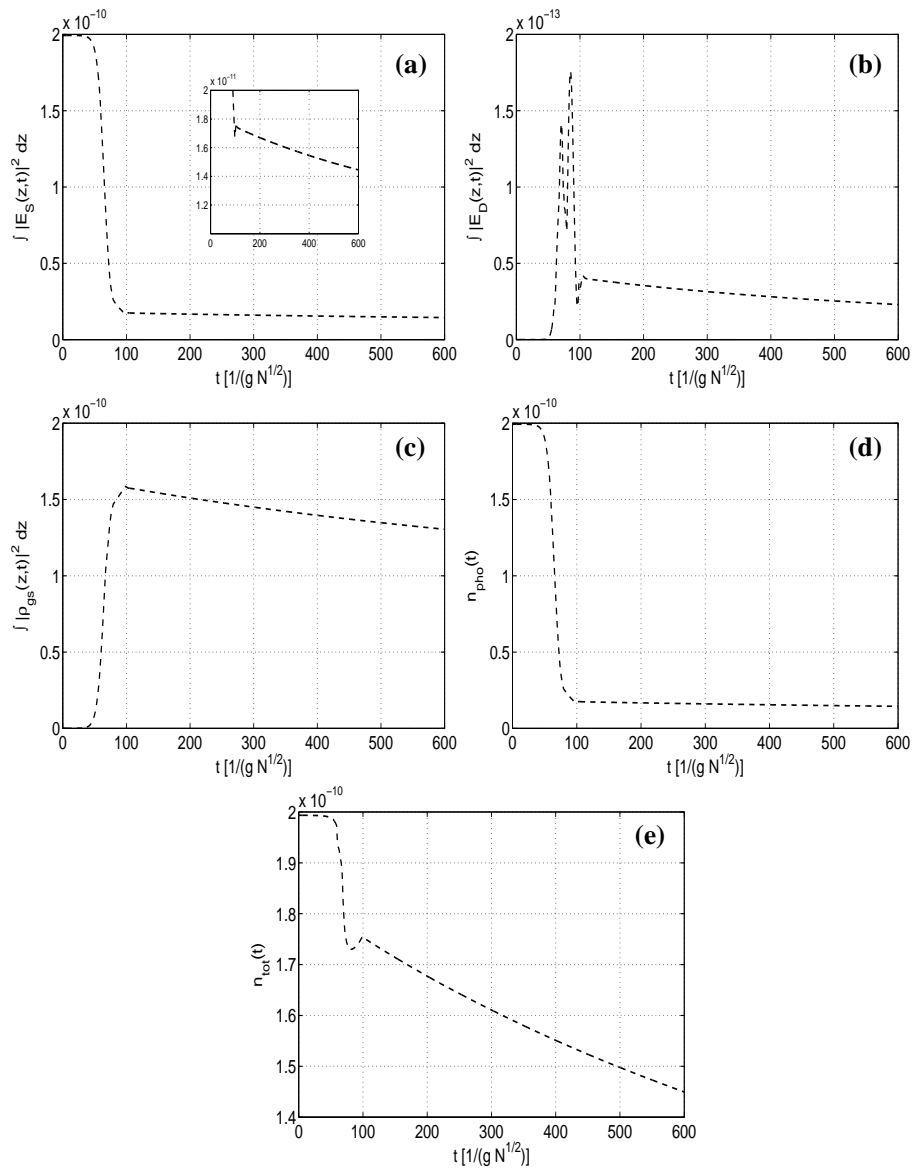
Figure 2.10: Temporal evolution of the number of excitations in (a) the sum mode and (b) the difference mode. Part (c) shows the evolution of the excitation stored in the spin coherence. The last two subfigures (d) and (e) show the dynamics of the total number of photons as well as the total excitation given by $n_{\mathrm{tot}} = n_{\mathrm{pho}} + \int |\rho_{gs}|^2 \mathrm{d}z$. Apparent is the non-exponential decay of the photon number as well as the total excitation. The numerical data is obtained from the simulation for fig. 2.11(b).

2.3.2 Temporal evolution of momenta beyond the adiabatic elimination of the difference-mode

In the previous section we have found a diffusive spreading of the field in the limit of large optical depth were the difference mode could be eliminated adiabatically. We want to drop the requirement of a large optical depth. The equations of motion eq. (2.63) and eq. (2.64) for the sum and difference mode have a special property, namely they do not couple between the even and odd share of the same field. Since any arbitrary function $f(x)$ can be decomposed into an even $f_e(x) = (f(x) + f(-x))/2$ and odd $f_o(x) = (f(x) - (f(-x))/2$ part we can deduce a set of four equations from the above set of equations. We find the even variant of equation (2.63)

$$\partial_t \hat{\mathcal{E}}_S^e(z,t) = v_{\text{gr}} \hat{\mathcal{E}}_D^o(z,t), \tag{2.83}$$

$$\partial_t \hat{\mathcal{E}}_S^o(z,t) = v_{\text{gr}} \hat{\mathcal{E}}_D^e(z,t). \tag{2.84}$$

An analog decomposition can be found for eq. (2.64). Based on this statement we are lead to the idea, that to determine the temporal evolution of the momenta, especially the field width of the sum mode, it is not necessary to calculate the fields based on the eqs. (2.63) and (2.64). It might be simpler to solve the set of coupled ordinary differential equations for the field momenta. We define the moments of an arbitrary field $\mathcal{F}(z,t)$ by

$$\langle \mathcal{F} \rangle_n(t) = \int z^n \, \mathcal{F}(z,t) \mathrm{d}z. \tag{2.85}$$

By multiplying eq. (2.63) with z^2 and integrating over z, we find

$$\partial_t \langle \mathcal{E}_S \rangle_2(t) = \int_{-\infty}^{\infty} z^2 \partial_z \hat{\mathcal{E}}_D(z,t) \mathrm{d}z, \tag{2.86}$$

and by partial integration we find

$$\partial_t \langle \mathcal{E}_S \rangle_2(t) = -2 \, v_{\text{gr}} \langle \mathcal{E}_D \rangle_1(t), \tag{2.87}$$

where we have assumed that the first derivative vanishes at the integration limits. By multiplying eq. (2.64) with z and integration we additionally find

$$\partial_t \langle \mathcal{E}_D \rangle_1(t) = -\frac{g^2 N}{\Gamma_{ge}} \langle \mathcal{E}_D \rangle_1(t) + c \int_{-\infty}^{\infty} z \partial_z \mathcal{E}_S(z,t)$$

$$= -\frac{g^2 N}{\Gamma_{\text{ge}}} \langle \mathcal{E}_D \rangle_1(t) - c \langle \mathcal{E}_S \rangle_0(t). \tag{2.88}$$

and finally for the zeroth moment of the sum field

$$\partial_t \langle \mathcal{E}_S \rangle_0(t) = 0. \tag{2.89}$$

Hence it is a constant of motion in the case of vanishing Raman decay rate. To compare with our numerical results we will simplify the set of equations by presuming one- and two-photon resonance. Furthermore we will apply the initial conditions: $\langle \mathcal{E}_S \rangle_2(0) = \delta_0$ and $\langle \mathcal{E}_D \rangle_1(0) = 0$, because we start with an sum field with an certain initial width, i. e. δ_0, and have no excitation initially in the difference mode. The last of the equations above can be integrated immediately to find

$$\langle \mathcal{E}_S \rangle_0(t) = \langle \mathcal{E}_S \rangle_0(0). \tag{2.90}$$

To solve equation (2.88) we make the ansatz

$$\langle \mathcal{E}_D \rangle_1(t) = B(t) \, e^{-ct/L_{\mathrm{abs}}} \tag{2.91}$$

and find a simple differential equation for B, which can easily be integrated. Using the initial condition for the first moment $\langle \mathcal{E}_D \rangle_1$ of the difference field we retrieve the solution of eq. (2.88)

$$\langle \mathcal{E}_D \rangle_1(t) = \langle \mathcal{E}_S \rangle_0(0) \, L_{\mathrm{abs}} \left(\exp\left\{ -\frac{c}{L_{\mathrm{abs}}} t \right\} - 1 \right). \tag{2.92}$$

Integration of eq. (2.87) and applying the initial condition $\langle \mathcal{E}_S \rangle_2(0) = \delta_0$ we find after some calculations the solution for the second moment of the sum field

$$\langle \mathcal{E}_S \rangle_2(t) = \langle \mathcal{E}_S \rangle_2(0) + 2 v_{\mathrm{gr}} L_{\mathrm{abs}} \langle \mathcal{E}_S \rangle_0(0) \left(t + \frac{L_{\mathrm{abs}}}{c} \left(\exp\left\{ -\frac{c}{L_{\mathrm{abs}}} t \right\} - 1 \right) \right). \tag{2.93}$$

One recognizes that a larger absorption length L_{abs} only affects the short-time evolution, where the width increases quadratically in time. After this initial period the increase of the field width of the sum mode is linear in time with a slope given by $2 D = 2 v_{\mathrm{gr}} L_{\mathrm{abs}}$ (normalized to the initial probe pulse area). Figure 2.11 compares the analytical result with a numerical simulation. In the analytical result we have substituted the time-independent group velocity by a time-dependent one, i. e. $v_{\mathrm{gr}} \to v_{\mathrm{gr}}(t)$. Apart from the initial time period, the agreement between analytical predictions and numerical simulation is nearly perfect. The initial deviations are caused by non-adiabatic couplings on the numerical side and in case of the analytical calculations by the time-dependence of the group velocity.

2.3.3   Non-equal control-field amplitudes

In the case of non-equal control-field amplitudes the trigonometric functions in eq. (2.59) and (2.60) do not vanish. Following again the adiabatic elimination procedure given in section 2.2.5 and thereby using (2.57) we find a closed equation for the sum normal mode.

$$\left(\partial_t + v_{\mathrm{gr}} \cos 2\varphi \, \partial_z \right) \hat{\mathcal{E}}_S = v_{\mathrm{gr}} \, L_{\mathrm{abs}} \, \sin^2 2\varphi \, \partial_z^2 \hat{\mathcal{E}}_S. \tag{2.94}$$

Eq. (2.94) is a Fokker-Planck type equation with a finite drift and diffusion term. However, by applying the Galilei transformation $z' = z - v_{\mathrm{gr}} \cos(2\varphi) \, t$ to go from the initial to a uniformly moving frame, we find again a diffusion equation with diffusion constant

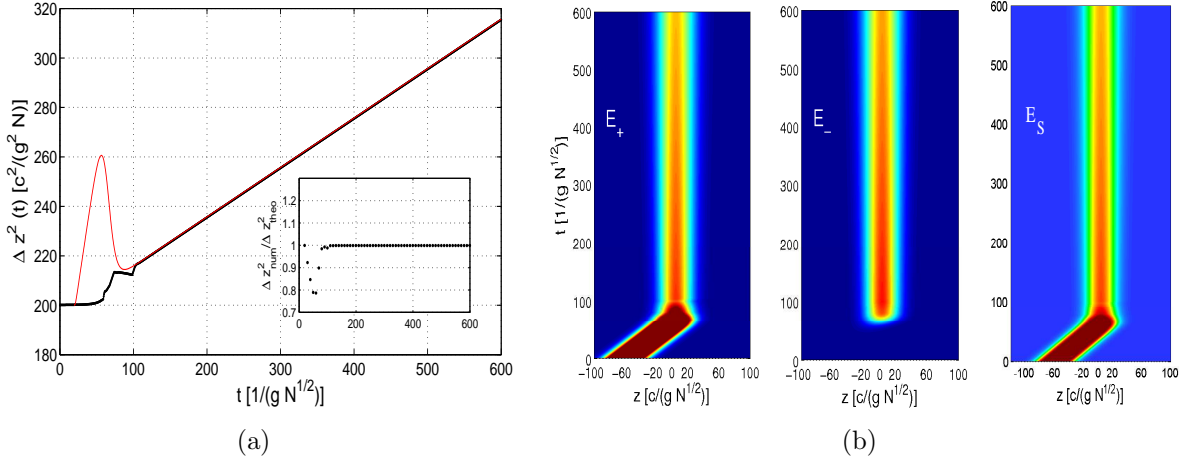$$\mathcal{D} = v_{\mathrm{gr}} \, L_{\mathrm{abs}} \, \sin^2(2\varphi). \tag{2.95}$$

Figure 2.11: (a) Shown is the temporal dynamics of the field widthof the envelope function of the sum mode. The red line corresponds to the analytic (see eq. (2.93)) and the black line to the corresponding numerical result. The later is based on the numerical propagation of the full set of Maxwell-Bloch equations after the secular approximation. The corresponding simulation is the one shown in subfigure (b). The inset shows the ratio of numerical and analytic solution. One recognizes nearly perfect agreement for large times, i. e. after the switching period. (b) The figures show that it is possible to directly convert an initial probe field pulse into a stationary pulse of light by simultaneously applying two-counterpropagating control fields with equal amplitudes while the probe pulse is still in the EIT-medium [87]. The diffusion behavior is suppressed compared to fig. 2.6, which is due the smaller final group velocity. All other numerical parameters are the same.

To summarize, the dynamics is described by a translational motion superimposed by a diffusive part. Thus the sum mode is only a quasi-stationary field, i. e. it still propagates, with a small but constant group velocity $v_{\mathrm{gr}} \cos(2\varphi)$.

Let us examine this in more detail. The group velocity of the sum mode $v_{\mathrm{gr}}^{(S)}$ is proportional to the difference of the Rabi frequencies $\Omega_\pm$

$$v_{\mathrm{gr}}^S = c \cos^2 \theta \cos 2\varphi = c \cos^2 \theta \frac{|\Omega_+|^2 - |\Omega_-|^2}{|\Omega_+|^2 + |\Omega_-|^2}. \tag{2.96}$$

Hence, propagation of the sum mode into the forward direction is achieved by choosing the Rabi frequency Ω_+ larger than that of the backward direction Ω_-. An example of such a process is shown in the figures 2.12, 2.13 and 2.14. Corresponding to the group velocities given in fig. 2.12 figure 2.13 shows the temporal evolution of the sum mode and the Raman coherence. We can see by comparing fig. 2.12 with fig. 2.13, that if the group velocity of either direction

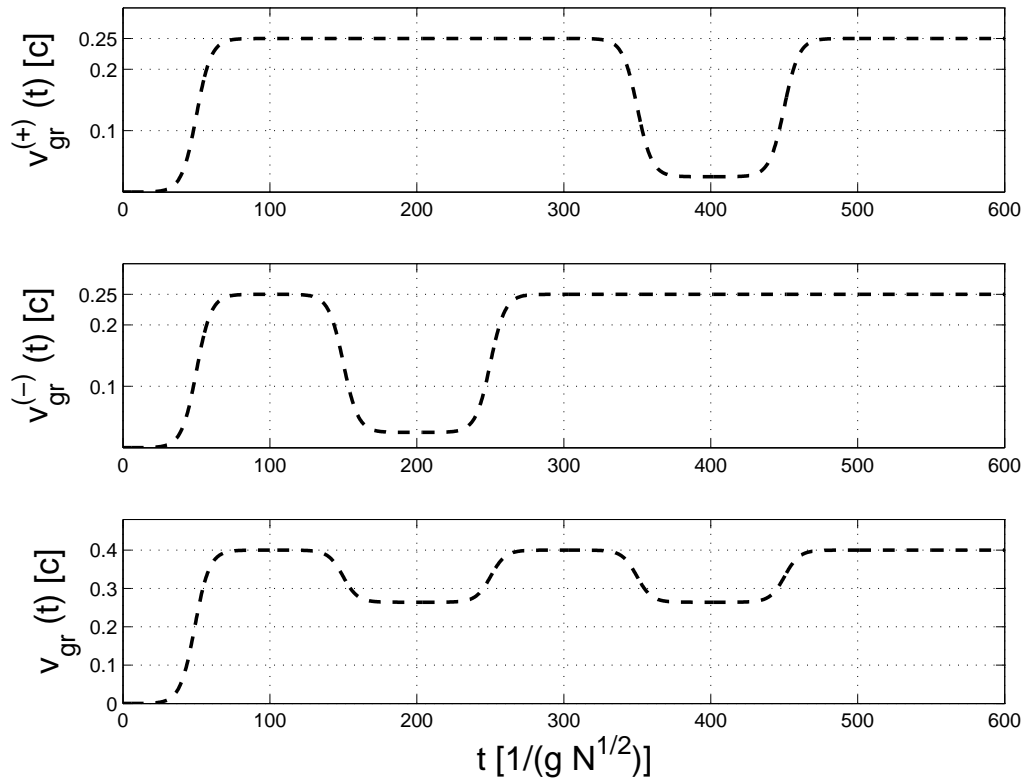$$v_{\mathrm{gr}}^{(\pm)} = c \cos^2 \theta_\pm = c \frac{\Omega_\pm^2}{\Omega_\pm^2 + g^2 N} \tag{2.97}$$

Figure 2.12: The independently controllable group velocities for the forward $(v_{\mathrm{gr}}^{(+)})$ and backward $(v_{\mathrm{gr}}^{(+)})$ propagating modes. The subfigure at the bottom shows the group velocity $v_{\mathrm{gr}} = c \cos^2 \theta$ computable by $v_{\mathrm{gr}}^{(+)}$ and $v_{\mathrm{gr}}^{(-)}$.

decreases, caused for example by the reduction of the corresponding Rabi frequency, the sum field will move into the direction defined by the wave-vector of the stronger coupling field.

2.4 Spatially *modulated* retrieve fields

Spatial manipulation of photonic excitation in collective atomic ensembles

In addition to its property to slow-down electromagnetic fields to incredibly low group velocities EIT is also a promising candidate to achieve nonlinear interaction at a low-light level [93]. It was shown that a light pulse may experience very large nonlinearities even at energy densities as low as one photon per atomic cross section [9, 10]. This has important potential applications to quantum computation, for new types of nonlinear spectroscopy [39], studies of correlation and noise at the few photon level [94] and resonant four-wave mixing of weak fields [95, 96]. With respect to quantum computation still one major challenge remains. To achieve a phase shift of π in a single-photon phase gate it is necessary to focus the pulses close to the diffraction limit of λ^2. Here we
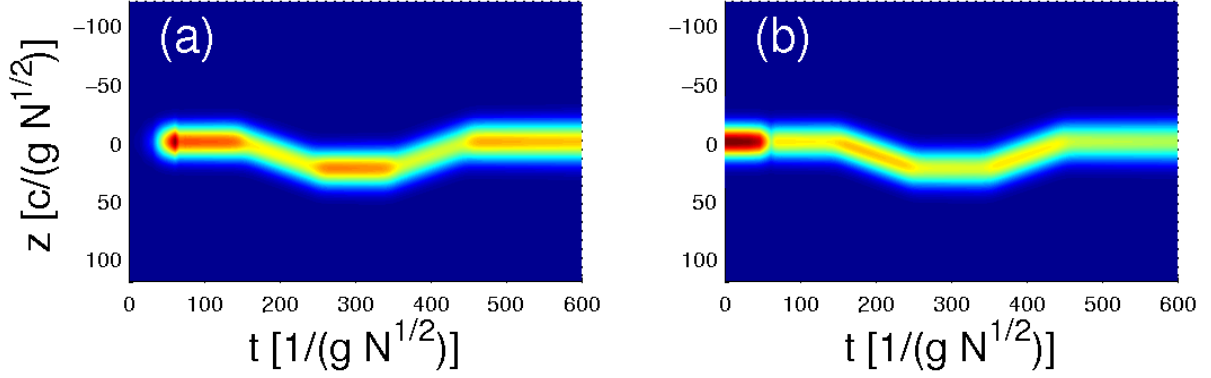
Figure 2.13: The figure shows the dynamics of the sum mode and the spin coherence for non-equal control-fields. The temporal evolution of the corresponding group velocities is depicted in fig. 2.12. (a) After the sum mode is read out of the Raman coherence it moves according to the dynamics of the control-fields first into the forward and later on into the backward direction. In fig. 2.14 the corresonding evolution of the forward and backward propagating modes is shown. (b) The Raman coherence follows adiabatically the temporal dynamics of the sum mode.

propose an approach which allows to coherently and adiabatically compress the probe-field excitation and thereby to achieve a higher nonlinear interaction energy. Compared to earlier approaches we also take advantage of the stationary light schemes to extend the
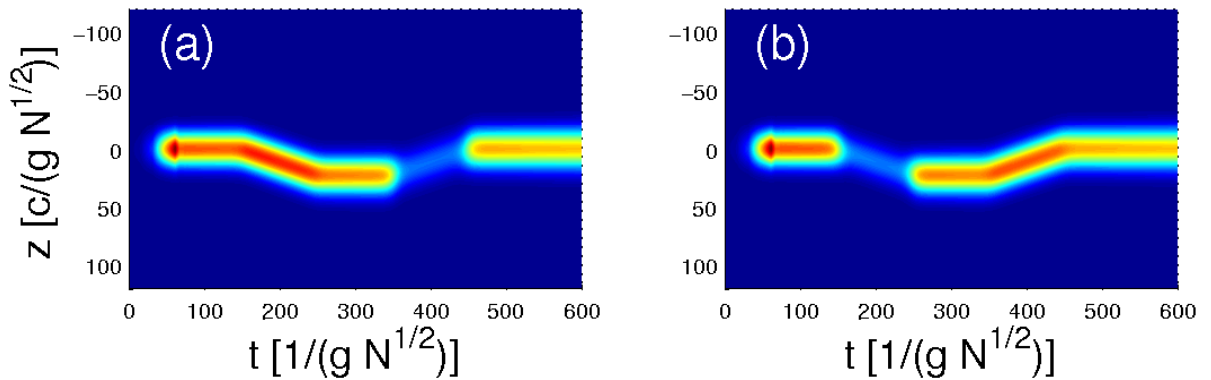

Figure 2.14: Temporal evolution of the (a) forward $(+)$ and (b) backward $(-)$ field modes. If the corresponding sum mode, shown in fig. 2.13, is stationary both modes are excited. In the case of forward propagation the backward mode is negligible (see (b)) and vice versa.
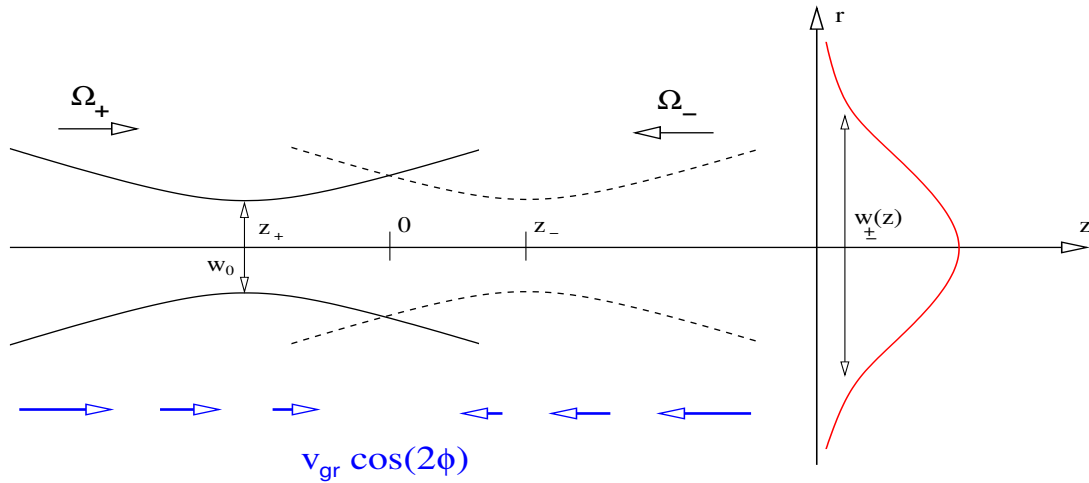
Figure 2.15: Field configuration for spatially varying group velocity. Shown are the lines of equal intensity for the Ω_+ and Ω_--control-field with their focal points located at z_+ and z_-. w_0 is the spot size of the Gaussian beams and $w_\pm(z)$ the beam width at a distance of z from of the foci at $z_\pm$. The effective group velocity of the sum mode for this configuration is indicated at the bottom. It leads to an effective force pointing towards the origin.

interaction time.

In section 2.3.3 we have shown, that it is possible to move the *center-of-mass* of a quasi-stationary light field using drive fields with non-equal intensities. Due to the more likely creation of a probe photon into the direction of the stronger coupling field, a drift motion of the sum mode occurs, and the difference mode as well as the spin coherence follow this motion. Hence it should be possible to move around and manipulate the probe pulse within the EIT-medium by applying control-fields with non-homogeneous control-fields as well as temporally and spatially varying intensity maxima. If the intensity maximum of one control-field component approaches the localized excitation, stored in the collective spin coherence the excitation is being *pushed*. The drift velocity imprinted by this process is given, according to eq. (2.94), by the effective group velocity $v_{\mathrm{gr}} \cos 2\varphi$. If a control-field configuration would render the value of the effective group velocity negative for positive values of z and positive for negative values of z, the associated drift would tend to compress the stationary field. This process may counteract the diffusive spread found in the last section.
A manipulation of the effective group velocity in such a way can be achieved by using two counter-propagating control-field beams with separated foci. The separation of the foci is assumed to be along the propagation direction of the forward and backward mode.

Linear spatial profile of intensity differences

The configuration mentioned above can be realized using paraxial Gaussian beams as shown in fig. 2.15, where the divergence of the beams is not neglected. Gaussian beams

are given by

$$E_{\mathrm{c}}^{\pm}(z, \mathbf{r}_{\perp}) = E_c^0 \frac{w_0}{w_{\pm}(z)} \exp\left(-\frac{\mathbf{r}_{\perp}}{w_{\pm}(z)}\right), \tag{2.98}$$

where $|\mathbf{r}_{\perp}|$ denotes the distance from the symmetry axis z of the set-up [97]. w_0 is the beam waist of the control-field and $w_{\pm}(z)$ is the width at a distance z from one of the corresponding foci $z_{\pm}$

$$w_{\pm}(z) = w_0 \sqrt{1 + \left(\frac{z - z_{\pm}}{z_{\mathrm{R}}}\right)^2}. \tag{2.99}$$

Here $z_{\mathrm{R}} = \pi w_0^2/\lambda_c$ is the Rayleigh length, the length along z, after which the width of the Gaussian beam increases to $\sqrt{2}w_0$ the width at the focus. The amplitude of the control field at the focus is denoted by E_c^0. After some algebra we find for the $\cos 2\varphi$-term in the effective group velocity

$$\cos 2\varphi = \frac{w_-^2(z) - w_+^2(z)}{w_+^2(z) + w_-^2(z)}, \tag{2.100}$$

where we have restricted our considerations to points on the z-axis. Furthermore, we have assumed that the peak intensities of both control-fields are equal. Since both fields drive the same transition all other terms cancel. Assuming equal Rayleigh length for both fields the expression simplifies to

$$\cos 2\varphi = \frac{(z - z_-)^2 - (z - z_+)^2}{(z - z_+)^2 + (z - z_-)^2 + 2z_{\mathrm{R}}^2} = \frac{2 z (z_+ - z_-) + (z_+^2 - z_-^2)}{(z - z_+)^2 + (z - z_-)^2 + 2z_{\mathrm{R}}^2}. \tag{2.101}$$

For the studies in the next sections we are interested in the case of two well separated foci and additionally assume that the entire dynamics takes place in the region of small $|z|$, i. e. $|z| \ll min\{|z_+|, |z_-|\}$. Assuming finally that the foci are located symmetrically with respect to the origin with absolute distance z_0, we find

$$\cos 2\varphi \approx -\frac{z}{L}, \tag{2.102}$$

where L is the characteristic length which is given by

$$L = \frac{1}{2}\left[z_0 + z_{\mathrm{R}}\left(\frac{z_{\mathrm{R}}}{z_0}\right)\right]. \tag{2.103}$$

For notational simplicity we have taken here the reference to the zero point of the coordinate system which is not necessary. In addition we find for the $\sin 2\varphi$-term

$$\sin 2\varphi \approx 1. \tag{2.104}$$

The linear approximation is of course only valid as long as $|z| \ll L$. The dependence of the $\cos 2\varphi$-term and the $\sin 2\varphi$-term on z following eq. (2.100) is shown in fig. 2.16.
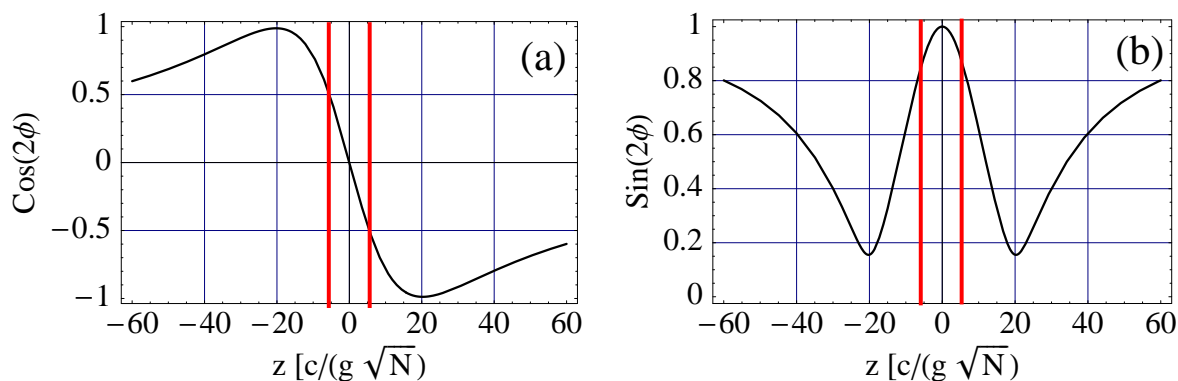
Figure 2.16: (a) The pre-factor of the force term for the configuration of two Gaussian beams with separated foci. The focal points of the two beams are located at $z_\pm = \pm 20c/(g\sqrt{N})$ like in the simulation for fig. 2.17. The linear regime near the origin is clearly visible. (b) The corresponding $\sin 2\varphi$-term, which shows the limitations of this approximation. The area enclosed by the red lines indicates the operation region.

2.4.1   Fokker-Planck equation for the *fast* normal mode

Within the approximation of paraxial Gaussian control fields with separated foci the equations of motion for the normal modes are given by

$$\left(\partial_t - \frac{v_{\text{gr}}}{L}z\partial_z\right)\hat{\mathcal{E}}_{\text{S}} = -\gamma_{gs}\sin^2\theta\hat{\mathcal{E}}_{\text{S}} + v_{\text{gr}}\partial_z\hat{\mathcal{E}}_{\text{D}} + v_{\text{gr}}\varphi'\left(\hat{\mathcal{E}}_{\text{S}} - \frac{z}{L}\hat{\mathcal{E}}_{\text{D}}\right), \tag{2.105}$$

$$\left(\partial_t + \frac{c}{L}z\partial_z\right)\hat{\mathcal{E}}_{\text{D}} = -\frac{c}{L_{\text{abs}}}\hat{\mathcal{E}}_{\text{D}} + c\partial_z\hat{\mathcal{E}}_{\text{S}} - c\varphi'\left(\hat{\mathcal{E}}_{\text{D}} + \frac{z}{L}\hat{\mathcal{E}}_{\text{S}}\right). \tag{2.106}$$

Here we have again neglected the time dependence of the external control-fields and hence set $\dot{\theta} = 0$ as well as $\dot{\varphi} = 0$. Furthermore we have $\varphi' \approx \frac{1}{2L}$. In order to adiabatically eliminate the difference mode $\hat{\mathcal{E}}_{\text{D}}$, we need $L_{\text{abs}} \ll L$ and $1 \ll cT/L_{\text{abs}}$, where T is the characteristic time on which the difference mode changes. The characteristic length on which the difference mode changes drops out of the considerations. By applying these conditions we find

$$\hat{\mathcal{E}}_{\text{D}} = -L_{\text{abs}}\left(\frac{z}{2L^2} - \partial_z\right)\hat{\mathcal{E}}_{\text{S}} \approx L_{\text{abs}}\partial_z\hat{\mathcal{E}}_{\text{S}}, \tag{2.107}$$

where we have used that $|z| \ll L$. Substituting this into equation (2.105) we arrive at

$$\left(\partial_t + \gamma_{\text{gs}}\sin^2\theta\right)\hat{\mathcal{E}}_{\text{S}} = \left(\frac{v_{\text{gr}}}{2L} + v_{\text{gr}}\frac{z}{L}\partial_z + L_{\text{abs}}\partial_z^2\right)\hat{\mathcal{E}}_{\text{S}}. \tag{2.108}$$

We can simplify the equation by making the ansatz

$$\hat{\mathcal{E}}_{\text{S}} = E_{\text{S}}\,e^{-\gamma_{gs}t\sin^2\theta}. \tag{2.109}$$

Furthermore, introducing the abbreviations

$$A_0 = \frac{v_{\mathrm{gr}}}{2L} + \partial_z \left(-\frac{v_{\mathrm{gr}}z}{L} \right) = -\frac{v_{\mathrm{gr}}}{2L}, \tag{2.110}$$

$$A_1 = \frac{v_{\mathrm{gr}}z}{L}, \tag{2.111}$$

$$B = 2D, \tag{2.112}$$

eq. (2.108) can be transformed into a Fokker-Planck equation with an additional decay term $A_0 E_{\mathrm{S}}$ [98]

$$\partial_t E_{\mathrm{S}} = A_0 E_{\mathrm{S}} + \partial_z (A_1 E_{\mathrm{S}}) + \frac{1}{2}\partial_z^2 (B E_{\mathrm{S}}). \tag{2.113}$$

After the separation of the simple decay term A_0 we identify the resulting Fokker-Planck equation to be of the Ornstein–Uhlenbeck type [99, 100]. The constant A_1 is called drift constant and B or equivalently D are called diffusion constant. The Ornstein–Uhlenbeck process has a stationary solution which we are going to determine now. Performing a Fourier transformation of the Ornstein-Uhlenbeck type Fokker-Planck equation with respect to the space variable leads to

$$\partial_t \tilde{E}_{\mathrm{S}}(k,t) = -\frac{v_{\mathrm{gr}}}{L}k \left(\partial_k + LL_{\mathrm{abs}}k \right) \tilde{E}_{\mathrm{S}}(k,t) = 0, \tag{2.114}$$

where the last equation holds since we are looking for the steady-state solution. The solution of the this differential equation is a Gaussian function. By a inverse Fourier transformation we then find the following expression for the sum mode

$$\hat{\mathcal{E}}_{\mathrm{S}}(z,t) = \frac{\hat{\mathcal{E}}_{\mathrm{S}}^{(0)}}{\sqrt{2\pi \, LL_{\mathrm{abs}}}} \exp\left\{ -(\gamma_{gs}\sin^2\theta + \frac{v_{\mathrm{gr}}}{2L})t \right\} \exp\left\{ -\frac{z^2}{2LL_{\mathrm{abs}}} \right\}. \tag{2.115}$$

Hence in the long-time limit, the field approaches a stationary Gaussian distribution of width $\sigma_{\mathrm{ss}} = \sqrt{LL_{\mathrm{abs}}}$, which decays in time with an effective rate $\gamma_{\mathrm{eff}} = \gamma_{gs}\sin^2\theta + v_{\mathrm{gr}}/2L$. The use of retrieve lasers with non-equal and spatially varying intensities thus acts like an effective cavity for the probe-field with an energy ring-down time given by the time a photon needs to travel the distance between the foci of the two control lasers. If we take in addition also the decay of the Raman coherence into account the ring down time decreases further.

Even though the interpretation of Fokker-Planck equations is in general not straightforward [34] it is the case for the Ornstein–Uhlenbeck process. Eq. (2.108) comprises of three terms on the right hand side, the first one is the decay term which we have already discussed. The next two terms are more interesting and respresent two competing physical processes. The first can be interpreted as an effective force acting on the field excitation which tries to drag it towards the origin (more generally towards the midpoint between the two intensity maxima of the control-fields). Hence this term acts compressing on the probe-field excitation. The last term is responsible for diffusion as we have already discussed in section 2.3.1, i. e. it leads to a spatial broadening of the stationary light
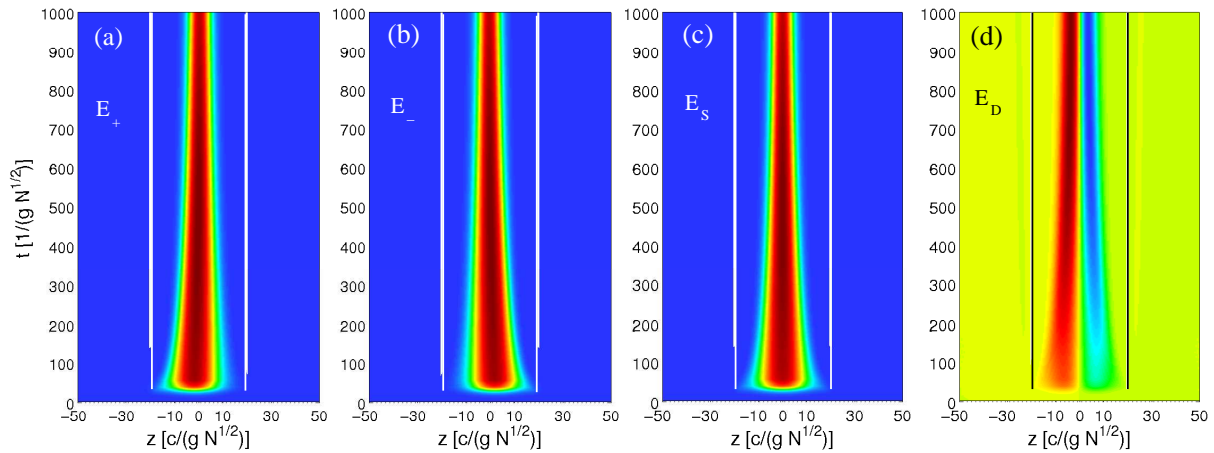
Figure 2.17: Temporal evolution of the (a) forward, (b) backward, (c) sum and (d) difference mode in the case of separated foci of the control-fields. The two competing processes of diffusion and Raman scattering towards the midpoint between the focal points lead to a stationary state behavior with decreasing amplitude of the fields. The white lines (a)-(c) and the black lines (d), denote the positions of the focal points of the two used control-fields.

pulse. In the situation we have considered here the action of this two processes leads to a stationary distribution given by (2.115).

It is noteworthy that the group velocity only appears in the decay term. The width of the field distribution only depends on the geometrical parameter L, i. e. the distance between the two foci, and the absorption length L_{abs} of the medium. This has an important consequence since the group velocity is a measure for the weight of the light- and matter-contributions in the polariton [1]. Even though the major part of the excitation is stored in the well protected spin coherence in the regime of small group velocities, it can be adiabaticly compressed by manipulating the tiny electromagnetic contribution of the polariton. This is because in the adiabatic limit the spin coherence follows the sum field. Hence by slowly reducing the distance between the two foci we can compress the spin coherence along withthe stationary light excitation.

In fig. 2.17 a numerical simulation of stationary light generated by two fields with separated foci is shown. Here the excitation was initially stored as a Gaussian distribution in the spin coherence with $e^{-1/2}$-width given by $2\sigma(0) = 7$. A small part of the distribution was not located within the region between the foci which has a width of forty in this example. By inspecting, e. g. part (a) of the figure, we see that initially the forward propagating mode is mainly created in the vicinity of the control-field focus of the Ω_+-field – the left white line. This is due to more probable creation of Raman scattered photons into the forward propagating mode. The same argumentation holds for the backward propagating mode in part (b).

Furthermore, we can see that the initial field width decreases until the field distribution

has reached a stationary width. From that point on only the height of the distribution decreases according to eq. (2.115). As will be discussed in the following the initial decrease is due to the excitation of higher-order eigensolutions of eq. (2.108) which decay faster than the lowest-order solution (2.115).

Second moment of the sum field in the adiabatic limit

If we use the definitions for the momenta, eq. (2.108), we can determine the equation of motion for the zeroth- and second-order moments of the sum mode. These are given by

$$\left[\partial_t + \gamma_{gs} \sin^2 \theta + \frac{5 v_{\mathrm{gr}}}{2L}\right] \langle \mathcal{E}_S \rangle_2 (t) = 2 v_{\mathrm{gr}} l_{\mathrm{abs}} \langle \mathcal{E}_S \rangle_0 (t), \tag{2.116}$$

$$\left[\partial_t + \gamma_{gs} \sin^2 \theta\right] \langle \mathcal{E}_S \rangle_0 (t) = -\frac{v_{\mathrm{gr}}}{2L} \langle \mathcal{E}_S \rangle_0 (t). \tag{2.117}$$

In the case of vanishing Raman decay rate, i. e. $\gamma_{gs} = 0$, we find the following solutions to these equations

$$\langle \mathcal{E}_S \rangle_0 (t) = \langle \mathcal{E}_S \rangle_0 (0) \, e^{-\frac{v_{\mathrm{gr}}}{2L} t}, \tag{2.118}$$

$$\langle \mathcal{E}_S \rangle_2 (t) = L_{\mathrm{abs}} L \langle \mathcal{E}_S \rangle_0 (0) \, e^{-\frac{v_{\mathrm{gr}}}{2L} t} \left(1 - e^{-\frac{2 v_{\mathrm{gr}}}{L} t}\right) + \langle \mathcal{E}_S \rangle_2 (0) \, e^{-\frac{5 v_{\mathrm{gr}}}{2L} t}. \tag{2.119}$$

The zeroth moment vanishes with the same decay rate as eq. (2.115). Considering the normalized width of the sum mode, i. e. the width divided by the time-dependent area eq. (2.118), one recognizes that it approaches for large times ($t \gg 2L/v_{\mathrm{gr}}$) a constant value. The constant is independent of the initial width of the wave-packet. It only depends on the medium ($L_{\mathrm{abs}} = \gamma_{ge} c / g^2 N$) and externally adjustable parameters (L). Numerical examples that support this statements are shown in fig. 2.18.

Spatial shift between forward/backward field distributions

For comparison with our numerical results and for a further understanding of the processes, we want to determine the location of the maxima of forward and backward propagating modes in the limit of the stationary Ornstein-Uhlenbeck solution. It will turn out, that the two maxima are not located at the same point and their separation only depends on the absorption length in absence of EIT.
The asymptotic solution for the sum mode is given by eq. (2.115). Hence, with the help of eq. (2.107) one can calculate, using this function, the difference mode in the vicinity of the origin, i. e. $z \ll L$,

$$\mathcal{E}_D(z,t) = L_{\mathrm{abs}} \partial_z \mathcal{E}_S(z,t) = -\frac{z}{L} \mathcal{E}_S(z,t). \tag{2.120}$$

To determine the forward and backward propagating modes, we use the inverse transformation of eq. (2.46). By applying simple trigonometric relations we find, in the limit $z \ll L$, that the mixing angle is given by

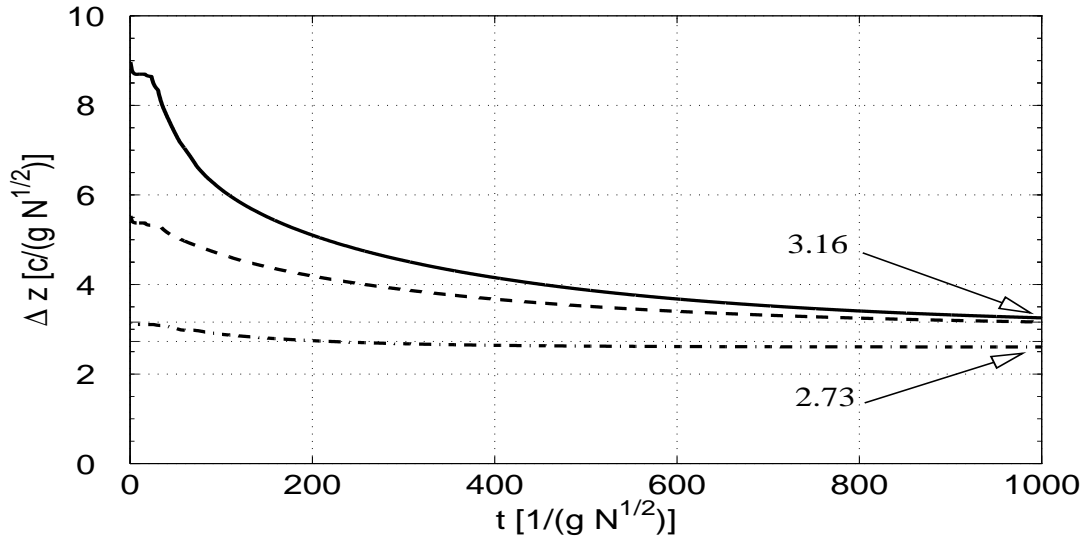$$\varphi \approx \frac{\pi}{4} - \frac{z}{2L}. \tag{2.121}$$

Figure 2.18: The figure shows the normalized variance of the sum mode as function of time. The solid and the dashed line converge towards the same steady-state value. The parameters used only differ in the initial value used for the sum field width ($L = 10$, $L_{abs} = 1$, solid $\Delta z(0) = 7$, dashed $\Delta z(0) = 5$). The dot-dashed curve corresponds to a different control-field configuration ($L = 15/2$, $\Delta z(0) = 3$). The numbers denote the steady state value of the variance given by $\Delta z_{ss} = \sqrt{L\,L_{abs}}$

This leads to the following approximate relations

$$\cos \varphi \approx \frac{1}{\sqrt{2}} \left(1 + \frac{z}{2L}\right), \tag{2.122}$$

$$\sin \varphi \approx \frac{1}{\sqrt{2}} \left(1 - \frac{z}{2L}\right). \tag{2.123}$$

and finally to

$$\mathcal{E}_{\pm}(z,t) = \frac{\mathcal{E}_S(z,t)}{\sqrt{2}} \left(1 \mp \frac{z}{L}\right). \tag{2.124}$$

One finds the location of the maxima for the forward and backward propagating modes by inserting the asymptotic solution eq. (2.115) and differentiation with respect to the spatial variable. Assuming again that we are only interested in the case $L_{abs} \ll L$, we find

$$z_{max}^{\pm} \approx \frac{L_{abs}}{2}. \tag{2.125}$$

Hence the asymptotic separation between the maxima only depends on the absorption length in absence of EIT. Fig. 2.19 shows an example of the motion of the distribution maxima towards their steady state points $z_{max}^{\pm}$. In discussing fig. 2.17 we have already
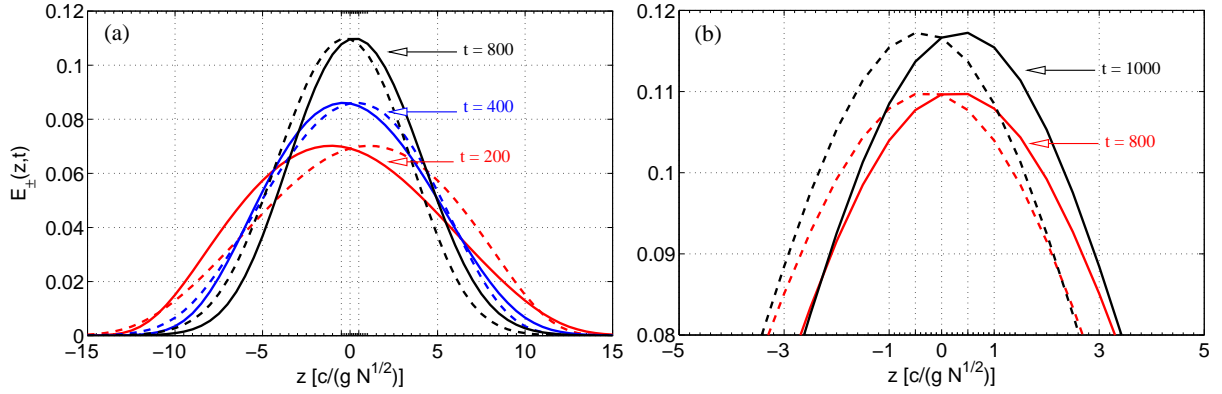
Figure 2.19: The figure shows the normalized field distributions of the forward (solid line) and backward (dashed line) propagating modes for different propagation times. The field distributions are normalized using their time-dependent pulse areas. (a) With increasing time the maxima of the field distributions move towards their steady state points $z^{\pm}_{\max}$. (b) Finally the distributions stay ever after at those points. The numerical data for this plot is based on fig. 2.17.

mentioned that the forward and backward propagating modes are created due to a higher probability of a stimulated Raman scattering processes in the vicinity of the foci of the Ω_+/Ω_--fields, respectively. During the evolution they move, due to the induced drift motion, towards their final points, which is shown in fig. 2.19 (a). In this process the field distributions of the modes always interchange their position and move thereby through each other.

2.4.2 Initial value problem of Ornstein–Uhlenbeck process

Given an initial distribution for the sum mode, how does the distribution evolve in time, when we consider the configuration with stationary, displaced foci? For this we have to solve the initial value problem for the Ornstein–Uhlenbeck process with decay. Before we deal with the specific problem, let us briefly review the general theory behind this. Assume that we want to solve an initial value problem of the form

$$\frac{\partial}{\partial t}\phi(z,t) = \hat{L}\phi(z,t) \text{ with } \phi(z,0) = \phi_0(z) \tag{2.126}$$

where $\hat{L}$ is some time-independent hermitian (differential) operator. Then the general solution of the problem is given by

$$\phi(z,t) = \sum_{n=0}^{\infty} c_n\, e^{-\lambda_n t}\phi_n(z), \tag{2.127}$$

where the λ_n and ϕ_n are eigenvalues and eigenfunctions of $\hat{L}$, i. e. we have

$$\left(\hat{L} + \lambda_n\right)\phi_n = 0, \tag{2.128}$$

where the ϕ_n form a complete, orthonormal set of functions with respect to a scalar product $(\phi, \psi) = \int w(z)\phi^*(z)\,\psi(z)\,\mathrm{d}z$ with $w(z)$ being some real-valued integral kernel. Finally the coefficients c_n are, because of this orthonormality, given by

$$c_n = \int w(z)\,\phi_n^*(z)\,\phi(z,0)\mathrm{d}z. \tag{2.129}$$

Hence our problem can be solved by making use of the eigenfunctions $\{\chi_n(z), \lambda_n\}$ of the backward (eigenvalue) equation of the Ornstein–Uhlenbeck type Fokker-Planck equation (2.113) (without trivial decay term) [98]. The backward equation is given by

$$\partial_t E_S = \frac{v_{\mathrm{gr}}}{L}\,E_S + \frac{v_{\mathrm{gr}}}{L}z\partial_z\,E_S + D\partial_z^2\,E_S \tag{2.130}$$

by making an ansatz like eq. (2.127), we find the corresponding eigenvalue equation

$$\phi_n''(z) + \frac{v_{\mathrm{gr}}}{D}\frac{z}{L}\phi_n'(z) + \left(\frac{\lambda_n}{D} + \frac{v_{\mathrm{gr}}}{DL}\right)\phi_n(z) = 0, \tag{2.131}$$

where the prime denotes again differentiation with respect to z. This differential equation can be transformed into the differential equation for Hermite polynomials by using $\phi_n(z) = \varphi_n(z)\exp(-\alpha^2 z^2)$ to find

$$\varphi_n''(z) - Az\varphi_n'(z) + \left(B\,z^2 + C\right)\varphi_n(z) = 0, \tag{2.132}$$

where

$$A = \frac{v_{\mathrm{gr}}}{2DL} - 4\alpha^2, \tag{2.133}$$

$$B = 2\,\alpha^2\left(\alpha^2 - \frac{v_{\mathrm{gr}}}{2DL}\right), \tag{2.134}$$

$$C = \left(\frac{\lambda_n}{D} + \frac{v_{\mathrm{gr}}}{DL}\right) - 2\,\alpha^2. \tag{2.135}$$

Setting $B = 0$ to eliminate the quadratic term, we can use the corresponding condition

$$\alpha^2 = \frac{v_{\mathrm{gr}}}{2DL} = \frac{1}{2\,L\,L_{\mathrm{abs}}} \tag{2.136}$$

to simplify the expression for A and C. Using furthermore the variable substitution $z = \beta\,x$, we can reformulate the differential equation above to find

$$\varphi_n''(x) - \beta^2\frac{v_{\mathrm{gr}}}{D\,L}x\varphi_n'(x) + \beta^2\frac{\lambda_n}{D}\varphi_n(z) = 0. \tag{2.137}$$

By comparing this equation with the differential equation for the Hermite polynomials H_n [101], we can eliminate the factor β and finally find the eigenvalues λ_n and normalized eigenfunctions Φ_n to eq. (2.131)

$$\lambda_n = n\frac{v_{\mathrm{gr}}}{L}, \tag{2.138}$$

$$\Phi_n(z) = \left(2^n n!\sqrt{\pi}\,L\,L_{\mathrm{abs}}\right)^{-1/2}\,H_n\left(\frac{z}{\sqrt{2\,L\,L_{\mathrm{abs}}}}\right)\exp\left\{-\frac{z^2}{2\,L\,L_{\mathrm{abs}}}\right\}, \tag{2.139}$$

with $n \in \mathbb{N}_0$. As is well known from various textbooks do the functions Φ_n form a complete set of functions [101]. Hence the general solution to the initial value problem including the global decay term reads

$$E_S(z,t) = \sum_{n=0}^{\infty} \frac{c_n}{\sqrt{2^{n+1} n! \sqrt{\pi} \, L \, L_{\text{abs}}}} \exp\left\{ -\frac{z^2}{2 L L_{\text{abs}}} \right\} \times$$

$$\times \, H_n\left(\frac{z}{\sqrt{2 L \, L_{\text{abs}}}} \right) \exp\left\{ -\frac{v_{\text{gr}}(n+1/2)t}{L} \right\}. \tag{2.140}$$

The expansion coefficients c_n are determined by the initial field $E_S(z,0)$

$$c_n = \int_{-\infty}^{\infty} E_S(z,0) \, H_n\left(\frac{z}{\sqrt{2 L \, L_{\text{abs}}}} \right) \mathrm{d}z. \tag{2.141}$$

Apart from the overall damping term and a factor of two in the exponent of the Gaussian is eq. (2.140) very similar to a damped harmonic oscillator with an oscillator length given by $\sqrt{L \, L_{\text{abs}}}$. If the initial light pulse, i. e. the stored excitation, is Gaussian and if the separation of the foci of the two retrieve lasers is chosen such that the width of the excitation is less than the effective oscillator length $\sqrt{L \, L_{\text{abs}}}$, only the fundamental mode Φ_0 gets excited in the retrieve process. In this case a spatially constant field distribution is created as shown in fig. 2.20. The field, however, has a finite lifetime determined by the overall damping rate $\gamma_{\text{eff}} = v_{\text{gr}}/2L$. As a consequence the photonic excitation $n_{\text{pho}} \sim |E_S(t)|^2$ decays in time and since the spin coherence follows adiabaticly the dynamics of the sum mode the total excitation decays according to

$$n_{\text{tot}}(t) = n_{\text{tot}}(0) \exp\left(-\frac{v_{\text{gr}}}{L} t \right). \tag{2.142}$$

In order to have negligible losses, the time over which the stationary light pulse can be maintained is limited by the same expression as in the diffusion case

$$t \ll \frac{L}{v_{\text{gr}}} \approx \frac{\Delta z^2(0)}{v_{\text{gr}} \, L_{\text{abs}}}. \tag{2.143}$$

If the separation between the focal points during the retrieve process is much smaller than the width of the stored excitation, the theory presented here is only applicable to the part of the pulse which is located between the focal points, i. e. in the region given by the linear slope in fig. 2.16 (a). The rest of the excitation is lost, since it separates from the initial distribution or it leads to excitation of the higher-order Gauss-Hermite modes. These decay very fast compared to the fundamental mode, see eq. (2.140)[102].

2.5 Spatial compression of stationary light pulses

2.5.1 Basic concept

In the last section we have seen that it is possible to manipulate the shape of the regenerate probe field by means of control field beams with spatially modulated intensities. In
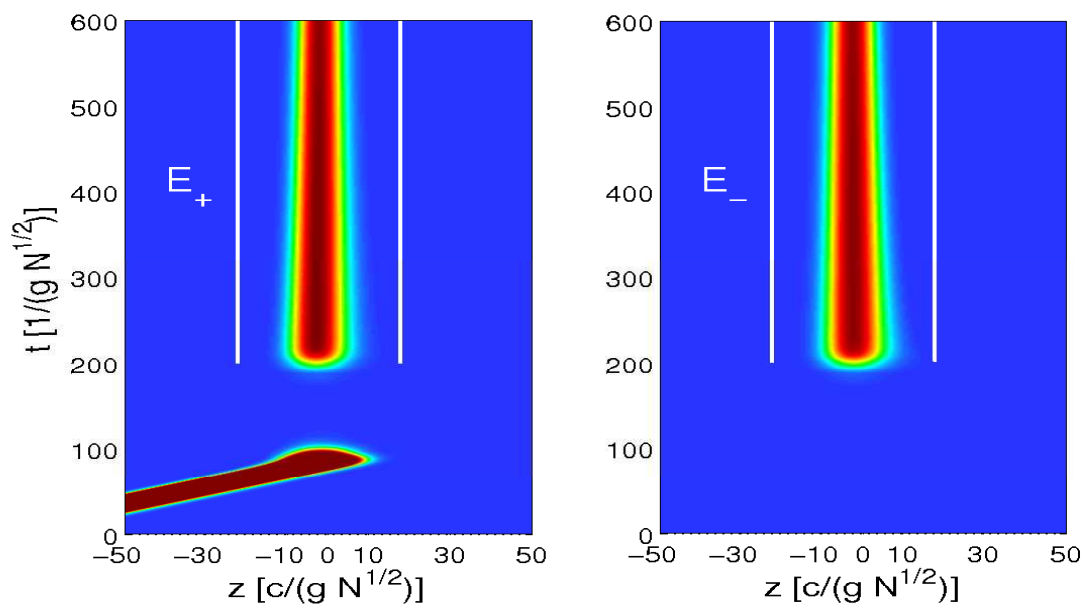
Figure 2.20: Storage of a Gaussian pulse and subsequent retrieval with two control beams with spatially varying intensity profiles. The maxima of the intensities of $\Omega_\pm$ are indicated by the two white lines. Close to the midpoint between these lines the normalized intensity difference $|\Omega_{+0}|^2/|\Omega_0|^2 - |\Omega_{-0}|^2/|\Omega_0|^2$ varies linearly with z. The generation of fields with constant spatial shape is apparent. The parameters are given by: $\delta = \Delta = \Delta\omega = 0$ and $\gamma_{ge} = N = c = 1$ and the width of the initial Gaussian wave-packet is $\Delta z(t=0) = \sqrt{10}$. The separation of the foci is $40\,c/(g\sqrt{N})$ which leads to $L \approx 10$ for a Rayleigh length of $z_R = 1.6$. The dependence of the control-field is given by $\Omega_+(t) = 100*0.5*[1-\tanh\{0.1*(t-60)\}] + 0.5*[1+\tanh\{0.1*(t-200)\}]$. For the minus direction a similar term was used consisting only of the second term.

this section we want to extend this ansatz and use it to actively compress the retrieved stationary probe field pulse.

To avoid losses the compression of a photonic excitation should start with a mode matched wave-packet, i. e. with an initial width smaller than the oscillator length $\sqrt{L\,L_{\mathrm{abs}}}$. Then only the fundamental mode Φ_0 gets excited and experiences in the small group velocity limit, i. e. the regime of interest, an unavoidable small loss with an effective decay rate of

$$\gamma_{\mathrm{eff}} = \frac{v_{\mathrm{gr}}}{2\,L} = \frac{c\,\cos^2\theta}{2\,L(t)}. \tag{2.144}$$

Compression of Φ_0, respectively $\hat{\mathcal{E}}_S$, can be achieved, according to eq. (2.140) by decreasing adiabatically the characteristic length L, i. e. by decreasing the distance between the control-field foci. If the process is sufficiently adiabatic, the width of the fundamental
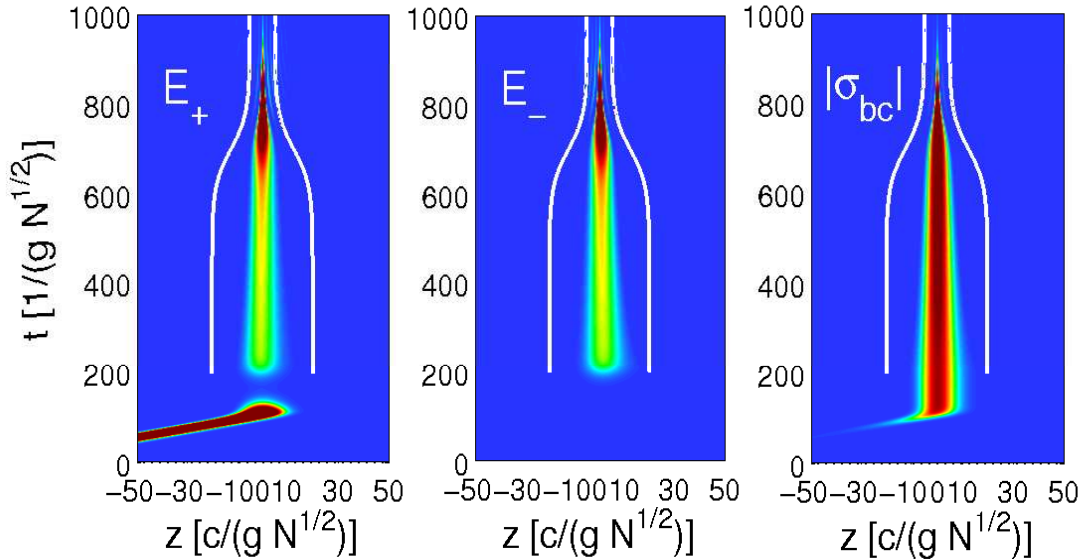
Figure 2.21: Retrieval of a stored pulse using drive fields with separated foci and subsequent reduction of their separation. The position of the focal points is indicated by white lines. One clearly recognizes a compression of the probe-field associated with an increase of the field density. However, the whole compression procedure is accompanied by strong losses. The parameters are the same as for fig. 2.20 except for $\gamma = 0.05$. The foci move like: $z_{\pm}(t) = \pm 20 \mp 10 * 0.5 * [1 + \tanh(0.0125 * (t - 700))]$.

mode should follow this motion without excitation of higher order modes. This is shown in fig. 2.21, where the location of the focal points is again denoted by the white lines. Apparent is the decreasing width of the photonic as well as the spin excitation. The compression is however accompanied by strong losses. This is shown in fig. 2.22 where the temporal evolution of the peak excitation density and the total excitation, i. e.

$$n_{\text{tot}} = \int \mathrm{d}z \left[|\hat{\mathcal{E}}_S|^2 + |\hat{\mathcal{E}}_D|^2 + |\hat{\sigma}_{gs}|^2 \right] \tag{2.145}$$

are depicted. In the next section we give a more quantitative discussion of the relevant loss mechanisms and discuss conditions for their minimization.

2.5.2 Nonadiabatic effects

In this section we want to consider nonadiabatic effects which may occur when compressing the stationary light pulse by adiabatically decreasing the distance between the two control field focal points. We will derive conditions which should be fulfilled to achieve adiabatic dynamics. To this end, we again consider eq. (2.51) and (2.52). For simplicity we assume
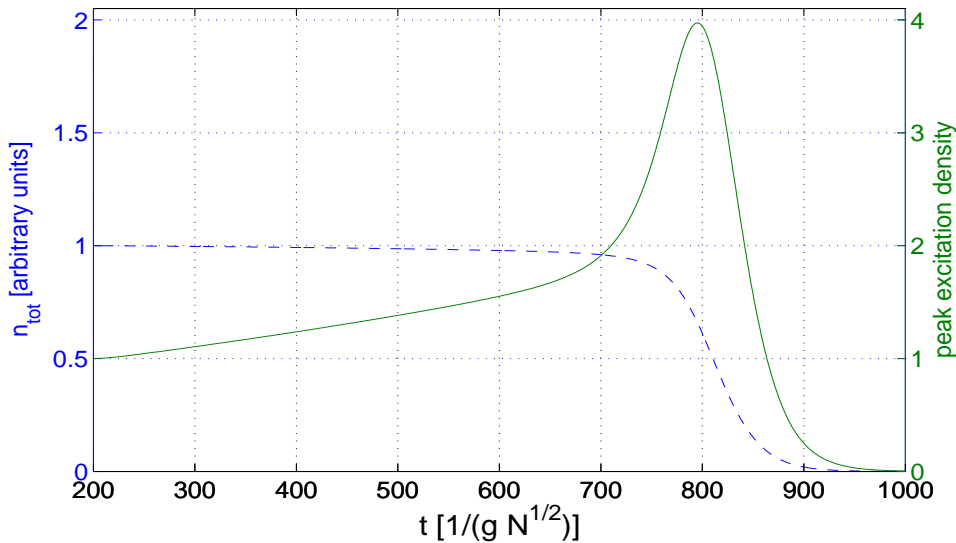
Figure 2.22:   Peak excitation density (solid line) and total excitation (dashed line) as a function of time for the numerical simulation of fig. 2.21. Both quantities are normalized to their value at $t = 200 \, (g\sqrt{N})^{-1}$.

one- and two-photon resonance, i. e. $\delta = \Delta = 0$ and a vanishing decay rate of the Raman coherence ($\gamma_{gs} = 0$). Furthermore, we assume that $\partial_t \theta = 0$ holds which is true in the present configuration if the group velocity stays constant in time. Using these assumptions the considered equations read

$$\left[\partial_t - \frac{v_{\mathrm{gr}} z}{L}\partial_z\right] \hat{\mathcal{E}}_S = v_{\mathrm{gr}} \left[\frac{\dot{\varphi}}{c} + \partial_z\right] \hat{\mathcal{E}}_D + v_{\mathrm{gr}}\varphi' \left[\hat{\mathcal{E}}_S - \frac{z}{L}\hat{\mathcal{E}}_D\right], \tag{2.146}$$

$$\left[\partial_t + \frac{c\,z}{L}\partial_z\right] \hat{\mathcal{E}}_D = -\frac{c}{L_{\mathrm{abs}}}\hat{\mathcal{E}}_D - \left[\dot{\varphi} - c\partial_z\right]\hat{\mathcal{E}}_S - c\varphi' \left[\frac{z}{L}\hat{\mathcal{E}}_S + \hat{\mathcal{E}}_D\right]. \tag{2.147}$$

Using $\varphi' = 1/2L$ and the conditions $T_D\, c \gg L_{\mathrm{abs}}$ and $z \ll L\, L_D/L_{\mathrm{abs}}$, where T_D and L_D and are the characteristic time and distance in which the difference mode changes, we can adiabatically eliminate the same. These conditions are easily fulfilled. We also used $L \gg L_{\mathrm{abs}}$ which is only justified if we do not compress the stationary light pulse down to the order of the absorption length L_{abs}. L_{abs} is usually on the order of a few millimeter in a dilute vapor cell or down to few micrometer in a Bose-Einstein condensate. The adiabatically eliminated difference field reads

$$\hat{\mathcal{E}}_D = -L_{\mathrm{abs}} \left[\frac{\dot{\varphi}}{c} + \frac{z}{2\,L^2} - \partial_z\right] \hat{\mathcal{E}}_S. \tag{2.148}$$

Substituting this into the equation of motion for the sum field (2.146) and, recalling that the mixing angle φ is time- as well as space-dependent, we find

$$\left[\partial_t - \frac{v_{\text{gr}}}{2L} - \frac{v_{\text{gr}}z}{L}\partial_z\right]\hat{\mathcal{E}}_S = v_{\text{gr}}L_{\text{abs}}\left[-\left(\frac{\dot{\varphi}}{c}\right)^2 + \left(\frac{z}{2L^2}\right)^2 + \partial_z^2\right]\hat{\mathcal{E}}_S +$$
$$+ v_{\text{gr}}L_{\text{abs}}\left[\frac{\dot{\varphi}}{c}\partial_z\hat{\mathcal{E}}_S - \frac{1}{c}\partial_z\left(\dot{\varphi}\hat{\mathcal{E}}_S\right) - \frac{z}{2L^2}\partial_z\hat{\mathcal{E}}_S - \frac{1}{2L^2}\partial_z\left(z\hat{\mathcal{E}}_S\right)\right]. \quad (2.149)$$

With the help of

$$\dot{\varphi} = -\frac{z}{2L}\partial_t\ln L \quad (2.150)$$

this can furthermore be evaluated and leads with the condition $\sqrt{L/L_{\text{abs}}}L \gg |z|$ to the following Fokker-Planck equation

$$\partial_t\hat{\mathcal{E}}_S = -\frac{v_{\text{gr}}}{2L}\left[1 - \frac{L_{\text{abs}}}{c}(\partial_t\ln L) + \frac{z^2 L_{\text{abs}}}{2Lc^2}(\partial_t\ln L)^2\right]\hat{\mathcal{E}}_S + \partial_z\left[\frac{v_{\text{gr}}z}{L}\hat{\mathcal{E}}_S\right] + v_{\text{gr}}L_{\text{abs}}\partial_z^2\hat{\mathcal{E}}_S. \quad (2.151)$$

One recognizes that apart from the explicit time dependence of L nonadiabatic corrections lead to two additional loss terms. The first can be neglected compared to $v_{\text{gr}}/2L$ since

$$|\partial_t\ln L| \ll \frac{c}{L_{\text{abs}}}. \quad (2.152)$$

The second term leads to losses for large values of z. The corresponding loss rate

$$\frac{z^2 L_{\text{abs}}}{4L^2}\frac{v_{\text{gr}}}{c^2}(\partial_t\ln L)^2 \quad (2.153)$$

can also be neglected for

$$z^2 \ll \left[\frac{L_{\text{abs}}}{2L}\left(\frac{1}{c}\partial_t\ln L\right)^2\right]^{-1}. \quad (2.154)$$

Since the typical scale of the width of the field distribution is $\Delta z \simeq \sqrt{L L_{\text{abs}}}$ this is again well justified because of $|\partial_t\ln L| \ll c/L_{\text{abs}}$. We thus can safely ignore the two additional loss terms. With the help of the ansatz

$$\hat{\mathcal{E}}_S(z,t) = \hat{\tilde{\mathcal{E}}}_S(z,t)\exp\left\{-\int\limits_0^t d\tau\frac{v_{\text{gr}}}{2L(\tau)}\right\} \quad (2.155)$$

equation (2.151) simplifies to the earlier found Fokker-Planck equation (2.113) for the Ornstein-Uhlenbeck process except for the time-dependence of the characteristic length L. We thus see that the losses during compression, found in the example of the last

section, cannot be attributed to the nonadiabatic corrections in eq. (2.151) but must be explained from the Ornstein-Uhlenbeck dynamics itself. To this end we reexamine eq. (2.140) for the general solution of the Ornstein-Uhlenbeck process but now, however, with time-dependent parameters. From eq. (2.140) we recognizes that higher order modes have a faster decay. Thus the most likely reason for the observed losses is a population of higher-order modes.

We now want to derive a set of rate equations, for the expansion coefficients of the general Ornstein-Uhlenbeck solution. Our intention is to study the population of higher-order modes during the compression process and to show how we can minimize their population. The general solution of the Fokker-Planck equation (2.113) with a time-depending characteristic length L is given by

$$\hat{\tilde{\mathcal{E}}}_S(z,t) = \sum_{n=0}^{\infty} d_n(t)\Phi_n(z,t) \tag{2.156}$$

where we have included all temporal dynamics except for the overall loss rate $v_{\mathrm{gr}}/2\,L$ into the expansion coefficient $d_n(t)$. For those we want to derive a system of rate equations. From section 2.4.2 we know that the functions Φ_n, see eq. (2.139), solve the eigenvalue problem eq. (2.131). Hence, we have

$$v_{\mathrm{gr}}\, L_{\mathrm{abs}}\, \partial_z^2 \hat{\tilde{\mathcal{E}}}_S + \partial_z \left(\frac{v_{\mathrm{gr}}\, z}{L}\, \hat{\tilde{\mathcal{E}}}_S \right) = -\sum_{n=0}^{\infty} \frac{v_{\mathrm{gr}}}{L}\, n\, \Phi_n(z,t) \tag{2.157}$$

and on the other hand

$$\partial_t \hat{\tilde{\mathcal{E}}}_S = \sum_{n=0}^{\infty} \left[(\partial_t d_n)\Phi_n(z,t) + d_n \partial_t \Phi_n(z,t) \right]. \tag{2.158}$$

The two expressions eq. (2.157) and (2.158) have to be equal due to the Fokker-Planck equation for $\hat{\tilde{\mathcal{E}}}_S$. To determine the expansion coefficients we have to find the time-derivative of $\Phi_n(z,t)$. After some algebra and using well known relations for Hermite polynomials we find

$$\partial_t \Phi_n(z,t) = \frac{1}{4} \frac{1}{\sqrt{2^{n+1}\, n!\, \sqrt{\pi}\, L\, L_{\mathrm{abs}}}} \left[H_{n+2} \left(\frac{z}{\sqrt{2\, L\, L_{\mathrm{abs}}}} \right) \right.$$
$$\left. + 2\, n\, H_n \left(\frac{z}{\sqrt{2\, L\, L_{\mathrm{abs}}}} \right) \right] e^{-z^2/(2\, L\, L_{\mathrm{abs}})} (\partial_t \ln L). \tag{2.159}$$

With the help of this we can finally use the orthonormality of the Hermite polynomial to determine the rate equation for the expansion coefficients

$$\partial_t d_n = -n \left[\frac{v_{\mathrm{gr}}}{L} + \frac{1}{2}(\partial_t \ln L) \right] d_n - \frac{1}{2}\sqrt{n\,(n-1)}(\partial_t \ln L)\, d_{n-2} \tag{2.160}$$

The first term $n\, v_{\mathrm{gr}}/L$ corresponds to the already found decay behavior of the Ornstein-Uhlenbeck solution eq. (2.140) without adiabatic corrections. The other two terms only
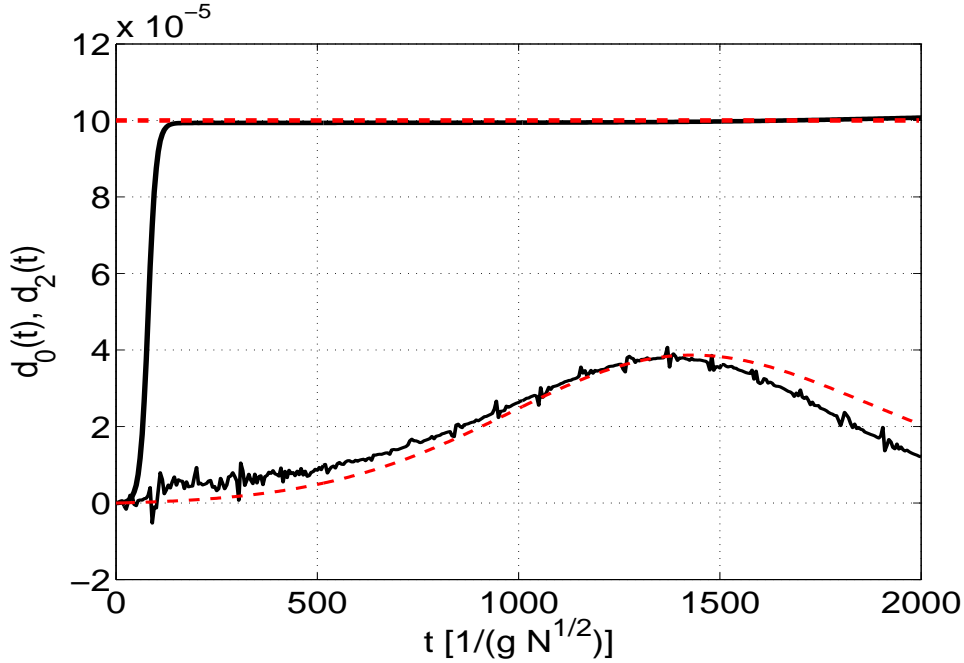
Figure 2.23: This figure compares the numerical results (black solid lines) with the analytical predictions (dashed red lines) for the expansion coefficients d_0 (upper curves) and d_2 (lower curves). The agreement of both approaches is quite good. The numerical results are based on the solution of the full set of Maxwell-Bloch equations after the secular approximation where as the analytical graphs are based on eq. (2.161) and (2.162). The difference between the numerical and the analytical result for d_0 at the beginning is due to the read-out procedure which is not taken into account in the analytic theory. For the simulation we used the following parameters: $\gamma_{gg} = \gamma_{ss} = 0.05$, $g = N = c = 1$, one- and two-photon resonance conditions, i. e. $\Delta = \delta = 0$, Rayleigh length $z_R = \pi/2$ and $z_\pm(t) = \mp 30 \pm 25 * 0.5 * [1 + \tanh(1.5625 * 10^{-3} * (t - 1000))]$ and $\Omega_\pm(t) = 0.1 * 0.5 * [1 + \tanh(0.05 * (t - 80))]$.

occure if the distance between the two focal points of the control-fields is changed in time. For the lowest coefficients we find

$$\partial_t d_0 = 0 \tag{2.161}$$

$$\partial_t d_2 = -2 \left[\frac{v_{\text{gr}}}{L} + \frac{1}{2}(\partial_t \ln L) \right] d_2 - \frac{1}{\sqrt{2}}(\partial_t \ln L)d_0. \tag{2.162}$$

Thus d_0 is constant while the higher-order modes are build up in time. In figure 2.23 an example is given where the coefficients $d_0(t)$, $d_2(t)$ are calculated from the numerical solution of the full Maxwell-Bloch equations and compared to the solution of eqs. (2.161) and (2.162). One recognizes very good agreement.

It is important to note that the eigenmodes of the Ornstein-Uhlenbeck process are

not orthogonal in the usual sense but that their orthogonality relation reads

$$\int\limits_{-\infty}^{\infty} \mathrm{d}z \, e^{z^2/2LL_{\mathrm{abs}}} \Phi_n(z) \, \Phi_m(z) = \delta_{nm}. \tag{2.163}$$

Thus the increase of the coefficients d_n for higher modes and $d_0 = const.$ and hence of the expansion coefficients of the Orstein-Uhlenbeck solution

$$c_n(t) = d_n(t) \exp\left\{ -\int\limits_0^t \frac{v_{\mathrm{gr}}(\tau)}{2L(\tau)} \mathrm{d}\tau \right\}, \tag{2.164}$$

does not mean that the photon number in the field increases. The latter is proportional to

$$\int\limits_{-\infty}^{\infty} \mathrm{d}z |\mathcal{E}_S|^2 \sim \sum_{m,n} \int\limits_{-\infty}^{\infty} \mathrm{d}z \Phi_n(z) \, \Phi_m(z) \, c_n^* \, c_m. \tag{2.165}$$

The population of higher order modes eventually leads to increased losses. We notice that during the compression $\partial_t \ln L$ is negative and thus can compensate the term $2 \, v_{\mathrm{gr}}/L$ or even overcompensate it. Overcompensation leads to an exponential increase of higher-order modes and would thus prevent compression. For this reason we require

$$|\partial_t \ln L| \leq \frac{2v_{\mathrm{gr}}}{L}. \tag{2.166}$$

On the other hand the compression should be as fast as possible and the stationary light should be transferred back to a spin excitation as fast as possible since losses occur only when a nonvanishing stationary light field is present. Thus it seems natural to consider the case

$$\partial_t \ln L = -\frac{2 \, v_{\mathrm{gr}}}{L}. \tag{2.167}$$

Noting that the sum mode $\hat{\mathcal{E}}_S$ is related to $\hat{\tilde{\mathcal{E}}}_S$ via eq. (2.155) we see that there is in addition an overall effective decay rate

$$\gamma_{\mathrm{eff}} = \frac{v_{\mathrm{gr}}(t)}{2 \, L(t)} = \frac{c \cos^2 \theta(t)}{2 \, L(t)}. \tag{2.168}$$

Thus when reducing L we should also reduce v_{gr} to keep γ_{eff} small. If γ_{eff} is for example chosen to be constant we find with eq. (2.167)

$$\partial_t \ln L(t) = -4\gamma_{\mathrm{eff}} \tag{2.169}$$

and thus

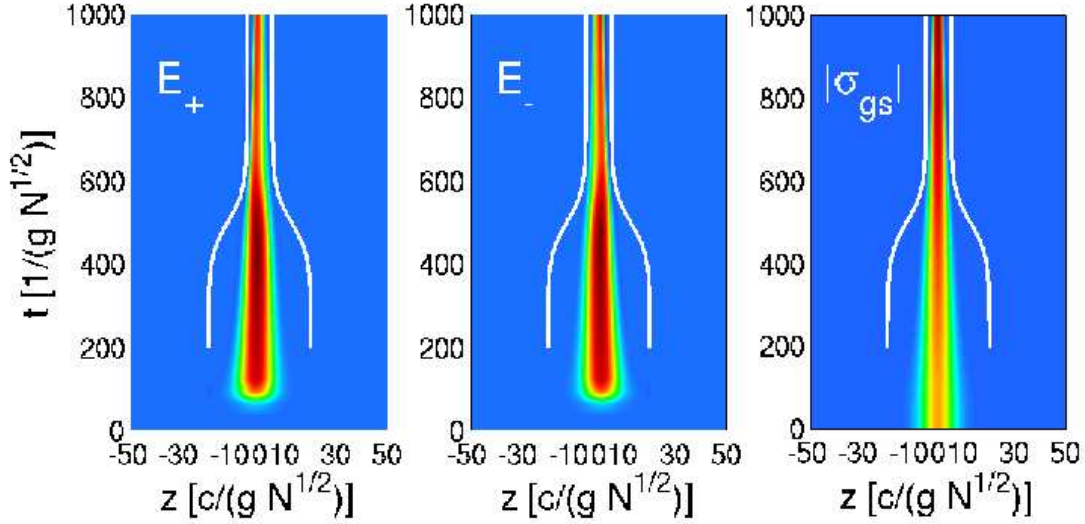$$L(t) = L(0) \, e^{-4 \, \gamma_{\mathrm{eff}} \, t}. \tag{2.170}$$

Figure 2.24: Retrieval of a stored pulse using drive fields with separated foci and subsequent reduction of their separation. The position of the focal points is indicated by white lines. One clearly recognizes a compression of the probe-field associated with an increase of the field density. The parameters are $\gamma = 0.05$, and the width of the initial Gaussian distribution $\Delta z = 5$. The foci move like: $z_{\pm}(t) = \pm 20 \mp 10 * 0.5 * [1 + \tanh(0.0125 * (t - 500))]$

In this case one finds for the coefficients d_n with $d_0(t = 0) = d_0$ and $d_m(t = 0) \equiv 0$ for $m \neq 0$

$$d_0(t) = d_0, \tag{2.171}$$

$$d_2(t) = 2\sqrt{2}\gamma_{\text{eff}}\, t\, d_0, \tag{2.172}$$

$$d_4(t) = 2\sqrt{24}\gamma_{\text{eff}}^2\, t^2\, d_0. \tag{2.173}$$

To illustrate that keeping γ_{eff} small leads to substantially reduced losses we present in fig. 2.24 and fig. 2.25 a numerical example. The figure shows an increase of the peak excitation density by a factor of 3 whereas the photon number in the probe field pulse decreases only by 5%-10%.

Hence, we have shown that the present approach is suitable to compress the long-lived stationary photonic excitation by adiabatically decreasing the distance between the control-field foci and dynamically keeping the overall effective damping rate γ_{eff} small. This leads to less loss since higher order modes are only minimally excited, see eqs. (2.172,2.173).
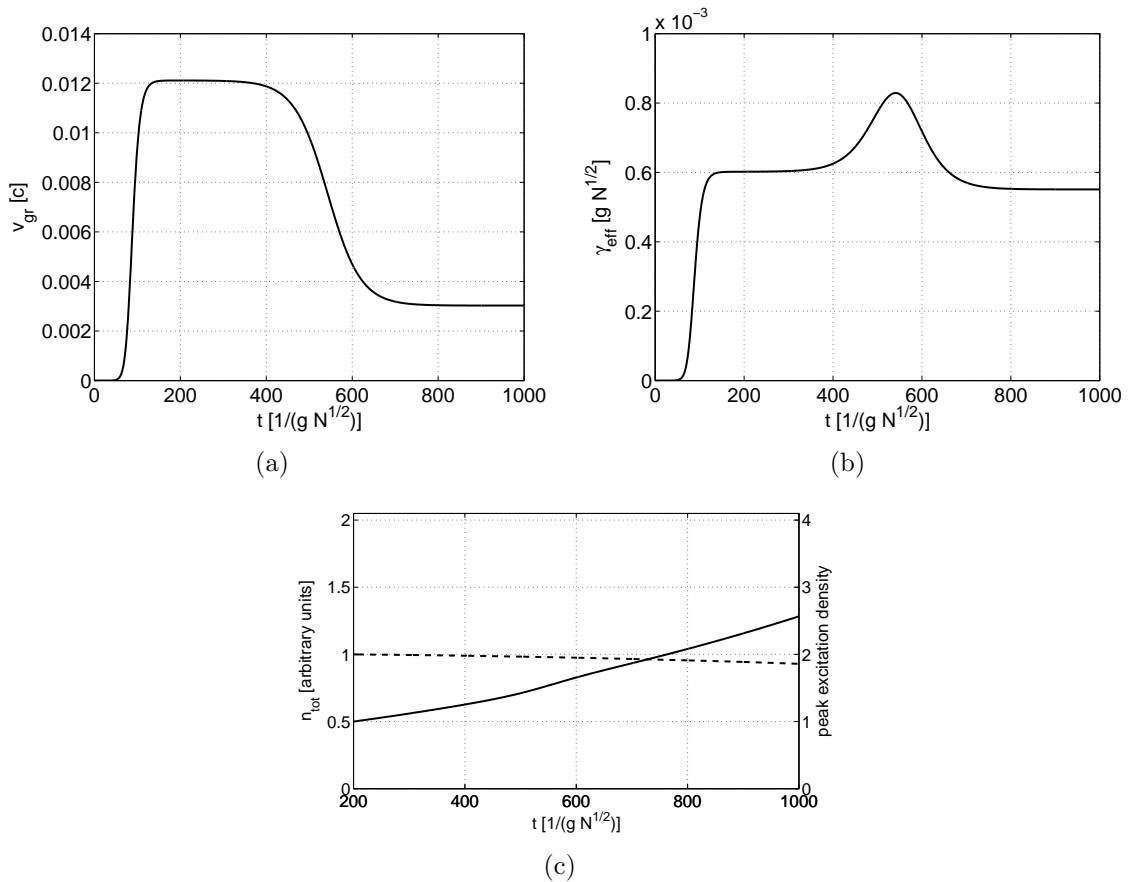
(a)

(b)

(c)

Figure 2.25: The plots given here show relevant parameters for the simulation of fig. 2.24. (a) gives the temporal evolution of the group velocity at $z = 0$. (b) shows the effective decay rate for the same cut. (c) presents the peak excitation density (solid line) and the total number of probe field photons n_{tot} (dashed line) as a function of time. Even though the peak excitation denstiy can be increase by a factor of 3 only little photon loss occurs.

2.6 Conclusion

In this chapter we have identified the phenomenon underlying the diffusive spreading of stationary light, i. e. the phenomenon of pulse matching, using a self-consistent set of field equations and introducing new normal modes. Moreover, we showed that in addition to diffusion also a drift motion may occur in the same scheme. The drift motion can be tailored in such a way that an effective force is created which points towards the midpoint between the focal points of the two control-field Gaussian laser beams used to create the stationary pulses of light. Using the effective force the stationary pulses of light can be coherently compressed. This compression is however accompanied by losses. In addition we have identified the main loss mechanism, i. e. the excitation of higher-order modes of a general Orstein-Uhlenbeck solution, and pointed out ways to suppress those excitations.

Finally, a new stationary light scheme was introduced at the beginning of the chapter which does not require a secular approximation. The new scheme leads to the same effects pointed out here, however, it also opens up new ways for the coherent manipulation of stored spin coherences and stationary light pulses by using the possibility to manipulate the single-photon detunings of the two different control-fields separately. Furthermore, this new scheme shows that neither a spatial periodic structure of the absorption profile [12] nor a periodically modulated refractive index [11] is necessary for the creation of stationary light.

Chapter 3

Sagnac-interferometer based on slow-light in ultra-cold quantum gases

3.1 Introduction

In contrast to inertial motion, rotation of an object is absolute in the sense that it can be defined intrinsically, i.e. independent of any inertial frame of reference. Moreover, all types of acceleration of the local frame of reference can be distinguished and determined by local measurements [58]. Rotation can be detected by means of the Sagnac effect [57], i.e. the relative phase shift $\Delta\phi_{\rm rot}$ of counterpropagating waves in a ring interferometer of area $\mathbf{A}$ attached to the laboratory frame rotating with angular velocity $\mathbf{\Omega}$. The phase shift is given by

$$\Delta\phi_{\rm rot} = \frac{4\pi}{\lambda v}\mathbf{\Omega}\cdot\mathbf{A}, \tag{3.1}$$

where λ is the wavelength and v the phase velocity of the corresponding wave phenomenon. Depending on the nature of the wave, one distinguishes two basic types of Sagnac interferometers: light and matter wave gyroscopes [103]. Both wave phenomena require a sufficient coherence length to be used in an interferometer. It is interesting to note, that the Sagnac phase shift per unit area in a matter wave device exceeds that of laser based gyroscopes by the ratio of rest energy per particle to photon energy $mc^2/\hbar\omega$. This factor is for alkali atoms and optical photons on the order of 10^{11}, which was first noted by L. A. Page [104]. Despite this very large number, matter wave gyroscopes have only recently reached the short-time sensitivities of laser based devices [105, 106]. This is primarily because of two reasons: First, fiber-optic interferometers can have a much larger area than matter wave systems [65]. Secondly, the large photon flux achievable in optical systems, leads to a much lower shot noise level [107] as compared to matter wave set-ups. Thus, in order to make full use of the much larger rotational sensitivity per unit area of a matter wave device one needs to find ways to increase *(i)* the interferometer area and *(ii)*

the particle flux. While a substantial increase of the interferometer area in matter wave devices is difficult, the use of novel cooling techniques has led to high-flux atom sources which have been employed to substantially improve the performance of atom interferometers [108]. Even though the particle throughput can now reach 10^8 s^{-1} as compared to a few atoms per second in the first interferometers, the noise level is still much higher than that achievable in optical fiber gyroscopes [109]. The latter has photon rates on the order of 10^{16} s^{-1} [109]. Continuously loaded Bose-Einstein condensates (BEC) could provide a source for coherent atoms with higher flux values. Substantial progress has been made over the past few years in this direction [110].

We here propose a gyroscope based on the propagation of dark-state polaritons in an ultra-cold gas of Λ-type 3-level atoms [15]. We argue that this interferometer combines the large rotational phase shift of matter wave systems with the large area typical for optical gyroscopes. The idea is based on the simultaneous coherence and momentum transfer associated with the Raman transition in EIT-systems under slow-light conditions [27]. The reduction of the group velocity of light in EIT media is based on the change of character of the dressed eigenmodes of the systems from electromagnetic to atomic excitations [1]. In the course of the velocity reduction electromagnetic excitations are coherently been transformed into spin excitations (waves). The current chapter presents a detailed theoretical description of the proposed gyroscope.

A naive interpretation of eq. (3.1) would suggest that an optical gyroscope with a reduced phase or group velocity would pick up an enhanced Sagnac phase per unit area. This issue has been discussed in the past quite controversial [111, 112, 113, 114]. The controversy has been settled however and it has been shown that the observed phase shift does not depend on the presence of a comoving refractive medium in the beam path [115, 116, 117]. As shown by Dufour and Prunier it also does not depend on whether the observation takes place in the rotating frame or not [118]. As a consequence proposals for laser gyroscopes, using EIT-media to reduce the group velocity of light, do not allow to detect rotation intrinsically with an enhanced sensitivity [13]. The conclusion that EIT-media are not suitable at all is however not true. We will show that a simultaneous coherence and momentum transfer can be used to overcome the problems encountered when we disregard the motion of the medium constituents but only allow for the dispersive properties of the medium. The momentum transfer creates a coherent matter wave that will pick up a Sagnac phase shift in an appropriate medium of ultra-cold atoms.

In the most relevant type of light-matter-interaction, namely dipole interaction, the electromagnetic field couples to the atomic polarization in which case the field phase couples to the phase *difference* of the two involved atomic states. In order for a rotational phase shift of the center-of-mass wavefunction to affect the polarization, it is necessary that the matter fields corresponding to the two atomic states acquire different rotational phases. We will show that this can be achieved if the atoms in the initial, highly populated state of the EIT-system form a superfluid in a ring configuration [119, 120]. We will calculate the rotationally induced phase shift emerging in such a hybrid light-matter gyroscope. We will show that for a vanishing momentum transfer the Sagnac phase shift is equal to that of a light interferometer as given by eq. (3.1) while with the momentum transfer matter wave sensitivity can be reached. We will discuss the necessity of

a superfluid in a ring-type confining potential and show that in other cases there is no enhancement effect as compared to the pure light case.

The necessity of a ring-type superfluid reduces the potential advantages of a large-area hybrid interferometer stated in [15]. We will show however, that the minimum detectable rotation rate at the shot noise limit corresponds to that of a matter wave gyroscope with a rather large particle flux given by the density of the ultra-cold gas, e.g. a BEC, multiplied by the recoil velocity. To determine the quantum sensitivity limit of the hybrid interferometer, the saturation of the Sagnac phase shift with the probe-light intensity and the probe-field absorption are taken into account. The Sagnac phase attains a maximum value for a certain probe-field power. We determine the optimum parameter values for a maximum signal-to-noise ratio (SNR) and derive the minimum detectable rotation rate $\Omega_{\min}$ per unit area.

3.2 The Sagnac-Hybrid Interferometer

3.2.1 The Principle

An intrinsic sensor attached to the laboratory detects the rotation of the frame without any reference to some other non-rotating frame of reference. It is most natural to describe the system from the point of view of a co-rotating observer [121]. We will give a microscopic description of the gyroscope in which we consider an ensemble of three-level atoms with internal states $|1\rangle$, $|2\rangle$, and $|3\rangle$. These states are coupled by two laser fields with (complex) Rabi frequencies Ω_c and Ω_p in a Raman configuration as shown in Fig. 3.1. The probe-field Ω_p is assumed to either co- or counter-propagate to the rotation, while Ω_c, which is assumed to be much stronger than Ω_p propagates in a different, ideally perpendicular direction. The ensemble and the laser sources are assumed to be attached to the laboratory frame rotating with an angular velocity , $\mathbf{\Omega}(t) = \Omega(t)\mathbf{e}_z$. The center-of-mass motion of the atoms shall be confined to the periphery of the circular loop with radius R. It is assumed that $|\Omega|R \ll c$ such that non-relativistic quantum mechanics applies. Under conditions of two-photon resonance, the control-field Ω_c generates EIT for the probe-field associated with a substantial reduction of the group velocity [14, 46]. The group velocity reduction is due to the coupling of the weak probe light to the atomic Raman coherence. In the quasi-particle picture of dark-state polaritons, introduced by M. Fleischhauer and M. D. Lukin. [1], the processes corresponds to an adiabatic rotation from the light to the matter degree of freedom. In the Introduction we have seen that the smaller the group velocity of the dark-state polariton the larger its admixture of the matter- or spin-wave component thus making slow-light a natural candidate for a hybrid light-matter interferometer [1, 122].

3.2.2 Dynamics in a rotating frame

The dynamics seen by a co-rotating observer can be deduced by transforming the system Hamiltonian to the rotating frame. We start our description from the standard
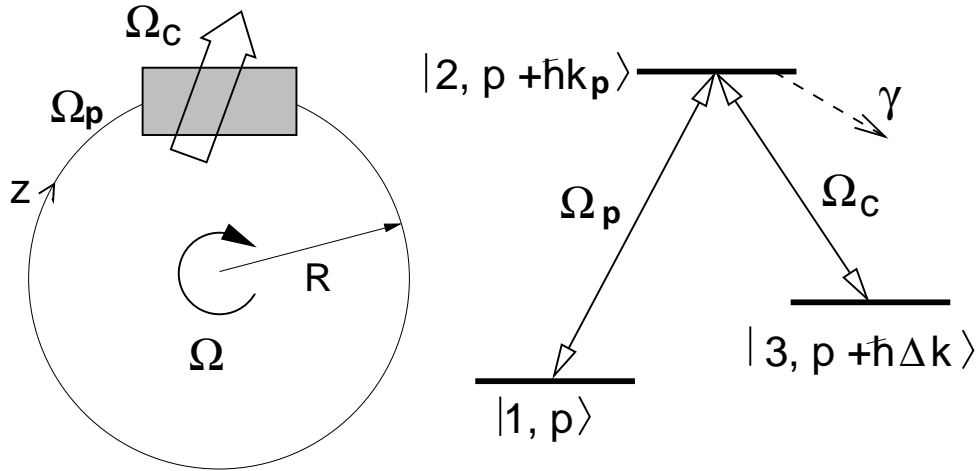
Figure 3.1: *left:* setup of light Sagnac interferometer with vapor cell or trap attached to rotating body with angular velocity Ω. *right:* level scheme of atoms. p denotes momentum along the peripheral direction z. k_p is the wavenumber of the probe field propagating parallel to z. $\Delta k = k_p - k_c^{\parallel}$, where $k_c^{\parallel}$ is the component of the control-field wave vector in z direction.

atom-light interaction Hamiltonian of quantum optics in Coulomb gauge after the Power-Zienau-Wolley transformation [18, 23]. Adding the free Hamiltonian of a 3-component nonrelativistic Schrödinger field the system Hamiltonian reads in the non-rotating frame and in second quantization

$$
\begin{aligned}
\hat{H} &= \hat{H}^{(A)} + \hat{H}^{(F)} + \hat{H}^{(I)} \\
&= \sum_{\mu} \int \mathrm{d}^3r \, \hat{\Psi}_{\mu}^{\dagger}(\mathbf{r}) \left[-\frac{\hbar^2}{2m}\nabla^2 + \hbar\omega_{\mu} + V_{\mu}^{\mathrm{ext}}(\mathbf{r},t) \right] \hat{\Psi}_{\mu}(\mathbf{r}) \\
&\quad + \frac{\epsilon_0}{2} \int \mathrm{d}^3r \left[\left(\frac{\hat{\mathbf{\Pi}}(\mathbf{r})}{\epsilon_0} \right)^2 + c^2 \left(\nabla \times \hat{\mathbf{A}}_{\perp}(\mathbf{r}) \right)^2 \right] \\
&\quad + \frac{1}{\epsilon_0} \sum_{\mu,\nu} \int \mathrm{d}^3r \, \hat{\Psi}_{\mu}^{\dagger}(\mathbf{r}) \left[\mathbf{d}_{\mu\nu} \cdot \left(\hat{\mathbf{\Pi}}(\mathbf{r}) - \epsilon_0 \mathbf{E}_{\mathrm{ext}}(\mathbf{r},t) \right) \right] \hat{\Psi}_{\nu}(\mathbf{r}).
\end{aligned}
\tag{3.2}
$$

$\hat{H}^{(A)}$ describes the motion of atoms in an external, possibly state- and time-dependent trapping potential $V_{\mu}^{\mathrm{ext}}(\mathbf{r},t)$. The three internal states are described by the three Schrödinger fields $\hat{\Psi}_1(\mathbf{r},t)$, $\hat{\Psi}_2(\mathbf{r},t)$, and $\hat{\Psi}_3(\mathbf{r},t)$ corresponding to the states of the Λ-system shown in fig. 3.1. $\hat{H}^{(F)}$ is the free Hamiltonian of the radiation field, where $\hat{\mathbf{A}}_{\perp}(\mathbf{r})$ is the transverse part of the vector potential and $\hat{\mathbf{\Pi}}(\mathbf{r}) = -\hat{\mathbf{D}} = -\left(\epsilon_0 \hat{\mathbf{E}}_{\perp} + \hat{\mathbf{P}}_{\perp} \right)$ is its conjugate momentum, which corresponds to the electric displacement field. For notational simplicity we will drop the subscript $''\perp''$, that denoted the transversality on the vector fields, in the following. Finally $\hat{H}^{(I)}$ describes the interaction of the atoms with the quantized field

as well as an additional external field in the dipole approximation. The transition to a rotating frame, having an angular velocity $\mathbf{\Omega}(t)$ with respect to the initial frame, is done via the unitary transformation

$$U(t) = \exp\left(-\frac{i}{\hbar}\int_{t_0}^{t}\mathrm{d}\tau\,\mathbf{\Omega}(\tau)\cdot\hat{\mathbf{L}}\right),\tag{3.3}$$

where $\hat{\mathbf{L}}$ is the total angular momentum operator of light and matter [123]. Restricting ourselves to a rotation about a fixed axis, the z axis, only the z component of $\hat{\mathbf{L}}$ is relevant

$$\begin{aligned}\hat{L}_{\mathrm{z}} &= \hat{L}_{\mathrm{z}}^{(A)} + \hat{L}_{\mathrm{z}}^{(F)}\\ &= \frac{\hbar}{i}\sum_{\mu}\int\mathrm{d}^3r\,\hat{\Psi}_{\mu}^{\dagger}\partial_{\varphi}\hat{\Psi}_{\mu}\\ &\quad -\frac{1}{2}\sum_{i}\int\mathrm{d}^3r\,\left[\hat{\Pi}_{\mathrm{i}}(\partial_{\varphi}\hat{A}_{\mathrm{i}}) + (\partial_{\varphi}\hat{A}_{\mathrm{i}})\hat{\Pi}_{\mathrm{i}}\right].\end{aligned}\tag{3.4}$$

The index μ denotes summation over the three internal states and the index i over the three spatial dimensions. The Hamiltonian operator in the rotating frame is then given by

$$\hat{H}_{\mathrm{rot}} = U(t)\,\hat{H}\,U^{\dagger}(t) + \Omega(t)\hat{L}_z.\tag{3.5}$$

Since $\hat{L}_{\mathrm{z}}^{(A)}$ and $\hat{L}_{\mathrm{z}}^{(F)}$ commute, the unitary transformation (3.3) can be decomposed into two operators which act on the matter wave and on the electromagnetic field respectively. One finds

$$\hat{H}_{\mathrm{rot}}^{(A)} = \Omega(t)\hat{L}_z^{(A)} + \sum_{\mu}\int\mathrm{d}^3r'\hat{\Psi}_{\mu}^{\dagger}(\mathbf{r}')\left[-\frac{\hbar^2}{2m}\nabla'^2 + \hbar\omega_{\mu} + V_{\mu}^{\mathrm{ext}}(\mathbf{r}')\right]\hat{\Psi}_{\mu}(\mathbf{r}'),\tag{3.6}$$

$$\hat{H}_{\mathrm{rot}}^{(F)} = \Omega(t)\hat{L}_z^{(F)} + \hat{H}_0^{(F)} + \frac{1}{\epsilon_0}\sum_{\mu,\nu}\int\mathrm{d}^3r'\,\hat{\Psi}_{\mu}^{\dagger}(\mathbf{r}')\left[\mathbf{d}_{\mu\nu}\cdot\left(\hat{\mathbf{\Pi}}(\mathbf{r}') - \epsilon_0\mathbf{E}_{\mathrm{ext}}(\mathbf{r}',t)\right)\right]\hat{\Psi}_{\nu}(\mathbf{r}').$$
$$\tag{3.7}$$

Here the prime denotes that the variables are given with respect to the rotating frame coordinates

$$\mathbf{r}' = \mathbf{r} + \int_{t_0}^{t}\mathrm{d}\tau\,\mathbf{e}_{\varphi}\,R\,\Omega(\tau),\tag{3.8}$$

with R being the distance from the rotation axis. For all field operators $\hat{\mathbf{F}}\in\{\hat{\mathbf{\Psi}},\hat{\mathbf{\Pi}},\hat{\mathbf{A}}\}$ we have

$$U\hat{\mathbf{F}}(\mathbf{r})U^{\dagger} = \hat{\mathbf{F}}\left(\mathbf{r} + \int_{t_0}^{t}\mathrm{d}\tau\,\mathbf{e}_{\varphi}\,R\,\Omega(\tau)\right) = \hat{\mathbf{F}}(\mathbf{r}').\tag{3.9}$$

The dynamics of the matter fields is governed in the rotating frame by the following Heisenberg equations of motion where we omitted the primes for notational simplicity

$$i\hbar\Big(\partial_t + \Omega(t)\partial_\varphi\Big)\hat{\Psi}_\mu(\mathbf{r}, t) = \left[-\frac{\hbar^2}{2m}\nabla^2 + \hbar\omega_\mu + V_\mu^{\text{ext}}(\mathbf{r})\right]\hat{\Psi}_\mu(\mathbf{r}, t)$$
$$+ \frac{1}{\epsilon_0}\sum_\nu \mathbf{d}_{\mu\nu}\cdot\left[\hat{\mathbf{\Pi}}(\mathbf{r}) - \epsilon_0\mathbf{E}_{\text{ext}}(\mathbf{r}, t)\right]\hat{\Psi}_\nu(\mathbf{r}). \tag{3.10}$$

Correspondingly the equations of motion for the conjugate momentum $\hat{\mathbf{\Pi}}$ and the transverse vector potential $\hat{\mathbf{A}}$ read

$$\Big(\partial_t + \Omega(t)\partial_\varphi\Big)\hat{\mathbf{\Pi}}(\mathbf{r}, t) = -\frac{1}{\mu_0}\nabla\times(\nabla\times\hat{\mathbf{A}}(\mathbf{r}, t)) \tag{3.11}$$

and

$$\Big(\partial_t + \Omega(t)\partial_\varphi\Big)\hat{\mathbf{A}}(\mathbf{r}, t) = \frac{1}{\epsilon_0}\hat{\mathbf{\Pi}}(\mathbf{r}, t) + \frac{1}{\epsilon_0}\hat{\mathbf{P}}(\mathbf{r}, t). \tag{3.12}$$

Here we have introduced the transverse polarization

$$\hat{\mathbf{P}}(\mathbf{r}, t) = \sum_{\mu,\nu}\hat{\Psi}_\mu^\dagger(\mathbf{r}, t)\,\mathbf{d}_{\mu\nu}\hat{\Psi}_\nu(\mathbf{r}, t). \tag{3.13}$$

It is immediately obvious that the transformation to the rotating frame just amounts to the replacement $\partial_t \longrightarrow \partial_t + \Omega(t)\,\partial_\varphi$ in the equations of motion with respect to the initial frame.

In the Coulomb gauge we have $\hat{\mathbf{\Pi}}(\mathbf{r}, t) = -\hat{\mathbf{D}}(\mathbf{r}, t)$ [18]. Using this and $\hat{\mathbf{D}}(\mathbf{r}) = \epsilon_0\hat{\mathbf{E}}(\mathbf{r}) + \hat{\mathbf{P}}(\mathbf{r})$ we find for the wave equation in the rotating frame

$$\left[\triangle - \frac{1}{c^2}\Big(\partial_t + \Omega(t)\partial_\varphi\Big)^2\right]\hat{\mathbf{E}}(\mathbf{r}, t) = \mu_0\Big[\partial_t + \Omega(t)\partial_\varphi\Big]^2\hat{\mathbf{P}}(\mathbf{r}, t). \tag{3.14}$$

In the following we are going to apply the slowly-varying envelope approximation, which still holds in the rotating frame. The approximation is applicable as long as the rate of change of the field is negligible on the distance of a wavelength of the field. Thus we introduce slowly-varying variables for the transverse field as well as the polarization by $\hat{\mathbf{E}}(\mathbf{r}, t) = \hat{\boldsymbol{\mathcal{E}}}^{(+)}(x, r_\perp, t)\,e^{-i(\omega_p t - k_p x)} + h.\,a.$ and $\hat{\mathbf{P}}(\mathbf{r}, t) = \hat{\boldsymbol{\mathcal{P}}}^{(+)}(x, r_\perp, t)\,e^{-i(\omega_p t - k_p x)} + h.\,a.$, where $x = R\varphi$ is the arclength of the circle. Restricting ourselves to propagation along the periphery of the interferometer we find within the slowly-varying envelope approximation and neglecting terms $\mathcal{O}(\Omega R/c)$

$$\Big(\partial_t + c\partial_x + ik_p\Omega R\Big)\hat{\boldsymbol{\mathcal{E}}}^{(+)}(x, t) = \frac{i\,\omega_p}{2\,\epsilon_0}\hat{\boldsymbol{\mathcal{P}}}^{(+)}(x, t). \tag{3.15}$$

The term proportional to the rotation rate Ω is responsible for the rotationally induced Sagnac phase shift in the pure light case, i. e. without any influence from the medium. As shown in [15] and in the next section the polarization term leads to an additional phase

shift if we fulfill the conditions mentioned section in 3.1.

Introducing also slowly-varying amplitudes for the matter fields $\hat{\Psi}_1 = \hat{\Phi}_1$, $\hat{\Psi}_2 = \hat{\Phi}_2\, e^{-\mathrm{i}(\omega_p t - k_p x)}$ and $\hat{\Psi}_3 = \hat{\Phi}_3\, e^{-\mathrm{i}(\Delta\omega t - \Delta k x)}$ with $\Delta\omega = \omega_p - \omega_c$ and $\Delta k = k_p - k_c^{\parallel}$, where $k_c^{\parallel}$ is the wave vector projection of the control-field on to the x-axis, we find

$$\left(\mathcal{D}_1 - V_1(x)\right)\hat{\Phi}_1 = \hbar\Omega_p^*\hat{\Phi}_2, \tag{3.16}$$

$$\left(\mathcal{D}_2 - V_2(x) + \hbar(\Delta_2 - k_p\Omega R)\right)\hat{\Phi}_2 = \hbar\Omega_p\hat{\Phi}_1 + \hbar\Omega_c\hat{\Phi}_3, \tag{3.17}$$

$$\left(\mathcal{D}_3 - V_3(x) + \hbar(\Delta_3 - \eta k_p\Omega R)\right)\hat{\Phi}_3 = \hbar\Omega_c^*\hat{\Phi}_2, \tag{3.18}$$

with

$$\mathcal{D}_\mu = \mathrm{i}\,\hbar\,\partial_t + \frac{\hbar^2\partial_x^2}{2m} + \mathrm{i}\,\hbar\,(\Omega R + \eta_\mu v_{\mathrm{rec}})\partial_x. \tag{3.19}$$

Here we have used the definitions $\Delta_2 = \omega_p - \omega_2 - \omega_{\mathrm{rec}}$ and $\Delta_3 = \Delta\omega - \omega_3 - \eta^2\omega_{\mathrm{rec}}$ for the one- and two-photon detuning including the recoil shift ($\omega_{\mathrm{rec}} = \hbar k_p^2/2m$). Additionally we have introduced the dimensionless parameter $\eta = \Delta k/k_p$ which describes the momentum transfer from the light fields to the atoms in state $|3\rangle$ as well as the abbreviation $\eta_\mu = \delta_{\mu,2} + \eta\,\delta_{\mu,3}$. The control and probe-field Rabi frequencies are defined by $\Omega_{p,c} = -\mathbf{d}_{p,c}\cdot\mathbf{E}_{\mathrm{ext}}^{(p,c)}/\hbar$.

3.3 Sagnac phase shift and influence of external trapping potentials

In this section we calculate the stationary Sagnac phase shift obtained in the hybrid interferometer in the perturbative limit of low probe light intensities. In particular we will take into account the effects of the confinement of the atoms along the direction of the interferometer path. In what follows we perform a perturbation theory in powers of the probe-field, i. e. our general solution may be expanded in powers of Ω_p^n

$$\hat{\Phi}_\mu(\mathbf{r}, t) = \sum_n \hat{\Phi}_\mu^{(n)}(\mathbf{r}, t). \tag{3.20}$$

Furthermore, we assume that all atoms are initially in the internal state $|1\rangle$. Therefore, we have $\langle\hat{\Phi}_2^{(0)}(x, t=0)\rangle = \langle\hat{\Phi}_3^{(0)}(x, t=0)\rangle = 0$. The stationary state is described in zeroth order according to eq. (3.16) by

$$\left(\frac{\hbar^2\partial_x^2}{2m} + i\hbar\Omega R\partial_x + (\epsilon_1 - V_1(x))\right)\hat{\Phi}_1^{(0)}(x) = 0, \tag{3.21}$$

where ϵ_1 is the energy (chemical potential) of the internal state $|1\rangle$. This equation holds also in first order of the perturbation theory due to the initial conditions mentioned above. Assuming $|\Omega_c| \gg |\Delta_2|, k_p|\Omega|R, V_2(x)/\hbar, \Omega R/L, v_{\mathrm{rec}}/L, \epsilon_2/\hbar$ and $\hbar/(2mL^2)$ one finds in first order from eq. (3.17)

$$\hat{\Phi}_3^{(1)}(x) = -\frac{\Omega_p(x)}{\Omega_c}\hat{\Phi}_1^{(0)}(x), \tag{3.22}$$

which amounts to an adiabatic elimination of the excited state. Using this, eq. (3.18) and the two-photon resonance condition $\Delta_3 = 0$, we find

$$
\hat{\Phi}_2^{(1)} = \eta k_p \frac{\Omega R}{|\Omega_c|^2} \hat{\Phi}_1^{(0)} \Omega_p - \frac{1}{|\Omega_c|^2} \left[\frac{\hbar}{2m} \partial_x^2 + \mathrm{i} \left(\Omega R + \eta v_{\mathrm{rec}} \right) \partial_x + \frac{\epsilon_3 - V_3(x)}{\hbar} \right] \hat{\Phi}_1^{(0)} \Omega_p,
$$

$$
\tag{3.23}
$$

$$
= \eta \frac{\hat{\Phi}_1^{(0)}}{|\Omega_c|^2} \left[k_p \Omega R - i v_{\mathrm{rec}} (\partial_x \ln \hat{\Phi}_1^{(0)}) \right] \Omega_p(x)
$$

$$
- \frac{\hat{\Phi}_1^{(0)}}{|\Omega_c|^2} \left[\frac{\hbar \partial_x^2}{2m} + i \left(\Omega R + \eta v_{\mathrm{rec}} - i \frac{\hbar}{m} (\partial_x \ln \hat{\Phi}_1^{(0)}) \right) \partial_x \right] \Omega_p(x).
$$

In deriving the second equation, which is useful for later discussions, we have made use of (3.21) and assumed equal trapping potentials for the internal states $V_1 = V_3$. Furthermore, an unimportant constant energy term proportional to $\epsilon_1 - \epsilon_3$ has been dropped. One recognizes that the fields $\hat{\Phi}_2^{(1)}$ and $\hat{\Phi}_3^{(1)}$ and thus the medium polarization

$$
\mathcal{P}_{12}^{(+)}(x) = d_{12} \langle \hat{\Phi}_1^\dagger(x) \hat{\Phi}_2(x) \rangle \tag{3.24}
$$

follow in a straight forward way from the solution of eq. (3.21). In the next two sections we will consider two important and fundamentally different cases. In the first case no longitudinal confining potential for atoms in state $|1\rangle$ is assumed. This is equivalent to a system with periodic boundary conditions such as a ring trap. In the second case a trapping potential in the peripheral direction is taken into account.

3.3.1 Periodic boundary conditions in state $|1\rangle$

Let us consider the case that atoms in state $|1\rangle$ do not experience any confining potential in the x direction. Since x is the coordinate along the periphery of the interferometer, this amounts to considering a ring-trap configuration with periodic boundary conditions as shown in fig. 3.2. With $V_1(x) \equiv 0$, eq. (3.21) has the solutions

$$
\hat{\Phi}_1^{(0)}(x) = \begin{cases} \hat{\Phi}_0 & \epsilon_1 = 0 \\ \hat{\Phi}_0 \, e^{-im\Omega Rx/\hbar} & \epsilon_1 = m\Omega^2 R^2/2 \end{cases}, \tag{3.25}
$$

where $\hat{\Phi}_0$ is constant. We assume that the atoms in state $|1\rangle$ form a Bose condensate and can thus be described by a coherent c-number field (or order parameter), i. e. we can substitute $\hat{\Phi} \to \Phi$. The ring-trap configuration then implies periodic boundary conditions

$$
\Phi(x + 2\pi R) = \Phi(x). \tag{3.26}
$$

As a consequence only the solution with $\epsilon_1 = 0$ applies as long as $m\Omega R^2/\hbar < 1$. This reflects the fact that the BEC forms a *superfluid* which is irrotational and thus will not
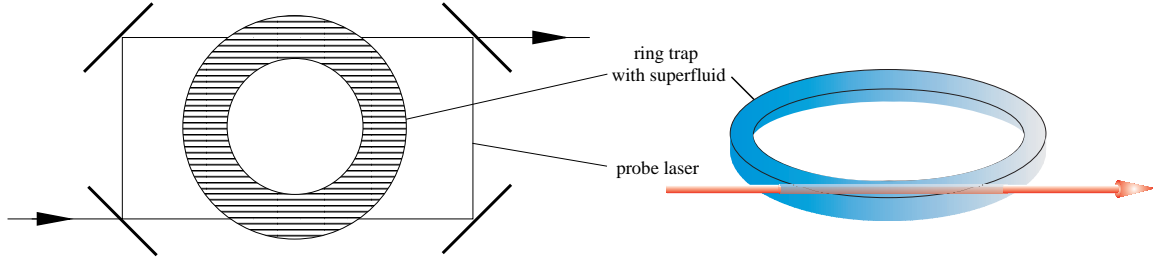
Figure 3.2: The picture shows the proposed setup of a ring-shaped trap configuration supporting a superfluid ultra-cold gas (BEC). The red arrow corresponds to the crossing probe-field laser. It is not necessary to use the symmetric set-up as shown on the left hand side, however, this approach allows for a distinction of rotational from linear acceleration.

pick up any rotational phase. This yields with eq. (3.23)

$$\Phi_2^{(1)}(x) = \eta k_p \frac{\Omega R}{|\Omega_c|^2} \Phi_0 \, \Omega_p(x) - \frac{i(\Omega R + \eta v_{\text{rec}})\Phi_0}{|\Omega_c|^2} \partial_x \, \Omega_p(x) \tag{3.27}$$

$$- \frac{1}{|\Omega_c|^2} \Phi_0 \frac{\hbar}{2m} \partial_x^2 \, \Omega_p(x).$$

Equation (3.27) allows us to finally determine the linear response of the medium. By substituting the expressions for $\Phi_2^{(1)}$ and $\Phi_1^{(0)}$ into eq. (3.24) and subsequently into the stationary, shortened wave equation, eq. (3.15), we find using the definition $g = d_{12}\sqrt{\omega_p/2\hbar\epsilon_0 F}$ for the coupling constant

$$\left(c\partial_x + i k_p \Omega R \right) \Omega_p(x) = -ig^2 \Phi_1^{(0)*} \Phi_2^{(1)}(x). \tag{3.28}$$

Here d_{12} denotes the dipole matrix element of the $|1\rangle \leftrightarrow |2\rangle$ transition and F the transversal cross section of the probe beam. The last two equations allow us to determine the equation for the weak probe-field

$$\left\{ \left[c\cos^2\theta + (\eta v_{\text{rec}} + \Omega R)\sin^2\theta \right] \partial_x - i \sin^2\theta \frac{\hbar\partial_x^2}{2m} \right\} \Omega_p$$

$$= -i k_p \Omega R \left(\cos^2\theta + \eta \sin^2\theta \right) \Omega_p(x). \tag{3.29}$$

For notational simplicity we have introduced the mixing angle θ through the definition $\tan^2\theta = g^2 n/|\Omega_c|^2$, where $n = \Phi_0^*\Phi_0$ is the density of atoms in state $|1\rangle$. Eq. (3.29) has a very intuitive interpretation. It describes the propagation of the probe-field with the group velocity

$$v_{\text{gr}} = c\cos^2\theta + \eta \, v_{\text{rec}} \, \sin^2\theta \tag{3.30}$$

in the rotating frame [124]. The propagation of light in an EIT medium is associated with the formation of a dark-state polariton, a superposition of electromagnetic and matter

wave components. If we neglect the motion of the atoms, the group velocity of this quasi-particle is proportional to $\cos^2\theta$, which is the square of the weight factor of the electromagnetic part of the polariton [1]. If the coherence transfer from light to atoms is accompanied by a finite momentum transfer of $\eta\, m\, v_{\text{rec}}$, then there is also a matter wave contribution to the total group velocity. This contribution is again proportional to the square of its weight factor in the polariton. Thus in the limit $\tan^2\theta > c/v_{\text{rec}} = \tan^2\theta_{\text{crit}}$, the light wave is turned into a propagating spin-polarization with velocity $\eta\, v_{\text{rec}}$. As a consequence of the admixture of a matter wave excitations, the equation of motion (3.29) also obtains a term corresponding to the kinetic energy of the matter wave. The right hand side of eq. (3.29) describes the light and matter wave contributions to the rotationally induced phase shift. Noteworthy is that the group-velocity term corresponding to the light part has no rotational admixture. The matter wave contribution to the phase shift is non-zero only if there is a finite momentum transfer, i.e. if $\eta \neq 0$. Eq. (3.29) can easily be solved in the limit of small rotation, $|\Omega|R \ll v_{\text{gr}}$, which is the case of interest. Neglecting the second-order derivative, eq. (3.29) reduces to eq. (11) of ref. [15]

$$\partial_x \ln \Omega_p(x) = -i \frac{2\pi\Omega R}{\lambda c} \left[\frac{\xi(x)}{\xi(x) + \eta} + \frac{mc^2}{\hbar\omega_p} \frac{\eta}{\xi(x) + \eta} \right], \tag{3.31}$$

where

$$\xi(x) \equiv \frac{\cot^2\theta}{\cot^2\theta_{\text{crit}}} \approx \frac{v_{\text{gr}}(x)}{v_{\text{rec}}} - \eta. \tag{3.32}$$

The last approximate equation is only valid for $v_{\text{gr}} \ll c$. When ξ is large the group velocity is much larger than the recoil velocity, while ξ approaching zero means that the group velocity is comparable to the recoil velocity. Eq. (3.31) describes the rotationally induced phase shift of the probe-field without taking its absorption into account, i. e. in the regime of perfect EIT. Two counterpropagating probe-fields will experience the Sagnac phase shift

$$\Delta\phi_{\text{sig}} = \frac{2\pi\Omega R}{\lambda c} \int \frac{\xi(x)}{\xi(x) + \eta}\, \mathrm{d}x + \frac{\Omega R}{\hbar/m} \int \frac{\eta}{\xi(x) + \eta}\, \mathrm{d}x. \tag{3.33}$$

This is the result obtained in [15]. The Sagnac phase has two terms, a light-contribution and, if $\eta \neq 0$, a matter wave contribution. If the group velocity becomes comparable to the recoil velocity, i.e. for $\xi \to 0$, the Sagnac phase approaches the matter wave value!

The assumption of periodic boundary conditions for $\hat{\Phi}_1^{(0)}$ practically requires a ring trap configuration and the solution $\hat{\Phi}_1^{(0)}(x) = \hat{\Phi}_0 = const.$ means that the atoms do not follow the motion of the rotating trap. This is strictly speaking only possible if the gas is superfluid. In a normal gas collisions with wall roughness's and between atoms, which are not taken into account here, would accelerate the vapor atoms in the initial phase of rotation. Eventually a stationary state would be reached where the atoms co-rotate with the trap. Whether the above given arguments can be applied to normal gases strongly depends on the time scales to reach the stationary state. Thus the extention to thermal gases made in [15] is problematic and needs more careful considerations. Secondly the
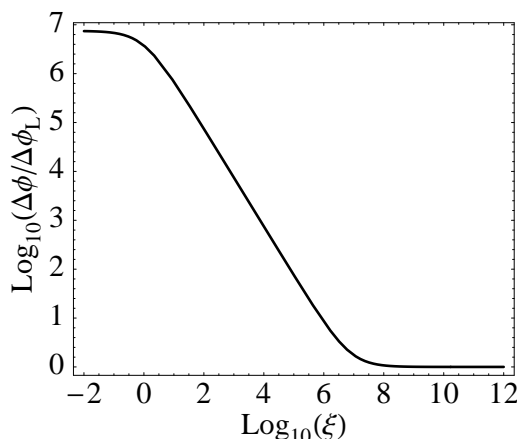
Figure 3.3: Sagnac phase-shift of the EIT hybrid interferometer relative to the phase shift of an optical gyroscope of the same area, a ratio of medium length to circumference of 10^{-3} and $\eta = 1$; for $\xi \gg \eta m c^2 / \hbar \omega_p$ we are in the light and for $\xi \ll \eta$ we are in the matter wave regime. A recoil velocity $v_{\mathrm{rec}} = \hbar \omega_p / mc$ of 4 cm/s was assumed.

need for a superfluid gas (e.g. BEC) in a ring trap puts restrictions to the achievable interferometer area. Although recently there has been substantial progress in realizing ring traps for BEC [119], the area achieved is only on the order of 10^{-1} cm^2, which cannot compete with the values reached in fiber-optical gyroscopes.

3.3.2 Effect of longitudinal confinement

Let us now discuss the case of a longitudinal trapping potential for atoms in state $|1\rangle$, i.e. $V_1(x) \neq 0$ in eq. (3.21). In this case the substitution

$$\Phi_1^{(0)}(x) = \Phi_0 \, f(x) \, \mathrm{e}^{-im\Omega Rx/\hbar} \tag{3.34}$$

leads to the steady-state equation

$$\left(\frac{\hbar^2 \partial_x^2}{2m} + \frac{m}{2}\Omega^2 R^2 + \epsilon_1 - V_1(x) \right) f(x) = 0. \tag{3.35}$$

If one disregards the small centrifugal energy shift proportional to Ω^2, this equation is just the stationary Schrödinger equation for a particle in the trap potential V_1. The solution of this equation is independent of the rotation rate except for the trivial centrifugal energy term. If we substitute (3.34) into the second equation of (3.23), one recognizes that all terms containing the rotation rate Ω in first order vanish exactly:

$$\Phi_2^{(1)}(x) = -i\frac{\Phi_1^{(0)}(x)}{|\Omega_c^2|} \left(\eta v_{\mathrm{rec}}(\partial_x \ln f(x))\Omega_p(x) - i\frac{\hbar \partial_x^2}{2m}\Omega_p(x) \right)$$

$$- i\frac{\Phi_1^{(0)}(x)}{|\Omega_c^2|} \left(\eta v_{\mathrm{rec}} - i\frac{\hbar}{m}\partial_x \ln f(x) \right) \partial_x \Omega_p. \tag{3.36}$$

Substituting this into the shortened wave equation for Ω_p yields

$$\left[c \cos^2 \theta + \left(\eta v_{\text{rec}} - i \frac{\hbar}{m} \partial_x \ln f(x) \right) \sin^2 \theta \right] \partial_x \Omega_p(x) - i \sin^2 \theta \frac{\hbar \partial_x^2}{2m} \Omega_p(x) = \tag{3.37}$$
$$- i k_p \Omega R \, \cos^2 \theta \Omega_p(x) - \eta v_{\text{rec}} \sin^2 \theta \Big(\partial_x \ln f(x) \Big) \Omega_p(x).$$

Neglecting the term with second derivatives as well as those containing derivatives of $f(x)$, i. e. taking into account that $f(x)$ is a slowly-varying ground-state wave function of a smooth potential, eq. (3.37) reduces to

$$\partial_x \ln \Omega_p(x) = -i \frac{2\pi \Omega R}{\lambda c} \frac{\cos^2 \theta}{\cos^2 \theta + \eta \frac{v_{\text{rec}}}{c} \sin^2 \theta} = -i \frac{2\pi \Omega R}{\lambda c} \frac{1}{1 + \eta/\xi}. \tag{3.38}$$

It is obvious that only the light part of the Sagnac phase survives, as we see from discussing the two limits of the parameter ξ. If ξ tends to zero, i. e. in the matter case, the right hand side vanishes and so does the Sagnac shift. On the other hand, if ξ tends to infinity, i. e. in the pure light case, the second term in the denominator of the right hand side of eq. (3.38) vanishes and only the pure light rotational phase shift survives. Thus in the EIT hybrid gyroscope a matter wave contribution to the Sagnac phase only emerges in the absence of a confining potential i. e. if periodic boundary conditions apply as e.g. in a ring trap.

The physical interpretation of this result is straight forward. In the presence of a confining potential the atoms trapped in this potential, especially the atoms in state $|1\rangle$, are bound to the motion of the confining potential. Hence they acquire a rotationally induced phase shift by following the motion of the potential which is attached to the rotating frame. The atoms in state $|2\rangle$ acquire the same phase shift since they are in the same frame. Therefore, the polarization eq. (3.24) attains no Sagnac phase since it is a sesquilinear function in terms of the wave-functions of the states $|1\rangle$ and $|2\rangle$. In the case of a superfluid BEC in a ring trap the order parameter does not pick up any phase as long as the rotation is sufficiently slow. This is due to the periodic boundary conditions and the superfluidity of the condensate [125, 126, 127].

3.4 Quantum limited sensitivity of the slow-light gyroscope

The aim of this section is to determine the sensitivity of the slow-light Sagnac interferometer in the case of periodic boundary conditions, i.e. in the absence of any confining potential in the propagation direction. We restrict ourselves to the case $\eta = 1$, i. e. to the configuration of perpendicular wave vectors of probe and control field. We assume that the error in determining the Sagnac phase is entirely determined by quantum fluctuations. If coherent laser light or Poissonian particle sources are used the shot noise limit of the phase measurement is given by [21]

$$\Delta \phi_{\text{noise}} = \frac{1}{\sqrt{n_{\text{D}}}}, \tag{3.39}$$

where $n_{\mathrm{D}} = I_{\mathrm{out}}t_{\mathrm{D}}$ is the total number of photons or atoms counted at the detector during the measurement time t_{D}. I_{out} is the photon or atom flux, i. e. the number of particles per time unit. The assumption that the quantum noise limit is set by shot noise is justified by two observations: First of all, it is known that using non-classical light or sub-Poissonian particle sources in interferometry does in general not lead to an improvement of the signal-to-noise ratio. This is because losses are usually already quite substantial at the optimum operation point. These tend to quickly destroy the fragile nonclassical and sub-Poissonian properties. Secondly, as has been shown in [31, 128], atomic noise contributions in EIT-type interferometer set-ups are small and can be neglected.

In the weak-signal limit discussed in the previous section, the Sagnac phase accumulated is independent of the signal field strength [15], hence the signal-to-noise ratio could become arbitrarily large when the input laser power is increased. This argumentation only holds as long as the lowest order of the perturbation theory in the signal field intensity used in the derivation of eq. (3.33) is applicable. In reality the Sagnac phase approaches a maximum value at a certain optimum probe laser power and decreases for larger intensities. As we will see later on, the optimum intensity is reached when the number density of photons in the EIT medium approaches that of the atoms. In order to calculate the maximum sensitivity and to find the optimum operation conditions we have to calculate the Sagnac phase to all orders of the signal Rabi frequency. In higher order perturbation the excited state $|2\rangle$ attains a finite population, therefore decay out of the excited state needs to be taken into account. In general the decay leads to a population redistribution among the states of the Λ system, see Fig. 3.4. It can also lead to loss out of the system. We will disregard the latter process. This allows us to describe the system by a set of equations for the single-particle density matrix $\rho_{\mu\nu}(x,x',t) = \langle \hat{\Phi}_\mu^\dagger(x,t)\hat{\Phi}_\nu(x',t)\rangle = \mathrm{Tr}\{\rho\hat{\Phi}_\mu^\dagger(x,t)\hat{\Phi}_\nu(x',t)\}$ in the internal states $\mu, \nu \in \{1, 2, 3\}$. Since the medium polarization of the $|1\rangle - |2\rangle$-transition is determined by the local density-matrix element $\rho_{12}(x,x,t)$ we consider only local quantities. For the density matrix elements diagonal in the internal states we find the equations of motion

$$\partial_t\rho_{11}(x,t) = \gamma_1\rho_{22}(x,t) - \mathrm{i}\,\Omega_{\mathrm{p}}^*(x,t)\rho_{21}(x,t) + \mathrm{i}\,\Omega_{\mathrm{p}}(x,t)\rho_{12}(x,t)$$
$$- \Omega R\,\partial_x\rho_{11}(x,t), \tag{3.40}$$

$$\partial_t\rho_{22}(x,t) = -\gamma_2\rho_{22}(x,t) + \mathrm{i}\,\Omega_{\mathrm{p}}^*(x,t)\rho_{21}(x,t) - \mathrm{i}\,\Omega_{\mathrm{p}}(x,t)\rho_{12}(x,t)$$
$$+ \mathrm{i}\,\Omega_{\mathrm{c}}^*(x,t)\rho_{23}(x,t) - \mathrm{i}\,\Omega_{\mathrm{c}}(x,t)\rho_{32}(x,t) - (\Omega R + v_{\mathrm{rec}})\partial_x\rho_{22}(x,t), \tag{3.41}$$

$$\partial_t\rho_{33}(x,t) = \gamma_3\rho_{22}(x,t) - \mathrm{i}\,\Omega_{\mathrm{c}}^*(x,t)\rho_{23}(x,t) + \mathrm{i}\,\Omega_{\mathrm{c}}(x,t)\rho_{32}(x,t)$$
$$- (\Omega R + v_{\mathrm{rec}})\partial_x\rho_{33}(x,t). \tag{3.42}$$

Likewise we find for the local coherence's

$$\partial_t\rho_{12}(x,t) = -[\mathrm{i}(\Delta_2 - \Omega R k_{\mathrm{p}}) + \gamma_2/2]\rho_{12}(x,t) + \mathrm{i}\,\Omega_{\mathrm{c}}^*(x,t)\rho_{13}(x,t)$$
$$- \mathrm{i}\,\Omega_{\mathrm{p}}^*(x,t)(\rho_{22}(x,t) - \rho_{11}(x,t)) - (\Omega R + v_{\mathrm{rec}})\partial_x\rho_{12}(x,t)$$
$$+ v_{\mathrm{rec}}\langle \hat{\Phi}_2^\dagger(\partial_x\hat{\Phi}_1)\rangle \tag{3.43}$$

$$\partial_t \rho_{13}(x,t) = -[\mathrm{i}(\Delta_3 - \Omega R k_p) + \gamma_{13}]\rho_{13}(x,t) - \mathrm{i}\,\Omega_\mathrm{p}^*(x,t)\rho_{23}(x,t)$$
$$+ \mathrm{i}\,\Omega_\mathrm{c}(x,t)\rho_{12}(x,t) - (\Omega R + v_\mathrm{rec})\partial_x\rho_{13}(x,t) + v_\mathrm{rec}\langle\hat{\Phi}_3^\dagger(\partial_x\hat{\Phi}_1)\rangle \qquad (3.44)$$

$$\partial_t \rho_{23}(x,t) = [\mathrm{i}(\Delta_2 - \Delta_3) - \gamma_2/2]\rho_{23}(x,t) - \mathrm{i}\,\Omega_\mathrm{p}(x,t)\rho_{13}(x,t)$$
$$- \mathrm{i}\,\Omega_\mathrm{c}(x,t)(\rho_{33}(x,t) - \rho_{22}(x,t)) - (\Omega R + v_\mathrm{rec})\partial_x\rho_{23}(x,t) \qquad (3.45)$$

where $\gamma_2 \equiv \gamma_1 + \gamma_3$. For the derivation of the decay terms we refer to the Appendix A.1. One recognizes that the local nondiagonal matrix elements are coupled to non-local quantities of the form $\langle\hat{\Phi}_\nu^\dagger(x)(\partial_x\hat{\Phi}_\mu(x))\rangle$. These terms cause the build-up of coherences between different internal states *and* different positions. The coherences are zero at the beginning, due to the initial conditions. We now argue that the above terms can be neglected. From eq. (3.16) we find that in steady-state and ignoring second-order derivatives (remember that there is no longitudinal confining potential, i. e. $V_1 \equiv 0$)

$$\mathrm{i}\hbar\Omega R\partial_x\Phi_1 = \hbar\Omega_p^*\Phi_2. \qquad (3.46)$$

In the adiabatic limit where the atoms are in the dark state defined by (3.22)

$$\Phi_3(x) = -\frac{\Omega_p(x)}{\Omega_c}\Phi_1(x) \qquad (3.47)$$

we have (see eq. (3.23))

$$\Phi_2 = \frac{k_p\Omega R}{|\Omega_c|^2}\Phi_1\Omega_p - \mathrm{i}\frac{\Omega R + v_\mathrm{rec}}{|\Omega_c|^2}\partial_x(\Phi_1\Omega_p). \qquad (3.48)$$

Substituting this into eq. (3.46) yields

$$\partial_x\Phi_1(x) = -\mathrm{i}s\frac{[k_p\Omega R - \mathrm{i}(\Omega R + v_\mathrm{rec})(\partial_x \ln\Omega_p)]}{\Omega R\,(1+s) + v_\mathrm{rec}\,s}\Phi_1(x), \qquad (3.49)$$

where $s = |\Omega_p|^2/|\Omega_c|^2$. Since the slowly-varying envelope of Ω_p picks up a Sagnac-phase shift according to eq. (3.38) we arrive with

$$\partial_x \ln\Omega_p \sim -\mathrm{i}\frac{\alpha}{c}k_p\Omega R \qquad (3.50)$$

at

$$\partial_x\Phi_1 = -\mathrm{i}\frac{k_p\Omega R}{v_\mathrm{rec}}\left(1 - \alpha\frac{v_\mathrm{rec}}{c}\right)\Phi_1 + \mathcal{O}((\Omega R)^2) \qquad (3.51)$$

As a consequence the term $v_\mathrm{rec}\langle\Phi_2^\dagger\partial_x\Phi_1\rangle$ in eq. (3.43) is of the order of

$$v_\mathrm{rec}\langle\Phi_2^\dagger\partial_x\Phi_1\rangle \simeq -\mathrm{i}k_p\Omega R\left(1 - \alpha\frac{v_\mathrm{rec}}{c}\right)\rho_{12} \qquad (3.52)$$

and is thus negligible as compared to $\gamma_2\rho_{12}/2$. Similarly the term $v_{\text{rec}}\langle\Phi_3^\dagger\partial_x\Phi_1\rangle$ in eq. (3.44) is of the order of

$$v_{\text{rec}}\langle\Phi_3^\dagger\partial_x\Phi_1\rangle \simeq -\mathrm{i}k_p\Omega R\left(1 - \alpha\frac{v_{\text{rec}}}{c}\right)\rho_{13}. \tag{3.53}$$

Since in the ideal case the ground-state coherence is long lived, one has $\gamma_{13} \to 0$, neglecting this term is not as straight forward as above. However, adiabatically eliminating the fast decaying optical coherence ρ_{12} in eq. (3.43) and substituting into eq. (3.44) yields a term proportional to $|\Omega_c|^2/\gamma_2\rho_{13}$ which is much larger than $k_p\Omega R\rho_{13}$. Thus also this term can be safely neglected.

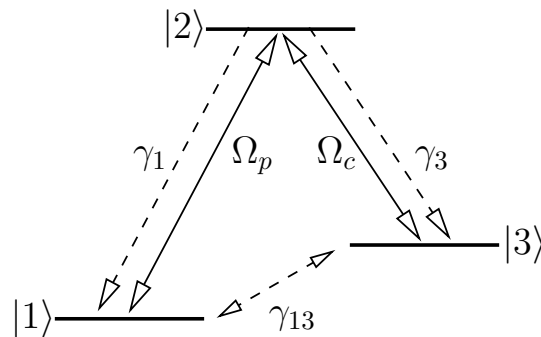In the following we assume one- and two-photon resonance, i.e. $\Delta_2 = \Delta_3 = 0$, and

Figure 3.4: Λ configuration in which the Rabi frequency Ω_p drives the $1 \leftrightarrow 2$-transition and Ω_c the $3 \leftrightarrow 2$-transition (solid lines). Radiative decay from the excited level to $|1\rangle$ or to $|3\rangle$ goes as γ_1 or γ_3 respectively (dashed lines). The dephasing rate of the $1 - 3$ coherence is denoted by γ_{13}.

solve the above system of equations in steady state for the coherence of the $1 \leftrightarrow 2$-transition.

3.4.1 Perturbation theory with respect to characteristic length

The density matrix equations (3.40-3.45) without the non diagonal terms $\langle(\partial_x\hat{\Phi}_\mu^\dagger(x))\hat{\Phi}_\nu(x)\rangle$ can be written in compact form as

$$\partial_t\rho(x,t) = \left(\mathbf{M}(x) + v_{\text{rec}}\mathbf{D}\partial_x\right)\rho(x,t) \tag{3.54}$$

where $\mathbf{M}$ and $\mathbf{D}$ are 9×9 matrices. Even under stationary conditions we are left with a set of first order linear differential equations with space dependent coefficient. Thus in order to find an analytic solution further approximations are needed. We neglect at this stage terms of the form $\Omega R\partial_x$ since they lead to higher order corrections with respect to the rotation rate. The Sagnac effect is a first order effect in Ω, see eq. (3.1). Furthermore, we make use of the fact that the off-diagonal density matrix elements are only slowly-varying

in space: Let l and T be characteristic length and time scales of changes. Normalizing time and space to these units by $\xi = x/l$ and $\tau = t/T$, eq. (3.54) reads

$$\partial_\tau \rho = \left(\tilde{\mathbf{M}} + \frac{v_{\text{rec}}T}{l} \tilde{\mathbf{D}} \partial_\xi \right) \rho \tag{3.55}$$

where typical matrix elements of $\tilde{\mathbf{M}} = \mathbf{M}T$ read as ΩT, with $|\Omega T| \gg 1$ and those of $\tilde{\mathbf{D}} = \mathbf{D}T$ are of order unity. Since the dimensionless parameter $v_{\text{rec}}T/l$ is typically small compared to unity we can apply a perturbation expansion in the recoil velocity.

In zeroth order we disregard the term containing $\mathbf{D}$. Hence in steady state we have to solve $\mathbf{M}\rho_{\text{ss}}^{(0)} = 0$ with the constraint $\sum_\mu \rho_{\mu\mu}(x) = n(x)$, which reflects the conservation of probability. Up to first order in v_{rec} we find

$$\underline{\rho}_{\text{ss}}^{(1)}(x) = \left(\underline{\mathbf{1}} - v_{\text{rec}}\underline{\mathbf{M}}^{-1}\underline{\mathbf{D}}\partial_x \right) \underline{\rho}_{\text{ss}}^{(0)}(x). \tag{3.56}$$

Here $\underline{\mathbf{M}}$ is a reduced 8×8 matrix obtained from $\mathbf{M}$ by incorporating the constraint $\sum_\mu \rho_{\mu\mu}(x) = n(x)$ and $\underline{\rho}_{\text{ss}}^{(0)}$ is the corresponding zeroth order density matrix. The explicit expressions of all matrices and vectors can be obtained from (3.40)-(3.45) in a straight forward manner. They are however lengthy and will not be given here.

3.4.2 Steady state Maxwell-Bloch equation

To obtain the rotationally induced phase shift we expand eq. (3.56) up to first order in the angular velocity Ω and use the stationary, shortend wave-equation for the probe-field in the rotating frame

$$\left(c\partial_x + \mathrm{i}k_{\text{p}}\Omega R \right)\Omega_{\text{p}}(x) = -\mathrm{i}\,g^2 n\rho_{21}^{\text{ss}}. \tag{3.57}$$

Furthermore, we neglect terms $\mathcal{O}(\gamma_{13}^2)$ and $\gamma_{13}\Omega_{\text{p}}^m$ with $m \in \mathbb{N}$ since we assume a long-lived coherence between the two lower states $|1\rangle$ and $|3\rangle$. In addition we make use of the EIT condition $\Omega_{\text{c}}^2 \gg \gamma_{13}\gamma_1$ [27] and assume for simplicity $\gamma_1 = \gamma_3 = \gamma$.
With these assumptions we find the following expressions for the real and imaginary part of the susceptibility, which determine the dispersion and absorption of the medium

$$\chi'(\Omega_{\text{p}}) = -\beta^{-1}\frac{\Omega\,R}{c}\left(1 + g^2 n \frac{\Omega_{\text{c}}^2}{(\Omega_{\text{c}}^2 + |\Omega_{\text{p}}|^2)^2} \right) \tag{3.58}$$

$$\chi''(\Omega_{\text{p}}) = -\beta^{-1}\frac{\gamma_{13}}{c}g^2 n\frac{\Omega_{\text{c}}^2}{(\Omega_{\text{c}}^2 + |\Omega_{\text{p}}|^2)^2} \tag{3.59}$$

with

$$\beta(\Omega_{\text{p}}) = 1 + \frac{v_{\text{rec}}}{c}g^2\,n\frac{\Omega_{\text{c}}^4}{(\Omega_{\text{c}}^2 + |\Omega_{\text{p}}|^2)^3}. \tag{3.60}$$

In the following we are interested in the correct description of the *phase shift* induced on the probe-field. Hence we may use a simplified description of the *absorption* of the probe-field, i. e. of the imaginary part of the susceptibility $\chi(\Omega_\mathrm{p}) = \chi' + \mathrm{i}\,\chi''$. One can easily see that the absorption constant is bounded from above by

$$\chi'' \to \kappa = -\frac{\gamma_{13}}{c} \frac{g^2 n}{\Omega_\mathrm{c}^2} = \frac{\gamma_{13}}{c} \tan^2 \theta. \tag{3.61}$$

This equation does not take into account the saturation of the absorption in the limit of large probe-field intensities $|\Omega_p| \sim \Omega_c$ and thus overestimates the losses slightly. In this limiting case the following stationary equation for the signal field arises

$$\partial_x \ln \Omega_\mathrm{p}(x) = -\frac{\gamma_{13}}{c} \tan^2 \theta - \mathrm{i}\,k_p\,\chi'(\Omega_\mathrm{p}(x)). \tag{3.62}$$

This is a non-linear differential equation, which does not lead to a simple integral. One may reformulate it in terms of an integral equation

$$\Omega_p(x) = \Omega_p(0)\,e^{-\kappa x} \exp\left[-\mathrm{i}\,k_p \int\limits_0^x \chi'\left(\Omega_p(x')\right) \mathrm{d}x'\right]. \tag{3.63}$$

The first term in eq. (3.62) describes absorption losses, the second term the rotationally induced or Sagnac phase. The same is true for eq. (3.63). An approximate solution to these equations will be given in the next section. We will persue an approach which allows us to derive analytical expression that are more suitable for interpretation.

3.4.3 Quantum limits of gyroscope sensitivity

Using the results from the last section we can now determine the minimum detectable rotation rate Ω_min of the slow-light gyroscope. We do so by maximizing the signal-to-noise ratio (SNR) of the interferometer with respect to the system parameters and set it equal to unity. The phase difference of two polaritons propagating in opposite directions is given by

$$\Delta\phi_\mathrm{sig} = \int \mathrm{d}x\,k_p\Big[\chi'\big(\Omega, \Omega_p(x)\big) - \chi'\big(-\Omega, \Omega_p(x)\big)\Big], \tag{3.64}$$

where we have ignored for notational simplicity the overall minus sign. Using this and eq. (3.58) we find

$$\Delta\phi_\mathrm{sig} = \Delta\phi_\mathrm{light} + \Delta\phi_\mathrm{matter}$$
$$= \frac{4\pi\Omega R}{\lambda c} \int \mathrm{d}x\,\frac{\xi(x)}{\xi(x) + \eta\frac{1}{(1+s(x))^3}} + \frac{2\Omega R}{\hbar/m} \int \mathrm{d}x\,\frac{\eta\frac{1}{(1+s(x))^2}}{\xi(x) + \eta\frac{1}{(1+s(x))^3}}, \tag{3.65}$$

where $s(x) = |\Omega_p(x)|^2/\Omega_c^2$ is a saturation parameter, and $\xi(x)$ was introduced in (3.32). One recognizes that the matter wave component of the signal phase shift – the second
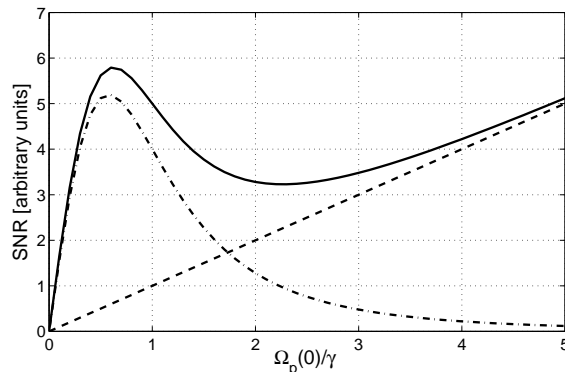
Figure 3.5: Schematic dependence of SNR on input probe-field Rabi frequency. The dash-dotted line indicates the contribution of the matter wave term, the dashed line that of the light term. The solid line is the sum of both contributions.

term on the right hand side of eq. (3.65) – decreases for increasing input probe intensity. The light component – first term in the same line of eq. (3.65) – approaches a constant in the same limit. At the same time the shot noise phase error

$$\Delta\phi_{\text{noise}} = \frac{1}{\sqrt{n_D}} \tag{3.66}$$

is inversely proportional to $|\Omega_p(0)| \, exp\,(-\kappa L)$, where L is the length of the medium. The source of the probe-field is located at $x = 0$. As a consequence of the different dependence of $\Delta\phi_{\text{sig}}$ and $\Delta\phi_{\text{noise}}$ on the signal field strength, the signal-to-noise ratio $SNR = \Delta\phi_{\text{sig}}/\Delta\phi_{\text{noise}}$ has the qualitative behavior shown in Fig. 3.5. For very large laser fields the SNR becomes arbitrarily large. This is because the light contribution to the Sagnac phase $\Delta\phi_{\text{light}}$ becomes independent on $\Omega_p(0)$ while the shot noise becomes arbitrarily small as was shown in the Introduction part of this thesis.

For small probe intensities the SNR has a local maximum due to the saturation of the matter wave phase shift. As the matter wave contribution to the Sagnac shift is orders of magnitude larger than the light contribution, extremely large input intensities would be required to exceed the sensitivity value at the first local maximum. We thus consider only this first maximum when determining the quantum-limited sensitivity of the slow-light gyroscope.

Although it is rather straight forward to calculate the minimum detectable rotation rate determined by $SNR = 1$ numerically, we are interested here in an analytic estimate. To derive a corresponding analytic expression we make a number of simplifying assumptions. We consider the propagation of polaritons through a homogeneous medium of length L. Furthermore, we ignore the space dependence of the functions $\xi(x)$ and $s(x)$ in the expression (3.65) for the signal phase, replacing $|\Omega_p(x)|$ by its input value $|\Omega_p(0)| \equiv |\Omega_p|$. As will be seen later on this only slightly overestimates the saturation of the signal at the optimum operation point. We also ignore the saturation of the probe-field absorption, which again only slightly overestimates the probe-field absorption at the
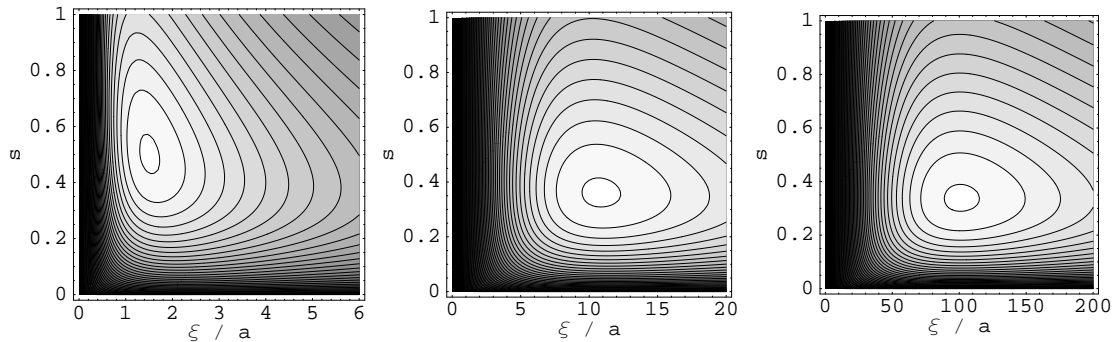
Figure 3.6: Signal-to-noise ratio (SNR) in units of the first two factors of eq. (3.72) as a function of the saturation parameter s and the light-matter-transition parameter ξ. The three graphs correspond to three different values of the loss parameter a. $a = 0.5$ (*left*), $a = 5$ (*middle*) and $a = 50$ (*right*) which are some of the values used for fig. 3.7. The *middle* and *right* plot support the statement that the location of the SNR-maximum is given, in the large a limit, by the expressions (3.73).

operation point. Finally, we only consider the dominant matter wave contribution to the signal phase. Thus we have

$$\Delta\phi_{\text{sig}} = \frac{2\,\Omega RL}{\hbar/m} \frac{(1+s)}{\xi(1+s)^3 + 1}. \tag{3.67}$$

Here $s = |\Omega_p|/\Omega_c$ is again the saturation parameter and the parameter ξ, introduced in eq. (3.32), describes the transition from a light-dominated ($\xi \gg 1$) to a matter-dominated ($\xi \ll 1$) operation of the hybrid gyroscope.

In order to estimate the signal-to-noise ratio SNR=$\Delta\phi_{\text{sig}}/\Delta\phi_{\text{noise}}$ we rewrite the shot noise expression (3.66) in terms of the parameters ξ and s. The number of probe photons at the detector can be written in terms of the probe-field Rabi frequency at the source via

$$n_{\text{D}} = \frac{P_{\text{D}}t}{\hbar\omega_{\text{p}}} = \frac{2\,\epsilon_0\,F\,c}{\hbar\omega_p} \left(\frac{\hbar\Omega_p(0)}{|\mathbf{d}_p|}\right)^2 t\,e^{-2\kappa L}, \tag{3.68}$$

where F is the cross-section of the signal beam, t the detection time interval, and $\kappa = \gamma_{13}/(v_{\text{rec}}\xi)$ the absorption coefficient introduced before. The radiative decay rate $\gamma = \gamma_1$ and the dipole matrix element $|\mathbf{d}_p|$, contained in the Rabi frequency $\Omega_p(0)$, are related through

$$\gamma = \frac{1}{4\,\pi\,\epsilon_0} \left(\frac{4}{3} \frac{|\mathbf{d}_p|^2\,\omega_p^3}{\hbar\,c^3}\right), \tag{3.69}$$

i. e. according to the Einstein A-coefficient [123]. After a straight forward calculation we find

$$n_{\text{D}} = F\,\varrho\,v_{\text{rec}}\,t\,\xi\,s\,e^{-2\,a/\xi} \tag{3.70}$$
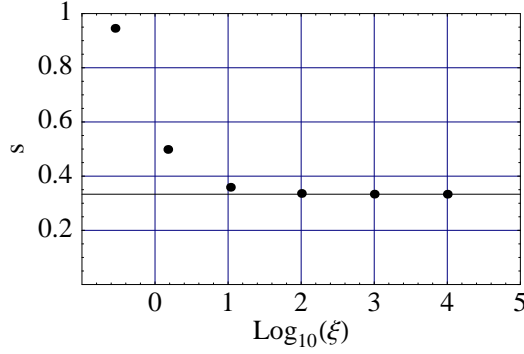
Figure 3.7: Optimum values of $s = |\Omega_p(0)|/\Omega_c$ and $\xi = v_{\mathrm{gr}}/v_{\mathrm{rec}} - 1$ for different values of the loss parameter $a = \gamma_{13}L/v_{\mathrm{rec}}$ ($= 0.05, 0.5, 5, 50, 500, 5000$). For large values of a the optimum values are $s_{\mathrm{opt}} = 1/3$ and $\xi_{\mathrm{opt}} = 2a$. For small values of a there is only a small deviation in the optimum parameters.

where ϱ is the density of atoms in the EIT medium, and

$$a \equiv \frac{\gamma_{13}L}{v_{\mathrm{rec}}} \tag{3.71}$$

characterizes the absorption due to a finite lifetime of the ground-state coherence. Since typical values of γ_{13} are in the kHz regime and $v_{\mathrm{rec}} \sim 1$ cm/s, a is typically large compared to unity for $L \gg 10^{-3}$ cm. With the above expressions we find for the signal-to-noise ratio

$$SNR = \frac{\Omega A}{\hbar/m} \Big(F \varrho v_{\mathrm{rec}} t \Big)^{1/2} \frac{\xi^{1/2}s^{1/2}(1+s)}{\xi(1+s)^3 + 1} \, \exp\big(-a/\xi\big). \tag{3.72}$$

The fist two factors in eq. (3.72) are the expression for the signal-to-noise ratio of a pure matter wave gyroscope with interferometer area $A = RL$ and flux $j = F \varrho v_{\mathrm{rec}}$, i. e. j is the number of atoms per second penetrating the cross section F [21]. In conventional atomic interferometers based on cold or ultra-cold atoms the flux that contributes to the interference signal of the device is considerably low, i. e. it is on the order of 10^8 atoms/s in comparison with 10^{16} photons/s in a conventional fiber optics gyroscope [109]. However, in the case studied here, the flux can be at least two orders of magnitude higher than the atom interferometer flux. In fig. 3.6 the dependence of the signal-to-noise ration is shown for typical values of the absorption parameter a.

The last two factors can be changed by optimizing the probe-field strength (s) and the group velocity in the medium (ξ). In Fig. 3.7 we have plotted the optimum values of s and ξ for different values of the loss parameter a. One finds that in the typical parameter regime $a \gg 1$ the maximum SNR is attained for

$$s_{\mathrm{opt}} = \frac{1}{3}, \quad \text{and} \quad \xi_{\mathrm{opt}} = 2a. \tag{3.73}$$

This approximation is still quite good even when a is about one as can be seen form fig. 3.6. Thus the optimum group velocity is according to eq. (3.32) given by

$$v_{\mathrm{gr}}^{\mathrm{opt}} = 2\gamma_{13}L + v_{\mathrm{rec}} \approx 2\gamma_{13}L, \tag{3.74}$$

where the last approximate equation holds if a is much bigger than unity. Thus we find a maximum SNR if the velocity is chosen such that during the propagation over the entire medium length L, a fraction of $1/\sqrt{e}$ of the initial polaritons got absorbed. Setting SNR=1, we eventually arrive at the minimal detectable rotation rate

$$\Omega_{\min} = \frac{\hbar/m}{A} \frac{1}{\left(F \varrho\, v_{\mathrm{rec}}\, t\right)^{1/2}} f\,\sqrt{a} \tag{3.75}$$

where $f \approx 7.19$ is a numerical prefactor. Apart from the term $\sqrt{a}$ and the unimportant numerical prefactor f, the minimal detectable rotation rate corresponds to that of a matter wave interferometer where all atoms propagate with recoil velocity. The densities achievable in the present set-up are however much larger than those in a typical beam, e.g. if we consider a BEC in a ring trap configuration.

To be more specific we give two estimates based on the already existing circular waveguides for Bose-Einstein condensates [119, 120]. To this end, we assume that the atomic density is $\rho = 10^{14}$ cm^{-3} with a cross-section $F \approx 10^{-2}$ cm^2 (smaller circle of the toroidal BEC). In case of the work of S. Gupta et al. the diameter of the waveguide is $d_{\mathrm{Gupta}} \approx 3$ mm and in the case of A. S. Arnold et al. it is $d_{\mathrm{Arnold}} \approx 96$ mm. Hence, we find in the first case the minimum detectable rotation to be $\Omega_{\min}^{\mathrm{Gupta}} \approx 1.4 \times 10^{-9}$ s^{-1} Hz$^{-1/2}$ and in the latter case $\Omega_{\min}^{\mathrm{Arnold}} \approx 1.4 \times 10^{-12}$ s^{-1} Hz$^{-1/2}$. These values compare very well to the state-of-the-art which for optical gyroscopes is 2×10^{-10} rad s^{-1} Hz$^{-1/2}$ [63] and for matter wave gyroscopes is 6×10^{-10} rad s^{-1} Hz$^{-1/2}$ [64].

3.5   Conclusion

We have proposed a novel type of light-matter wave hybrid Sagnac interferometer based on ultraslow light. We have shown that unlike in earlier proposals of slow-light gyroscopes, it is not sufficient to utilize the dispersive properties of the media to achieve an enhancement of the rotational sensitivity of an EIT-based Sagnac interferometer. According to the studies presented it is necessary to harness simultaneous coherence and momentum transfer in the associated Raman transition of the EIT-medium. Moreover, the medium has to be prepared initially in a state in which it does not acquire any rotational phase shift. This can be achieved, for example, by using a superfluid BEC in a ring trap. The latter requirement reduces the potential benifit of the hybrid interferometer idea as compared to the statements in [15]. It is not possible to build large area interferometers under this conditions with current technology. However, the potential large flux of the proposed interferometer leads to a reduction of the acquired shot noise as compared to present day pure matter wave gyroscopes and thus still leads to a sensitivity enhancement.

Chapter 4

Studies on transient Velocity Selective Coherent Population Trapping

This chapter is the result of a joint experimental and theoretical project within the Graduiertenkolleg 792: ,,Ultrakurzzeitphysik und nichtlineare Optik". In the course of the project I worked in the group of Prof. Dr. Dr. h.c. K. Bergmann together with Dr. F. Vewinger [129]. The aim of the project was the first experimental verification of the so-called transient trapping states (dark states) predicted by E. Arimondo et al. [130] for the scheme of velocity selective coherent population trapping (VSCPT).

4.1 Introduction

The idea of coherent population trapping (CPT) [21, 131] and especially of VSCPT [132, 133] is to prepare atoms in special superposition states in which there is no absorption or induced emission of the incident light fields even in the presence of a resonant coupling. In the present case these dark states are superpositions of different tensor products of internal and external states, i. e. of atoms in Zeeman sublevels with fixed momenta. The preparation of the system in these states is reflected by the generation of certain momentum distributions. In an atomic beam experiment the momentum distribution, which we want to measure, is translated into a spatial distribution at the detector which is sufficiently far enough downstream from the preparation or interaction region.

Transient velocity selective dark states were discussed first theoretically by E. Arimondo et al. [130] for the case of a $J_g = 2 \leftrightarrow J_e = 1$-transition coupled by counterpropagating σ^+ and σ^- laser-fields. Beside a stable dark state this scheme also possesses a transient dark state, i. e. a dark state that has a finite lifetime. The transient dark states have been experimentally used before [134] but have so far not been studied for their own sake. In this chapter we will present our experimental results and compare the experimental momentum distributions corresponding to the transient dark state with a

full numerical solution of the generalized optical Bloch equations. To our knowledge this is the first direct experimental observation of the transient velocity-selective dark state.

4.2 Principles of VSCPT

4.2.1 VSCPT in a Λ-configuration

In this section we follow references [132, 133] to give a brief explanation of the mechanism of velocity selective coherent population trapping. We consider two Zeeman manifolds with total angular momentum $J_g = 1$ of the ground state-manifold and $J_e = 1$ for the excited state-manifold. Atoms of this configuration are irradiated by two counter-propagating circular-polarized classical electric fields as depicted in fig. 4.1 (a).

In the first stage of the description we do not take spontaneous emission into account except for the optical pumping process into the Λ-type subsystem of the $J_g = 1 \leftrightarrow J_e = 1$ -transition given by the states $\{|g_{-1}\rangle = |J_g, m_g = -1\rangle, |e\rangle = |J_e, m_e = 0\rangle, |g_{+1}\rangle = |J_g, m_g = 1\rangle\}$. Due to the applied $\sigma^+ - \sigma^-$-laser fields and the vanishing Clebsch-Gordon coefficient of the $|J_g = 1, m_g = 0\rangle \leftrightarrow |J_e = 1, m_e = 0\rangle$ -transition spontaneous emission leads to the depopulation of the V-configuration represented by the set of states $\{|J_e, m_e = -1\rangle, |J_g, m_g = 0\rangle, |J_e, m_e = 1\rangle\}$. Hence, it is only necessary to consider in the following the Λ-subsystem. The Hamiltonian which describes the motion of atoms, stimulated emission and absorption processes is given by

$$H = \frac{\mathbf{p}^2}{2M} + \hbar\omega_e |e\rangle\langle e| - \mathbf{d} \cdot \mathbf{E}(z, t), \tag{4.1}$$

where M is the mass of the atoms and $P_e = |e\rangle\langle e|$ the projector on the excited state $|e\rangle = |J_e, m_e = 0\rangle$. This state has an energy of $\hbar\omega_e$ with respect to the ground state manifold J_g. Here $\mathbf{d}$ is the electric dipole moment operator. The representation of the classical electric field propagating in the $\pm$ z-direction is given by

$$\mathbf{E}(z, t) = \frac{1}{2} \left(\mathcal{E}_+ \boldsymbol{\epsilon}_+ e^{-\mathrm{i}\omega t} e^{\mathrm{i}kz} + \mathcal{E}_- \boldsymbol{\epsilon}_- e^{-\mathrm{i}\omega t} e^{-\mathrm{i}kz} + c.c. \right), \tag{4.2}$$

where $\boldsymbol{\epsilon}_\pm$ are the unit vectors of the left $(-)$ /right $(+)$ circular polarized fields [135]. The carrier frequency is denoted by ω, its corresponding wave number by k and $\mathcal{E}_\pm$ are the slowly varying field amplitudes (positive frequency part) for the forward respectively backward propagating component of the applied electric field. The Rabi frequencies for these fields are defined via $\Omega_\pm = -d_\pm \mathcal{E}_\pm / \hbar$ with $d_\pm = \langle e | \boldsymbol{\epsilon}_\pm \cdot \mathbf{d} | g_\mp \rangle$. Due to the selection rules we have $\langle e | \boldsymbol{\epsilon}_\pm \cdot \mathbf{d} | g_\pm \rangle = 0$. Furthermore, because of linear momentum conservation the dipole interaction Hamiltonian leads only to an interaction between states belonging to a closed momentum family

$$\mathcal{F}(q) = \{|e, q\rangle, |g_-, q - \hbar k\rangle, |g_+, q + \hbar k\rangle\}. \tag{4.3}$$
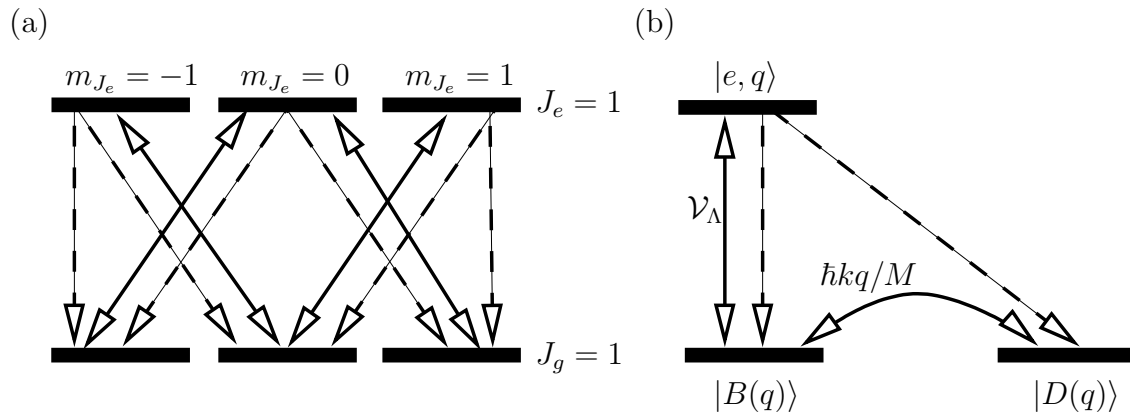
Figure 4.1: (a) Solid lines represent the possible coupling due to the radiation field. The dashed lines illustrate the pathways allowed by selection rules for spontaneous decay. The $m_{J_e} = 0 \rightarrow m_{J_g} = 0$ is forbidden due to these. (b) The relevant Λ-system in an appropriate dressed state picture. The excited states $|e, q\rangle$ couples to $|B(q)\rangle$ due to the radiation field $\mathcal{V}_\Lambda$, which itself is coupled to $|D(q)\rangle$ by the kinetic energy part of the Hamiltonian. Only in the case, q=0, the state $|D(q)\rangle$ does not participate to the absorption and fluorescence cycles; in this case it is a true trapping state.

Following this line one finds the interaction Hamiltonian in the momentum family basis after the rotating wave approximation

$$\mathcal{V}_\Lambda = \sum_q \frac{\hbar}{2} \Big(\Omega_+ |e, q\rangle\langle g_-, q - \hbar k| + \Omega_- |e, q\rangle\langle g_+, q + \hbar k| \Big) e^{-i\omega t} + \text{h.a.}. \tag{4.4}$$

Here $|\mu, p\rangle = |\mu\rangle \otimes |p\rangle$ denotes that the atom is in the internal state $|\mu\rangle$ and has a momentum p along the z-axis, i. e. the quantization axis of the system defined by the propagation direction of the external laser field. The family momentum q is, according to the above definition, the real momentum p of the excited state $|e\rangle$. In a later section we will give a more detailed derivation of the above expressions.

4.2.2   Dynamics in dark- and bright state basis

One can understand VSCPT in a simple way by introducing the so-called dark and bright states of the Λ-configuration. The dark state of the Hamiltonian (4.4) with family momentum q is defined as

$$|D(q)\rangle = \frac{\Omega_-}{\Omega} |g_-, q - \hbar k\rangle - \frac{\Omega_+}{\Omega} |g_+, q + \hbar k\rangle \tag{4.5}$$

and the bright state as

$$|B(q)\rangle = \frac{\Omega_+}{\Omega} |g_-, q - \hbar k\rangle + \frac{\Omega_-}{\Omega} |g_+, q + \hbar k\rangle, \tag{4.6}$$

where the effective Rabi frequency Ω is $\Omega = \sqrt{\Omega_+^2 + \Omega_-^2}$. The Rabi frequencies $\Omega_\pm$ are chosen to be real which can always be done by choosing an appropriate coordinate system. The dark and bright states are called like this because of the following properties

$$\langle q, e | \mathcal{V}_\Lambda | D(q) \rangle = 0 \quad \text{and} \quad \langle q, e | \mathcal{V}_\Lambda | B(q) \rangle = \frac{\hbar}{2} \Omega e^{-i\omega t}. \tag{4.7}$$

Consequently, the atoms in the dark state do not couple to the laser field for any family momentum, whereas the atoms in the bright state absorb a laser photon irrespectively of their family momentum. If we suppose that initially the atoms are prepared in the dark state, than the subsequent time evolution of the corresponding density matrix element is determined by

$$\partial_t \langle D(q) | \rho | D(q) \rangle = -i \frac{k\, q}{M} \frac{2\, \Omega_+ \Omega_-}{\Omega^2} \langle D(q) | \rho | B(q) \rangle + c.c. \tag{4.8}$$

Now suppose that the initial dark state has zero family momentum, i. e. $q = 0$, in this case the right-hand side of eq. (4.8) vanishes. Hence, atoms prepared in the dark state cannot leave it due to their free motional evolution. Even spontaneous emission does not lead to a destruction of the dark state because it is, according to eq. (4.5), a superposition of two ground states which are radiatively stable. The use of meta-stable states is also possible as long as the lifetime of the states is much longer than the interaction and measurement time. In summary, the state $|D(q = 0)\rangle$ is a perfectly trapped state. Because of this $|D(0)\rangle$ is also called *stable* VSCPT state.

In the case of $q \neq 0$, eq. (4.8) results in a coupling induced by the free evolution of the dark state $|D(q)\rangle$ to the bright state $|B(q)\rangle$. The states $|D(q \neq 0)\rangle$ thus participate in the absorption and fluorescence cycles. This dynamics is sketched in fig. 4.1 (b), where we have also noted that the coupling rate between the dark- and bright state is proportional to kq/M.

4.2.3 Transient VSCPT states

As predicted by Papoff et al. [130] the interaction of freely moving atoms with two counter-propagating right and left circular polarized laser beams on a $J_g = 2 \leftrightarrow J_e = 1$ -transition leads to the creation of transient VSCPT-states. These are *not* exact eigenstates of the kinetic energy Hamiltonian as was the case for the stable dark state in a $J_g = 1 \leftrightarrow J_e = 1$-configuration discussed in the last section. Even for a vanishing family momentum the corresponding state does not turn into a stable dark state.

The coupling scheme of a $J_g = 2 \leftrightarrow J_e = 1$ -transition, shown in fig. 4.2, suggests the introduction of two distinct subsystems. Both systems are coupled to each other only by optical pumping. By inspecting fig. 4.2, we see that these systems are the already discussed Λ-configuration (blue, dashed-line) and the so-called inverted-W-configuration (red, solid line). The transient dark state, which we are interested in, is an eigenstate of the inverted-W system. The nomenclature of the states used here has to be read in analogy to the one used in the last section.

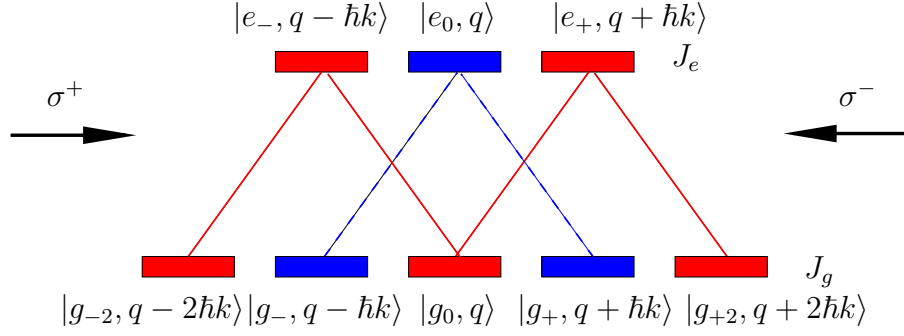As mentioned before, the dipole interaction with the radiation field only leads to a

$$|e_-, q - \hbar k\rangle \quad |e_0, q\rangle \quad |e_+, q + \hbar k\rangle$$

$$J_e$$

$$\sigma^+ \qquad\qquad\qquad\qquad\qquad\qquad \sigma^-$$

$$J_g$$

$$|g_{-2}, q - 2\hbar k\rangle \, |g_-, q - \hbar k\rangle \; |g_0, q\rangle \; |g_+, q + \hbar k\rangle \; |g_{+2}, q + 2\hbar k\rangle$$

Figure 4.2: Coupling scheme of the $J_g = 2 \leftrightarrow J_e = 1$-transition for the classical laser field in a $\sigma^+ - \sigma^-$- configuration. The Λ-system consists of the family of states $\mathcal{F}_\Lambda(q) = \{|e_0, q\rangle, |g_-, q - \hbar k\rangle, |g_+, q + \hbar k\rangle\}$ and the inverted-W system of $\mathcal{F}_{IW}(q) = \{|e_0, q\rangle, |g_\pm, q \pm \hbar k\rangle, |g_{\pm 2}, q \pm 2\hbar k\rangle\}$.

coupling between states of the same momentum family. Since there are now two subsystems two momentum families emerge

$$\mathcal{F}_\Lambda(q) = \{|e, q\rangle, |g_-, q - \hbar k\rangle, |g_+, q + \hbar k\rangle\}, \tag{4.9}$$

$$\mathcal{F}_{IW}(q) = \{|g, q\rangle, |e_\pm, q \pm \hbar k\rangle, |g_{\pm 2}, q \pm 2\hbar k\rangle\}. \tag{4.10}$$

With the assumption of equal field amplitudes of the counterpropagating electric fields and using the appropriate Clebsch-Gordon coefficients, the interaction Hamiltonian of the inverted-W configuration reads

$$\mathcal{V}_{IW} = \sum_q \frac{\hbar \Omega}{2} \Big[\sqrt{\frac{6}{10}} |e_{-1, q - \hbar k}\rangle \langle g_{-2}, q - 2\hbar k|$$

$$+ \sqrt{\frac{1}{10}} \big(|e_{-1}, q - \hbar k\rangle \langle g_0, q| + |e_{+1}, q + \hbar k\rangle \langle g_0, q| \big)$$

$$+ \sqrt{\frac{6}{10}} |e_{+1}, q + \hbar k\rangle \langle g_{+2}, q + \hbar k| \Big] e^{-\mathrm{i}\omega t} + \text{h.a.} \tag{4.11}$$

By diagonalization of this interaction operator we can transform the momentum family for the inverted-W configuration into a new representation $\mathcal{F}_{IW}(q) = \{|\Psi_{NC}\rangle, |\Psi_{C1}\rangle, |\Psi_{C2}\rangle, |e_\pm, q \pm \hbar k\rangle\}$ with

$$|\Psi_{NC}\rangle = \frac{1}{\sqrt{8}} \Big(|g_{-2}, q - 2\hbar k\rangle - \sqrt{6}|g_0, q\rangle + |g_{+2}, q + 2\hbar k\rangle \Big), \tag{4.12}$$

$$|\Psi_{C1}\rangle = \frac{1}{\sqrt{2}} \big(|g_{-2}, q - 2\hbar k\rangle - |g_{+2}, q + 2\hbar k\rangle \big), \tag{4.13}$$

$$|\Psi_{C2}\rangle = \frac{1}{\sqrt{24}} \Big(3|g_{-2}, q - 2\hbar k\rangle + \sqrt{6}|g_0, q\rangle + 3|g_{+2}, q + 2\hbar k\rangle \Big). \tag{4.14}$$

The state vector $|\Psi_{NC}\rangle$ has a vanishing eigenvalue with respect to the interaction Hamiltonian (4.11) and does not involve excited states hence it is the dark state of the inverted-W

configuration. Yet, it is not an exact eigenstate of the kinetic energy Hamiltonian. This can be seen by considering the free evolution of the state in the Schrödinger picture, which is given by

$$
\begin{aligned}
\mathrm{i}\hbar\frac{\partial|\Psi_{NC}\rangle}{\partial t} &= \frac{\hat{p}^2}{2M}|\Psi_{NC}\rangle \\
&= \frac{q^2}{2M}|\Psi_{NC}\rangle + \frac{\hbar^2 k^2}{\sqrt{2}M}\left[\frac{1}{\sqrt{2}}|\Psi_{NC}\rangle + \sqrt{\frac{3}{2}}|\Psi_{C1}\rangle\right] + \frac{\hbar k q}{M}|\Psi_{C2}\rangle.
\end{aligned}
\tag{4.15}
$$

Hence, even for a vanishing family momentum, $q = 0$, there exists a coupling of the dark state to one of the bright-states of the system, i. e. the dark state $|\Psi_{NC}\rangle = |\Psi_{NC}(q)\rangle$ is not a real *trapping state* for any q. As we see from eq. (4.15) the lifetime of the dark state is maximal if the family momentum q is zero. Because of this, the state $|\Psi_{NC}(q = 0)\rangle$ is called *transient trapping state*. The transient dark state is characterized, as we can see from eq. (4.12), by three peaks in the momentum distribution which are located at $p = 0$ and $p = \pm 2\hbar k$. From eq. (4.15) we see, furthermore, that the lifetime of the state is on the order of the recoil time $\tau_{\mathrm{rec}} = \hbar/E_{\mathrm{rec}} = 2M/\hbar k^2$. In the most relevant cases this time scale is sufficiently long for an experimental verification of these states. In the next sections we will give a more detailed calculation of the corresponding lifetime.

4.3 Theoretical description

This section gives a derivation of the interaction Hamiltonians mentioned in the introduction of the chapter. In addition we review the derivation of the generalized optical Bloch equations that we used for the simulation. As stated above we want to study the evolution of freely moving atoms irradiated on the $J_g = 2 \leftrightarrow J_e = 1$ transition by two counter-propagating laser fields in a $\sigma^+ - \sigma^-$-laser configuration. The coupling scheme is shown in fig. 4.2. The total Hamiltonian of the system

$$
\hat{H} = \hat{H}_{\mathrm{sys}} + \hat{H}_f + \hat{H}_{\mathrm{int}},
\tag{4.16}
$$

consists of three parts, the first part $\hat{H}_{\mathrm{sys}}$ describes the free motion of the atoms and the interaction with the classical laser fields, the second part the free quantized electromagnetic field $\hat{H}_f$ (bath) and the last part the interaction of the quantized electromagnetic field with the atoms $\hat{H}_{\mathrm{int}}$.

4.3.1 Interaction with the classical laser field

In the $\sigma^+ - \sigma^-$-configuration [135] the laser radiation $\mathbf{E}(z, t) = \boldsymbol{\mathcal{E}}(z, t) + \boldsymbol{\mathcal{E}}^*(z, t)$ is composed of two counterpropagating beams with left- (σ^-) and right-circular (σ^+) polarization

$$
\boldsymbol{\mathcal{E}}(z, t) = \frac{1}{2}\left(\mathcal{E}_+\boldsymbol{\epsilon}_+ e^{-\mathrm{i}\omega t}e^{\mathrm{i}kz} + \mathcal{E}_-\boldsymbol{\epsilon}_- e^{-\mathrm{i}\omega t}e^{-\mathrm{i}kz}\right),
\tag{4.17}
$$

where $\mathcal{E}_\pm$ denote the corresponding slowly varying amplitudes. Since the classical laser field couples two Zeeman manifolds we have to apply the Wigner-Eckart theorem [136], i. e. we can write the dipole operator as

$$\hat{\mathbf{d}} = \sum_{i=0,\pm} (\hat{d}_i \boldsymbol{\epsilon}_i + h.a.), \tag{4.18}$$

where the sum runs over all possible polarizations (linear (0), left circular (-) and right circular (+)) of the electromagnetic field. The dipole operators with respect to the polarization axis are thus given by

$$\hat{d}_m = d \sum_{\substack{-J_e \leq m_e \leq J_e \\ -J_g \leq m_g \leq J_g}} C^{J_e,J_g,J}_{m_e,m_g,m} |J_e, m_e\rangle \langle m_g, J_g|. \tag{4.19}$$

The $C^{J_e,J_g,J}_{m_e,m_g,m}$ are the Clebsch-Gordan coefficients, and $d = \langle J_e \| \hat{d} \| J_g \rangle$ is the reduced dipole matrix element. By inserting eq. (4.18) and the expression for the electric field into the Hamilton operator in dipole approximation we find

$$V_{AL} = \frac{\hbar}{2} \left(\sum_{\substack{-J_e \leq m_e \leq J_e \\ -J_g \leq m_g \leq J_g}} C^{J_e,J_g,J}_{m_e,m_g,+1} |J_e, m_e\rangle \langle m_g, J_g| \Omega_+ e^{-i\omega t} e^{ikz} \right.$$

$$\left. + \sum_{\substack{-J_e \leq m_e \leq J_e \\ -J_g \leq m_g \leq J_g}} C^{J_e,J_g,J}_{m_e,m_g,-1} |J_e, m_e\rangle \langle m_g, J_g| \Omega_- e^{-i\omega t} e^{-ikz} + \text{h.a.} \right), \tag{4.20}$$

where the Rabi frequencies $\Omega_\pm = -d\mathcal{E}_\pm / \hbar$. Since we want to study subrecoil dynamics we have to quantize both internal and external degrees of freedom of the atoms [137]. Hence we represent the interaction Hamiltonian operator (4.20) in the basis of the eigenfunctions of the momentum operator, i. e.

$$\mathcal{V}_{AL} = \int d^3\mathbf{p} \int d^3\mathbf{p}' |\mathbf{p}\rangle \langle \mathbf{p}'| \langle \mathbf{p}|V_{AL}|\mathbf{p}'\rangle. \tag{4.21}$$

Using the relation $e^{\pm ikz}|\mathbf{p}\rangle = |\mathbf{p} \pm \hbar k \mathbf{e}_z\rangle$ and the orthonormality of the eigenfunctions of the momentum operator $\langle \mathbf{p}|\mathbf{p}' \pm \hbar k \mathbf{e}_z\rangle = \delta(\mathbf{p} \mp \hbar k \mathbf{e}_z - \mathbf{p}')$ one finds

$$\mathcal{V}_{AL} = \frac{\hbar}{2} \left(\sum_{\substack{-J_g \leq m_g \leq J_g \\ -J_g \leq m_g \leq J_g}} \int d^3\mathbf{p}\, C^{J_e,J_g,J}_{m_e,m_g,m} |J_e, m_e\rangle \langle m_g, J_g| \otimes |\mathbf{p}\rangle \langle \mathbf{p} - \hbar k \mathbf{e}_z| \Omega_+ e^{-i\omega t} \right.$$

$$\tag{4.22}$$

$$\left. + \sum_{\substack{-J_e \leq m_e \leq J_e \\ -J_g \leq m_g \leq J_g}} \int d^3\mathbf{p}\, C^{J_e,J_g,J}_{m_e,m_g,m} |J_e, m_e\rangle \langle m_g, J_g| \otimes |\mathbf{p}\rangle \langle \mathbf{p} + \hbar k \mathbf{e}_z| \Omega_- e^{-i\omega t} + \text{h.a.} \right).$$

In the rest of this paragraph we will restrict our considerations to the motion of atoms along the z-axis. The Clebsch-Gordan coefficients show that, especially in the case of the examined $J_g = 2 \leftrightarrow J_e = 1$ transition, only states within the Λ- and inverted-W subsystems are coupled to each other. To transform the above interaction Hamiltonian in his present representation into the one given in the last sections we replace the integral by the sum over momenta, i. e. $\int \mathrm{d}p_z \rightarrow V_p \sum_{p_z}$, where V_p is the corresponding integration volume. In this case we also have to redefine the corresponding state vectors. The state vector in the discrete case are related to the ones in the continuous case through: $\sqrt{V_p}|p\rangle_{con} \rightarrow |p\rangle_{dis}$. For notational simplicity we drop however the distinction using the subscripts. If we instead of using the standard momentum representation of the state vectors introduce the family momentum representation we find the interaction Hamiltonian given below. The usage of the family momentum notation transforms the sum over the real momenta p_z into a sum over the family momenta q, e. g. $|e_-\rangle\langle g_0| \otimes |p_z\rangle\langle p_z + \hbar k|$ transforms to $|e_-\rangle\langle g_0| \otimes |q - \hbar k\rangle\langle q|$. Our interaction Hamiltonian $\mathcal{V}_{AL} = \mathcal{V}_\Lambda + \mathcal{V}_{IW}$ consists of two parts. One describes the interaction within the Λ-system, the other one within the inverted-W configuration

$$\mathcal{V}_\Lambda = \sum_q \frac{\hbar}{2}\sqrt{\tfrac{3}{10}}\{\Omega_+|e_0,q\rangle\langle g_{-1},q-\hbar k| \tag{4.23}$$

$$+ \Omega_-|e_0,q\rangle\langle g_{+1},q+\hbar k|\}\exp(-i\omega t) + \text{h.a.},$$

$$\mathcal{V}_{IW} = \sum_q \frac{\hbar}{2}\left[\sqrt{\tfrac{6}{10}}\Omega_+|e_{-1},q-\hbar k\rangle\langle g_{-2},q-2\hbar k| \tag{4.24}\right.$$

$$+\sqrt{\tfrac{1}{10}}\big(\Omega_-|e_{-1},q-\hbar k\rangle + \Omega_+|e_{+1},q+\hbar k\rangle\big)\langle g_0,q|$$

$$\left.+\sqrt{\tfrac{6}{10}}\Omega_-|e_{+1},q+\hbar k\rangle\langle g_{+2},q+2\hbar k|\right]\exp(-i\omega t) + \text{h.a.},$$

where we note again that $\Omega_\pm = -d\,\mathcal{E}_\pm/\hbar$ are the Rabi frequencies of the coupling laser fields. This interaction Hamiltonian has been used for the numerical simulation of the system in terms of the generalized optical Bloch equations and for calculations in the context of a resolvent approach.

4.3.2 Derivation of the generalized optical Bloch equation

The generalized optical Bloch equations (GOBE), which we will derive in this section, form the basis for our numerical simulations of the experiment. Therefore, we here give a brief derivation. To derive the GOBE we use the master equation (A.17) deduced in appendix A.1

$$\partial_t \rho = -\frac{1}{\hbar^2}\int\limits_0^t \mathsf{Tr}_f\left\{[H_{int}(t),[H_{int}(t'),\rho(t)\otimes\rho_f(0)]]\right\}\mathrm{d}t'. \tag{4.25}$$

The density matrix of the electromagnetic field is given by ρ_f and we assume that the interaction starts at $t = 0$. Furthermore, $\mathsf{Tr}_f\{\}$ denotes tracing over the bath states,

i. e. the states of the electromagnetic field. To evaluate this expression we write the interaction Hamiltonian with the quantized electromagnetic field in dipole approximation in the form

$$
\begin{aligned}
H_{\mathrm{int}}(t) &= -\hbar \left[\boldsymbol{\Delta}^{(+)} \cdot \hat{\mathbf{E}}^{(+)} e^{\mathrm{i}\omega_e t} + \boldsymbol{\Delta}^{(-)} \cdot \hat{\mathbf{E}}^{(-)} e^{-\mathrm{i}\omega_e t} \right] \\
&= -\hbar \sum_{s=0,\pm} \left[\Delta_s^{(+)} \hat{E}_s^{(+)} e^{\mathrm{i}\omega_e t} + \Delta_s^{(-)} \hat{E}_s^{(-)} e^{-\mathrm{i}\omega_e t} \right],
\end{aligned}
\tag{4.26}
$$

where we have already applied the rotating wave approximation and included the atomic dipole matrix element into the definition of the quantized electromagnetic field. Hence, $\hat{\mathbf{E}}^{(+)} = (\hat{\mathbf{E}}^{(-)})^\dagger$ now have the meaning of a Rabi frequency. The second equal sign holds if we represent the vector operators in the orthonormal basis of left-, right- and linear-polarized light with respect to the propagation direction of the laser field. The $\boldsymbol{\Delta}^{(\pm)}$ are vectorial raising and lowering operators which have the form

$$
\boldsymbol{\Delta}^{(+)} = \sum_{s=0,\pm} C_{m_{\mathrm{e}},m_{\mathrm{g}},s}^{J_{\mathrm{e}},J_{\mathrm{g}},J} |J_{\mathrm{e}}, m_{\mathrm{e}}\rangle\langle m_{\mathrm{g}}, J_{\mathrm{g}}| \boldsymbol{\epsilon}_s = \sum_{s=0,\pm} \Delta_s^{(+)} \boldsymbol{\epsilon}_s = (\boldsymbol{\Delta}^{(-)})^\dagger.
\tag{4.27}
$$

To evaluate the Master equation 4.25, it is necessary to make some assumptions about the bath. To this end, we assume that the field modes are δ-correlated in time [21, 123], i. e. we have

$$
\langle \hat{E}_s^{(+)}(\mathbf{r}, t)\hat{E}_{s'}^{(-)}(\mathbf{r}, t')\rangle = \frac{\Gamma}{2}\delta(t - t')\delta_{s,s'},
\tag{4.28}
$$

$$
\langle \hat{E}_s^{(+)}(\mathbf{r}, t)\hat{E}_{s'}^{(-)}(\mathbf{r}, t')\rangle = \langle \hat{E}_s^{(+)}(\mathbf{r}, t)\hat{E}_{s'}^{(+)}(\mathbf{r}, t')\rangle = \langle \hat{E}_s^{(-)}(\mathbf{r}, t)\hat{E}_{s'}^{(-)}(\mathbf{r}, t')\rangle = 0,
\tag{4.29}
$$

for $s, s' \in \{0, \pm 1\}$. By determining the double commutator of (4.25) we find that it is necessary to consider four terms. Two of these include the product of the interaction Hamiltonian with itself but for two different moments in time. Using eq. (4.26) and the relations $\Delta_s^{(+)}\Delta_{s'}^{(+)} = \Delta_s^{(-)}\Delta_{s'}^{(-)} = 0$, which hold for all s and s', we find for these products

$$
\begin{aligned}
H_{\mathrm{int}}(t)H_{\mathrm{int}}(t') = \hbar^2 \sum_{s,s'} \Big[&\Delta_s^{(+)}\Delta_{s'}^{(-)} \hat{E}_s^{(+)}(t)\hat{E}_{s'}^{(-)}(t') e^{\mathrm{i}\omega_e(t-t')} \\
&+\Delta_s^{(-)}\Delta_{s'}^{(+)} \hat{E}_s^{(-)}(t)\hat{E}_{s'}^{(+)}(t') e^{-\mathrm{i}\omega_e(t-t')} \Big].
\end{aligned}
\tag{4.30}
$$

In the following we will give the results after tracing over the bath variables. To evaluate these terms we have used eq. (4.28) and (4.29). The result is

$$
\mathsf{Tr}_f\{H_{\mathrm{int}}(t)H_{\mathrm{int}}(t')\rho(t) \otimes \rho_f\} = \frac{\hbar^2\Gamma}{2} e^{\mathrm{i}\omega_e(t-t')}\delta(t - t') \left(\boldsymbol{\Delta}^{(+)} \cdot \boldsymbol{\Delta}^{(-)} \right) \rho(t),
\tag{4.31}
$$

$$
\mathsf{Tr}_f\{\rho(t) \otimes \rho_f H_{\mathrm{int}}(t')H_{\mathrm{int}}(t)\} = \frac{\hbar^2\Gamma}{2} e^{-\mathrm{i}\omega_e(t-t')}\delta(t - t')\rho(t) \left(\boldsymbol{\Delta}^{(+)} \cdot \boldsymbol{\Delta}^{(-)} \right).
\tag{4.32}
$$

These two terms represent the loss from the excited state manifold due to spontaneous emission. The other two terms of the double commutator represent the feeding terms

of the ground state manifold. To evaluate them we have to determine the following expression

$$\mathsf{Tr}_f\{H_{\text{int}}(t')\rho(t) \otimes \rho_f H_{\text{int}}(t)\}$$
$$= \hbar^2 \mathsf{Tr}_f \left\{ \left(\boldsymbol{\Delta}^{(-)} \cdot \hat{\mathbf{E}}^{(-)}(\mathbf{r},t) \right) \rho(t) \otimes \rho_f \left(\boldsymbol{\Delta}^{(+)} \cdot \hat{\mathbf{E}}^{(+)}(\mathbf{r},t') \right) \right\} e^{-\mathrm{i}\omega_e(t-t')}. \tag{4.33}$$

Using the mode expansion of the quantized electromagnetic fields with the coupling constant $g_k = \wp\sqrt{\omega_k/2\hbar\epsilon_0 V}$ of mode k in a quantization volume V

$$\hat{\mathbf{E}}^{(+)}(\mathbf{r},t) = \sum_{\mathbf{k},s} g_k a_{\mathbf{k},s} \boldsymbol{\epsilon}_{\mathbf{k},s} e^{\mathrm{i}(\mathbf{k}\cdot\mathbf{r}-\omega t)} = \left(\hat{\mathbf{E}}^{(-)}(\mathbf{r},t) \right)^{\dagger} \tag{4.34}$$

and $\mathsf{Tr}_f\{\rho_f a_{\mathbf{k},s} a_{\mathbf{k},s'}^{\dagger}\} = \delta_{\mathbf{k},\mathbf{k}'}\delta_{s,s'}$, we find

$$\mathsf{Tr}_f\{H_{\text{int}}(t')\rho(t)\otimes\rho_f H_{\text{int}}(t)\} = \hbar^2 \sum_{\mathbf{k},s} g_k^2 \left(\boldsymbol{\Delta}^{(-)} \cdot \boldsymbol{\epsilon}_{\mathbf{k},s} \right) e^{-\mathrm{i}\mathbf{k}\cdot\hat{\mathbf{r}}} \rho(t) e^{\mathrm{i}\mathbf{k}\cdot\hat{\mathbf{r}}} \left(\boldsymbol{\Delta}^{(+)} \cdot \boldsymbol{\epsilon}_{\mathbf{k},s} \right) e^{\mathrm{i}(\omega-\omega_e)(t-t')}. \tag{4.35}$$

This can be furthermore simplified if we replace the sum over the field modes in eq. (4.35) by an integral. Doing this we assume that the modes are closely spaced in frequency space [21]

$$\sum_{\mathbf{k}} = \frac{V}{(2\pi)^3} \int \mathrm{d}\Omega \int_0^{\infty} \mathrm{d}k\, k^2. \tag{4.36}$$

Using eq. (4.36) we finally arrive at

$$\mathsf{Tr}_f\{H_{\text{int}}(t')\rho(t) \otimes \rho_f H_{\text{int}}(t)\}$$
$$= \frac{\wp^2 c}{2(2\pi)^3\hbar\epsilon_0} \sum_s \int \mathrm{d}\Omega \int_0^{\infty} \mathrm{d}k \left[k^3 \left(\boldsymbol{\Delta}^{(-)} \cdot \boldsymbol{\epsilon}_{\mathbf{k},s} \right) e^{-\mathrm{i}\mathbf{k}\cdot\hat{\mathbf{r}}} \rho(t) e^{\mathrm{i}\mathbf{k}\cdot\hat{\mathbf{r}}} \left(\boldsymbol{\Delta}^{(+)} \cdot \boldsymbol{\epsilon}_{\mathbf{k},s} \right) \right] e^{\mathrm{i}c(k-k_e)(t-t')}. \tag{4.37}$$

Since the term in the square brackets of eq. (4.37) is slowly varying with respect to the wave number we can make the replacement $k \to k_e$, where k_e is the wavenumber corresponding to the transition frequency ω_e. Furthermore, we can extend the lower integration limit in the k-integration to $-\infty$. This amounts to a Wigner-Weisskopf approximation [21]. Identifying the definition of the delta-function

$$\int_{-\infty}^{\infty} \mathrm{d}k\, e^{\mathrm{i}c(k-k_e)(t-t')} = \frac{2\pi}{c}\delta(t-t'), \tag{4.38}$$

we finally find

$$\mathsf{Tr}_f\{H_{\text{int}}(t')\rho(t) \otimes \rho_f H_{\text{int}}(t)\}$$
$$= \frac{3}{8\pi}\Gamma \sum_s \int d\Omega \left[\left(\mathbf{\Delta}^{(-)} \cdot \boldsymbol{\epsilon}_{\mathbf{k},s}\right) e^{-i\mathbf{k}\cdot\hat{\mathbf{r}}}\rho(t)e^{i\mathbf{k}\cdot\hat{\mathbf{r}}} \left(\mathbf{\Delta}^{(+)} \cdot \boldsymbol{\epsilon}_{\mathbf{k},s}\right)\right] \delta(t - t'). \tag{4.39}$$

with the free-space spontaneous emission rate

$$\Gamma = \frac{\wp^2 \omega_e^3}{3\pi\hbar\epsilon_0 c^3} \tag{4.40}$$

from Wigner-Weisskopf theory [24, 123]. One finds the same result for the fourth term $\mathsf{Tr}_f\{H_{\text{int}}(t)\rho(t) \otimes \rho_f H_{\text{int}}(t')\}$. By collecting the results of eq. (4.31), (4.32) and (4.39) we finally find the generalized optical Bloch equation in the Schrödinger picture [138, 139]

$$\frac{\partial\rho}{\partial t} = \frac{i}{\hbar}\left[\frac{\hat{\mathbf{p}}^2}{2M} + \hbar\omega_e\hat{P}_e + V, \rho\right]$$
$$- \frac{\Gamma}{2}\left[(\mathbf{\Delta}^{(+)} \cdot \mathbf{\Delta}^{(-)})\rho + \rho(\mathbf{\Delta}^{(+)} \cdot \mathbf{\Delta}^{(-)})\right]$$
$$+ \frac{3}{4\pi}\Gamma \int d\Omega \sum_s \left[\left(\mathbf{\Delta}^{(-)} \cdot \boldsymbol{\epsilon}_{\mathbf{k},s}\right) e^{-i\mathbf{k}\cdot\hat{\mathbf{r}}}\rho(t)e^{i\mathbf{k}\cdot\hat{\mathbf{r}}} \left(\mathbf{\Delta}^{(+)} \cdot \boldsymbol{\epsilon}_{\mathbf{k},s}\right)\right], \tag{4.41}$$

where $\mathcal{V} = \mathcal{V}_\Lambda + \mathcal{V}_{IW}$. In order to simplify the notation we have omitted subscripts that denote the difference between Schrödinger and interaction picture. This should, however, not lead to any confusion. The first line represents the unitary evolution of the atomic system whereas the second line corresponds to the decay out of the excited state manifold and the last line to the feeding of the ground state manifold by spontaneous emission. A derivation of the equations of motion for the density matrix elements in the momentum family basis [138, 139] can easily be found from eq. (4.41)

$$\partial_t\rho_{m_e,m'_e}(q) = \left[-\Gamma - i\frac{kq}{M}(m_e - m'_e) - i\frac{\hbar k^2}{2M}(m_e^2 - m'^2_e)\right]\rho_{m_e,m'_e}(q)$$
$$- \frac{i}{2}\sum_{s,m_g}\left(\Omega_s C^{J_e,J_g,J}_{m_e,m_g,m}\rho_{m_g,m'_e}(q) - \Omega_s C^{J_e,J_g,J}_{m'_e,m_g,m}\rho_{m_e,m_g}(q)\right), \tag{4.42}$$

$$\partial_t\rho_{m_e,m_g}(q) = \left[i\Delta - \frac{\Gamma}{2} - i\frac{kq}{M}(m_e - m_g) - i\frac{\hbar k^2}{2M}(m_e^2 - m_g^2)\right]\rho_{m_e,m_g}(q)$$
$$- \frac{i}{2}\sum_s \left(\Omega_s C^{J_e,J_g,J}_{m_e,m'_g,s}\rho_{m'_g,m_g}(q) - \Omega_s C^{J_e,J_g,J}_{m'_e,m_g,s}\rho_{m_e,m'_e}(q)\right), \tag{4.43}$$
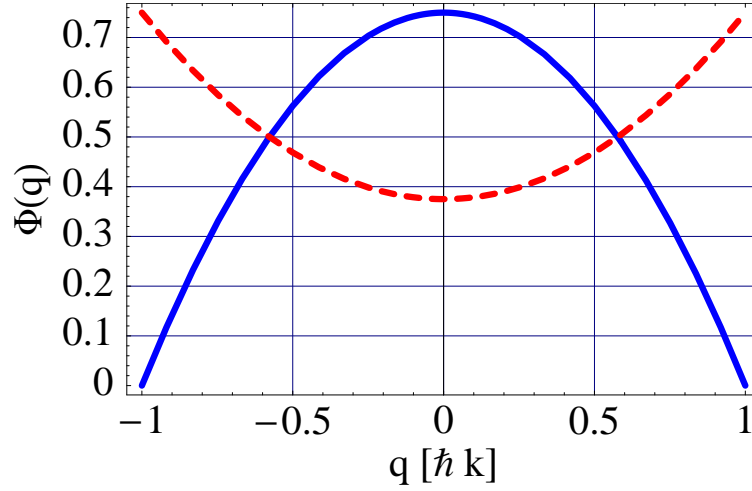
Figure 4.3: Emission characteristics for linear (blue solid line) and left/right circular polarized (red dashed line) light as a function of the family momentum q. Linear polarized light leads to momentum change which is more probable for small family momenta whereas in the case of circular polarized light it is more probable for high momenta.

$$\partial_t \rho_{m_g,m_g'}(q) = \left[-\mathrm{i}\frac{kq}{M}(m_g - m_g') - \mathrm{i}\frac{\hbar k^2}{2M}(m_g^2 - m_g'^2) \right] \rho_{m_g,m_g'}(q)$$

$$- \frac{\mathrm{i}}{2} \left(\sum_{s,m_e'} \Omega_s\, C_{m_e,m_g,s}^{J_e,J_g,J}\, \rho_{m_e,m_g'}(q) - \sum_{s,m_e'} \Omega_s\, C_{m_e,m_g',s}^{J_e,J_g,J}\, \rho_{m_g,m_e}(q) \right)$$

$$+ \Gamma \sum_s \int_{-\hbar k}^{\hbar k} \mathrm{d}q'\, C_{m_g,m_e,s}^{J_e,J_g,J}\, \rho_{m_e,m_e'}(q - \hbar s k + q')\, C_{m_g',m_e',s}^{J_e,J_g,J}\, \Phi_s(q'). \tag{4.44}$$

The functions $\Phi_s(q)$ are called dipole radiation pattern and are given by [138]

$$\Phi_0(q) = \frac{3}{4\hbar k}\left(1 - \frac{q^2}{(\hbar k)^2}\right), \tag{4.45}$$

$$\Phi_\pm(q) = \frac{3}{8\hbar k}\left(1 + \frac{q^2}{(\hbar k)^2}\right). \tag{4.46}$$

These are probability density distributions for spontaneous emission with polarization 0 or ± 1 with z-projection q of the wave vector, i. e. the probability to find a linear polarized, spontaneously emitted photon with a momentum along z between q and $q + \mathrm{d}q$ is given by $\Phi_0(q)\mathrm{d}q$. The probability distributions are shown in fig. 4.3. The above set of equations can in general not be solved analytically. However, we can discretize them in space and time and integrate them numerically. Results of simulations based on this approach will be given in section 4.5.

4.3.3 Effective Hamiltonian and ground states loss rates

The transient VSCPT-state discussed in section 4.2.3 is given by the dark state of the corresponding interaction Hamiltonian $\mathcal{V}_{IW}$. Due to the decomposition found by Morris and Shore [140], we know that two further states exist that only include bare ground state eigenfunctions. These couple, however, due to the radiation field, to the excited state manifold.

We will show now using resolvent theory that due to the free motional evolution the dark state with respect to the interaction Hamiltonian is not a perfect trapped state, i. e. it couples to the bright states of the system. This occurs, in contrast to the former Λ-system, even for a vanishing family momentum.

The resolvent theory is based on the adiabatic elimination of the excited state manifold [17]. This is justified as long as the Rabi frequency is small compared to the decay rate of or the detuning from the excited state, i. e. as long as $|\Omega| \ll |i\Gamma/2 + \Delta|$. In this case the evolution of the ground state manifold is isolated from the rest of the system. Moreover, there exist two isolated subsystems of the ground state manifold which correspond to the ground states of the Λ- and inverted-W configuration respectively [130]. Mathematically this means that the matrix representation of the full effective Hamiltonian is in block diagonal form. Hence, the resolvent theory allows for the derivation of two effective, non-hermitian Hamiltonians corresponding to these subsystems.

The momentum family basis allows the diagonalization of these non-hermitian Hamiltonians for the determination of the complex eigenvalues as a function of the family momentum. In particular it is possible to calculate the decay rates of the eigenstates of these subsystems. In lowest order of the resolvent theory one finds [130]

$$H_{\text{res}} = \tilde{\mathcal{V}}_{\text{AL}} \, \hat{P}_e \frac{1}{-\hbar \left(i\Gamma/2 - \Delta \right)} \hat{P}_e \, \tilde{\mathcal{V}}_{\text{AL}} \tag{4.47}$$

Here $\hat{P}_e$ is the projector on the excited state manifold, which in the case of the $J_g = 2 \leftrightarrow J_e = 1$ -transition is given by $\hat{P}_e = |e_-, q - \hbar k\rangle\langle e_-, q - \hbar k| + |e_0, q\rangle\langle e_0, q| + |e_+, q + \hbar k\rangle\langle e_+, q + \hbar k|$. The atom-light interaction Hamiltonian in the interaction picture reads

$$\tilde{\mathcal{V}}_{\text{AL}} = e^{i\omega_{\text{L}} \hat{P}_e t} \, \mathcal{V}_{\text{AL}} \, e^{-i\omega_{\text{L}} \hat{P}_e t}. \tag{4.48}$$

The effective Hamiltonian is then only acting on the ground state manifold

$$H_{\text{eff}} = \frac{\hat{p}^2}{2M} + H_{\text{res}}. \tag{4.49}$$

It is non-hermitian since the absorption of a photon leads to loss of population. In order to understand the more involved results of the $J_g = 2 \leftrightarrow J_e = 1$-system we will present first the results for the Λ-subsystem. To this end we normalize the effective Hamiltonian with respect to $\hbar\Gamma$

$$\mathcal{H}_{\text{eff}} = \frac{E_{\text{rec}}}{\hbar\Gamma} \left[\left(\frac{\hat{p}}{\hbar k} \right)^2 + \alpha \, \tilde{V}_{\text{AL}} \hat{P}_e \frac{1}{-\hbar \left(i/2 - \Delta/\Gamma \right)} \hat{P}_e \tilde{V}_{\text{AL}} \right], \tag{4.50}$$
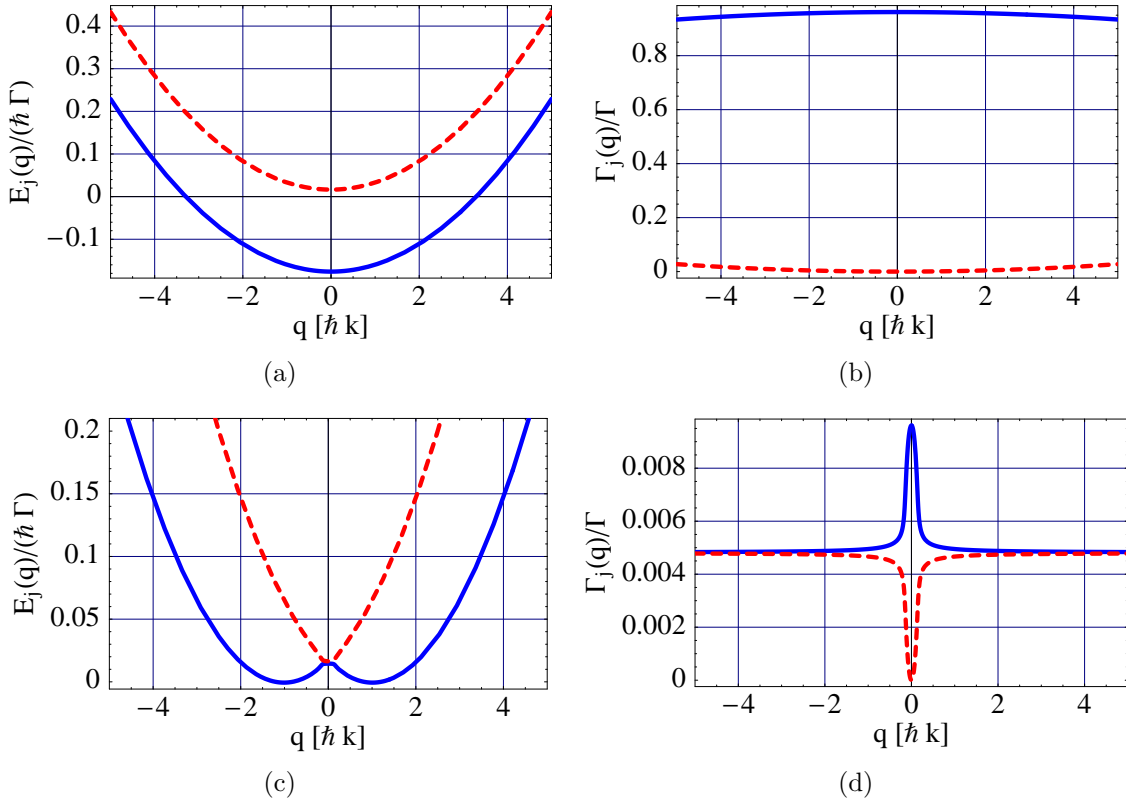
(a)

(b)

(c)

(d)

Figure 4.4: The subfigures show the real and imaginary parts of the complex eigenvalues $E_j(q) + i\hbar\Gamma_j(q)$ of the Λ-subsystem effective Hamiltonian 4.49 as a function of the family momentum. (a) and (b) show the case $\alpha \approx 15 > 1$ and the (c) and (d) show the opposite case $\alpha \approx 0.15 < 1$. For a physical explanation see main text. The calculations are based on a fictitious Λ-system with the physical parameters given in section 4.4 for the $J_g = 2 \leftrightarrow J_e = 1$-transition studied in the experiment.

where $\tilde{V}_{AL} = \tilde{\mathcal{V}}_{AL}/(\hbar\Omega/2)$ is the normalized interaction Hamiltonian. The factor

$$\alpha = \frac{\hbar\Omega^2}{4\Gamma E_{rec}} = \frac{\Omega^2/\Gamma}{4\,\omega_{rec}}, \tag{4.51}$$

is the ratio of the resonant optical pumping rate Ω^2/Γ to the recoil frequency defined by $\omega_{rec} = \hbar^2 k^2/(2M)$. This factor determines whether the dynamics of the system is dominated by the radiation field ($\alpha > 1$) or by the free motional evolution ($\alpha < 1$) [130]. This distinction can be understood qualitatively by the following discussion. By considering the absorption spectrum of one of the applied fields we see that it shows a transparency window at two-photon resonance of width $\Delta\omega_{tr} = \Omega^2/\Gamma$ (see Introduction chapter section 1.2.1). The case $\alpha \gg 1$ implies now that the transparency window is much larger than the recoil frequency. Hence, atoms which are frequency shifted due to motion by a few recoil frequencies $n\omega_{rec} \ll \Delta\omega_{tr}$ ($n \in \mathbb{N}$) do not participate to the cycles of absorption and spontaneous emission but are in a dark state and are hence long-lived. On the other hand if $\omega_{rec} \gg \Delta\omega_{tr}$, i. e. $\alpha \ll 1$, all states contribute to the cycles except

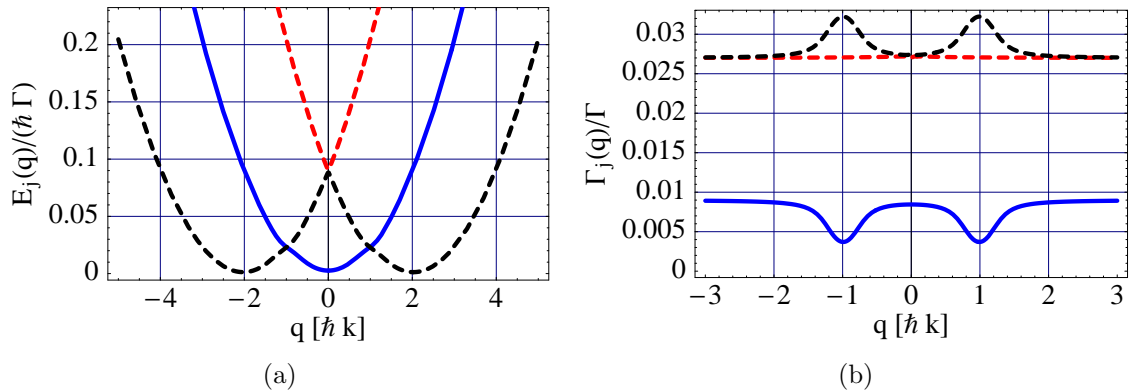(a)   (b)

Figure 4.5: The figure shows the real (a) and imaginary (b) part of the complex eigenvalues for the inverted-W subsystem. The figure of merit $\alpha \approx 1$ and corresponds to a later on shown numerical simulations with $\Omega = 0.3\Gamma$.

for the stable dark state $|\Psi_\Lambda(q = 0)\rangle$ which does not couple to the radiation field. This discussion is supported by the following consideration of the complex eigenvalues of the effective Hamiltonian (4.49) as a function of the family momentum.

In appendix A.2 a mathematica-code is given that allows, based on the scaled version of the Hamiltonian eq. (4.50), to determine the complex eigenvalues

$$E_j(q) + i\hbar\Gamma_j(q) \tag{4.52}$$

for the inverted-W configuration. The results for the Λ-system are given in fig. 4.4 for the limiting cases discussed above. By diagonalizing the effective Hamiltonian for the ground state manifold we find in that case two different eigenstates i. e. $j = 1, 2$. As suggested by the Morris-Shore transformation [140] and depicted in fig. 4.1 (b), one of the states is the dark state (red dashed line in fig. 4.4) which is stable for $q = 0$, i. e. $\Gamma(q = 0) = 0$, and the other the bright state (blue solid line). If the coupling of the radiation field dominates the system dynamics (upper row in fig. 4.4), the loss rate is almost independent of the family momentum q. This is in contrast to the weak field regime ($\alpha < 1$) shown in the lower row of fig. 4.4. One clearly sees that in both cases the dark state turns into a real trapped state if the family momentum approaches zero. On the other hand the bright state destabilizes in the small family momentum regime. In the interaction free case the two ground states $|g_{-1}, q - \hbar k\rangle$ and $|g_{+1}, q + \hbar k\rangle$ are represented by two parabolas with minima located at $q = \pm\hbar k$ respectively. The atom-laser interaction leads, as depicted in fig. 4.4 (a) and (c), to a splitting of the two eigenvalue parabolas. Figure 4.5 gives the real and imaginary part of the complex eigenvalues for the inverted-W subsystem. The shown example corresponds to parameters used later on for a numerical simulation based on the generalized optical Bloch equations. Similar to the Λ-configuration the parabolas corresponding to the free motional evolution (see real part) split up, i. e. show an avoided crossing (they have different colors), due to the interaction of the atoms with the radiation field. Furthermore, we see that the meta-stable transient dark state, corresponding to the eigenvalue with the smallest imaginary part, has no vanishing decay rate for $q = 0$.

Furthermore, we can read of fig. 4.5(b) that the lifetime of the bright state of the inverted-W subsystem is shorter by a factor 1/3 as compared to the lifetime of the transient dark state.

4.3.4 Conditions for detectability of meta-stable, transient trapping states

We now discuss the conditions under which the metastable transient trapping state $|\Psi_{IW}^{NC}(q=0)\rangle$ can be observed in the experiment. To this end we discuss three limits. On one hand there is the case of large Rabi frequency Ω with respect to the natural linewidth Γ of the transition. This corresponds to the regime $\alpha \gg 1$ since typically we have for optical transitons $\Gamma\tau_{\mathrm{rec}} \gg 1$. i. e. motional evolution is unimportant and can be neglected. In the second case we have $\Omega \approx \Gamma$ which will turn out to be the most interesting situation and finally we have $\Omega \ll \Gamma$. In the last case the number of fluorescence cycles passed through is not sufficient to transfer the initial population into the final dark state. We do not consider this limit any further.

In the first case ($\Omega \gg \Gamma$), the contribution of stimulated emitted photons is much bigger than the spontaneously emitted photons. Absorption and stimulated emission lead to an absolute momentum transfer from the radiation field to the atomic system of $2\hbar k$ as the initial state $|g_0, q\rangle$ is coherently coupled to the bare states $|g_{\pm 2}, q \pm 2\hbar k\rangle$. The state generated by this coupling has three peaks in the momentum distribution, similar to $|\Psi_{IW}^{NC}(q=0)\rangle$, and thus can be mistaken with the transient dark state. Only the height of the corresponding peaks in the distribution is different compared to the ones given by the metastable dark state $|\Psi_{NC}^{IW}\rangle$.

We give in fig. 4.6 a numerical example of the case $\Omega \gg \Gamma$ to show its characteristic features in momentum space. Since in the strong drive limit $\Omega \gg \Gamma$ population redistribution due to spontaneous emission is negligible the population of the transient dark state $|\Psi_{NC}^{IW}\rangle$ as well as that of the bright state $|\Psi_{C2}\rangle$ stay actually constant.

Hence, for transient VSCPT to become visible there has to be a certain balance between stimulated and spontaneous processes. One should keep in mind, that the longer the coherence build-up process takes, the more probable will be a destruction of the dark states due to decoherence processes. Even in the intermediate case $\Omega \approx \Gamma$ the observation of transient VSCPT will be difficult.

To understand the dynamics of VSCPT in more detail we now discuss the numerical solution of the generalized optical Bloch equations for experimental relevant parameters ($\Omega \approx \Gamma$, $\alpha \approx 1$). In what follows we disregard however decay out of the system. This is different to the real physical situation where spontaneous emission from the $^3\mathrm{P}_1$-state into the $^3\mathrm{P}_0$-state is allowed. This restriction is necessary to keep the problem numerically tractable but will lead to differences between simulation and measurement. The numerical simulation consisted of the integration of 64 times the number of family momentum states ordinary differential equations. The equations were integrated stepwise with a time increment of $1/20\,\Gamma^{-1}$ and a momentum increment of $\hbar k/20$. The considered momentum interval was $[-8\hbar k, 8\hbar k]$. The initial momentum distribution was given by a Gaussian
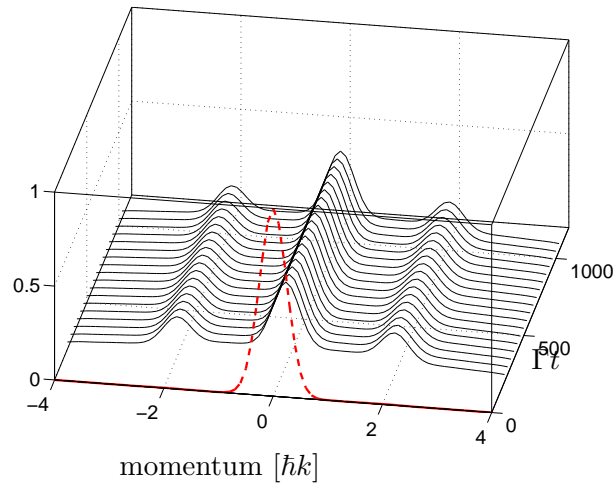
Figure 4.6: This figure gives a simulation for the case of strong optical pumping, i. e. $\alpha \gg 1$ ($\Omega = 10\Gamma$). The red-lines at $\Gamma t = 0$ represent the initial momentum distribution. The figure clearly shows that the stable dark state, represented by two peaks at $p = \pm \hbar k$, is not populated up to $\Gamma t \approx 1000$. The curve is normalized with respect to the maximum of the initial distribution.

profile of width $\Delta q = 0.15 \hbar k$ centered at $p = 0$. This corresponds to the experimental value as we will see in the next section. Initially all Zeeman states in the ${}^3 P_2$ manifold are equally populated without any coherence between them. Even though the atoms experienced in the experiment a time-dependent Rabi frequency, because the atomic beam crossed the laser beams, we assumed it to be constant in the simulation.

The result of the simulation is shown in fig. 4.7 for $\Omega \approx 0.3\Gamma$. Initially all atoms have a momentum in the vicinity of zero momentum. For a short interaction $\Gamma t < 50$, (see 4.7(a)) the momentum diffusion process is still suppressed. The main processes are absorption and stimulated emission. This leads, as discussed above, to a change in momentum of $\Delta p = \pm 2 \hbar k$ and to peaks in the momentum distribution at $p = 0$ and $p = \pm 2 \hbar k$ respectively. It is important to note that the stimulated process described does not lead to a broadening of the considered momentum peaks in contrast to spontaneous emission. Since here $\Omega \lesssim \Gamma$ stimulated and spontaneous processes occur in parallel. Due to the latter the population of the transient dark state increases.

The slower process of spontaneous emission leads to a random walk in momentum space as spontaneous emission of photons goes in an arbitrary direction. This causes a spreading of the distribution in momentum space [141]. The Clebsch-Gordan coefficients shown in fig. 4.8 lead to an enhancement of this effect. Due to them spontaneous emission of circular polarized photons is more likely, which have a larger projection of their momentum on the z-axis. The accompanied diffusive process eventually leads to a successive preparation of the stable dark state of the Λ-subsystem $|\Psi_\Lambda^{NC}(q = 0)\rangle$. The characterization of the stable dark state in momentum space is given by two peaks at $p = \pm \hbar k$. Due to the accumulation of the atoms in that state the width of these peaks decreases for longer interaction time, $\Gamma t > 200$.
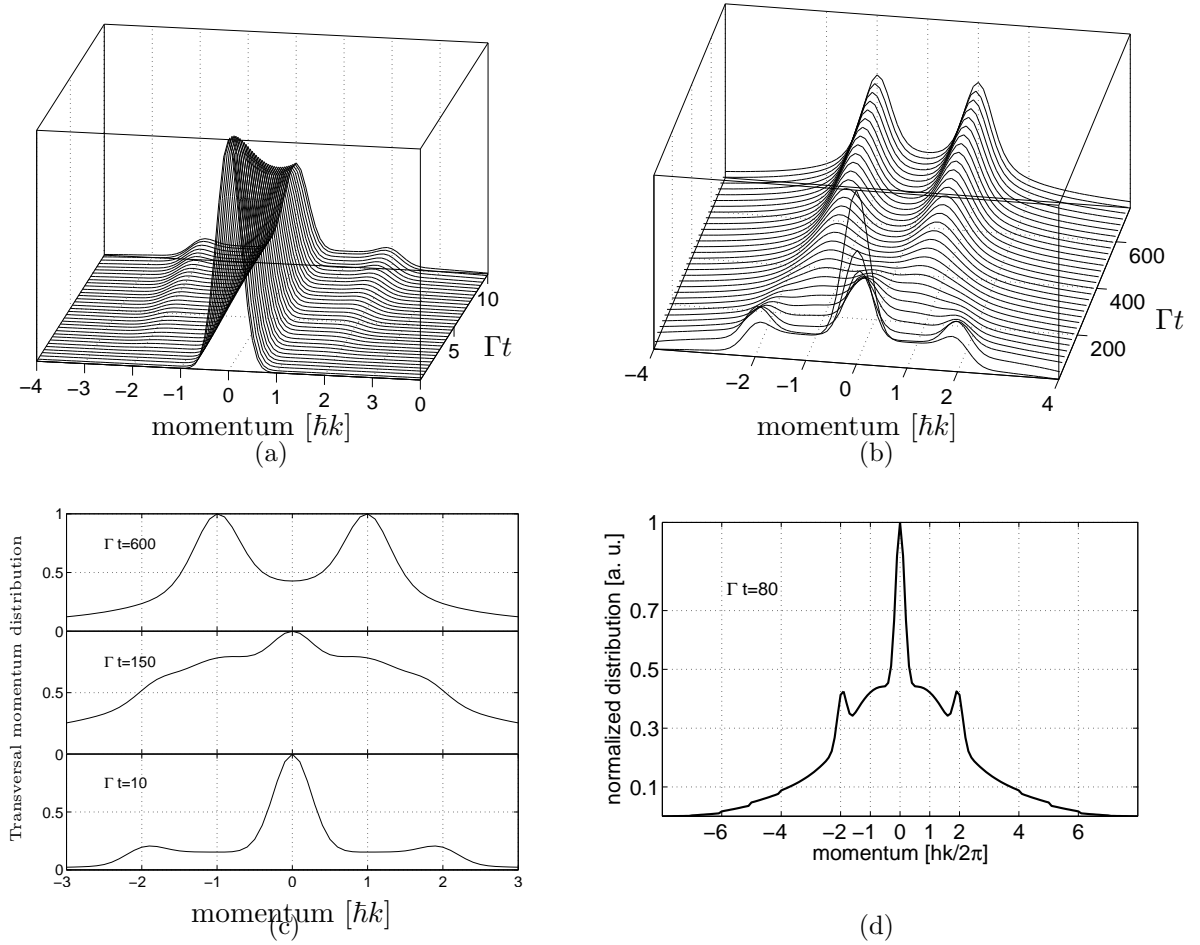
Figure 4.7: (b) shows the result of simulation corresponding to the experimental parameter with $\Omega = 0.3\Gamma$ (b) gives cuts through the momentum distribution shown in part (c) of the figure for certain values of the interaction time. For $\Gamma t = 10$ we see the transient dark state, for $\Gamma t = 600$ the stable dark state and for $\Gamma t = 150$ we see a five peak structure corresponding to the five peak structure given by the experimental data of fig. 4.11. (d) shows the cut through a simulation we a slightly different Rabi frequency of $\Omega \approx 0.45\Gamma$. The signatures of the bright state $|\Psi_{C2}\rangle$ are clearly visible by the peaks at $\pm 2\hbar k$ with the same width as the initial distribution.

For intermediate times, i. e. between $\Gamma t = 100$ and 200 the stable dark state of the Λ-configuration $|\Psi_\Lambda^{NC}(q = 0)\rangle$ and the meta-stable transient dark state of the inverted-W system $|\Psi_{IW}^{NC}(q = 0)\rangle$ as well as the bright state $|\Psi_{C2}(q = 0)\rangle$ are visible. The momentum distribution shows in this case five peaks at $p = 0$, $p = \pm\hbar k$ and $p = \pm 2\hbar k$ respectively. Fig. 4.7(c) shows a simulation where the bright state appears as narrow peak with the same width as the initial momentum distribution. Hence, a distinction of bright and transient dark state should be achievable with a sufficiently narrow initial momentum distribution. The bright state is short-lived due to strong optical pumping out of this state. Since $|\Psi_{NC}^{IW}(q = 0)\rangle$ is only metastable all population will eventually be lost from
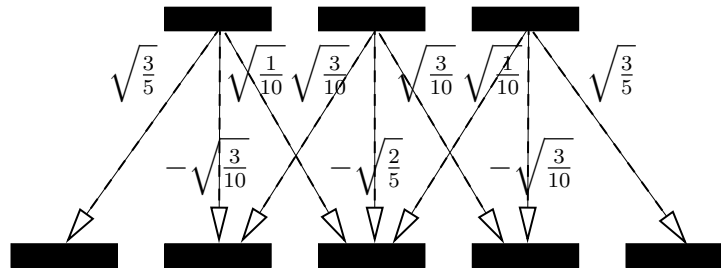
Figure 4.8: The figure shows the Clebsch-Gordon coefficients relevant for $J_g = 2 \leftrightarrow J_e = 1$-transition. The lead to a less probable emission of linear polarized photons than circular polarized photons. Due to the different emission characteristics of these photon types does spontaneous emission lead to a pronounced broadening of the momentum distribution.

that state and in the long time limit only two momentum peaks survive which correspond to the stable dark state $|\Psi_{NC}^\Lambda\rangle$. Finally, we note that for intermediate interaction times the five peak structure corresponding to the simultaneous occurrence of stable dark state and transient dark state and/or bright state can not be resolved very well in fig. 4.7(c).

We note that the notion of dark states makes sense only in the interaction region. After leaving this region the atoms are fixed in momentum eigenstates. Since momentum and kinetic energy Hamiltonian commutate these are also eigenstates of the latter. Hence, free motional evolution does not lead to a modification of the states after the interaction region. This allows us to measure later on both transient and stable dark state even though the time of flight to the detector is much longer then the decay time of the excited state or the recoil time.

In summary we have seen that an observation of $|\Psi_{IW}^{NC}(q = 0)\rangle$ requires Rabi $\Omega \approx \Gamma$ and intermediate interaction times.

4.4 Experimental background

This section gives a brief overview of the experimental setup and the procedure to measure the (transient) VSCPT dark state. For a more detailed description of the setup we refer to [129] and [142].

Experimental setup and preparation

The setup consists of three major parts: (a) a source of meta-stable neon atoms, (b) a free-flow area for the atomic beam with a preparation- and a interaction-region and (c) the detection unit. The neon discharge nozzle source, cooled by liquid nitrogen, excites a fraction on the order of 10^{-4} atoms to the metastable states ${}^3P_0$ or ${}^3P_2$ of the $2p^53s$ electronic configuration [143]. In fig. 4.9 the neon level scheme is shown. The neon beam is formed using differential pumping, where the pumping stages are separated by a skimmer with $1\,mm$ diameter. The transversal velocity distribution of the beam is controlled via a
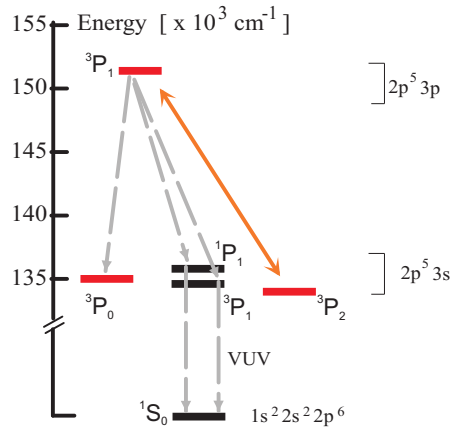
Figure 4.9: Level scheme of neon including the relevant levels for the experiment.

geometrical collimation of the beam using two slits $120\,cm$ apart, leading to a FWHM of the momentum distribution of about $0.15\hbar k$. This results in a Doppler broadening with respect to the transversal laser beams of less than 1 MHz. Hence, Doppler broadening is less than the natural linewidth ($\approx$ 8-9 MHz) of the used transitions. Finally, at the end of the setup, about $120\,cm$ behind the experimental region, one finds a movable channeltron detector. It is used to determine the spatial distribution of the atoms in the states $^3P_0$ and $^3P_2$, which corresponds, due to their induced transversal motion, to their momentum distribution. The response of the detector is neither state nor isotope specific. Since the detector is located behind a comoving slit of width $25\,\mu m$ and height $3\,mm$, the resolution of the momentum measurement is given by $\Delta p \approx 0.2\hbar k$. The used gas is a mixture of three neon isotopes, i. e. ^{20}Ne (90,5%), ^{21}Ne (0,27%) and ^{22}Ne (9,2%). The measurements shown in this chapter correspond to the ^{20}Ne isotope. The isotope frequency shift of the considered transition is on the order of 2 GHz which is much larger than the natural linewidth of the transition. This circumstance allows for a isotope selective addressing of the transition. In addition to the metastable atoms also VUV-photons, created by the discharge source, are detected by the channeltron. All these contributions, i. e. isotopes, VUV-photons and atoms in other metastable states lead to a background in the measurement data.

For the preparation of the experiment the population of the metastable state $^3P_0$ is depleted by optical pumping in a preparation region which is about $60\,cm$ upstream of the interaction region. Furthermore, in the interaction region the magnetic field is actively compensated to less than $1\,\mu$T to assure the degeneracy of all Zeeman states to better than 130 kHz.

Experimental procedure

To prepare transient velocity selective dark states proposed by E. Arimondo et al. [130] we apply light fields in a $\sigma^+ - \sigma^-$-configuration to a $J_g = 2 \leftrightarrow J_e = 1$-transition. This configuration was created in our case by the optical setup given in fig. 4.10. The laser beam passes through a polarizer, two quarter wave plates and optionally two cylindrical lenses
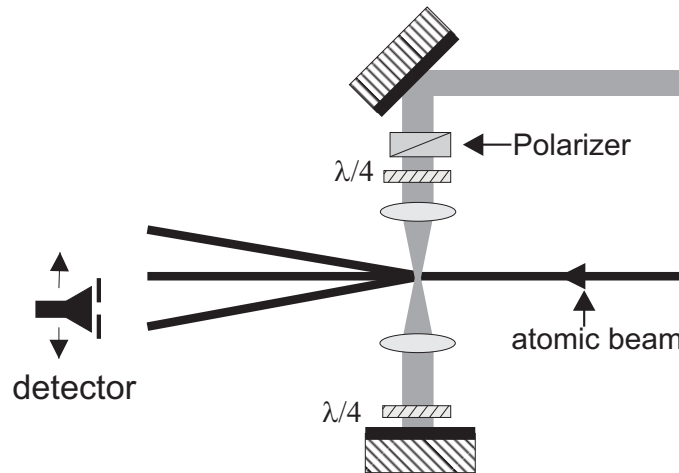
Figure 4.10: Schematic setup of the experiment. The cylindrical lenses have a focal length of 250 mm and they are in a confocal arrangement. Further details can be found in the text.

before being retroreflected. The polarizer and the first quarter wave plate establishes a right circular polarized laser beam incident perpendicular onto the atomic beam. The second quarter wave plate turns the laser beam into a linearly polarized beam, that is retroreflected by the mirror. The same quarter wave plate transforms this beam finally into a left circular polarized beam and establishes then the $\sigma^+ - \sigma^-$-configuration of two counter-propagating beams with orthogonal, circular polarization.

To study the temporal dynamics of the stable dark state $|\Psi_{NC}^{\Lambda}(q = 0)\rangle$ and the transient dark state $|\Psi_{NC}^{IW}(q = 0)\rangle$ we used three different laser beam width configurations. This corresponds to three different interaction times due to the constant longitudinal velocity of the atoms given by 470 m/s. The width of the longitudinal velocity distribution is about 100 m/s (FWHM) which is a measure of the interaction time error [129].

In a first setup we used cylindrical lenses in a confocal arrangement with the atomic beam crossing the laser beams in the vicinity of the foci. The transit time of the atoms is estimated to be a few $100 \, ns$; corresponding to $\Gamma t \approx 10$, where Γ is the linewidth of the transition between the $^3P_1$ and the $^3P_2$ state. The laser beam profile is not measured directly but inferred from the the dimensions of the optical setup. Hence the above value is only a lower bound for the interaction time, which is only reached for ideal optical elements.

In a second step we removed the cylindrical lenses to increase the interaction time between the atoms and the laser light. This leads to an approximate interaction time of $\Gamma t \approx 200$. Using a telescope in front of the polarizer, the beam diameter can be widened further to 8 mm, resulting in $\Gamma t \approx 800$.

We estimated that the laser beams were parallel to within 10^{-5} rad and that the reachable peak Rabi frequency is of the order of 500 MHz. The laser was detuned form the $|J_g = 2, m_g = 0\rangle \leftrightarrow |J_e = 1, m_e = 0\rangle$ -transition by 100 MHz to reduce the influence of stray light from the windows.

In the next section we will compare the experimental results measured in collaboration with F. Vewinger [129] with the simulations based on the full numerical solution of the generalized optical Bloch equations.

4.5 Comparison: experimental and theoretical results

This section will give a comparison of the measured data with the data obtained by the numerical integration of the generalized optical Bloch equations as derived in section 4.3.2. The section consists of two subsections including a more detailed explanation of (a) the short- and intermediate-time dynamics and (b) the long-term dynamics of the system.

4.5.1 Short and intermediate interaction time

In the short interaction time limit, i. e. $t < 20\Gamma^{-1}$, we anticipate from our simulation, see fig. 4.7, that only the transient dark state is prepared by optical pumping out of the bright state $|\Psi_{C2}\rangle$. This is a very fast process, it occurs on the time scale of Ω^{-1}. Since we have $\Omega \approx \Gamma$ emptying $|\Psi_{C2}\rangle$ only takes a few inverse lifetimes Γ^{-1}. The optical pumping process leads to an increase of population not only of $|\Psi_{NC}^{IW}\rangle$ but also of $|\Psi_{NC}^{\Lambda}\rangle$. The latter process is however somewhat slower due to the Clebsch-Gordon coefficients.

The transit time of the atoms through the beam is estimated by geometric arguments from the experimental setup. In the case of short interaction time we focused the laser beams onto the atomic beam. For ideal optical elements we find a minimum transit time corresponding to $\Gamma t \approx 10$.

Fig. 4.11 shows a measured momentum distribution. The initial momentum distribution is given by the grey area which is appropriately scaled down to fit into the plot. The initial peak contains contributions from population of the $^3P_0$, which is populated by spontaneous emission from the upper state $^3P_1$, as well as contributions of other neon isotopes whose momentum distributions are not changed due to the laser interaction because they are sufficiently far off resonant. The contribution due to other isotopes is on the order of 10% of the initial peak. The momentum distribution in the VSCPT-configuration clearly shows five maxima located at $p \approx n\hbar k$ with $n = -2, \cdots, 2$. These correspond to contributions from the transient and the stable dark state. In addition there should also be contributions from the bright state $|\Psi_{C2}\rangle$ since the interaction time is very short. In contrast to the simulation, shown in fig. 4.7, the symmetry of the distribution is broken with respect to $p = 0$. This is due to the not perfectly collinear setup of the laser beams in the creation of the $\sigma^+ - \sigma^-$-configuration by retroreflection. The retroreflected beam passes twice through a window and the (uncoated) cylindrical lens before crossing the atomic beam again. Thus also the Rabi frequencies of the two laser beams are not equal, i. e. $\Omega_+ \neq \Omega_-$, which leads to an asymmetric population distribution within the dark states. By comparing experimental, fig. 4.11 (a), with numerical results, fig. 4.7(c) , we see that we can resolve the experimental peaks much better. The broad nature of the peaks in the simulation is due to possible momentum change of $-\hbar k \leq p \leq \hbar k$ in a spontaneous emission process. We anticipate that the strong broadening in the simulation
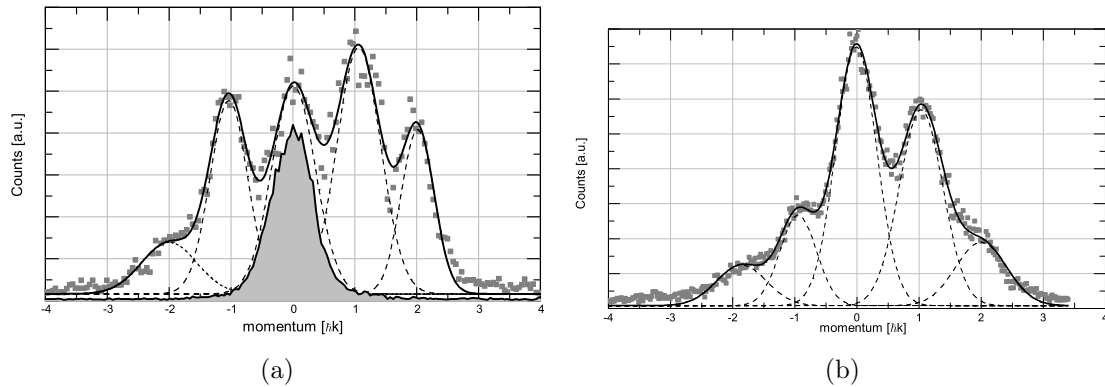
Figure 4.11: (a) Transverse atomic momentum profile after a short interaction time ($\Gamma t \approx 10$). The grey area shows the initial momentum distribution (scaled down) created by cooling the source and collimation of the atomic beam. The dashed lines are Gaussian fits to the individual peaks. The full line is the sum of the Gaussian fits. (b) Transversal momentum distribution for atoms that passed a σ^--beam after they traveled through the σ^+-σ^--configuration. The asymmetry of the distribution is an indicator for the observation of VSCPT. The dashed lines are Gaussian fits to the individual peaks, the solid line is their sum.

is due to neglection of spontaneous emission from the upper state $^3P_1$ into other states than $^3P_2$. However, it also leads to lower signal-to-noise ratio which we observed during the experiment.

Supplementary tests

As suggested by A. Aspect et al. [132] we conducted a consistency check to confirm the observation of VSCPT. We arranged the counter-propagating laser beams in such a way that they do not exactly overlap at the end of the σ^+-σ^--interaction region.

To this end we tilted the retroreflected beam slightly. At the end of the interaction zone only the σ^--beam interacted with the atoms after passing the σ^+-σ^--region. The dark states formed in the σ^+-σ^--interaction region are no-longer dark in this configuration and are therefore destroyed. In this configuration only the states $|g_{-2}\rangle$, $|g_{-1}\rangle$ and $|g_0\rangle$ couple to the excited state manifold and are hence depopulated by optical pumping. Due to the correlation between the internal m_J-Zeeman sublevels and the momentum family states $|q + m_J \hbar k\rangle$, found in section 4.3, this leads to the decrease of the peaks height at negative family momenta. The measurement with tilted lasers, shown in fig. 4.11 (b), shows a good agreement with the expectations, except for the zero momentum peak. This peak shows no depletion which indicates that it is mainly given by other neon isotopes which have a negligible coupling to the radiation field. Their motion is thus not modified by the radiation field and hence the zero momentum peak mainly represents the initial momentum distribution of these isotopes. An additional contribution to the zero momentum peak is given by atoms in the $^3P_0$-state of ^{20}Ne which is populated by spontaneous emission
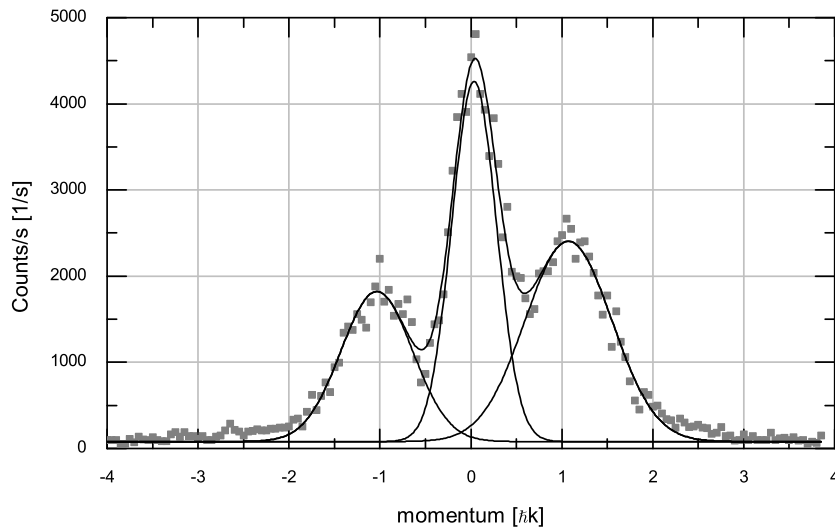
Figure 4.12: Transverse atomic momentum profile after an interaction time of $8\mu s$ ($\Gamma t \approx 800$). The lines are Gaussian fits to the peaks. The peaks at $p = \pm\hbar k$ reflect the stable dark state $|\Psi^\Lambda_{NC}(q = 0)\rangle$.

and which are also detected by the channeltrons. However, the latter contribution should be much smaller than the former. A more thorough discussion on the dependence of the dark states on the overlap of the counterpropagating beams can be found in [144].

There are further supplementary tests [132] that may support the observation of VSCPT. The replacement of the σ^+- and σ^--polarized beams by two orthogonal linearly polarized beams should lead to the observation of the same momentum distributions since the field configurations are equivalent. On the other hand, by applying two parallel linearly polarized beams the peak structure should disappear because the nonabsorbing atomic superpositions are not veloctiy selective. These test were, however, not performed.

4.5.2 Long interaction time

In the long interaction time limit we expect from our simulation and our earlier considerations that the momentum distribution only reflects the existence of the stable dark state $|\Psi^\Lambda_{NC}(q = 0)\rangle$. This is due to the accumulation of the atoms in the course of velocity selective coherent population trapping in the corresponding state. In fig. 4.12 a measured momentum distribution for an interaction time of $8\mu s$ ($\Gamma t \approx 800$) is shown which clearly reflects the characteristic features of the stable dark state $|\Psi^\Lambda_{NC}(q = 0)\rangle$. The asymmetry in the momentum profile is again due to asymmetry in the laser beam setup.

As in the short time limit the peak at $p = 0$ is caused by the atoms in state $^3P_0$ and contributions from other neon isotopes, i. e. ^{21}Ne (0,27%) and ^{22}Ne (9,2%). The long interaction time limit shows excellent qualitative agreement with our numerical simulation of the generalized optical Bloch equations.

4.6 Summary

The present chapter discussed the first observation of the transient dark state of VSCPT predicted by E. Arimondo et al. [130]. We compared the measured data with the numerical solution of the generalized optical Bloch equations which showed a qualitative agreement between theory and experiment. Finally we note once more that we can not distinguish very well the bright state $|\Psi_{C2}\rangle$ and the transient dark state $|\Psi_{NC}^{IW}\rangle$ using momentum distribution measurement. Even though the former has a much shorter lifetime, due to optical pumping, further experiments would be necessary for an unambiguous experimental verification.

Publications

Parts of this work have been already published or are submitted for publication:

1. F. Zimmer and M. Fleischhauer,
   Sagnac Interferometry based on ultra-slow polaritons in cold atomic vapors
   Phys. Rev. Lett. **92**, 253201 (2004)

2. F. E. Zimmer, A. André, M. D. Lukin and M. Fleischhauer
   Coherent control of stationary pulses of light
   Opt. Comm. **264**, 441-453 (2006)
   Dedicated to Bruce W. Shore on the occasion of his 70th birthday.

3. F. E. Zimmer and M. Fleischhauer,
   Quantum sensitivity limits of a Sagnac hybrid interferometer based on slow-light
   propagation in ultra-cold gases
   accepted by Phys. Rev. A

Preprints

4. F. Vewinger and F. E. Zimmer,
   Experimental observation of transient velocity-selective coherent population trapping in one dimension
   quant-ph/0501164

and earlier publications until the Diplom (German equivalent of the master degree)

5. Hans Jürgen Korsch and Frank Zimmer
   Chaotic Billards
   Computational Statistical Physics – From Billards to Monte Carlo
   15 (2001), Springer Verlag, ed. K. H. Hoffmann, M. Schreiber

6. B. Rosam, K. Leo, M. Glück, F. Keck, H. J. Korsch, F. Zimmer and K. Köhler,
   Lifetime of Wannier-Stark States in Semiconductor Superlattices under Strong Zener
   Tunneling to Above-Barrier Bands
   Phys. Rev. B **68**, 125301 (2003)

7. M. Glück, A. R. Kolovsky, H. J. Korsch and F. Zimmer,
   Wannier-Stark resonances in semiconductor superlattices
   Phys. Rev. B **65**, 115302 (2002)

The publications 1. and 3. are connected to the chapter (3) on the slow-light gyroscope and the publication 2. to the chapter (2) on stationary light. The 4. publication originated from an laboratory in the group of Prof. Dr. Klaas Bergmann while I was fellow of the Graduiertenkolleg 792: ,,Ultrakurzzeitphysik und nichtlineare Optik".

Appendix A

Appendix

A.1 Spontaneous emission in the presence of atomic motion

In this Appendix we deal with spontaneous emission in the presence of atomic motion. The motion of the atoms is described in the formalism of second quantization. For notational simplicity we perform all calculations for a two-level system. The generalization to the three level system under consideration is straight forward. The system is described by the Hamiltonian

$$H = H_{at} + H_f + H_{int}, \tag{A.1}$$

where H_{at} is the Hamiltonian, that describes the atom, H_f is responsible for the quantized field and H_{int} is the interaction Hamiltonian. We restrict ourselves to dipole-interaction between the radiation field and the atom. For simplicity we assume that the field vector direction coincides with the unit vector of the dipole-moment, hence we can write the interaction Hamiltonian in first quantization in the form

$$H_{int} = -\hbar \left[\hat{\sigma}_{eg} \, \hat{E}^{(+)} + h.a. \right]. \tag{A.2}$$

We have already applied here the rotating wave approximation and assumed resonance condition. The quantized electromagnetic field is given by

$$\hat{E}^{(+)}(x,t) = \sum_k \frac{\wp}{\hbar} \sqrt{\frac{\hbar \omega_k}{2\epsilon_o V}} \hat{a}_k(t) e^{i k x} \tag{A.3}$$

where $\wp$ is the dipole moment of the transition, ω the frequency of the field and V the quantization volume. We introduce the coupling constant for each mode $g_k = \frac{\wp}{\hbar} \sqrt{\frac{\hbar \omega_k}{2\epsilon_o V}}$. With the ansatz

$$\hat{\Psi}(x,t) = \sum_{\mu \in \{g,e\}} \hat{\Psi}_\mu(x,t) |\mu\rangle, \tag{A.4}$$

we can rewrite eq. (A.2) in the formalism of second quantization

$$\mathcal{H}_{int} = -\hbar \int \left[\hat{\Psi}_e^\dagger(x,t) \hat{\Psi}_g(x,t)\, \hat{E}^{(+)} + h.a. \right] \mathrm{d}x. \tag{A.5}$$

We note, that the system Hamiltonian reads in the formalism of second quantization

$$\begin{aligned}
\mathcal{H} &= \mathcal{H}_{at} + H_f + \mathcal{H}_{int} \\
&= \sum_{\mu \in \{g,e\}} \int \hat{\Psi}_\mu^\dagger(x,t) \left[-\frac{\hbar^2}{2m} \partial_x^2 + \hbar\omega_\mu + V_\mu(x,t) \right] \hat{\Psi}_\mu(x,t)\mathrm{d}x + H_f + \mathcal{H}_{int}.
\end{aligned} \tag{A.6}$$

Master equation

If a quantum mechanical system is in a mixed state, one describes it in general by a statistical operator χ [145]. In the Schrödinger picture, the atom+field system is described [21] by

$$\mathrm{i}\hbar\partial_t\chi(x,t) = [\mathcal{H}, \chi]. \tag{A.7}$$

To simplify the discussion and to use the fact, that the states of the field and the atomic system can be calculated at least approximately, we transform each operator $\mathcal{O}$ via

$$\tilde{\mathcal{O}} = \exp\left[\frac{\mathrm{i}}{\hbar}(\mathcal{H}_{at} + H_f)t \right] \mathcal{O} \exp\left[-\frac{\mathrm{i}}{\hbar}(\mathcal{H}_{at} + H_f)t \right] \tag{A.8}$$

into the interaction picture. Here the interaction picture is denoted by the tilde over the operator. With the help of this definition the von Neumann equation is given by

$$\mathrm{i}\hbar\partial_t\tilde{\chi}(t) = \left[\tilde{\mathcal{H}}_{int}(t), \tilde{\chi}(t) \right] \tag{A.9}$$

This equation can formally be integrated, and one obtains

$$\tilde{\chi}(t) = \tilde{\chi}(t_i) - \frac{\mathrm{i}}{\hbar} \int_{t_i}^t \left[\tilde{\mathcal{H}}_{int}(t'), \tilde{\chi}(t') \right] \mathrm{d}t'. \tag{A.10}$$

Here t_i is the time, when the interaction between the system and the bath starts. Substituting this equation into eq. (A.9), we find an integro-differential equation for the density matrix $\tilde{\chi}$.

$$\mathrm{i}\hbar\partial_t\tilde{\chi}(t) = \left[\tilde{\mathcal{H}}_{int}(t), \tilde{\chi}(t_i) \right] - \frac{\mathrm{i}}{\hbar} \int_{t_i}^t \left[\tilde{\mathcal{H}}_{int}(t), \left[\tilde{\mathcal{H}}_{int}(t'), \tilde{\chi}(t') \right] \right] \mathrm{d}t'. \tag{A.11}$$

Before we proceed a few essential assumptions should be summarized [34]:

(a) at $t = t_i$, when there is no interaction yet, the atomic part and the field part are independent, i. e. there is no correlation between them. Mathematically this can be expressed as

$$\chi(t_i) = \chi_{at}(t_i) \otimes \chi_f(t_i). \tag{A.12}$$

(b) We assume that the state of the field part is not changed due to the interaction with the atomic system. This means that the reservoir part is so large that its statistical nature stays the same during the whole process. Mathematically this can be formulated as follows. In general the density matrix can be decomposed as

$$\chi(t) = \chi_{at}(t) \otimes \chi_f(t_i) + \chi_{corr}(t). \tag{A.13}$$

Here χ_{corr} denotes the part that is responsible for the correlation between atomic and field system. The requirement mentioned above is fulfilled if

$$\mathsf{Tr}_f\{\chi_{corr}\} = 0 \tag{A.14}$$

for all t. This is the so-called *Born approximation*.

(c) The final assumption will turn eq. (A.11) into a differential equation. Physically we assume that the atom-field correlation time is negligible as compared to the evolution time of the atomic system. Hence we perform the following replacement

$$\tilde{\chi}(t') \rightarrow \tilde{\chi}(t). \tag{A.15}$$

This *Markov approximation* means that the knowledge of $\tilde{\chi}(t)$ at time $t = t_i$ is sufficient to determine $\tilde{\chi}(t)$ for all $t > t_i$.

In general we are only interested in the atomic observables, which depend only on the atomic density operator, hence we define the reduced density operator by tracing over all field states

$$\tilde{\rho} = \mathsf{Tr}_f\{\tilde{\chi}\}. \tag{A.16}$$

Applying this to eq. (A.11) we finally find the master equation for the reduced density operator after Born-Markov approximation

$$\partial_t \tilde{\rho}_{at} = -\frac{1}{\hbar^2} \int_0^t \mathsf{Tr}_f \left\{ \left[\tilde{\mathcal{H}}_{int}(t), \left[\tilde{\mathcal{H}}_{int}(t'), \tilde{\rho}_{at}(t) \otimes \rho_f(t_i) \right] \right] \right\} \mathrm{d}t'. \tag{A.17}$$

To derive this equation we have furthermore used that

$$\mathsf{Tr}_f\{\tilde{\mathcal{H}}_{int}(t)\tilde{\chi}(t_i)\} = 0, \tag{A.18}$$

which means that we assume that the interaction has no diagonal elements in the representation in which H_f is diagonal. This is not a very serious assumption since it can

always be accomplished by redefining H_f and H_{at} in such a way that the diagonal elements are included in H_{at}. For the further evaluation we will use the following relations

$$\langle \hat{E}_i^{(+)}(x,t)\hat{E}_j^{(-)}(x',t')\rangle = \frac{1}{2}\gamma\,\delta(x-x')\delta(t-t')\,\delta_{ij}, \tag{A.19}$$

$$\langle \hat{E}_i^{(-)}(x,t)\hat{E}_j^{(+)}(x',t')\rangle = \langle \hat{E}_i^{(+)}(x,t)\hat{E}_j^{(+)}(x',t')\rangle = \langle \hat{E}_i^{(-)}(x,t)\hat{E}_j^{(-)}(x',t')\rangle = 0. \tag{A.20}$$

To simplify eq. (A.17) further, we expand the double commutator and make use of the relation eqs. (A.19-A.20). After some tedious algebra one finds for the reduced density matrix in the interaction picture (we omitted the tilde for notational simplicity)

$$\begin{aligned}
\partial_t\rho(t) &= -\frac{\gamma}{2}\int dx\,\Big\{\hat{\Psi}_e^\dagger(x,t)\hat{\Psi}_g(x,t)\hat{\Psi}_g^\dagger(x,t)\hat{\Psi}_e(x,t)\rho(t) \\
&+ \rho(t)\hat{\Psi}_e^\dagger(x,t)\hat{\Psi}_g(x,t)\hat{\Psi}_g^\dagger(x,t)\hat{\Psi}_e(x,t) \\
&- 2\hat{\Psi}_e^\dagger(x,t)\hat{\Psi}_g(x,t)\rho(t)\hat{\Psi}_g^\dagger(x,t)\hat{\Psi}_e(x,t)\Big\}.
\end{aligned} \tag{A.21}$$

The structure of the equation does not change when we transform it to the Schrödinger picture except for the occurrence of additional terms which describe the unitary dynamics and the substitution $\hat{\Psi}_\mu(x,t) \to \hat{\Psi}_\mu(x)$. The density matrix elements are calculated in the same way as in section 3.4

$$\rho_{\mu\nu}(x,x',t) = \langle \hat{\Psi}_\mu^\dagger(x)\hat{\Psi}_\nu(x')\rangle = \mathsf{Tr}\{\rho(t)\hat{\Psi}_\mu^\dagger(x)\hat{\Psi}_\nu(x')\} \tag{A.22}$$

Unfortunately this approach with continuous variables leads to diverging contribution due the quantum field theoretical nature hence we use a similar ansatz as in [146] and discretize the problem. To do this we introduce a equidistant grid, with grid constant Δx and Δp, respectively. The position and quasimomentum constants should fulfill: $\Delta x\Delta p = 2\pi\hbar/M$, with M being the number of grid points. This means we consider a system in a box with length $L = M\Delta x$ and assume periodic boundary conditions. The quasimomentum is restricted to an interval of length $L_p = M\Delta p$. The Liouville equation then becomes using the replacement

$$\hat{\Psi}_\mu(x_j) = \frac{\hat{b}_{\mu,j}}{\sqrt{\Delta x}} \text{ with } \hat{b}_{\mu,j} = \frac{1}{\sqrt{M}}\sum_{j=0}^{M-1}\hat{a}_{\mu,j}e^{ik_jx_j} \tag{A.23}$$

and the substitution of the integrals by summations

$$\begin{aligned}
\dot{\rho}(t) &= -\frac{\gamma}{2\Delta x}\sum_{k=0}^{M-1}\Big\{\hat{b}_{e,k}^\dagger\hat{b}_{g,k}\hat{b}_{g,k}^\dagger\hat{b}_{e,k}\rho(t) \\
&+ \rho(t)\hat{b}_{e,k}^\dagger\hat{b}_{g,k}\hat{b}_{g,k}^\dagger\hat{b}_{e,k} - 2\hat{b}_{e,k}^\dagger\hat{b}_{g,k}\rho(t)\hat{b}_{g,k}^\dagger\hat{b}_{e,k}\Big\}.
\end{aligned} \tag{A.24}$$

Here the Bose field with discretized modes a_j and wave-number $k_j = p_j/\hbar$ is related to local bosonic operators, eq. (A.23) and $[\hat{b}_{\mu,j},\hat{b}_{\nu,i}] = \delta_{\mu\nu}\delta_{ij}$, via a discrete Fourier transformation. With the help of the definition for the density matrix elements in the discretized model

$$\rho_{\mu,\nu}(j,j',t) = \frac{1}{\Delta x}\langle 0|\hat{b}_{\mu,j}\rho(t)\hat{b}_{\nu,j'}^\dagger|0\rangle \tag{A.25}$$

one arrives at the following equations for the density matrix elements

$$\partial_t \rho_{g,g}(j, j', t) = \gamma\, \rho_{e,e}(j, j', t)\, \delta_{j,j'}, \tag{A.26}$$

$$\partial_t \rho_{e,e}(j, j', t) = -\gamma\, \rho_{e,e}(j, j', t), \tag{A.27}$$

$$\dot{\rho}_{g,e}(j, j', t) = -\frac{1}{2}\gamma\, \rho_{e,e}(j, j', t). \tag{A.28}$$

One should not that the decay leads to a decoherence of the spatial off-diagonal elements, i. e. $j \neq j'$, of the excited state and of the internal coherence. In the case of the Λ-type 3-level system as discussed in section 3.4 the equation have the form

$$\dot{\rho}_{1,1} = \gamma_1\, \rho_{2,2}(j, j', t)\, \delta_{j,j'}, \tag{A.29}$$

$$\dot{\rho}_{2,2} = (-\gamma_1 - \gamma_2)\, \rho_{2,2}(j, j', t), \tag{A.30}$$

$$\dot{\rho}_{3,3} = \gamma_2\, \rho_{2,2}(j, j', t)\, \delta_{j,j'}, \tag{A.31}$$

$$\dot{\rho}_{1,2} = -\frac{1}{2}\,(\gamma_1 + \gamma_2)\, \rho_{2,2}(j, j', t), \tag{A.32}$$

$$\dot{\rho}_{1,3} = 0, \tag{A.33}$$

$$\dot{\rho}_{1,2} = -\frac{1}{2}\,(\gamma_1 + \gamma_2)\, \rho_{2,2}(j, j', t). \tag{A.34}$$

By adding these equations to the von-Neumann equations one arrives at the proper density matrix equations for this system under consideration. In addition to the two state system there is also decay of the Raman spin coherence. In our model we assume that this is equal to zero.

A.2 mathematica-code for resolvent theory calculations

This appendix reports the mathematic-code used to calculate the complex eigenvalues of the effective Hamiltonian operators (4.49) or (4.50) for the case of the inverted-W subsystem. The programm can easily be rewritten to be suitable for the simpler Λ-subsystem.

```
<< LinearAlgebra'Orthogonalization'

%  free motional evolution of 8 state system

hfree[p_] = SparseArray[{{1, 1} -> p^2, {2, 2} -> (p + 1)^2,
     {3, 3} -> (p - 1)^2, {4, 4} ->p^2,
{5, 5} -> (p + 1)^2,{6, 6} -> (p - 1)^2,
{7,7} -> (p + 2)^2, {8, 8}-> (p - 2)^2},{8, 8}];

% decay out of the excited state with equal
% probability; only decay out of the system
```

```
hdecay = SparseArray[{{1, 1} -> 1, {2, 2} -> 1, {3, 3} -> 1}, {8, 8}];

% projection operator on excited state manifold

pj1 = SparseArray[{{1, 1} -> 1, {2, 2} -> 1, {3, 3} -> 1}, {8, 8}];

% definition of classical dipol interaction Hamiltonian

help1 = SparseArray[{{2, 4} -> Sqrt[1/10], {2, 7} -> Sqrt[6/10],
    {3, 4} -> Sqrt[1/10], {3, 8} -> Sqrt[6/10]}, {8, 8}];

hdipoleinteractionInvertedW = help1 + Transpose[help1];

help2 = SparseArray[{{1, 5} ->Sqrt[3/10], {1, 6} -> Sqrt[3/10]}, {8, 8}];

hdipoleinteractionLambda = help2 + Transpose[help2];

hval = hdipoleinteractionInvertedW + dipolinteractionLambda;

% definition of resolvent operator

help3[Deltas_] = Inverse[-(I/2*hdecay - Deltas*IdentityMatrix[8])];

% definition of resolvent operator

hresolvent[alpha_,Delta_] = alpha*vAL.pj1.help3[Delta].pj1.vAL;

% definition of effective operator
heff[q_, Delta_, alpha_] = Erec/(hbars*Gammas)*
        (hfree[q] +hresolvent[alpha,Delta]);

% projection on ground states of inverted-W subsystem
% (using the mathmatica command: part)

heffredIW[q_, Delta_, alpha_] = heff[q,Delta, alpha][[{4, 7, 8}, {4, 7, 8}]];

% definition of physical parameter

(* standard parameters *)

u    = 1.66053886*10^(-27); (*kg*)
hbar = 1.0545*10^(-34);      (* kg m^2/s *)

(* neon parameter *)
```

```
Gamma  = 1/(20*10^(-9))/2/Pi; (*s^(-1)*)
Lambda = 589*10^(-9); (*m*)
M = 20*u; (*kg*)

(* scaled parameter *)
hbars = 1;
Gammas = 1;
Deltas = 0.000001;
OmegaOptimals = 0.45;

(* compute needed numbers *)
k = 2*Pi/Lambda; (*m^-1*)

Erec = hbar^2*k^2/(2*M)/(hbar*Gamma);

% definition of function which calculates complex
% eigenvalues as a function of the Rabi frequency Omega and the
% family momentum q

f[Omega_, q_] := N[Eigenvalues[
                hEffRediW[q,Delta, hbar*Omega^2/(4*Gamma*Erec)]]];

% ordering of the resulting eigenvalues with respect to
% the value of their imaginary part

ordiW[Omega_, q_] := Ordering[Im[f[Omega, q]]];
```

Bibliography

[1] M. Fleischhauer and M. D. Lukin. Dark-state polaritons in electromagnetically induced transparency. *Phys. Rev. Lett.*, 84(22):5094–5097, 2000. (document), 1.3, 1.3.3, 2.1, 2.2.3, 2.2.4, 2.4.1, 3.1, 3.2.1, 3.3.1

[2] S. E. Harris. Electromagnetically induced transparency. *Physics Today*, 50:36, 1997. (document), 1.2.1

[3] M. Fleischhauer and M. D. Lukin. Quantum memory for photons: Dark-state polaritons. *Phys. Rev. A (Atomic, Molecular, and Optical Physics)*, 65(2):022314, 2002. (document), 1.2.2, 1.2.2, 1.3, 1.3.3, 2.1, 2.2.3

[4] M. Masalas and M. Fleischhauer. Scattering of dark-state polaritons in optical lattices and quantum phase gate for photons. *Phys. Rev. A (Atomic, Molecular, and Optical Physics)*, 69(6):061801, 2004. (document)

[5] I. Friedler, D. Petrosyan, M. Fleischhauer, and G. Kurizki. Long-range interactions and entanglement of slow single-photon pulses. *Phys. Rev. A (Atomic, Molecular, and Optical Physics)*, 72(4):043803, 2005. (document), 2.1

[6] M. D. Lukin and A. Imamoğlu. Nonlinear optics and quantum entanglement of ultraslow single photons. *Phys. Rev. Lett.*, 84:1419, 2000. (document), 1.2.2

[7] H. Schmidt and A. Imamoğlu. Giant Kerr nonlinearities obtained by electromagnetically induced transparency. *Opt. Lett.*, 21:1936, 1996. (document), 1.2

[8] S. E. Harris and Y. Yamamoto. Photon switching by quantum interference. *Phys. Rev. Lett.*, 81:3611, 1998. (document), 1.2.2

[9] S. E. Harris and L. V. Hau. Nonlinear optics at low light levels. *Phys. Rev. Lett.*, 82:4611, 1999. (document), 1.2.2, 2.1, 2.4

[10] D. A. Braje, V. Balic, G. Y. Yin, and S. E. Harris. Low-light-level nonlinear optics with slow light. *Phys. Rev. A (Atomic, Molecular, and Optical Physics)*, 68(4):041801, 2003. (document), 2.1, 2.4

[11] A. André and M. D. Lukin. Manipulating light pulses via dynamically controlled photonic band gap. *Phys. Rev. Lett.*, 89(14):143602, 2002. (document), 2.1, 2.2.2, 2.2.4, 2.6

[12] M. Bajcsy, A. S. Zibrov, and M. D. Lukin. Stationary pulses of light in an atomic medium. *Nature*, 426:638–641, 2003. (document), 2.1, 2.2.2, 2.2.4, 2.6

[13] U. Leonhardt and P. Piwnicki. Ultrahigh sensitivity of slow-light gyroscope. *Phys. Rev. A*, 62:055801, 2000. (document), 3.1

[14] L. V. Hau, S. E. Harris, Z. Dutton, and C. H. Behroozi. Light speed reduction to 17 metres per second in an ultracold atomic gas. *Nature*, 397:594–598, Feb 1999. (document), 1.1.1, 1.2, 1.2.2, 3.2.1

[15] F. Zimmer and M. Fleischhauer. Sagnac interferometry based on ultraslow polaritons in cold atomic vapors. *Phys. Rev. Lett.*, 92(25):253201, 2004. (document), 3.1, 3.2.2, 3.3.1, 3.3.1, 3.3.1, 3.4, 3.5

[16] M. S. Shahriar, G. S. Pati, R. Tripathi, V. Gopal, M. Messal, and K. Salit. Ultrahigh precission absolute and relative rotation sensing using fast and slow light. quant-ph/0505192. (document)

[17] C. Cohen-Tannoudji, J. Dupont-Roc, and G. Grynberg. *Atom-Photon-Interactions: Basic Processes and Applications.* John Wiley & Sons, Inc, 1992. 1.1, 1.1.1, 1.1.1, 1.1.1, 1.2, 1.2.1, 4.3.3

[18] C. Cohen-Tannoudji, J. Dupont-Roc, and G. Grynberg. *Photons and Atoms: Introduction to Quantum Electrodynamics.* John Wiley & Sons, Inc., 1997. 1.1, 1.1.1, 1.1.1, 3.2.2, 3.2.2

[19] C. Liu, Z. Dutton, C. H. Behroozi, and L. V. Hau. Observation of coherent optical information storage in an atomic medium using halted light pulses. *Nature*, 409:490–493, 2001. 1.1.1, 2.1

[20] D. F. Phillips, A. Fleischhauer, A. Mair, and R. L. Walsworth. Storage of light in atomic vapor. *Phys. Rev. Lett.*, 86:783–786, 2001. 1.1.1, 2.1

[21] M. O. Scully and M. S. Zubairy. *Quantum Optics.* Cambridge University Press, Cambridge, 1997. 1.1.1, 1.1.1, 1.2, 1.2.1, 1.2.2, 1.4.2, 2.2.1, 2.2.1, 2.2.3, 3.4, 3.4.3, 4.1, 4.3.2, 4.3.2, 4.3.2, A.1

[22] D. Ebert. *Eichtheorien: Grundlagen der Elementarteilchenphysik.* Akademie-Verlag Berlin, Berlin, 1989. 1.1.1

[23] E. A. Power. *Introductory Quantum Electrodynamics.* Longmans, London, 1964. 1.1.1, 3.2.2

[24] W. H. Louisell. *Quantum Statistical Properties of Radiation.* Wiley, New York, 1973. 1.1.1, 4.3.2

[25] P. W. Milonni and C. Eberlein. The quantum vacuum: An introduction to quantum electrodynamics. *American Journal of Physics*, 62(12):1154–1154, 1994. 1.1.1

[26] P. W. Milonni. *The Quantum Vacuum*. Academic Press, 1994. 1.1.1

[27] M. Fleischhauer, A. Imamoğlu, and J. P. Marangos. Electromagnetically induced transparency: Optics in coherent media. *Rev. Mod. Phys.*, 77(2):633, 2005. 1.2, 1.2.1, 2.1, 2.2.3, 2.2.3, 3.1, 3.4.2

[28] K. J. Boller, A. Imamoğlu, and S. E. Harris. Observation of electromagnetically induced transparency. *Phys. Rev. Lett.*, 66:2593–2596, 1991. 1.2

[29] S. E. Harris, J. E. Field, and A. Kasapi. Dispersive properties of electromagnetically induced transparency. *Phys. Rev. A*, 46:R29–R32, 1992. 1.2, 1.2.1, 1.2.2

[30] S. E. Harris. Refractive-index control with strong fields. *Optics Lett.*, 19:2018–2020, 1994. 1.2

[31] M. O. Scully and M. Fleischhauer. High-sensitivity magnetometer based on index-enhanced media. *Phys. Rev. Lett.*, 69:1360–1363, 1992. 1.2, 3.4

[32] R. W. Boyd. *Nonlinear Optics*. Acad. Press, Amsterdam, 2. edition, 2003. 1.2

[33] A. Imamoğlu and S. E. Harris. Lasers without inversion - interference of dressed lifetime-broadened states. *Optics Lett.*, 14:1344–1346, 1989. 1.2.1

[34] C. W. Gardiner and P. Zoller. *Quantum Noise*. Springer Series in Synergetics. Springer, third edition, 2004. 1.2.1, 2.2.1, 2.4.1, A.1

[35] M. Sargent III, M. O. Scully, and Jr. W. E. Lamb. *Laser Physics*. Addison-Wesly Publishing Company, Inc., Reading, Mass. 01867, 1987. 1.2.1, 1.2.1, 1.3.3, 2.2.1

[36] M. D. Lukin. Colloquium: Trapping and manipulating photon states in atomic ensembles. *Rev. Mod. Phys.*, 75(2):457, 2003. 1.2.1, 1.2.1

[37] A. Javan, O. Kocharovskaya, H. Lee, and M. O. Scully. Narrowing of electromagnetically induced transparency resonance in a Doppler-broadened medium. *Phys. Rev. A*, 66, 2002. 1.2.1

[38] S. H. Autler and C. H. Townes. Stark effect in rapidly varying fields. *Phys. Rev.*, 100(2):703–722, Oct 1955. 1.2.1

[39] M. D. Lukin, M. Fleischhauer, A. S. Zibrov, H. G. Robinson, V. L. Velichansky, L. Hollberg, and M. O. Scully. Spectroscopy in dense coherent media: Line narrowing and interference effects. *Phys. Rev. Lett.*, 79:2959–2962, 1997. 1.2.1, 2.2.3, 2.4

[40] M. Fleischhauer, C. H. Keitel, M. O. Scully, C. Su, B. T. Ulrich, and S. Y. Zhu. Resonantly enhanced refractive-index without absorption via atomic coherence. *Phys. Rev. A*, 46:1468–1487, 1992. 1.2.1

[41] J. D. Jackson. *Classical Electrodynamics.* John Wiley & Sons, Inc., New York, third edition, 1999. 1.2.1

[42] J. Kästel. Strahlungswechselwirkung von Atomen in Medien mit negativem Brechungsindex, Dezember 2004. 1.2.1

[43] A. Kasapi, Maneesh Jain, G. Y. Yin, and S. E. Harris. Electromagnetically induced transparency: Propagation dynamics. *Phys. Rev. Lett.*, 74(13):2447–2450, Mar 1995. 1.2.2

[44] M. Xiao, Y.-q. Li, S.-z. Jin, and J. Gea-Banacloche. Measurement of dispersive properties of electromagnetically induced transparency in rubidium atoms. *Phys. Rev. Lett.*, 74(5):666–669, Jan 1995. 1.2.2

[45] D. Budker, D. F. Kimball, S. M. Rochester, and V. V. Yashchuk. Nonlinear magneto-optics and reduced group velocity of light in atomic vapor with slow ground state relaxation. *Phys. Rev. Lett.*, 83(9):1767–1770, Aug 1999. 1.2.2

[46] M. M. Kash, V. A. Sautenkov, A. S. Zibrov, L. Hollberg, G. R. Welch, M. D. Lukin, Y. Rostovtsev, E. S. Fry, and M. O. Scully. Ultraslow group velocity and enhanced nonlinear optical effects in a coherently driven hot atomic gas. *Phys. Rev. Lett.*, 82:5229, 1999. 1.2.2, 3.2.1

[47] J. Oreg, F. T. Hioe, and J. H. Eberly. Adiabatic following in multilevel systems. *Physical Review A (General Physics)*, 29(2):690–697, 1984. 1.2.2

[48] S. E. Harris and Z. F. Luo. Preparation energy for electromagnetically induced transparency. *Phys. Rev. A*, 52:R928–R931, 1995. 1.2.2, 2.2.1

[49] R. W. Boyd, D. J. Gauthier, A. L. Gaeta, and A. E. Willner. Maximum time delay achievable on propagation through a slow-light medium. *Phys. Rev. A (Atomic, Molecular, and Optical Physics)*, 71(2):023801, 2005. 1.2.2

[50] K. Bergmann, H. Theuer, and B. W. Shore. Coherent population transfer among quantum states of atoms and molecules. *Rev. Mod. Phys.*, 70(3):1003–1025, 1998. 1.3

[51] M. Fleischhauer, S. F. Yelin, and M. D. Lukin. How to trap photons? Storing single-photon quantum states in collective atomic excitations. *Opt. Comm.*, 179:395–410, 2000. 1.3.3

[52] M. D. Lukin, S. F. Yelin, and M. Fleischhauer. Entanglement of atomic ensembles by trapping correlated photon states. *Phys. Rev. Lett.*, 84(18):4232–4235, 2000. 1.3.3

[53] R. H. Dicke. Coherence in spontaneous radiation processes. *Phys. Rev.*, 93(1):99–110, 1954. 1.3.3

[54] M. Gross and S. Haroche. Super-radiance - an essay on the theory of collective spontaneous emission. *Phys. Reports-review Section Phys. Lett.*, 93:301–396, 1982. 1.3.3

[55] A. S. Zibrov, A. B. Matsko, O. Kocharovskaya, Y. V. Rostovtsev, G. R. Welch, and M. O. Scully. Transporting and time reversing light via atomic coherence. *Phys. Rev. Lett.*, 88(10):103601, 2002. 1.3.3

[56] F. Harres. *Die Geschwindigkeit des Lichtes in bewegten Körpern*. PhD thesis, Universität Jena, 1911. 1.4

[57] M. G. Sagnac. L'éther lumineux démonstré par l'effect du vent relatif d'éther dans un interféromètre en rotation uniforme. *Comp. Rend. Acad. Sci.*, 157:708, 1913. Paris. 1.4, 3.1

[58] E. J. Post. Sagnac effect. *Rev. Mod. Phys.*, 39(2):475–493, Apr 1967. 1.4.1, 3.1

[59] O. Avenel, Y. Mukharsky, and E. Varoquaux. Superfluid gyrometers. *J. Low Temperature Phys.*, 135:745–772, 2004. 1.4.3

[60] K. F. Woodman, P. W. Franks, and M. D. Richards. The nuclear-magnetic-resonance gyroscope - a review. *J. Navigation*, 40:366–384, 1987. 1.4.3

[61] T. W. Kornack, R. K. Ghosh, and M. V. Romalis. Nuclear spin gyroscope based on an atomic comagnetometer. *Phys. Rev. Lett.*, 95(23):230801, 2005. 1.4.3

[62] S. Buchman, C. W. F. Everitt, B. Parkinson, J. P. Turneaure, and G. M. Keiser. Cryogenic gyroscopes for the relativity mission. *Physica B*, 280:497–498, 2000. 1.4.3

[63] G. E. Stedman, K. U. Schreiber, and H. R. Bilger. On the detectability of the Lense-Thirring field from rotating laboratory masses using ring laser gyroscope interferometers. *Classical Quantum Gravity*, 20:2527–2540, 2003. 1.4.3, 3.4.3

[64] T. L. Gustavson, A. Landragin, and M. A. Kasevich. Rotation sensing with a dual atom-interferometer Sagnac gyroscope. *Classical Quantum Gravity*, 17:2385–2398, 2000. 1.4.3, 3.4.3

[65] B. Culshaw. The optical fibre Sagnac interferometer: an overview of its principles and applications. *Measurement Science & Technology*, 17:R1–R16, 2006. 1.4.3, 3.1

[66] D. P. DiVincenzo. The physical implementation of quantum computation. *Fortschritte der Physik - Progress Phys.*, 48:771–783, 2000. 2.1

[67] J. I. Cirac and P. Zoller. Quantum computations with cold trapped ions. *Phys. Rev. Lett.*, 74:4091, 1995. 2.1

[68] N. A. Gershenfeld and I. L. Chuang. Bulk spin-resonance quantum computation. *Science*, 275:350, 1997. 2.1

[69] G. P. Berman, G. D. Doolen, P. C. Hammel, and V. I. Tsifrinovich. Solid-state nuclear-spin quantum computer based on magnetic resonance force microscopy. *Phys. Rev. B*, 61(21):14694–14699, Jun 2000. 2.1

[70] G. P. Berman, G. D. Doolen, P. C. Hammel, and V. I. Tsifrinovich. Magnetic resonance force microscopy quantum computer with tellurium donors in silicon. *Phys. Rev. Lett.*, 86(13):2894–2896, Mar 2001. 2.1

[71] H. J. Kimble. Strong interactions of single atoms and photons in cavity qed. *Physica Scripta*, T76:127–137, 1998. 2.1

[72] A. Kuhn, M. Hennrich, and G. Rempe. Deterministic single-photon source for distributed quantum networking. *Phys. Rev. Lett.*, 89(6):067901, Jul 2002. 2.1

[73] T. Pellizzari, S. A. Gardiner, J. I. Cirac, and P. Zoller. Decoherence, continuous observation, and quantum computing: A cavity QED model. *Phys. Rev. Lett.*, 75:3788, 1995. 2.1

[74] Y. Makhlin, G. Schön, and A. Shnirman. Quantum-state engineering with Josephson-junction devices. *Rev. Mod. Phys.*, 73:357, 2001. 2.1

[75] L. M. Duan, M. D. Lukin, J. I. Cirac, and P. Zoller. Long-distance quantum communication with atomic ensembles and linear optics. *Nature*, 414:413–418, 2001. 2.1

[76] B. Julsgaard, J. Sherson, J. I. Cirac, J. Fiurasek, and E. S. Polzik. Experimental demonstration of quantum memory for light. *Nature*, 432:482–486, 2004. 2.1

[77] M. D. Eisaman, A. André, F. Massou, M. Fleischhauer, A. S. Zibrov, and M. D. Lukin. Electromagnetically induced transparency with tunable single-photon pulses. *Nature*, 438:04327, December 2005. 2.1

[78] C. W. Chou, H. de Riedmatten, D. Felinto, S. V. Polyakov, S. J. van Enk, and H. J. Kimble. Measurement-induced entanglement for excitation stored in remote atomic ensembles. *Nature*, 438:832, December 2005. 2.1

[79] T. Chaneliere, D. N. Matsukevich, S. D. Jenkins, S.-Y. Lan, T. A. B. Kennedy, and A. Kuzmich. Storage and retrieval of single photons transmitted between remote quantum memories. *Nature*, 438:836, December 2005. 2.1

[80] E. Knill, R. Laflamme, and G. J. Milburn. A scheme for efficient quantum computation with linear optics. *Nature*, 409:46–52, 2001. 2.1

[81] J. L. O'Brien, G. J. Pryde, A. G. White, T. C. Ralph, and D. Branning. Demonstration of an all-optical quantum controlled-NOT gate. *Nature*, 426:264–267, 2003. 2.1

[82] S. Gasparoni, J.-W. Pan, P. Walther, T. Rudolph, and A. Zeilinger. Realization of a photonic controlled-[small-caps not] gate sufficient for quantum computation. *Phys. Rev. Lett.*, 93(2):020504, 2004. 2.1

[83] M. D. Lukin, M. Fleischhauer, R. Cote, L. M. Duan, D. Jaksch, J. I. Cirac, and P. Zoller. Dipole blockade and quantum information processing in mesoscopic atomic ensembles. *Phys. Rev. Lett.*, 87:037901, 2001. 2.1

[84] D. Tong, S. M. Farooqi, J. Stanojevic, S. Krishnan, Y. P. Zhang, R. Cote, E. E. Eyler, and P. L. Gould. Local blockade of rydberg excitation in an ultracold gas. *Phys. Rev. Lett.*, 93(6):063001, 2004. 2.1

[85] K. Singer, M. Reetz-Lamour, T. Amthor, L. G. Marcassa, and M. Weidemüller. Suppression of excitation and spectral broadening induced by interactions in a cold gas of rydberg atoms. *Phys. Rev. Lett.*, 93(16):163001, 2004. 2.1

[86] A. André, M. Bajcsy, A. S. Zibrov, and M. D. Lukin. Nonlinear optics with stationary pulses of light. *Phys. Rev. Lett.*, 94(6):063902, 2005. 2.1, 2.2.4

[87] A. André. private communication, 2005. 1, 2.3.1, 2.11

[88] A. André. *Nonclassical states of light and atomic ensembles: Generation and New Applications.* Phd thesis, Harvard University, Departement of Physics, Harvard University, Cambridge, Massachusetts, May 2005. 2.2.1, 2.2.4

[89] P. D. Drummond and M. G. Raymer. Quantum-theory of propagation of nonclassical radiation in a near-resonant medium. *Phys. Rev. A*, 44:2072–2085, 1991. 2.2.1

[90] V. Chaltykyan, G. Grigoryan, and G. Nikogosyan. Dark-state evolution and self-phase modulation in a lambda medium. *Phys. Rev. A (Atomic, Molecular, and Optical Physics)*, 68(1):013819, 2003. 2.2.3

[91] S. E. Harris. Electromagnetically induced transparency with matched pulses. *Phys. Rev. Lett.*, 70:552, February 1993. 2.2.5

[92] E. Cerboneschi and E. Arimondo. Transparency and dressing for optical pulse pairs through a double-lambda absorbing medium. *Phys. Rev. A*, 52:R1823–R1826, 1995. 2.2.5

[93] M. D. Lukin and A. Imamoğlu. Controlling photons using electromagnetically induced transparency. *Nature*, 413:273, 2001. 2.4

[94] M. D. Lukin, P. R. Hemmer, M. Löffler, and M. O. Scully. Resonant enhancement of parametric processes via radiative interference and induced coherence. *Phys. Rev. Lett.*, 81:2675, 1998. 2.4

[95] S. E. Harris, J. E. Field, and A. Imamoğlu. Nonlinear optical processes using electromagnetically induced transparency. *Phys. Rev. Lett.*, 64:1107–1110, 1990. 2.4

[96] K. Hakuta, L. Marmet, and B. P. Stoicheff. Electric-field-induced second-harmonic generation with reduced absorption in atomic hydrogen. *Phys. Rev. Lett.*, 66(5):596–599, Feb 1991. 2.4

[97] A. E. Siegman. *Lasers.* University Science Books, 20 Edgehill Road, Mill Valley, CA 94941, 1986. 2.4

[98] C. W. Gardiner. *Handbook of Stochastic Methods.* Springer Series in Synergetics. Springer, third edition, 2003. 2.4.1, 2.4.2

[99] G. E. Uhlenbeck and L. S. Ornstein. On the theory of the brownian motion. *Phys. Rev.*, 36:823, September 1930. 2.4.1

[100] H. J. Carmichael. *Statistical Methods in Quantum Optics 1.* Texts and Monographs in Physics. Springer Verlag, Berlin and Heidelberg, 1999. 2.4.1

[101] N. N. Lebedev. *Special Functions and their applications.* Dover Publications, Inc., 1972. 2.4.2, 2.4.2

[102] F. E. Zimmer, A. André, M. D. Lukin, and M. Fleischhauer. Coherent control of stationary light pulses. *Optics Comm.*, 264:441–453, 2006. 2.4.2

[103] G. E. Stedman. Ring-laser tests of fundamental physics and geophysics. *Rep. Prog. Phys.*, 60:615, 1997. 3.1

[104] L. A. Page. Effect of earth's rotation in neutron interferometry. *Phys. Rev. Lett.*, 35(8):543, Aug 1975. 3.1

[105] T. L. Gustavson, P. Bouyer, and M. A. Kasevich. Precision rotation measurements with an atom interferometer gyroscope. *Phys. Rev. Lett.*, 78(11):2046–2049, 1997. 3.1

[106] J. M. McGuirk, M. J. Snadden, and M. A. Kasevich. Large area light-pulse atom interferometry. *Phys. Rev. Lett.*, 85(21):4498–4501, 2000. 3.1

[107] W. W. Chow, J. Gea-Banacloche, L. M. Pedrotti, V. E. Sanders, W. Schleich, and M. O. Scully. The ring laser gyro. *Rev. Mod. Phys.*, 57:61, 1985. 3.1

[108] C. Orzel, A. K. Tuchman, M. L. Fenselau, M. Yasuda, and M. A. Kasevich. Squeezed States in a Bose-Einstein Condensate. *Science*, 291(5512):2386–2389, 2001. 3.1

[109] M. A. Kasevich. Coherence with Atoms. *Science*, 298(5597):1363–1368, 2002. 3.1, 3.4.3

[110] A. P. Chikkatur, Y. Shin, A. E. Leanhardt, D. Kielpinski, E. Tsikata, T. L. Gustavson, D. E. Pritchard, and W. Ketterle. A Continuous Source of Bose-Einstein Condensed Atoms. *Science*, 296(5576):2193–2195, 2002. 3.1

[111] A. Einstein. Bemerkungen zu *P. Harzers* Abhandlungen: Über die Mitführung des Lichtes in Glas und die Aberation. *Astronomische Nachrichten*, 199(4753), 1914. 3.1

[112] A. Einstein. Antwort auf eine Replik *Paul Harzers* (Nr. 4753, S.10 und 11). *Astronomische Nachrichten*, 199(4755):47, 1914. 3.1

[113] P. Harzer. Über die Mitführung des Lichtes in Glas und die Aberation. *Astronomische Nachrichten*, 198(4748):26, 1914. 3.1

[114] P. Harzer. Bemerkungen zu meinem Artikel in Nr. 4748 im Zusammenhange mit den vorstehenden Bemerkungen des *Herrn Einstein. Astronomische Nachrichten*, 199(4753):10, 1914. 3.1

[115] B. Pogany. Über die Wiederholung des Harress-Sagnacschen Versuches. *Annalen der Physik*, 80:217, 1926. 3.1

[116] B. Pogany. Über die Wiederholung des Harress-Sagnacschen Versuches. *Annalen der Physik*, 85:244, 1928. 3.1

[117] A. Dufour and F. Prunier. Sur un deplacément de franges enregistré sur une plateforme en rotation uniforme. *J. Phys. Radium*, 3:153, 1942. 3.1

[118] A. Dufour and F. Prunier. *Comp. Rend. Acad. Sci.*, 204:1322, 1937. 3.1

[119] S. Gupta, K. W. Murch, K. L. Moore, T. P. Purdy, and D. M. Stamper-Kurn. Bose-einstein condensation in a circular waveguide. *Phys. Rev. Lett.*, 95(14):143201, 2005. 3.1, 3.3.1, 3.4.3

[120] A. S. Arnold, C. S. Garvie, and E. Riis. Large magnetic storage ring for Bose-Einstein condensates. *Phys. Rev. A (Atomic, Molecular, and Optical Physics)*, 73(4):041606, 2006. 3.1, 3.4.3

[121] B. H. W. Hendriks and G. Nienhuis. Sagnac effect as viewed by a co-rotating observer. *Quantum Optics: Journal of the European Optical Society Part B*, 2(1):13–21, 1990. 3.2.1

[122] A. B. Matsko, O. Kocharovskaya, Y. Rostovtsev, G. R. Welch, A. S. Zibrov, and M. O. Scully. Slow, ultraslow, stored, and frozen light. *Adv. In Atomic, Molecular, Opt. Physics, Vol 46*, 46:191–242, 2001. 3.2.1

[123] L. Mandel and E. Wolf. *Optical coherence and quantum optics*. Cambridge University Press, Cambridge, 1995. 3.2.2, 3.4.3, 4.3.2, 4.3.2

[124] I. Carusotto, M. Artoni, and G.C. La Rocca. Atomic recoil effects in slow light propagation. *JETP Letters*, 72(6):289–293, 2000. 3.3.1

[125] K. W. Madison, F. Chevy, W. Wohlleben, and J. Dalibard. Vortex formation in a stirred Bose-Einstein condensate. *Phys. Rev. Lett.*, 84(5):806–809, Jan 2000. 3.3.2

[126] J. R. Abo-Shaeer, C. Raman, J. M. Vogels, and W. Ketterle. Observation of vortex lattices in Bose-Einstein condensates. *Science*, 292:476–479, 2001. 3.3.2

[127] M. W. Zwierlein, J. R. Abo-Shaeer, A. Schirotzek, C. H. Schunck, and W. Ketterle. Vortices and superfluidity in a strongly interacting Fermi gas. *Nature*, 435:1047–1051, 2005. 3.3.2

[128] M. Fleischhauer and M. O. Scully. Quantum sensitivity limits of an optical magnetometer based on atomic phase coherence. *Phys. Rev. A*, 49:1973–1986, 1994. 3.4

[129] Frank Vewinger. *Manipulation und Charakterisierung kohärenter Überlagerungszustände in Mehrniveausystemen.* Dissertation, Technische Universität Kaiserslautern, Fachbereich Physik, 67663 Kaiserslautern, Erwin-Schrödinger-Strasse, Dezember 2004. 4, 4.4, 4.4

[130] F. Papoff, F. Mauri, and E. Arimondo. Transient velocity-selective coherent population trapping in one dimension. *J. Opt. Soc. Am. B*, 9(3):321, march 1992. 4, 4.1, 4.2.3, 4.3.3, 4.3.3, 4.4, 4.6

[131] E. Arimondo. Coherent population trapping in laser spectroscopy. *Progress In Optics, Vol 35*, 35:257–354, 1996. 4.1

[132] A. Aspect, E. Arimondo, R. Kaiser, N. Vansteenkiste, and C. Cohen-Tannoudji. Laser cooling below the one-photon recoil energy by velocity-selective coherent population trapping. *Phys. Rev. Lett.*, 61(7):826, August 1988. 4.1, 4.2.1, 4.5.1

[133] A. Aspect, E. Arimondo, R. Kaiser, N. Vansteenkiste, and C. Cohen-Tannoudji. Laser cooling below the one-photon recoil energy by velocity-selective coherent population trapping: theoretical analysis. *J. Opt. Soc. Am. B*, 6(11):2112, November 1989. 4.1, 4.2.1

[134] M. Weitz, T. Heupel, and T. W. Hänsch. Multiple beam atomic interferometer. *Phys. Rev. Lett.*, 77(12):2356–2359, Sep 1996. 4.1

[135] H. J. Metcalf and P. van der Straten. *Laser Cooling and Trapping.* Springer, 2002. 4.2.1, 4.3.1

[136] A. R. Edmonds. *Angular momentum in Quantum Mechanics.* Princeton University Pres, Princeton, 1957. 4.3.1

[137] C. Menotti, G. Morigi, J. H. Müller, and E. Arimondo. Scaling laws in velocity-selective coherent population trapping in the presence of polarization-gradient cooling. *Physical Review A (Atomic, Molecular, and Optical Physics)*, 56:4327, 1997. 4.3.1

[138] Y. Castin, H. Wallis, and J. Dalibard. Limit of doppler cooling. *J. Opt. Soc. Am. B-optical Phys.*, 6:2046–2057, 1989. 4.3.2, 4.3.2, 4.3.2

[139] H. Wallis. Quantum-theory of atomic motion in laser-light. *Phys. Reports-review Section Phys. Lett.*, 255:204–287, 1995. 4.3.2, 4.3.2

[140] J. R. Morris and B. W. Shore. Reduction of degenerate 2-level excitation to independent 2-state systems. *Phys. Rev. A*, 27:906–912, 1983. 4.3.3, 4.3.3

[141] S. Stenholm. Redistribution of molecular velocities by optical processes. *Appl. Phys.*, 15:287–296, 1978. 4.3.4

[142] H. Theuer. *Anwendung von STIRAP in der kohärenten Teilchenoptik am Beispiel eines laserpräperierten Ne*-Atomstrahls.* Dissertation, Universität Kaiserslautern, January 2000. 4.4

[143] J. M. Weber, K. Hansen, M.-W. Ruf, and H. Hotop. Penning ionization of C_{60} and C_{70}. *Chem. Phys.*, 239:271–286, 1998. 4.4

[144] T. Esslinger, F. Sander, M. Weidemüller, and T. W. Hänsch. Subrecoil laser cooling with adiabatic transfer. *Phys. Rev. Lett.*, 76:2432–2435, 1996. 4.5.1

[145] A. Klein. Wechselwirkung von Störstellenatomen in Bose-Einstein-Kondensaten, 2004. A.1

[146] B. Schmidt, L. I. Plimak, and M. Fleischhauer. Stochastic simulation of a finite-temperature one-dimensional Bose gas: From the Bogoliubov to the Tonks-Girardeau regime. *Phys. Rev. A (Atomic, Molecular, and Optical Physics)*, 71(4):041601, 2005. A.1

Curriculum vitae

Frank Egon Zimmer

Personal data:

Date of birth:	July 3rd, 1974
Place of birth:	Hermeskeil
Nationality:	German
Marital status:	single

School education:

1981-1985	Grundschule in Thalfang
1986-1990	Hauptschule in Thalfang
1990-1991	Hauptschule in Hermeskeil
	leaving certificate: qualifizierter Sekundarabschluß 1
1991-1994	Balthasar-Neumann-Schule Trier
	Berufliches Gymnasium Bildungsgang Technik
	school leaving certificate: Allgemeine Hochschulreife (Abitur)

University education:

1996-1998	Grundstudium at the University of Kaiserslautern
	(major subject: physics, subsidiary subject: computer sience)
1998-2001	Hauptstudium period at the University of Kaiserslautern
	(major subject: physics, subsidiary subject: mathematics)
10/26/2001	Diploma in Physics, title of diploma thesis:
	Resonanzstrukturen in Wannier-Stark Systemen
	Supervisor: apl. Prof. Dr. H.-J. Korsch
2001-2006	Doctoral Program, Technical University of Kaiserslautern
	Supervisor: Prof. Dr. M. Fleischhauer

Danksagung

Ich möchte nicht eine Reihe von Menschen auflisten, die zum Gelingen dieser Arbeit beigetragen haben, sondern möchte mich mit einem kurzen Gedicht bei allen herzlich für die letzten Jahre und Ihre Unterstützung bedanken.

Demut

Seh ich die Werke der Meister an,
So seh ich das, was sie getan;
Betracht ich meine Siebensachen,
Seh ich, was ich hätt sollen machen.

J. W. v. Goethe